2010

Design, Synthesis And Characterization Of New Two-photon Absorbing (2pa) Fluorescent Dyes And Bioconjugates, And Their Applications In Bioimaging

Carolina D. Andrade
University of Central Florida

DESIGN, SYNTHESIS AND CHARACTERIZATION OF NEW TWO-PHOTON ABSORBING (2PA) FLUORESCENT DYES AND BIOCONJUGATES, AND THEIR APPLICATIONS IN BIOIMAGING

by

CAROLINA D. ANDRADE
B. S. Universidad Simon Bolivar, 2004

A dissertation submitted in partial fulfillment of the requirements
for the degree of Doctor of Philosophy
in the Department of Chemistry
in the College of Sciences
at the University of Central Florida
Orlando, Florida

Fall Term
2010

Major Professor: Kevin D. Belfield

ABSTRACT

The development of new multiphoton absorbing materials has attracted the attention of researchers for the last two decades. The advantages that multiphoton absorbing materials offer, versus their one-photon absorbing counterparts, rely on the nature of the nonlinearity of the absorption process, where two photons are absorbed simultaneously offering increased 3D resolution, deeper penetration, and less photobleaching and photodamage as a result of a more confined excitation. The applications of efficient two-photon absorbing materials have been extensively expanding into the fields of photodynamic therapy, microscopy, and optical data storage. One of the fields where an increased interest in multiphoton absorbing materials has been most evident is in bioimaging, in particular, when different cellular processes and organelles need to be studied by fluorescence microscopy. The goal of this research was to develop efficient two-photon absorption (2PA) compounds to be used in fluorescence bioimaging, meaning that such compounds need to posses good optical properties, such as high fluorescence quantum yield, 2PA cross section, and photostability.

In the first chapter of this dissertation, we describe the synthesis and structural characterization of a new series of fluorescent donor–acceptor and acceptor-acceptor molecules based on the fluorenyl ring system that incorporated functionalities such as alkynes and thiophene rings, through efficient Pd-catalyzed Sonogashira and Stille coupling reactions, in order to increase the length of the conjugation in our systems. These new molecules proved to have high two-photon absorption (2PA), and the effect of these functionalities on their 2PA cross section values was evaluated. Finally, their use in two-photon fluorescence microscopy (2PFM) imaging was demonstrated.

One of the limitations of the compounds described in Chapter 1 was their poor water solubility; this issue was addressed in Chapter 2. The use of micelles in drug delivery has been shown to be an area of increasing interest over the last decade. In the bioimaging field, it is key to have dye molecules with a high degree of water solubility to enable cells to uptake the dye. By enclosing a hydrophobic dye in Pluronic® F-127 micelles, we developed a system that facilitates the use of 2PA molecules (typically hydrophobic) in biological systems for nonlinear biophotonic applications, specifically to image the lysosomes. Furthermore, we report in this chapter the efficient microwave-assisted synthesis of the dye used in this study.

In addition, linear photophysical and photochemical parameters, two-photon absorption (2PA), and superfluorescence properties of the dye studied in Chapter 2, were investigated in Chapter 3. The steady-state absorption, fluorescence, and excitation anisotropy spectra of this dye were measured in several organic solvents and aqueous media.

In Chapter 4, we describe the preparation and the use of an efficient and novel two-photon absorbing fluorescent probe conjugated to an antibody that confers selectivity towards the vascular endothelial growth factor receptor 2 (VEGFR-2) in porcine aortic endothelial cells that express this receptor (PAE-KDR). It is known that this receptor is overexpressed in certain cancer processes. Thus, targeting of this receptor will be useful to image the tumor vasculature. It was observed that when the dye was incubated with cells that do not express the receptor, no effective binding between the bioconjugate and the cells took place, resulting in very poor, non-specific fluorescence images by both one and two-photon excitation. On the other hand, when the dye was incubated with cells that expressed VEGFR-2, efficient imaging of the cells was obtained, even at very low concentrations (0.4 μM). Moreover, incubation of the bioconjugate

with tissue facilitated successful imaging of vasculature in mouse embryonic tissue.

PUBLICATIONS TO DATE FROM DISSERTATION WORK

1. Andrade, C. D.; Yanez, C. O.; Qaddoura, M. A.; Wang, X.; Arnett, C. L.; Coombs, S. A.; Yu, J.; Bassiouni, R.; Bondar, M. V.; Belfield, K. D. "Two-Photon Lysosomal Bioimaging with Micelle-Encapsulated 2PA Fluorescent Dye" Journal of Fluorescence. Accepted on November **2010**.
2. Belfield, K. D.; Andrade, C. D.; Yanez, C. O.; Bondar, M. V.; Hernandez, F. E.; Przhonska, O. V. "New Two-Photon Absorbing Probe With Efficient Superfluorescent Properties" Journal of Physical Chemistry B. **2010**, *114*, 14087-14095.
3. Andrade, C. D.; Yanez, C. O.; Rodriguez, L.; Belfield, K. D. "A Series of Fluorene-Based Two-Photon Absorbing Molecules: Synthesis, Linear and Nonlinear Characterization, and Bioimaging." Journal of Organic Chemistry. **2010**, *75* (12), 3975-3982.
4. Yanez, C. O.; Belfield, K. D.; Andrade, C. D.; Yao, S.; Bondar, M. V. "Photosensitive Polymeric Materials for Two-Photon 3D WORM Optical Data Storage and Microfabrication." *Organic Thin Films for Photonic Applications, ACS Symposium Series.* **2010,** *1039,*Chapter 8.
5. Yanez, C. O.; Andrade, C. D.; Belfield, K. D. "Characterization of Novel Sulfonium Photoacid Generators and Their Microwave-Assisted Synthesis" Chemical Communications. **2009,** *7*, 827-829.
6. Yanez, C. O.; Andrade, C. D.; Yao, S.; Luchita, G.; Bondar, M. V.; Belfield, K. D. "Photosensitive Polymeric Materials for Two-Photon 3-D WORM Optical Data Storage Systems". ACS Applied Materials & Interfaces. **2009**, *1*, 2219-2229.

7. Belfield, K. D.; Yanez, C. O.; Andrade, C. D.; Yao, S. “New photosensitive polymeric materials for two-photon 3D WORM optical data storage.” Polymer Preprints (American Chemical Society, Division of Polymer Chemistry). **2008**, *49* (2), 980-981.

CONFERENCES AND PRESENTATIONS TO DATE FROM DISSERTATION WORK

1. Carolina D. Andrade, Ciceron O. Yanez, Hyo-Yang Ahn, Kevin D. Belfield. VEGFR-2 Selective Two-Photon Absorbing (2PA) Bioconjugate Probe for Bioimaging. The 9th International Symposium on Functional pi-Electron Systems. Atlanta, Georgia, 2010.
2. Carolina D. Andrade, Mykhailo V. Bondar, Ciceron O. Yanez, Hyo-Yang Ahn, Kevin D. Belfield. Photophysics and Bioimaging of an Efficient Two-Photon Absorbing, Superfluorescent Bisthiophenyl Fluorene Derivative. The 9th International Symposium on Functional pi-Electron Systems. Atlanta, Georgia, 2010.
3. Ciceron O. Yanez, Carolina D. Andrade, Xuhua Wang, Shen Yao, Sabrina A. Coombs, Curtesa L. Arnett, Kevin D. Belfield. Design of 2PA Lysosomal Specific Fluorescent Probes. The 9th International Symposium on Functional pi-Electron Systems. Atlanta, Georgia, 2010.
4. Carolina D. Andrade, Ciceron O. Yanez, Hyo-Yang Ahn, Kevin D. Belfield. VEGFR-2 Selective Two-Photon Absorbing (2PA) Bioconjugate. Biomedical Optics and 3-D Imaging: OSA Optics & Photonics Congress. Miami, Florida, 2010.
5. Ciceron O. Yanez, Alma R. Morales, Dao M. Nguyen, Xuhua Wang, Carolina D. Andrade, Sanchita Biswas, Hyo-Yang Ahn, Sheng Yao, and Kevin D. Befield. Biophotonics: Two-photon Fluorescence Microscopy, Probes & Target-specific Bioimaging. 2010 Industrial Affiliates Day, CREOL, The College of Optics & Photonics, University of Central Florida, Orlando, Fl, United States, 2010.

6. Ciceron O. Yanez, Carolina D. Andrade, Xuhua Wang, Shen Yao, Sabrina A. Coombs, Curtesa L. Arnett, Kevin D. Belfield. Lysosome-specific fluorene dyes for two-photon fluorescence microscopy. SPIE Photonics West. San Francisco, California, United States, 2010.
7. Carolina D. Andrade, Maher A. Qaddoura, Ciceron O. Yanez, Mykhailo V. Bondar, and Kevin D. Belfield. Two-photon absorbing fluorescent dye-containing micelles for bioimaging. 238th ACS National Meeting, Washington, D.C., United States, 2009.
8. Carolina D. Andrade, Ciceron O. Yanez, Kevin D. Belfield. Synthesis and characterization of novel fluorene-based two-photon absorbing molecules. 85th Florida Annual Meeting and Exposition (FAME), Orlando, Florida, United States, 2009.
9. Ciceron O. Yanez, Carolina D. Andrade, Sheng Yao, Gheorghe Luchita, Kevin D. Belfield. Photosensitive Polymeric Materials for Two-Photon 3D WORM Optical Data Storage Systems. 85th Florida Annual meeting (FAME), Orlando, Florida, United States, 2009.
10. Ciceron O. Yanez, Carolina D. Andrade, Sheng Yao, Gheorge Luchita, Kevin D. Belfield Photosensitive Polymeric Materials for Two-Photon 3D WORM Optical Data Storage Systems. 2009 Industrial Affiliates Day, CREOL, The College of Optics & Photonics, University of Central Florida, Orlando, Fl, United States, 2009.
11. Carolina D. Andrade, Ciceron O. Yanez, and Kevin D. Belfield. Synthesis and characterization of novel fluorene-based two photon absorbing molecules, 236th ACS National Meeting, Philadelphia, PA, United States, 2008.
12. Kevin D. Belfield, Ciceron O. Yanez, Carolina D. Andrade, Sheng Yao. New photosensitive polymeric materials for two-photon 3-D WORM optical data storage, 236th

ACS National Meeting, Philadelphia, PA, United States, 2008.

13. Ciceron O. Yanez, Carolina D. Andrade, Kevin D. Belfield. Formation of new sulfonium photoacid generators by microwave assisted reaction of diphenyl sulfides with diphenyl iodonium salts, 236th ACS National Meeting, Philadelphia, PA, United States, 2008.

I dedicate this dissertation to my wonderful family,

especially to my loving parents *Ada* and *Jose Luis*,

to my loved husband *Ciceron*,

and to my beautiful baby *Stephanie*.

ACKNOWLEDGMENTS

I would like to express my deepest appreciation and gratitude to my advisor Dr. Kevin D. Belfield for his support and guidance throughout this journey. Without his continued motivation and advice this dissertation wouldn't have been possible.

I wish to thank all the current and former members of Dr. Belfield's research group, with whom I've shared intense hours of lab work and tons of fun. In particular, thanks to Dr. M. Bondar, Dr. L. Rodriguez and Hyo-Yang Ahn for their contribution and help with the measurement of the nonlinear properties of the compounds synthesized. I also would like to acknowledge Maher Qaddoura for his assistance with the preparation of micelles. I would like to specially thank Dr. Ciceron O. Yanez for all his generosity and his dedication in all the microscopy and cell work required to complete this dissertation.

Thanks also to Drs. Karl Chai and Li-Mei Chen from the Burnett School of Biomedical Sciences, UCF for their participation and help in the tissue experiments.

TABLE OF CONTENTS

LIST OF FIGURES

LIST OF TABLES

LIST OF SCHEMES

LIST OF ACRONYMS AND ABREVIATIONS

^{13}C	Carbon 13 isotope
^{1}H	Hydrogen 1 isotope
2PA	Two-photon absorption
2PFM	Two-Photon fluorescence microscopy
3D	Tridimentional
A-π-A	Acceptor-π-acceptor
ACN	Acetonitrile
Anal.	Analysis
APCI	Atmospheric Pressure Chemical Ionization
Ar	Aromatic system
Calcd.	Calculated
$CDCl_3$	Deuterated chloroform
cm^{-1}	Wavenumber
d	Doublet
D-π-A	Donor-π-acceptor
dd	Doublet of doublets
DIC	Differential interference contrast
DMSO	Dimethylsulfoxide
DOL	Degree of labeling
DPA	9,10-diphenylanthracene
EtOAc	Ethyl acetate

EtOH	Ethanol
FITC	Fluorescein isothiocyanate
FLIM	Fluorescence Lifetime imaging
fs	Femtosecond (10^{-15} s)
FWHM	Full width at half maximum
g	Gram
GM	Goppert-Mayer unit for the 2PA cross section ($1x10^{-50}$ cm^4 s $photon^{-1}molecule^{-1}$)
h	Hour
Hz	Hertz
J	Coupling constant
KHz	Kilohertz (10^3 Hertz)
L	Liter
m	Multiplet
M	Molar
m.p.	Melting point
mAb	monoclonal antibody
mg	Milligram (10^{-3} grams)
MHz	Megahertz (10^6 Hertz)
min	Minute
mL	Milliliter (10^{-3} Liters)
mmol	Millimoles (10^{-3} moles)

MS	Mass spectrum
ms	Millisecond (10^{-3} seconds)
MVD	Microvascular density
n-BuLi	*n*-Butyllithium
N. A.	Numerical aperture
NIR	Near Infrared
nm	Nanometer (10^{-9} meters)
NMR	Nuclear magnetic resonance
PAE	Porcine aortic endothelial
PMT	Photomultiplier tube
ppm	Parts per million
psi	Pounds per square inch
r. t.	Room temperature
s	Seconds
S_1	First excited state, singlet
S_n	A Higher excited state
S_o	Ground state, singlet
t	Triplet
THF	Tetrahydrofurane
TLC	Thin layer chromatography
UV	Ultraviolet
VEGF	Vascular endothelial growth factor

VEGFR-2 or KDR	Vascular endothelial growth factor receptor 2
W	Watts
δ	ppm or 2PA cross section
$\Delta\lambda_{St}$	Stokes shift
ε	Molar absorptivity coefficient
λ^{abs}_{max}	Wavelength of maximum absorption
λ^{em}_{max}	Wavelength of maximum emission
μJ	microjoules (10^{-6} Joules)
μM	micromolar (10^{-6} Molar)
μm	micrometer (10^{-6} meters)
μL	microliter (10^{-6} Liters)
τ_F	Fluorescence lifetime
Φ	Fluorescence quantum yield

CHAPTER 1. A SERIES OF FLUORENE-BASED TWO-PHOTON ABSORBING MOLECULES: SYNTHESIS, LINEAR AND NONLINEAR CHARACTERIZATION, AND BIOIMAGING

Reproduced with permission from: Carolina D. Andrade, Ciceron O. Yanez, Luis Rodriguez, Kevin D. Belfield, *Journal of Organic Chemistry*, **2010**, *75* (12), 3975-3982.

1.1 Abstract

The synthesis, structural, and photophysical characterization of a series of new fluorescent donor–acceptor and acceptor-acceptor molecules, based on the fluorenyl ring system, with two-photon absorbing properties is described. These new compounds exhibited large Stokes shifts, high fluorescent quantum yields, and, significantly, high two-photon absorption cross sections, making them well suited for two-photon fluorescence microscopy (2PFM) imaging. Confocal and two-photon fluorescence microscopy imaging of COS-7 and HCT 116 cells incubated with probe **I** showed endosomal selectivity, demonstrating the potential of this class of fluorescent probes in multiphoton fluorescence microscopy.

Keywords: Fluorescent dyes, multiphoton absorption, fluorescence, two-photon, bioimaging.

1.2 Introduction

The development of multiphoton absorbing materials has attracted the interest of the scientific community in the last decade due to their potential applications in areas as optical data storage systems, microscopy imaging, optical limiting materials, and photodynamic therapy. In one-photon absorption processes, the absorbed light is directly proportional to the incident light intensity, whereas in two-photon absorption (2PA) processes, the probability of absorbing two

photons simultaneously is proportional to the square of the incident light intensity.[*1*] This nonlinear dependence provides several advantages, including highly confined excitation, increased 3D resolution (Figure 1-1), and the potential increase of penetration depth in tissue, important features in fields such as optical data storage,[*2-4*] 3D microfabrication,[*5-7*] and fluorescence microscopy.[*1, 8*]

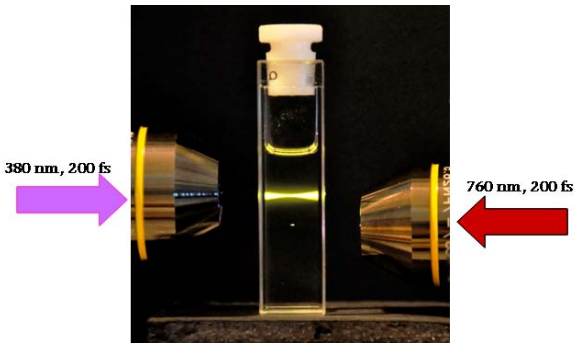

Figure 1-1 One-photon (left arrow) vs. two-photon (right arrow) excitation, showing the high 3D spatially-localized excitation in 2PA in a solution of dye **I.**

We previously reported a series of fluorescent dyes and photoacid generators that use fluorene as a core structure.[*9-14*] This core exhibited high thermal and photochemical stability making this class of compounds promising in areas such as lasing applications.[*15*]

Recently, a computational quantum chemical study of numerous fluorene derivatives was reported in order to predict and rationalize certain 2PA parameters, such as 2PA cross sections and 2PA wavelength. Though insightful, little comparison and validation of computed results with experimental data was presented, emphasizing the need to accurately measure 2PA spectra and cross sections of new compounds.[*16*]

In the interest of developing more efficient 2PA fluorophores, it is essential to improve the key photophysical properties such as quantum yield, absorption maxima, and 2PA cross sections in the tuning range of commercial Ti:sapphire lasers (700-1000 nm). In this work, we

present the design, synthesis, and photophysical (linear and nonlinear) characterization of a new series of two-photon absorbing molecules based on a fluorenyl core and demonstration of their use in *in vitro* confocal and two-photon fluorescence microscopy (2PFM) bioimaging.

In this approach, a series of dyes were developed with the general structural design donor-pi-acceptor (D-π-A) and acceptor-pi-acceptor (A-π-A) using benzothiazole moieties as electron-acceptor groups and diphenylamino groups as electron-donor moieties. To enhance the solubility of the fluorene core in organic solvents, both protons on the 9-position of fluorene were substituted by alkyl chains. Functionalities including thiophene and alkynes were incorporated in order to increase the length of the π -conjugation and to evaluate the effect of these functionalities on the linear absorption maxima, fluorescence quantum yields, and 2PA cross sections. The chemical structures of the new fluorescent compounds presented in this paper are illustrated in Figure 1-2.

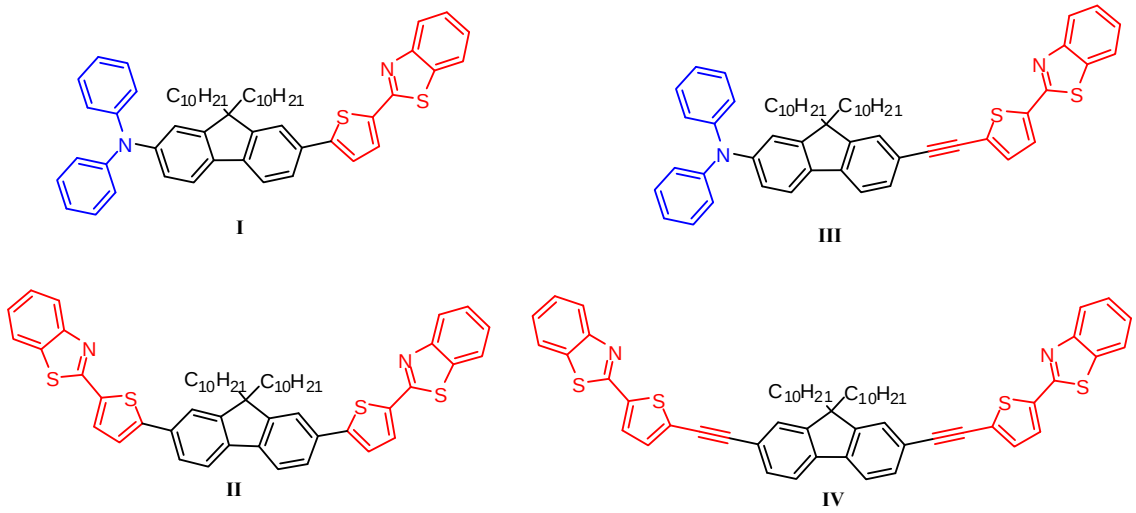

Figure 1-2 Structures of new donor-pi-acceptor (D-π-A) (**I** and **III**) and acceptor-pi-acceptor (A-π-A) (**II** and **IV**) fluorenyl derivatives. Benzothiazole moieties were used as acceptor groups while diphenylamino groups were used as donor moieties. Thiophene groups and alkynes were incorporated to extend the π-conjugation.

For the work described herein, the thiophene ring was chosen as a π electron bridge because it has a higher degree of aromaticity than other five member rings, e.g., furan, it is stable towards oxidation, and its chemical reactivity to allow functionalization is higher than that observed for benzene or furan. Incorporation of these heterocyclic rings in the molecular design of chromophores has been reported to enhance the optical properties, increasing both the maximum of absorption (λ^{abs}_{max}) and the 2PA cross section values, particularly when the thiophene ring is close to the fluorene core.[*17, 18*]

One of our goals was to compare this new series of compounds with our previously prepared and studied probes that contain benzothiazole groups. Thus, the bezothiazole ring system was used as an electron withdrawing group. Previous studies suggested that compounds containing this moiety are more robust than analog compounds containing benzoxazole groups. Moreover, benzothiazole groups are relatively strong electron withdrawing groups, and their ability to accept charge transferred from a diphenylamino moiety appears to be higher than that observed for benzoxazolyl containing compounds.[*19, 20*]

1.3 Results and Discussion

1.3.1 Synthesis of new fluorescent probes

The model 2PA fluorescent probe **I** was synthesized starting from the transformation of benzothiazole derivative **1** into tin derivative **2**, followed by Pd-catalyzed Stille coupling with key fluorenyl intermediate **3** was accomplished, as shown in Scheme 1-1, to yield nitrofluorenyl **4** in excellent yield.[*19, 21*] Reduction of the nitrofluorenyl **4**, and subsequent reaction of resulting amine **5** with iodobenzene under Ullman conditions, generated the D-π-A type

fluorescent dye **I**.[*19, 22*] Stille coupling between dibromofluorene derivative **6** and the tin thiophene benzothiazole intermediate **2** yielded symmetrical dye **II**[*11, 19, 21*] (Scheme 1-1).

Scheme 1-1

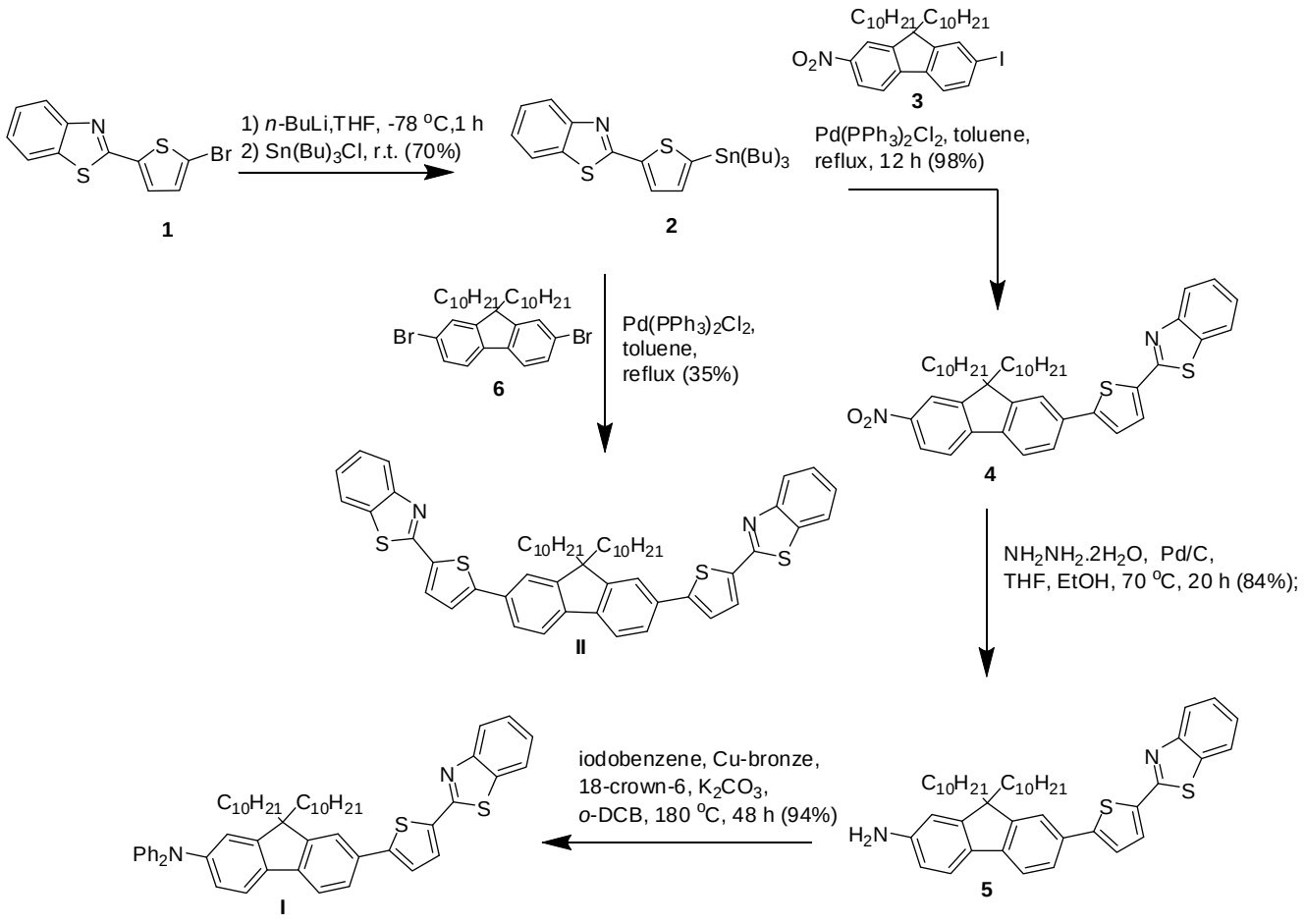

The synthesis of alkyne-containing dyes was achieved by means of successive Sonogashira coupling.[*23*] To prepare the asymmetrical compound **III**, 2-(5-bromothiophen-2-yl)benzothiazole **1** was converted into protected alkyne **7** which, after hydrolysis in toluene with KOH, generated alkyne **8** (Scheme 1-2).[*24, 25*] Pd-catalyzed Sonogashira coupling between the

alkyne **8** and key intermediate **3** yielded nitro derivative **9**, which was reduced with hydrazine to produce amine **10** in high yield. Amine **10** was treated with iodobenzene under Ullman conditions to generate the asymmetrical D̃π-A **III** (Scheme 1-2). [*19, 22*]

Scheme 1-2

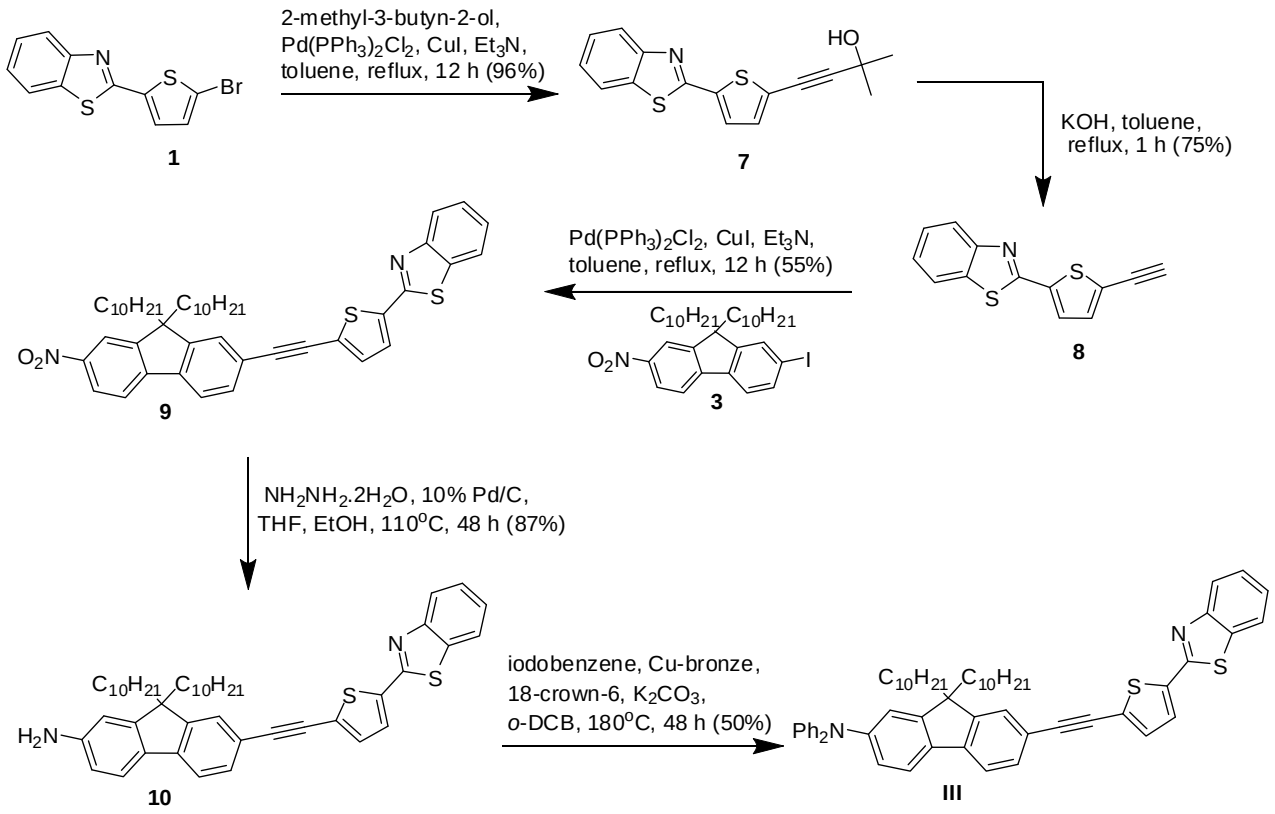

The symmetrical intermediate **11** was prepared using Sonogashira coupling between 9,9-didecyl-2,7-dibromofluorene **6** and 2-methylbut-3-yn-2-ol.[*24, 25*] After hydrolysis, the dialkyne **12** was coupled through a second Sonogashira reaction with **1**, yielding symmetrical Ãπ-A fluorenyl dye **IV** (Scheme 1-3).

Scheme 1-3

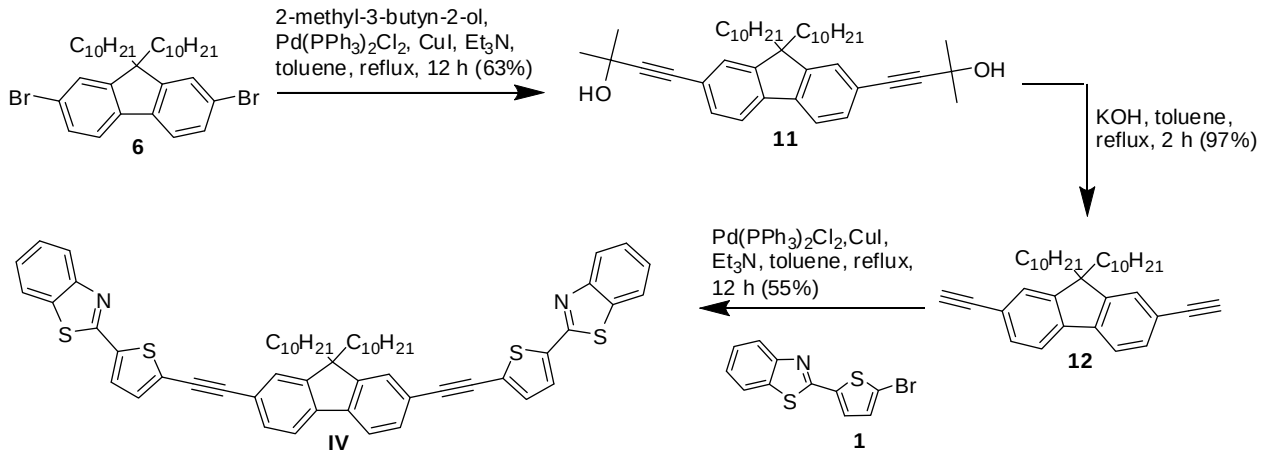

1.3.2 Linear photophysical properties

Table 1-1 summarizes the photophysical properties of the four new fluorescent dyes (**I**-**IV**). As can be seen in Figure 1-3, all molecules exhibited an intense absorption between 397-405 nm, fluorescent maximum in the range of 433-452 nm, and significant Stokes shift values in hexane (see Table 1-1). The new compounds also exhibited high fluorescence quantum yields (0.86-0.98), while a slight blue shift in the absorption maximum was observed when alkynyl moieties were incorporated in both symmetrical and asymmetrical derivatives.

Table 1-1 Photophysical characterization of new fluorene derivatives I, II, III, and IV in hexane.

Compound	λ^{abs}_{max}, nm	λ^{em}_{max}, nm	$\Delta\lambda_{St}$, nm	Φ^{1}	$\varepsilon^{max}.10^{-3}$, $M^{-1}.cm^{-1}$
I	403±1	452±1	49±2	0.86±0.05	53
II	405±1	446±1	41±2	0.98±0.05	31
III	398±1	444±1	46±2	0.92±0.05	50
IV	397±1	433±1	36±2	0.95±0.05	135

[1]Fluorescence quantum yield measured relative to 9,10-diphenylanthracene in cyclohexane.

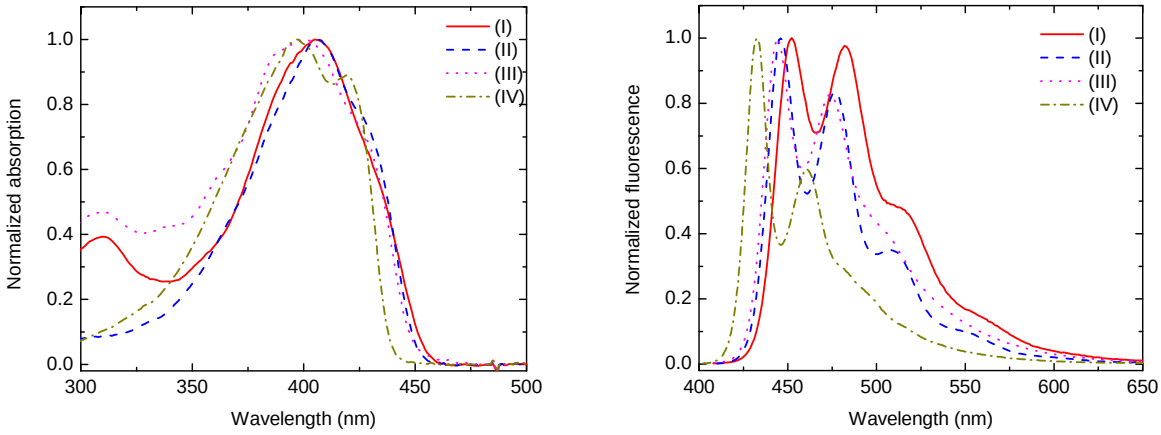

Figure 1-3 Normalized absorption (left) and fluorescence (right) spectra for **I**, **II**, **III**, and **IV** in hexane. Absorption and emission spectra were collected at room temperature using hexanes solutions with optical density of ~0.1 (approximately 10^{-6} M) without degassing the solutions. Emission was collected by exciting samples at their λ^{abs}_{max} value.

1.3.3 Nonlinear photophysical properties

Two-photon absorption (2PA) values were determined by the fluorescent method, measuring the two-photon exited fluorescence of the dyes in the range of 730-860 nm in hexane. The 2PA cross section measurements were performed with a tunable Ti:sapphire femtosecond

laser system (220 fs pulse width, 76 MHz repetition rate) pumped by a 10 W diode laser (532 nm) as the excitation source and a spectrofluorimeter with PMT detectors.

The 2PA spectra for this series of compounds are shown in Figure 1-4. Compound **I** exhibited a maximum 2PA cross section of ~248 GM at 730 nm which can be attributed to the tail of the band corresponding to the two-photon allowed $S_0 \rightarrow S_2$ transition; a second maximum of ~217 GM at 800 nm, assigned to $S_0 \rightarrow S_1$ 2PA forbidden transition, was also observed. Compound **II** exhibits a maximum 2PA cross section of ~335 GM at 730 nm. Comparing these results with our previously reported data for similar molecules that did not contain the thiophene moiety a significant increase in the 2PA cross section values was observed when the thiophenyl moiety is introduced in the fluorophore.[*9-14*]

To observe the effect of the presence of alkynyl triple bonds in the new derivatives, comparisons of compound **I** to compound **III** (D-π-A) and compound **II** to compound **IV** (A-π-A) were conducted. Compound **III** exhibited a maximum 2PA cross section of ~563 GM at 730 nm while a second maximum of ~356 GM at 800 nm was observed. Comparing these values to those obtained for compound **I**, it can be inferred that incorporating alkynyl triple bonds in these molecules results in an enhancement in the 2PA cross section for this unsymmetrical compound.

The 2PA cross section value obtained for compound **II** (~335 GM at 730 nm) can be compared with the large value obtained for compound **IV** at the same wavelength (~1093 GM). A significant increase in the 2PA cross section was observed when the number of alkynyl triple bonds was doubled.

Since the number of π electrons in these molecules is different, it is also useful to compare the ratios of 2PA cross section (δ) over the number of π-electrons (N_e) in the

chromophores (normalized cross section).[*18, 26*] When comparing **I** to **III**, it was observed that the incorporation of a triple bond in the π system resulted in a two-fold increase in the normalized cross section value (7 to 14 GM per π electron). Similarly, a three-fold increase of the normalized cross section was observed when comparing **II** and **IV** (9 and 27 GM per π electron, respectively).

In general, a considerable increase in the value of 2PA cross section was obtained when thiophene moieties were introduced in both fluorophore archetypes (D-π-A and A-π-A) studied in this series. In addition, extending the π-conjugation with alkynyl triple bond functionalities also significantly increased the 2PA for this class of molecules.

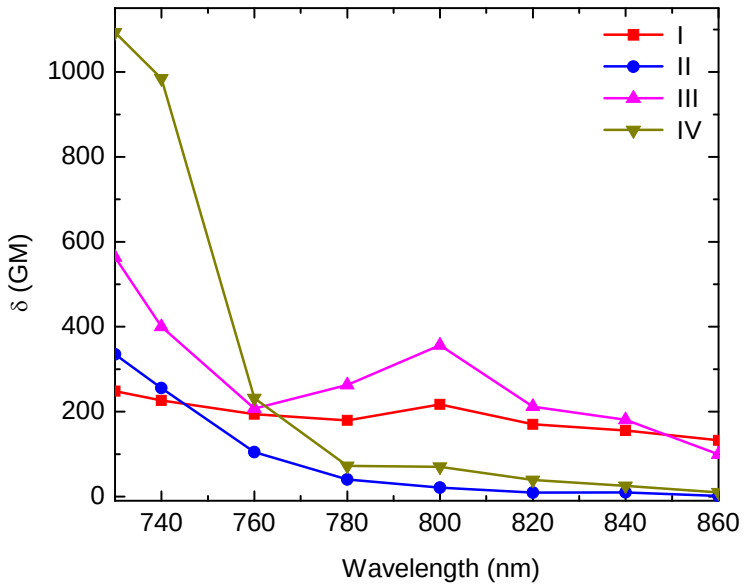

Figure 1-4 2PA spectra obtained for compounds **I-IV** in hexane. Incorporation of thiophene and alkynyl moieties resulted in an increase in the 2PA cross section values.

1.3.4 Fluorescence imaging

In order to evaluate the efficiency of these archetypes as fluorophores in 2PFM cell imaging, fluorene **I** was incubated in COS-7 and HCT 116 cell lines at different concentrations and incubation times. Probe **I** was chosen as model compound due to its relatively constant two-photon absorptivity across a useful NIR wavelength range (750-860 nm for the Ti:sapphire laser, Figure 1-4) and because it exhibited better solubility in DMSO than the more symmetrical compounds **II** and **IV** (important for cell incubation). Fluorescence micrographs indicated the distinct localization the probe in well confined areas within the cytosol in both COS-7 and HCT 116 cell lines (Figures 1-5 and 1-6). Probe **I** was incubated with a commercially available lysosomal selective dye (Lysotracker Red) and incubated for 10 min, 30 min, 50 min, 1 h 10 min, 1 h 30 min and 1 h 50 min, after incubation the cells were fixed, mounted, and imaged. Early colocalization with Lysotracker dye suggests a similar uptake mechanism for both the Lysotracker dye and probe **I**. However, longer incubation times (50 min and 1 h 50 min) indicates a difference in the progression of the probe from the endosomal vesicles to the lysosomes, where the Lysotracker dye reached the lysosomes more quickly than probe **I** (see Figure 1-5). The slower progression of probe **I** may prove useful for the study of late endosomal processes.

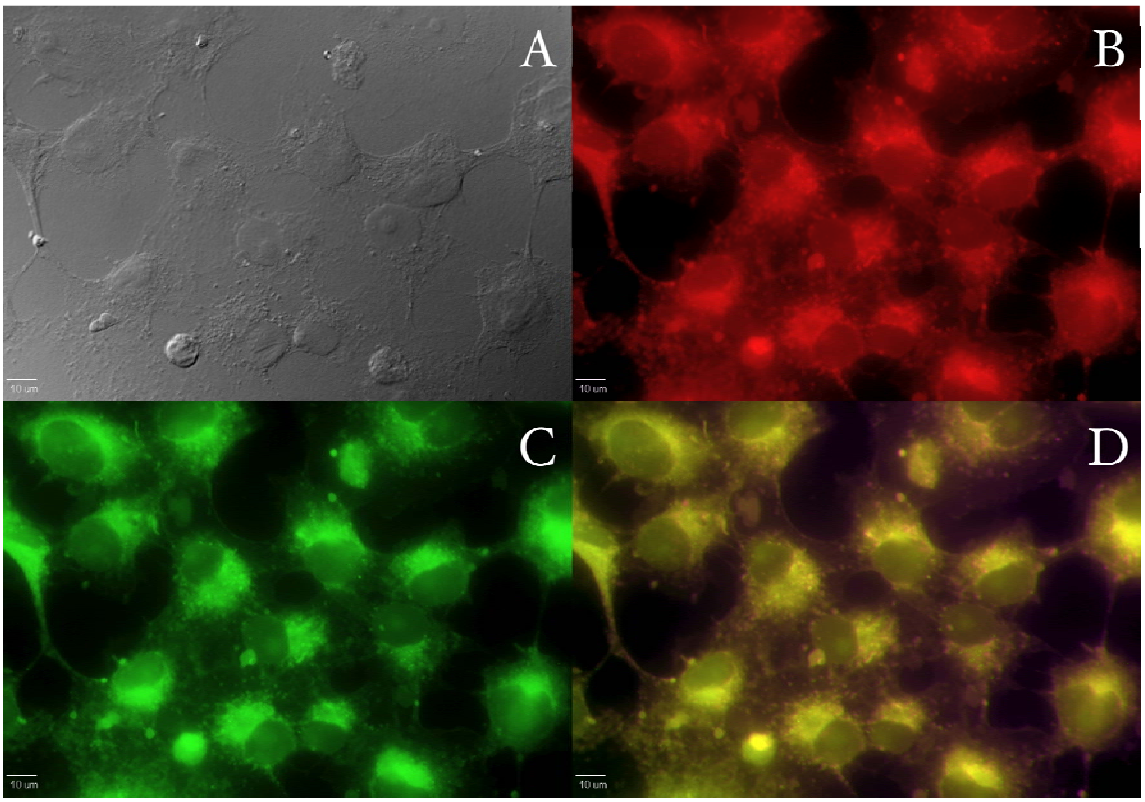

Figure 1-5 Confocal fluorescence images of COS-7 cells incubated with probe **I** (20 μM, 1 h 50 min) and Lysotracker Red (100 nM, 1 h 50 min). (A) DIC, one-photon fluorescence image showing (B) Lysotracker Red (Texas Red filter cube (Ex:562/40; DM: 593; Em:624/40)), (C) probe **I** (custom made filter cube (Ex:377/50; DM: 409; Em:525/40)) , and (D) colocalization (overlay of B and C). 10 μm scale bar.

The high contrast and good resolution observed in 2PFM images of HCT 116 cells, incubated with probe **I**, support use of the fluorenyl core as an integral part of the fluorescent probe's molecular architecture. The excellent linear and nonlinear photophysical properties points towards their potential as efficient 2PA fluorophores. The 2PFM image, shown in Figure 1-6, where the vesicles (presumably late endosomes) are clearly visualized in both 2D and 3D, is a testament of the efficacy of the 2PA fluorophore. The potential of these dyes exceeds that of imaging the endosomes, as further functionalization of the dye can be performed to modulate the

solubility properties and, more importantly, impart selectivity to other organelles or biomarkers of interest, aspects of current investigation. The new fluorenyl derivatives provide the basis for the development of fluorescent probes for 2PFM.

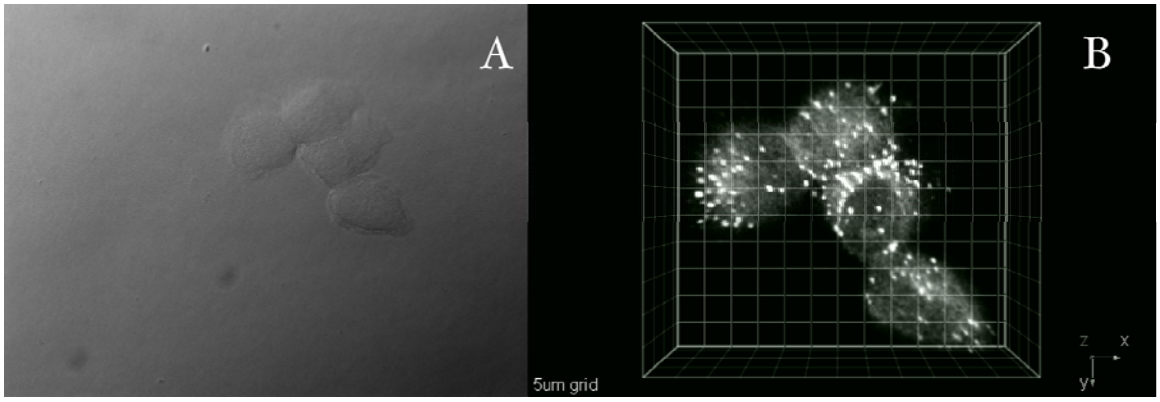

Figure 1-6 Two-photon fluorescence micrograph of HCT 116 cells incubated with probe **I** (20 μM, 1 h 50 min). A) DIC, B) 3D reconstruction from overlaid 2PFM images obtained from a modified laser scanning confocal microscopy system equipped with a broadband, tunable Ti:sapphire laser (220 fs pulse width, 76 MHz repetition rate), pumped by a 10 W frequency doubled Nd:YAG laser. (60x objective, NA= 1.35). Scale: 5 μm grid.

1.4 Experimental Section

1.4.1 Materials and methods

2-(5-Bromothiophen-2-yl)benzothiazole **1,** 9,9-didecyl-2-iodo-7-nitro-9H-fluorene **3**, and 2,7-dibromo-9,9-didecyl-9H-fluorene **6** were prepared as described in the literature.[*19, 27, 28*] All reactions were carried out under N_2. All other reagents and solvents were used as received from commercial suppliers. ^{1}H and ^{13}C NMR spectra were recorded in $CDCl_3$ on a NMR spectrometer at 500 and 125 MHz, respectively. MALDI MS analyses were performed at the University of Florida.

1.4.2 Synthetic procedures and characterization

Synthesis of 2-(5-(tributylstannyl)thiophen-2-yl)benzothiazole (2). At -78 °C 2-(5-bromothiophen-2-yl)benzothiazole **1** (200 mg, 0.67 mmol) was dissolved in dry THF (5 mL). A solution of *n*-BuLi in hexanes (0.27 mL, 2.5 M, 0.68 mmol) was added dropwise into the reaction mixture. After stirring for 1 h, $Sn(Bu)_3Cl$ (360 mg, 1.10 mmol) was added and the mixture was allowed to reach room temperature, and stirred overnight. The mixture was added to water, extracted with Et_2O twice, dried over $MgSO_4$, and purified by column chromatography using a mixture of hexanes:EtOAc (9:1) as an eluent to yield 240 mg (70%) of viscous oil. ^{1}H NMR (500 MHz, $CDCl_3$) δ8.02(d, *J*= 8.2 Hz, 1H, Ph-H), 7.82 (d, *J*= 8.0 Hz, 1H, Ph-H), 7.74 (d, *J*= 3.5 Hz, 1H, Thy-H), 7.43-7.47 (m, 1H, Ph-H), 7.31-7.35 (m, 1H, Ph-H), 7.18 (d, *J*= 3.5 Hz, 1H, Thy-H), 1.55-1.63 (m, 6H, CH_2), 1.31-1.39 (m, 6H, CH_2), 1.12-1.19 (m, 6H, CH_2), 0.90 (t, *J*= 7.34 Hz, 9H, CH_3). ^{13}C NMR (125 MHz, $CDCl_3$) δ 161.4, 153.9, 143.5, 142.4, 136.2, 134.7, 129.6, 126.2, 125.1, 122.9, 121.4, 28.9, 27.3, 13.7, 11.0. Anal. Calcd for $C_{23}H_{33}NS_2Sn$: C, 54.56; H, 6.57; N, 2.77. Found: C, 54.85; H, 6.67; N, 2.86.

Synthesis of 2-(5-(9,9-didecyl-7-nitro-9H-fluoren-2-yl)thiophen-2-yl)benzothiazole (4). 9,9-Didecyl-2-iodo-7-nitro-9H-fluorene **3** (200 mg, 0.32 mmol), 2-(5-(tributylstannyl)thiophen-2-yl)benzothiazole **2** (191 mg, 0.38 mmol), and $Pd(PPh_3)_2Cl_2$ (6 mg, 0.008 mmol) were dissolved in toluene (4 mL). The mixture was heated under reflux for 5 h. The solvent was removed under reduced pressure and the crude was purified by column chromatography using a mixture of hexanes:EtOAc (9.5:0.5) as an eluent to yield 222 mg (98%) of yellow oil that solidified upon standing (m.p. 73.2-74.9 °C). ^{1}H NMR (500 MHz, $CDCl_3$) δ 8.28 (dd, *J*= 8.3 Hz, *J*= 2.0 Hz, 1H, Ph-H), 8.22 (d, *J*= 2.0 Hz, 1H, Ph-H), 8.05 (d, *J*= 8.0 Hz,

1H, Ph-H), 7.88 (d, *J*= 7.8 Hz, 1H, Ph-H), 7.79-7.84 (m, 2H, Ph-H), 7.72-7.76 (m, 1H, Ph-H), 7.69 (d, *J*= 1.4 Hz, 1H, Ph-H), 7.66 (d, *J*= 3.7 Hz, 1H, Thy-H), 7.48-7.53 (m, 1H, Ph-H), 7.46 (d, *J*= 3.7 Hz, 1H, Thy-H), 7.37-7.42 (m, 1H, Ph-H), 2.01-2.09 (m, 4H, CH_2), 0.99-1.24 (m, 28H, CH_2), 0.82 (t, *J*= 7.0 Hz, 6H, CH_3), 0.54-0.69 (m, 4H, CH_2). ^{13}C NMR (125 MHz, $CDCl_3$) δ 161.0, 153.7, 153.4, 152.2, 147.9, 147.2, 146.8, 139.0, 136.6, 134.7, 134.4, 129.5, 126.6, 125.3, 124.40, 124.36, 123.5, 122.0, 121.9, 121.5, 120.4, 120.0, 118.3, 55.9, 40.1, 31.8, 29.8, 29.49, 29.47, 29.24, 29.19, 23.8, 22.6, 14.1. Anal. Calcd for $C_{44}H_{54}N_2O_2S_2$: C, 74.74; H, 7.70; N, 3.96. Found: C, 74.97; H, 7.85; N, 3.97.

Synthesis of 7-(5-(benzothiazol-2-yl)thiophen-2-yl)-9,9-didecyl-9H-fluoren-2-amine (5). 2-(5-(9,9-Didecyl-7-nitro-9H-fluoren-2-yl)thiophen-2-yl)benzothiazole **4** (160 mg, 0.23 mmol) and 10% Pd/C (16 mg) were dissolved in a mixture 1:1 of THF:EtOH (8 mL). $NH_2NH_2.2H_2O$ (136 mg, 2.7 mmol) was added to the mixture slowly at room temperature, and then heated to 70 °C for 20 h. The mixture was filtered though a silica plug with CH_2Cl_2, and, after removing the solvent under reduced pressure, the material was purified by column chromatography using as a solvent a mixture of hexanes:EtOAc (9:1), to yield 130 mg (84%) of dark yellow oil that was used directly since the primary amine is prone to oxidation. ^{1}H NMR (500 MHz, $CDCl_3$) δ8.04 (d, *J*= 8.0 Hz, 1H, Ph-H), 7.85 (d, *J*= 8.0 Hz, 1H, Ph-H), 7.59-7.64 (m, 2H, Ph-H, Thy-H), 7.54-7.58 (m, 2H, Ph-H), 7.45-7.51 (m, 2H, Ph-H), 7.34-7.39 (m, 2H, Ph-H, Thy-H), 6.65-6.69 (m, 2H, Ph-H), 3.80 (s, 2H, NH_2), 1.83-2.00 (m, 4H, CH_2), 0.99-1.28 (m, 28H, CH_2), 0.83 (t, *J*= 7.0 Hz, 6H, CH_3), 0.62-0.73 (m, 4H, CH_2). ^{13}C NMR (125 MHz, $CDCl_3$) δ 161.4, 153.8, 153.1, 150.7, 149.6, 146.4, 142.4, 135.0, 134.6, 131.6, 130.5, 129.5, 126.4, 125.1,

124.7, 123.0, 122.8, 121.4, 120.8, 120.1, 118.8, 114.1, 109.7, 54.9, 40.6, 31.9, 30.1, 29.6, 29.5, 29.29, 29.28, 23.8, 22.7, 14.1.

Synthesis of 7-(5-(benzothiazol-2-yl)thiophen-2-yl)-9,9-didecyl-N,N-diphenyl-9H-fluoren-2-amine (I). 7-(5-(Benzothiazol-2-yl)thiophen-2-yl)-9,9-didecyl-9H-fluoren-2-amine **5** (130 mg, 0.19 mmol), iodobenzene (157 mg, 0.77 mmol), Cu-bronze (61 mg, 0.96 mmol), 18-crown-6 (15 mg, 0.058 mmol), and K_2CO_3 (212 mg, 1.54 mmol) were combined with 1,2-dichlorobenzene (3 mL). The mixture was heated to 180 °C for 48 h. The crude product was passed through a silica plug with CH_2Cl_2. The solvent was removed under reduced pressure and the crude was purified by column chromatography on silica gel using as a solvent a mixture of hexanes:EtOAc (9:1) to yield 150 mg (94%) of yellow solid (m.p. 107.5-109.5 °C). ^{1}H NMR (500 MHz, $CDCl_3$) δ 8.04 (d, *J*= 8.0 Hz, 1H, Ph-H), 7.84 (d, *J*= 8.0 Hz, 1H, Ph-H), 7.58-7.65 (m, 4H, Ph-H, Thy-H), 7.56 (d, *J*= 8.0 Hz, 1H, Ph-H), 7.45-7.50 (m, 1H, Ph-H), 7.33-7.39 (m, 2H, Ph-H, Thy-H), 7.22-7.30 (m, 5H, Ph-H), 7.11-7.16 (m, 5H, Ph-H), 7.00-7.05 (m, 2H, Ph-H), 1.82-1.95 (m, 4H, CH_2), 1.01-1.23 (m, 28H, CH_2), 0.85 (t, *J*= 7.0 Hz, 6H, CH_3), 0.66-0.75 (m, 4H, CH_2). ^{13}C NMR (125 MHz, $CDCl_3$) δ 161.3, 153.8, 152.5, 151.6, 149.2, 147.9, 147.5, 141.6, 135.4, 134.6, 131.4, 129.6, 129.5, 129.24, 129.16, 125.2, 125.0, 124.0, 123.9, 123.4, 123.3, 122.8, 122.6, 121.5, 121.4, 120.1, 105.0, 55.2, 40.2, 31.9, 30.0, 29.6, 29.6, 29.3, 23.9, 22.7, 14.1. Anal. Calcd for $C_{56}H_{64}N_2S_2$: C, 81.11; H, 7.78; N, 3.38. Found: C, 80.81; H, 7.74; N, 3.30.

Synthesis of 2,2'-(5,5'-(9,9-didecyl-9H-fluorene-2,7-diyl)bis(thiophene-5,2-diyl))dibenzothiazole (II). 2-(5-(Tributylstannyl)thiophen-2-yl)benzothiazole **2** (460 mg, 0.90 mmol), 2,7-dibromo-9,9-didecyl-9H-fluorene **6** (250 mg, 0.41 mmol), and $Pd(PPh_3)_2Cl_2$ (7.2 mg, 0.01mmol) were dissolved in toluene. The mixture was heated under reflux for 24 h. The

solvent was removed under reduced pressure and the crude was purified by column chromatography using a mixture of hexanes:EtOAc (9.9:0.1) to yield 126 mg (35%) of yellow oil that solidified upon standing (m.p. 125.2-126.5 °C). ^{1}H NMR (500 MHz, $CDCl_3$) δ 8.05 (d, *J*= 7.76 Hz, 2H, Ph-H), 7.87 (d, *J*= 7.82 Hz, 2H, Ph-H), 7.74 (d, *J*= 7.63 Hz, 2H, Ph-H), 7.68-7.71 (m, 2H, Ph-H), 7.64-7.67 (m, 4H, Ph-H, Thy-H), 7.47-7.52 (m, 2H, Ph-H), 7.43 (d, *J*= 4.10 Hz, 2H, Thy-H), 7.36-7.40 (m, 2H, Ph-H), 2.00-2.06 (m, 4H, CH_2), 1.04-1.23 (m, 28H, CH_2), 0.80 (t, *J*= 7.04 Hz, 6H, CH_3), 0.67-0.74 (m, 4H, CH_2). ^{13}C NMR (125 MHz, $CDCl_3$) δ 161.2, 153.7, 152.1, 148.8, 140.9, 135.8, 134.7, 132.6, 129.5, 126.5, 125.2, 125.0, 123.7, 122.9, 121.5, 120.5, 120.3, 55.4, 40.4, 31.9, 30.0, 29.6, 29.5, 29.3, 29.2, 23.8, 22.6, 14.1. HRMS (MALDI) *m/z* calcd 877.3712 $[M+H]^+$, *m/z* found 877.3702 $[M+H]^+$.

Synthesis of 4-(5-(benzothiazol-2-yl)thiophen-2-yl)-2-methylbut-3-yn-2-ol (7). 2-(5-Bromothiophen-2-yl)benzothiazole **1** (200 mg, 0.67 mmol), 2-methyl-3-butyn-2-ol (170 mg, 2.02 mmol), $Pd(PPh_3)_2Cl_2$ (19 mg, 0.027 mmol), and CuI (5 mg, 0.027 mmol) were dissolved in a 1:4 mixture of Et_3N:toluene (5 mL). The mixture was heated under reflux for 12 h. After cooling to room temperature, the mixture was filtered through a celite plug, and purified by column chromatography using a mixture of hexanes:EtOAc (1:1) to yield 192 mg (96%) of pale yellow solid (m.p. 163.9-164.6 °C). ^{1}H NMR (500 MHz, $CDCl_3$) δ 8.02 (d, *J*= 8.04 Hz, 1H, Ph-H), 7.85 (d, *J*= 7.87 Hz, 1H, Ph-H), 7.50 (d, *J*= 3.95 Hz, 1H, Thy-H), 7.46-7.49 (m, 1H, Ph-H), 7.35-7.40 (m, 1H, Ph-H), 7.18 (d, *J*= 3.95 Hz, 1H, Thy-H), 2.11 (s, 1H, -OH), 1.64 (s, 6H, CH_3). ^{13}C NMR (125 MHz, $CDCl_3$) δ 160.4, 153.6, 137.9, 134.7, 132.9, 128.3, 126.4, 125.4, 123.1, 121.5, 121.4, 100.2, 75.2, 65.8, 31.3. Anal. Calcd for $C_{16}H_{13}NOS_2$: C, 64.18; H, 4.38; N, 4.68. Found: C, 64.10; H, 4.33; N, 4.64.

Synthesis of 2-(5-ethynylthiophen-2-yl)benzothiazole (8). 4-(5-(Benzothiazol-2-yl)thiophen-2-yl)-2-methylbut-3-yn-2-ol **7** (300 mg, 1.0 mmol) and KOH (300 mg, 5.3 mmol) were heated under reflux in toluene for 1 h. The mixture was filtered, then purified by column chromatography eluting with hexanes to yield 180 mg (75%) of a white solid (m.p. 117.3-118.3 °C). ^{1}H NMR (500 MHz, $CDCl_3$) δ 8.03 (d, *J*= 8.21Hz, 1H, Ph-H), 7.86 (d, *J*= 8.21Hz, 1H, Ph-H), 7.51 (d, *J*= 3.94 Hz, 1H, Thy-H), 7.47-7.50 (m, 1H, Ph-H), 7.37-7.42 (m, 1H, Ph-H), 7.28 (d, *J*= 3.94 Hz, 1H, Thy-H), 3.50 (s, 1H, C≡C-H). ^{13}C NMR (125 MHz, $CDCl_3$) δ ı60.2, 153.6, 138.5, 134.8, 133.9, 133.7, 127.8, 126.5, 125.4, 123.2, 121.6, 84.0, 76.5. Anal. Calcd for $C_{13}H_7NS_2$: C, 64.70; H, 2.92; N, 5.80. Found: C, 64.64; H, 2.91; N, 5.75.

Synthesis of 2-(5-((9,9-didecyl-7-nitro-9H-fluoren-2-yl)ethynyl)thiophen-2-yl)benzothiazole (9). 2-(5-Ethynylthiophen-2-yl)benzothiazole **8** (180 mg, 0.75 mmol), 9,9-didecyl-2-iodo-7-nitro-9H-fluorene **3** (460 mg, 0.75 mmol), $Pd(PPh_3)_2Cl_2$ (20 mg, 0.03 mmol), and CuI (5.6 mg, 0.03 mmol),were dissolved in a 1:4 mixture of Et_3N:toluene (5 mL). The mixture was heated under reflux for 12 h. After cooling to room temperature, the mixture was filtered through a celite plug and purified by column chromatography eluting with a mixture of hexanes:EtOAc (9:1), and then recrystallized from hexane to yield 300 mg (55%) of yellow solid (m.p. 142.3-143.6 °C). ^{1}H NMR (500 MHz, $CDCl_3$) δ 8.28 (dd, *J*= 8.40 Hz, *J*= 2.18 Hz, 1H, Ph-H), 8.21 (d, *J*= 2.05 Hz, 1H, Ph-H), 8.05 (d, *J*= 7.74 Hz, 1H, Ph-H), 7.88 (d, *J*= 7.74 Hz, 1H, Ph-H), 7.77-7.82 (m, 2H, Ph-H), 7.55-7.61 (m, 3H, Ph-H, Thy-H), 7.48-7.52 (m, 1H, Ph-H), 7.39-7.42 (m, 1H, Ph-H), 7.33 (d, *J*= 4.08 Hz, 1H, Thy-H), 2.01-2.08 (m, 4H, CH_2), 0.99-1.29 (m, 28H, CH_2), 0.84 (t, *J*= 6.93 Hz, 6H, CH_3), 0.50-0.64 (m, 4H, CH_2). ^{13}C NMR (125 MHz, $CDCl_3$) δ ı60.3, 153.7, 152.5, 152.3, 147.4, 146.6, 139.3, 138.4, 134.8, 132.8, 131.2, 128.5,

128.3, 126.7, 126.2, 126.0, 123.2, 123.1, 121.6, 121.5, 120.2, 118.3, 105.0, 96.3, 83.8, 55.9, 40.0, 31.9, 29.9, 29.51, 29.48, 29.2, 23.8, 22.6, 14.14, 14.06. Anal. Calcd for $C_{46}H_{54}N_2O_2S_2$: C, 75.57; H, 7.45; N, 3.83. Found: C, 75.69; H, 7.47; N, 3.85.

Synthesis of 7-((5-(benzothiazol-2-yl)thiophen-2-yl)ethynyl)-9,9-didecyl-9H-fluoren-2-amine (10). 2-(5-((9,9-Didecyl-7-nitro-9H-fluoren-2-yl)ethynyl)thiophen-2-yl)benzothiazole **9** (180 mg, 0.24 mmol) and 10% Pd/C (18 mg) were dissolved in a 1:1 mixture of THF:EtOH (4 mL). $NH_2NH_2.2H_2O$ (146 mg, 2.8 mmol) was added to the mixture dropwise at room temperature, followed by heating to 110 °C for 48 h. The mixture was filtered though a silica plug with CH_2Cl_2, and, after removing the solvent under reduced pressure, the material was purified by column chromatography using a mixture of hexanes:EtOAc (9:1) as eluent to yield 150 mg (87%) of dark yellow oil that was used immediately due to the oxidative lability of the primary amine. ^{1}H NMR (500 MHz, $CDCl_3$) δ 8.03 (d, *J*= 7.45 Hz, 1H, Ph-H), 7.86 (d, *J*= 7.67 Hz, 1H, Ph-H), 7.56 (d, *J*= 3.99 Hz, 1H, Thy-H), 7.52 (d, *J*= 7.75 Hz, 1H, Ph-H), 7.46-7.50 (m, 3H, Ph-H), 7.43-7.44 (m, 1H, Ph-H), 7.36-7.40 (m, 1H, Ph-H), 7.27 (d, *J*= 3.99 Hz, 1H, Thy-H), 6.65-6.68 (m, 2H, Ph-H), 3.83 (s, 2H, NH_2), 1.84-1.97 (m, 4H, CH_2), 1.03-1.27 (m, 28H, CH_2), 0.85 (t, *J*= 7.16 Hz, 6H, CH_3), 0.56-0.68 (m, 4H, CH_2). ^{13}C NMR (125 MHz, $CDCl_3$) δ 161.0, 160.6, 153.8, 153.1, 150.2, 149.9, 146.6, 146.0, 144.4, 142.7, 141.6, 136.1, 134.6, 133.7, 132.7, 132.2, 131.5, 128.4, 122.9, 121.6, 118.5, 114.0, 109.8, 97.7, 81.9, 54.9, 40.5, 31.9, 30.2, 29.7, 29.6, 29.4, 29.3, 23.9, 22.7, 14.2.

Synthesis of 7-((5-(benzothiazol-2-yl)thiophen-2-yl)ethynyl)-9,9-didecyl-N,N-diphenyl-9H-fluoren-2-amine (III). 7-((5-(Benzothiazol-2-yl)thiophen-2-yl)ethynyl)-9,9-didecyl-9H-fluoren-2-amine **10**, (0.135 mg, 0.19 mmol), iodobenzene (157 mg, 0.77 mmol), Cu-

bronze (61 mg, 0.96 mmol), 18-crown-6 (15 mg, 0.058 mmol), and K_2CO_3 (212 mg, 1.54 mmol) were combined with, 1,2-dichlorobenzene (3 mL). The mixture was heated at 180 °C for 48 h. The crude product was passed through a silica plug with CH_2Cl_2. The solvent was removed under reduced pressure, and the crude product was purified by column chromatography on silica gel using a mixture of hexanes:EtOAc (9.5:0.5) as eluent to yield 81 mg (50%) of yellow viscous oil. ^{1}H NMR (500 MHz, $CDCl_3$) δ 8.04 (d, *J*= 8.11 Hz, 1H, Ph-H), 7.85 (d, *J*= 8.11 Hz, 1H, Ph-H), 7.59 (d, *J*= 7.90 Hz, 1H, Ph-H), 7.56 (d, , *J*= 3.72 Hz, 1H, Thy-H), 7.45-7.52 (m, 4H, Ph-H), 7.35-7.39 (m, 1H, Ph-H), 7.24-7.30 (m, 5H, Ph-H), 7.10-7.15 (m, 5H, Phe-H), 7.00-7.05 (m, 3H, Phe-H), 1.80-1.92 (m, 4H, CH_2), 1.03-1.28 (m, 28H, CH_2), 0.85 (t, *J*= 7.14 Hz, 6H, CH_3), 0.62-0.69 (m, 4H, CH_2). ^{13}C NMR (125 MHz, $CDCl_3$) δ 160.5, 153.7, 152.6, 150.8, 147.8, 147.8, 141.9, 137.7, 135.2, 134.7, 132.4, 130.8, 129.2, 128.4, 127.4, 126.6, 125.7, 125.4, 124.0, 123.3, 123.01 122.7, 121.5, 120.9, 119.6, 119.1, 118.9, 97.4, 82.2, 55.2, 40.2, 31.9, 30.0, 29.6, 29.6, 29.4, 29.3, 23.9, 22.7, 14.1. Anal. Calcd for $C_{58}H_{64}N_2S_2$: C, 81.64; H, 7.56; N, 3.28. Found: C, 81.63; H, 7.62; N, 3.05.

Synthesis of 4,4'-(9,9-didecyl-9H-fluorene-2,7-diyl)bis(2-methylbut-3-yn-2-ol) (11). 2,7-Dibromo-9,9-didecyl-9H-fluorene **6** (1.0 g, 1.65 mmol), 2-methyl-3-butyn-2-ol (0.83 g, 9.92 mmol), $Pd(PPh_3)_2Cl_2$ (95 mg, 0.135 mmol), and CuI (25 mg, 0.13 mmol) were dissolved in a 1:4 mixture of Et_3N:toluene (15 mL). The mixture was heated under reflux for 12 h. After it was cooled down, the mixture was filtered through a celite plug and purified by column chromatography using hexanes as a eluent, followed by a mixture of hexanes:EtOAc (10:1) to yield 0.64 g (63%) of white solid (m.p. 89.0-89.9 °C). ^{1}H NMR (500 MHz, $CDCl_3$) δ 7.58-7.61 (m, 2H, Ph-H), 7.35-7.41 (m, 4H, Ph-H), 2.05 (s, 2H, -OH), 1.89-1.96 (m, 4H, CH_2), 1.63-1.68

(s, 12H, CH_3), 0.98-1.27 (m, 28H, CH_2), 0.85 (t, *J*= 6.49 Hz, 6H, CH_3), 0.50-0.58 (m, 4H, CH_2). ^{13}C NMR (125 MHz, $CDCl_3$) δ 150.9, 140.6, 130.7, 126.0, 121.4, 119.8, 93.9, 83.0, 65.7, 55.2, 40.4, 31.9, 31.6, 30.0, 29.6, 29.5, 29.3, 29.2, 23.7, 22.6, 14.1. Anal. Calcd for $C_{43}H_{62}O_2$: C, 84.53; H, 10.23. Found: C, 84.46; H, 10.25.

Synthesis of 9,9-didecyl-2,7-diethynyl-9H-fluorene (12). 4,4'-(9,9-Didecyl-9H-fluorene-2,7-diyl)bis(2-methylbut-3-yn-2-ol) **11** (450 mg, 0.736 mmol) and KOH (206 mg, 3.68 mmol) were heated under reflux in toluene for 2 h. The mixture was filtered, then purified by column chromatography using hexanes to yield 350 mg (97%) of light yellow oil. ^1H NMR (500 MHz, $CDCl_3$) δ 7.63 (dd, *J*= 7.73 Hz, *J*= 0.65 Hz, 2H, Ph-H), 7.48 (dd, *J*= 7.73 Hz, *J*= 1.42 Hz, 2H, Ph-H), 7.45-7.46 (m, 2H, Ph-H), 3.15 (s, 2H, C≡C-H), 1.90-1.96 (m, 4H, CH_2), 0.99-1.25 (m, 28H, CH_2), 0.85 (t, *J*= 7.0 Hz, 6H, CH_3), 0.52-0.58 (m, 4H, CH_2). ^{13}C NMR (125 MHz, $CDCl_3$) δ 151.0, 141.0, 131.2, 126.5, 120.8, 119.95, 84.5, 77.3, 55.2, 40.2, 31.9, 29.9, 29.5, 29.5, 29.2, 23.7, 22.7, 14.1. Anal. Calcd for $C_{37}H_{50}$: C, 89.81; H, 10.19. Found: C, 89.79; H, 10.24.

Synthesis of 2,2'-(5,5'-(9,9-didecyl-9H-fluorene-2,7-diyl)bis(ethyne-2,1-diyl)bis(thiophene-5,2-diyl))dibenzothiazole (IV). 9,9-Didecyl-2,7-diethynyl-9H-fluorene **12** (300 mg, 0.61 mmol), 2-(5-bromothiophen-2-yl)benzothiazole **1** (377 mg, 1.27 mmol), $Pd(PPh_3)_2Cl_2$ (34 mg, 0.05 mmol), and CuI (10 mg, 0.05 mmol) were dissolved in a 1:4 mixture of Et_3N:toluene (5 mL). The mixture was heated under reflux for 12 h. After it was cooled down, the mixture was filtered through a celite plug, and purified by column chromatography using a mixture of hexanes:EtOAc (10:1) as eluent to yield 310 mg (55%) of yellow solid (m.p. 74.0-75.5 °C). ^1H NMR (500 MHz, $CDCl_3$) δ 8.04 (dd, *J*= 8.09 Hz, *J*= 0.54 Hz, 2H, Ph-H), 7.87 (dd, *J*= 8.04 Hz, *J*= 0.53 Hz, 2H, Ph-H), 7.70 (d, *J*= 7.83 Hz, 2H, Ph-H), 7.57 (d, *J*= 3.89 Hz,

2H, Thy-H), 7.54-7.56 (m, 2H, Ph-H), 7.52-7.53 (m, 2H, Ph-H), 7.48-7.51 (m, 2H, Ph-H), 7.37-7.41 (m, 2H, Ph-H), 7.31 (d, *J*= 3.89 Hz, 2H, Thy-H), 1.97-2.04 (m, 4H, CH_2), 1.04-1.23 (m, 28H, CH_2), 0.84 (t, *J*= 6.96 Hz, 6H, CH_3), 0.58-0.65 (m, 4H, CH_2). ^{13}C NMR (125 MHz, $CDCl_3$) δ 160.5, 153.7, 151.3, 141.1, 138.0, 134.7, 132.6, 130.8, 128.4, 127.1, 126.6, 125.9, 125.5, 123.1, 121.5, 121.3, 120.2, 97.0, 82.9, 55.4, 40.3, 31.9, 30.0, 29.6, 29.5, 29.3, 29.3, 23.8, 22.7, 14.1. Anal. Calcd for $C_{59}H_{60}N_2S_4$: C, 76.58; H, 6.54; N, 3.03. Found: C, 76.79; H, 6.75; N, 2.79.

1.4.3 Measurements

Absorption spectra were recorded with an UV–visible spectrophotometer. Steady-state fluorescence spectra were measured with a spectrofluorimeter in the photon counting regime of the PMT using an L-format configuration. The fluorescence spectra were corrected for the spectral dependence of the PMT. All measurements were performed in hexane at room temperature in 1 cm quartz cuvettes, with dye concentrations on the order of 10^{-6} M. Fluorescence quantum yields were determined relative to 9, 10-diphenylanthracene in cyclohexane as a standard.[*29*]

Two-photon absorption (2PA) cross sections of the final compounds were determined by the two-photon induced fluorescence method.[*30*] In this method, the sample is excited simultaneously by two photons of low energy, resulting in fluorescence emission. The number of photons emitted can be measured by a PMT, and the latter related to the numeric value of the 2PA cross section relative to a reference.

The 2PA cross section measurements were performed with a tunable 10 W pumped Ti:sapphire femtosecond laser system (220 fs pulse width, 76 MHz repetition rate) as the excitation source and a spectrofluorimeter with PMT detectors (Figure 1-7).

The linear polarization and the power of the laser light were adjusted by the optical attenuator (OA), which consists of two Glan-Thompsom polarizers and a half-waveplate. The laser beam was divided with a beam splitter (BS) from where the transmitted beam was expanded with a bean expander (BE) and passed through the sample (S) after being focused with an objective lens (10X). The reflected beam was sent to the power meter (PM) to monitor the variation of the incident power on the sample (S). The two-photon emission (2PE) light was focused by the lens (L) and the upconverted fluorescence was collected by the PMT of the spectrofluorimeter used for fluorescence quantum yield methods at a direction perpendicular to the pump beam. During these measurements this PMT was set to analog mode. A computer was used to record and process all the experimental data. The numerical estimation of the 2PA cross section δ was performed by comparison with a known reference by using equation (i):

$$\delta = \delta_R \frac{\langle I \rangle}{\langle I_R \rangle} \frac{C_R}{C} \frac{n^2}{n_R{}^2} \frac{Q_R}{Q} \frac{P_R{}^2}{P^2} \qquad \text{(i)}$$

where the subscript *R* refers to the reference, $<I>$ is the integrated intensity from two-photon excitation, *C* is the concentration, *n* is the refractive index, *Q* is the quantum yield and *P* is the incident power on the sample.

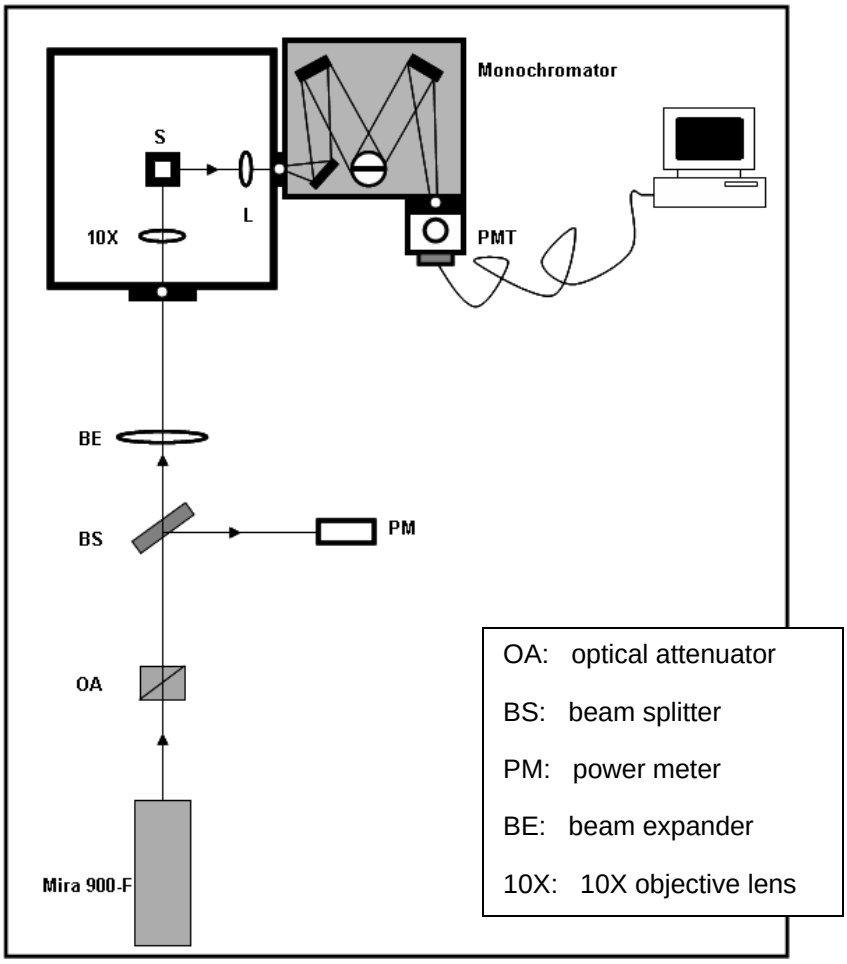

Figure 1-7 Experimental setup used to measure the 2PA cross sections of the dyes.

1.4.4 Cell culture and incubation

COS-7 and HCT 116 cell were cultured in DMEM, supplemented with 10% FBS, and 1% penicillin, and 1% streptomycin at 37 °C, under 5% CO_2 environment. N° 1 round 12 mm coverslips were treated with poly-D-lysine to improve cell adhesion, and washed (3x) with PBS buffer solution. The treated cover slips were placed in 24-well plates, seeded with 80,000 cells/well, and incubated at the same conditions as indicated above until 75-85% confluency was reached on the coverslips. From a 4.10 x 10^{-4} M stock solution of dye **I** a series of 0.1, 1, 10, 20,

and 50 μM solutions in DMSO were prepared with all solutions also containing 75 nM of Lysotracker Red. These solutions were used to incubate the cells for 10 min to 3h. The dye solutions were extracted and the coverslipped cells were washed abundantly with PBS (4x).

1.4.5 Cell fixing and mounting

Cells were fixed with 3.7% solution of paraformaldehyde in pH=7.4 PBS buffer for 10 min. The fixing agent was extracted and washed (2x) with PBS. To reduce autofluorescence, a fresh solution of $NaBH_4$ (1 mg/mL) in pH=8 PBS buffer was used to treat the fixed cells (2x). The coverslipped cells were then washed with buffer PBS (2x) and mounted on microscope slides using an antifade mounting media.

1.4.6 Confocal one-photon fluorescence imaging

One-photon (conventional) fluorescence microscopy images were recorded on an inverted confocal microscope equipped with a EM-CCD digital camera. One-photon confocal fluorescence images of the fixed cells were taken using a custom made filter cube (Ex:377/50; DM: 409; Em:525/40) and a Texas Red filter cube (Ex:562/40; DM: 593; Em:624/40) for probe **I** and Lysotracker Red, respectively.

1.4.7 Two-photon upconverted fluorescence imaging

Two-photon fluorescence microscopy (2PFM) imaging was performed on a modified laser scanning confocal microscopy system equipped with a broadband, tunable Ti:sapphire laser (220 fs pulse width, 76 MHz repetition rate), pumped by a 10 W frequency doubled Nd:YAG laser. The Ti:sapphire laser, tuned 700 nm and modelocked, was used as the two-photon excitation source. Two-photon induced fluorescence was collected by a 60x microscope objective (UPLANSAPO 60x, N.A.=1.35). A high transmittance (>95%) short-pass filter (cutoff

685 nm) was placed in front of the PMT detector within the scanhead in order to filter off background radiation from the laser source (700 nm).

1.5 Conclusions

Efficient synthetic routes were developed to prepare four new fluorescent compounds containing functionalities such as thiophene and alkynyl moieties on a fluorene core, affording systematic variation of molecular symmetry and extent of conjugation. Comprehensive characterization of the new compounds revealed excellent linear and nonlinear photophysical properties, such as high fluorescent quantum yields (0.86-0.98) and high two-photon absorptivity (220-1060 GM). Incorporation of thiophene and alkynyl moieties resulted in an increase in the 2PA cross section values. Probe **I** proved to have low cytotoxocity when incubated with COS-7 and HCT 116 cells, exhibiting endosomal selectivity, as evidenced by one-photon fluorescence imaging and colocalization studies. The advantageous properties of probe **I** facilitated 2PFM endosomal imaging, with the 2PFM images providing much better resolution, allowing the visualization of individual endosomes. Due to their linear and nonlinear photophysical properties, these new fluorenyl derivatives should find use in a number of emerging photonics applications such as targeted two-photon fluorescence imaging and two-photon based optical data storage.

CHAPTER 2. TWO-PHOTON LYSOSOMAL BIOIMAGING WITH MICELLE-ENCAPSULATED 2PA FLUORESCENT DYE

Carolina D. Andrade, Ciceron O. Yanez, Maher A. Qaddoura, Xuhua Wang, Curtesa L. Arnett, Sabrina A. Coombs, Jin Yu, Rania Bassiouni, Mykhailo V. Bondar and Kevin D. Belfield. *Journal of Fluorescence*. Accepted on November **2010**.

2.1 Abstract

We report two-photon fluorescence microscopy (2PFM) imaging and *in vitro* cell viability of a new, efficient, lysosome-selective system based on a two-photon absorbing (2PA) fluorescent probe (**IV**) encapsulated in micelles formed with Pluronic® F-127. Preparation of probe **IV** was accomplished via microwave-assisted synthesis, resulting in improved yields and reduced reaction times. Photophysical characterization revealed notable 2PA efficiency of this probe.

Keywords: Fluorescent dyes, pluronics, multiphoton absorption, bioimaging, fluorescence microscopy, lysosomes.

2.2 Introduction

The advantages that 2PA materials offer over their one-photon absorbing counterparts relies on the very nature of the nonlinear absorption process, where two photons are absorbed simultaneously, offering increased 3D resolution as a result of a significantly confined excitation volume.[*31*] This inherent advantage has increased the interest of the scientific community in multiphoton imaging over the last decades, which has spawned the development of novel multiphoton absorbing materials and their applications. The variety of applications of these materials is witnessed in a number of fields, including microscopy,[*1, 8*] lasing,[*15*] and optical data storage.[*4, 32, 33*] In the field of bioimaging, there has been increased attention in labeling

different cell components or certain cells within a specific type of tissue by direct and indirect immunostaining with efficient 2PA fluorescent dyes.[*34, 35*]

The lysosomes and their enzymes are the centerpiece of the digestive cycle of the cell and, as such, are key in many cellular processes such as apoptosis and phagocytosis. Lysosomal activity has been associated with an array of conditions including cancer,[*36*] aging,[*37*] autophagy,[*36, 38*] and apoptotic and necrotic cell deaths,[*36, 39*] but the specific role of the lysosomes in such processes remains a matter of some speculation. Furthermore, the less common yet still severe conditions classified as Lysosomal Storage Disorders have very serious clinical manifestations, such as mental retardation, progressive cognitive decline, and behavioral inappropriateness.[*40*] Thus, methods and materials to that can specifically probe lysosomes are of considerable interest.

The advent of fluorescence microscopy techniques that surpass the diffraction limit, including 2PFM,[*1*] stimulated emission depletion (STED) microscopy,[*41, 42*] photo-activated localization microscopy (PALM),[*43*] and interferometric photo-activated localization microscopy (iPALM),[*44*] have set the foundations for unforeseen resolution, and will undoubtedly lead to more exciting discoveries, especially when these techniques are combined to exploit superresolution to its very limit.[*30*] Even though there are commercially available alternatives for imaging the lysosomes by fluorescence, very few of the dyes or proteins employed possess the photostability and high two-photon absorption cross sections to be *efficient* 2PA probes, particularly for prolonged imaging.

Pluronic® F-127 has been used in drug delivery applications to enhance the solubility of hydrophobic substances such as anticancer drugs.[*45, 46*] Pluronic® micelles are known

to be uptaken by MDCK cells by means of clathrin-mediated endocytosis when present above the critical micelle concentration (CMC).[*47-49*] Probe **IV** was encapsulated in Pluronic® F-127, with the purpose of it being endocytosed, and subsequently tracked through the vesicle maturation process (Figure 2-1). After the micelles are endocytosed they can either reach full endosomal maturation, reaching the lysosomes, or follow exocytosis before attaining the endolysosomal stage.

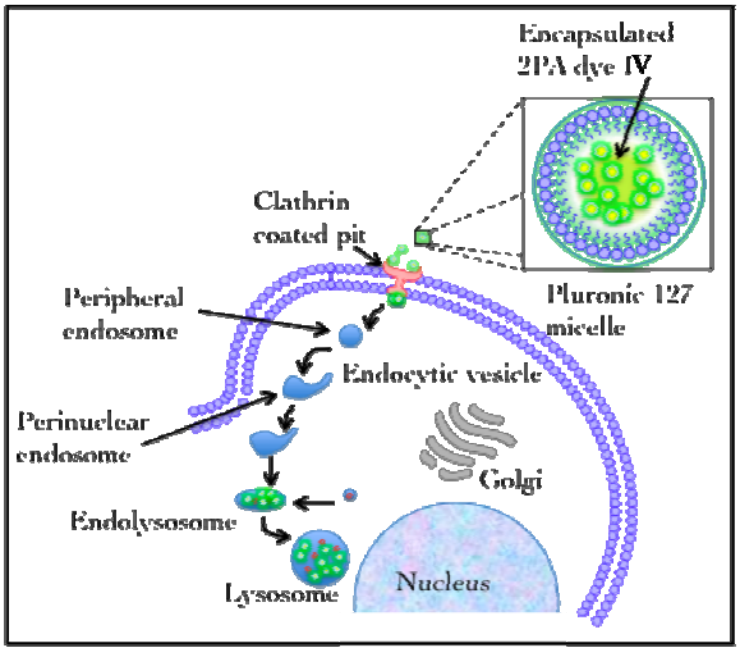

Figure 2-1 Depiction of Pluronic® F-127-encapsulated 2PA probe **IV** being uptaken into an HCT 116 cell by means of clatherin-mediated endocytosis. After 3 h of incubation, **IV** can be found in lysosomes.

2.3 Results and Discussion

2.3.1 Synthesis of new fluorescent probes

The strategy for the synthesis of probe **IV** is outlined in Scheme 2-1. Thiophene **1** underwent Sonogashira coupling with a protected terminal alkyne to yield intermediate **7** (12

h). The microwave-assisted equivalent of this reaction reached completion 360 times faster.[*14*] Deprotection of the triple bond in intermediate **7** was also performed under microwave irradiation, generating **8** in higher yield and shorter reaction time when compared to conventional thermal deprotection. A second Sonogashira coupling, between **8** and **6**, was required to generate probe **IV**; this microwave-assisted reaction afforded the product in slightly higher yield and shorter time (20 times faster) than conventional heating.

Scheme 2-1

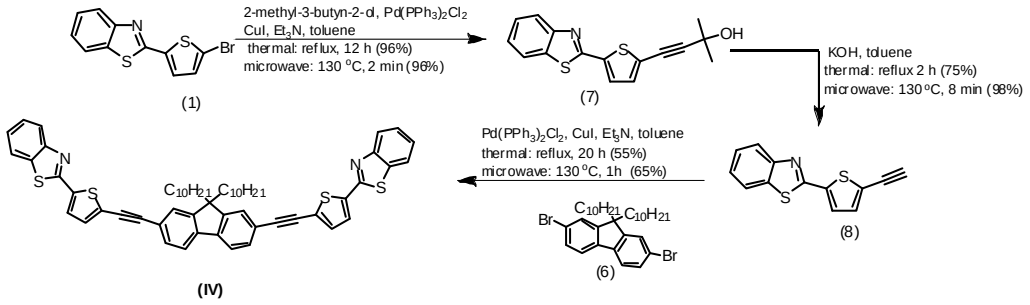

2.3.2 Linear photophysical properties

The hydrophobic character of probe **IV** made it an ideal candidate for encapsulation in Pluronic® F-127. Steady state, linear absorption, and fluorescence properties of solutions of **IV** in hexane and with the Pluronic® surfactant in PBS buffer were measured (Figure 2-2). Absorption maxima at around 400 nm were observed for **IV** in both solvent systems. The emission maximum shifted towards longer wavelengths when **IV** was prepared in Pluronic® solution as a consequence of the increase in polarity of the media. In hexane, the fluorescence quantum yield of **IV** was 0.95, while nonradiative decay led to a reduction to one third of this value when the dye was dissolved in the aqueous Pluronic® solution (see Table 2-1).

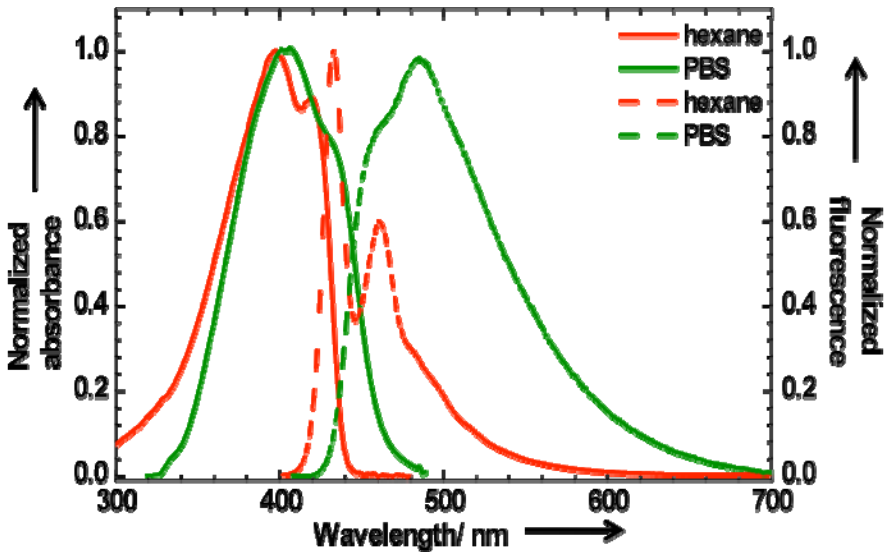

Figure 2-2 Absorption (solid) and emission (broken) spectra of 2PA probe **IV** in hexane (red) and encapsulated in Pluronic® F-127 (PBS solution, green).

Table 2-1 Linear optical properties of probe **IV.**

Compound	λ^{abs}_{max} (nm)	λ^{em}_{max} (nm)	Φ^{1}
IV in hexane	397±1	433±1	0.95±0.05
IV in Pluronic®F-127 /PBS	403±1	485±1	0.35±0.05

[1] Fluorescence quantum yield, Φ, measured relative to 9,10-diphenylanthracene in cyclohexane.

2.3.3 Nonlinear photophysical properties

Two-photon absorption cross section values of solutions of **IV** in cyclohexane, DMSO, and 5 wt% aqueous DMSO were determined using the two-photon fluorescence method from 640 to 920 nm, a convenient wavelength range for 2PFM imaging (Figure 2-3). 2PA at these wavelengths was consistent for symmetrical 2PA dyes. Since adherence to the selection rules are typically more stringent for symmetrical dyes, high cross 2PA sections at twice the linear λ_{max} are seldom observed for this type of compound (Figure 2-2).[*29, 50*] The highest 2PA cross section values were observed at 680 nm for all solvents used, which is likely the maximum of the lower energy two-photon allowed transition. Even though the lowest 2PA cross sections were observed in the aqueous mixture, a value of 250 GM at ca. 700 nm is quite good. This and the fluorescence quantum yield of **IV** proved favorable for 2PFM imaging.

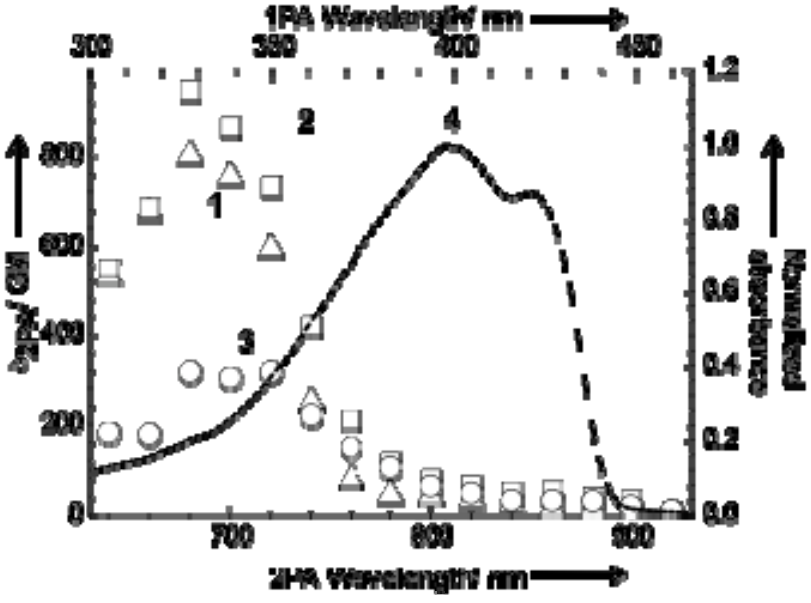

Figure 2-3 2PA spectra of 2PA probe **IV** in cyclohexane (1), DMSO (2) and 5 wt% aqueous DMSO (3). Normalized one-photon absorption spectrum of IV in cyclohexane (4).

2.3.4 Fluorescence imaging

HCT 116 cells were incubated in Pluronic® F-127 encapsulated 2PA probe **IV**. A series of 0.1, 1, 10, 25, and 50 μM solutions of the micelle-encapsulated probe in culture media was prepared. Another identical series, also containing 75 nM of Lysotracker Red (Invitrogen), was prepared for colocalization studies to determine whether the micelle-encapsulated probe reached the lysosomes. HCT 116 cells were incubated in these solutions for 3 h. After fixation, the one-photon fluorescence images exhibited good agreement between the Lysotacker Red (Figure 2-4B) and the Pluronic® F-127-encapsulated 2PA probe **IV** (Figure 2-4C), as shown by the overlay of micrographs of these two channels (Figure 2-4D). The excellent colocalization agreement was further confirmed by the calculation of the colocalization coefficient which was determined to be ≅ 0.91.[*51*]

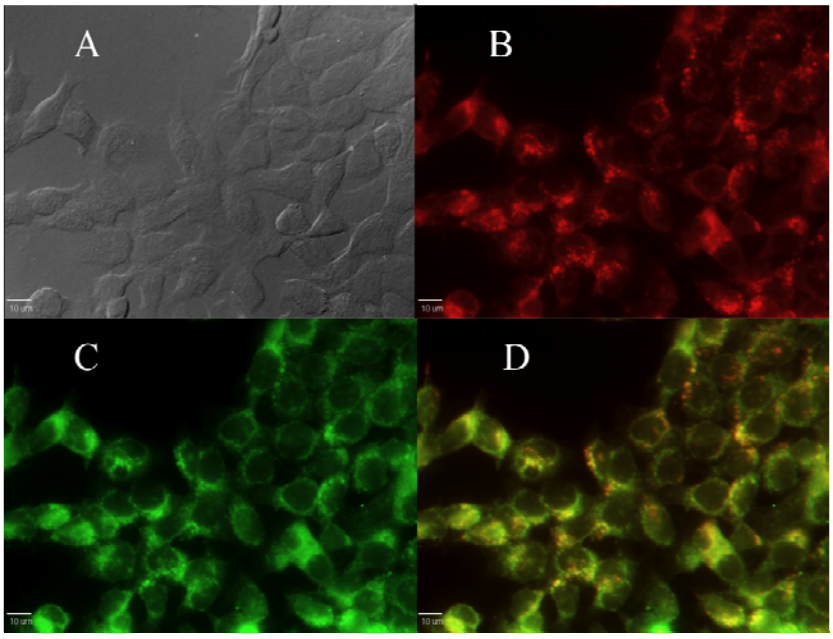

Figure 2-4 Confocal fluorescence images of HCT 116 cells incubated with 2PA probe **IV** encapsulated in Pluronic® F-127 (25 μM, 3 h) and Lysotracker Red (100 nM, 3 h). DIC (A), one-photon fluorescence image showing Lysotracker Red (B) and 2PA probe **IV** encapsulated in Pluronic® F-127 micelles (C). (D) is colocalization (overlay of B and C). 10 μm scale bar.

Cell viability assays were conducted with CellTiter® 96 AQ (Promega). In this assay, the ability of the cell to metabolize MTS to formazan was evaluated. Formazan has an absorption (λ_{max} ≈490 nm) that is significantly red-shifted with respect to MTS. Hence, by interrogation at 490 nm, one can approximate the proportion of cells that are metabolically active or viable. To evaluate the effect of the micelle-encapsulated probe **IV**, COS-7 and HCT 116 cells were seeded (5 x 10^3 cells/well) in a 96 well plate and incubated for 24 h in DMEM (Invitrogen). The cells were incubated with 60, 50, 25, 10, and 1 μM solutions of Pluronic® F-127-encapsulated probe **IV** for 24 h. The results indicated that these concentrations did not significantly affect either cell line. Even at concentrations above those used for imaging, the cell viability is practically 100% (see Figure 2-5), compelling data to support the use of this probe for *in vivo* two-photon fluorescence imaging.

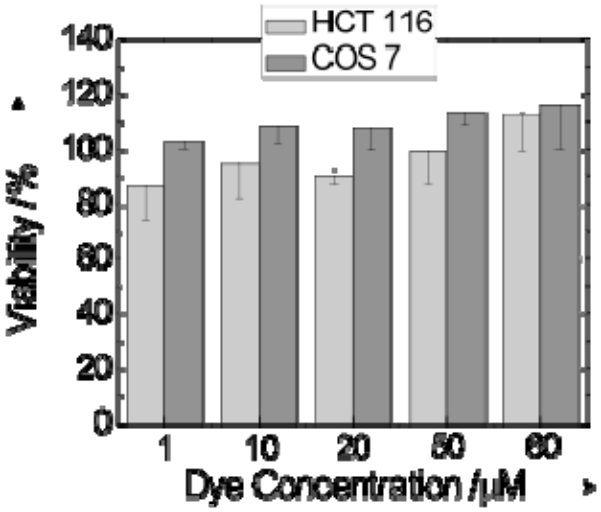

Figure 2-5 Cell viability assays of COS-7 and HCT 116 cells incubated with Pluronic® F-127-encapsulated 2PA probe **IV.**

Two-photon fluorescence microscopy (2PFM) images of fixed HCT 116 cells incubated with probe **IV** encapsulated in Pluronic® F-127 (50 μM, 3 h) were collected on a modified Olympus Fluoview FV300 microscope system coupled to a tunable Coherent Mira 900F Ti:sapphire, 76 MHz, modelocked, 200 fs laser tuned to 700 nm (Figure 2-6C).

Two-photon fluorescence imaging, Figure 2-6C, revealed remarkable contrast when compared to one-photon (conventional) fluorescence imaging, Figure 2-6B, in which individual lysosomes become evident. This demonstrates the potential that this probe-micelle formulation has for following the endocytotic process by 2PFM. Furthermore, the versatility of this system should allow one to encapsulate a wide variety of 2PA hydrophobic dyes, an aspect of further investigation.

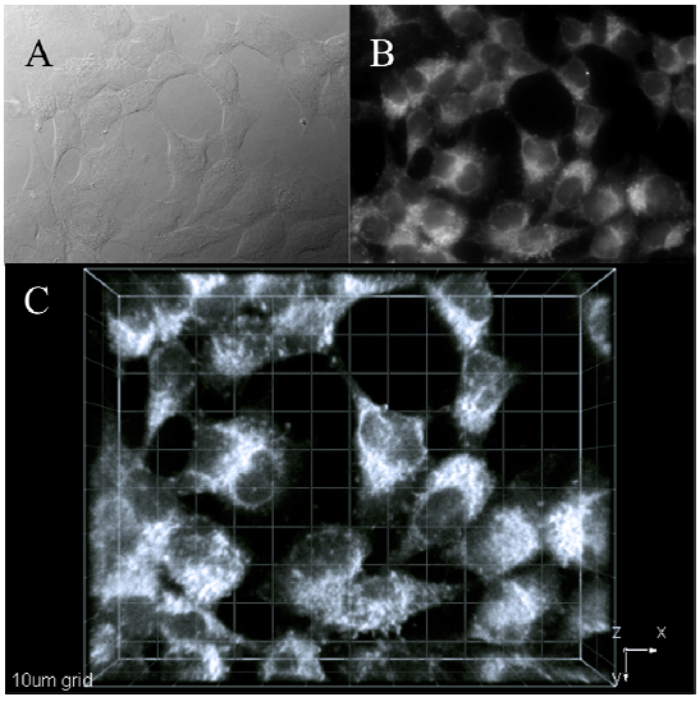

Figure 2-6 One-and two-photon fluorescence micrographs of HCT 116 cells incubated with probe **IV** encapsulated in Pluronic® F-127 (50 μM, 3 h). DIC (A), one-photon fluorescence (B), and 3D reconstruction from overlaid 2PFM images (C), 76 MHz, 200 fs laser 700 nm, 60x objective (NA= 1.35, Olympus). Scale: 10 μm grid.

2.4 Experimental Section

2.4.1 Materials and methods

2-(5-Bromothiophen-2-yl)benzothiazole **1** and 2,7-dibromo-9,9-didecyl-9H-fluorene **6** were prepared as described previously.[*27, 28*] Synthesis of compounds **7** and **8** has been achieved previously by conventional heating, and dye **IV** was prepared trough a different methodology.[*52*] All microwave reactions were carried out under N_2 in a CEM Discover unit microwave in 10 mL closed vessels programmed at a maximum temperature of 130 ^{o}C, maximum pressure of 100 psi and maximum power of 100 Watts. All other reagents and solvents were used as received from commercial suppliers. ^{1}H and ^{13}C NMR spectra were recorded in $CDCl_3$ on a Varian NMR spectrometer at 500 and 125 MHz, respectively. Elemental analyses were performed by Atlantic Microlab, Inc.

2.4.2 Synthetic procedures and characterization

Synthesis of 4-(5-(benzothiazol-2-yl)thiophen-2-yl)-2-methylbut-3-yn-2-ol (7): 2-(5-Bromothiophen-2-yl)benzothiazole **1** (200 mg, 0.67 mmol), 2-methyl-3-butyn-2-ol (170 mg, 2.02 mmol), $Pd(PPh_3)_2Cl_2$ (19 mg, 0.027 mmol) and CuI (5 mg, 0.027 mmol) were dissolved in a 1:4 mixture of Et_3N:toluene (5 mL). The mixture was either heated under reflux for 12 hours or irradiated in the microwave for 2 minutes, when it was determined by TLC that the reaction was completed. The mixture was filtered through a celite plug, and purified by column chromatography using as a solvent a mixture of hexane:ethyl acetate (1:1) to yield 192 mg (96%) of a pale yellow solid when the heating was achieved by either method. m.p. 163.9-164.6 ^{o}C. ^{1}H NMR (500 MHz, $CDCl_3$) δ8.02 (d, *J*=8.04Hz, 1H, Ph-H), 7.85 (d, *J*=7.87Hz, 1H, Ph-H), 7.50 (d, *J*=3.95 Hz, 1H, Thy-H), 7.47 (m, 1H, Ph-H), 7.38 (m, 1H, Ph-H), 7.18 (d, *J*=3.95 Hz, 1H, Thy-

H), 2.11 (s, 1H, -OH), 1.64 (s, 6H, CH3). ^{13}C NMR (125 MHz, $CDCl_3$) δ 160.4, 153.6, 137.8, 134.7, 132.9, 128.3, 126.4, 125.3, 123.1, 121.5, 121.4, 100.2, 75.2, 65.8, 31.3.Anal. Calcd for $C_{16}H_{13}NOS_2$: C, 64.18; H, 4.38; N, 4.68. Found: C, 64.10; H, 4.33; N, 4.64.

Synthesis of 2-(5-ethynylthiophen-2-yl)benzothiazole (8): 4-(5-(Benzothiazol-2-yl)thiophen-2-yl)-2-methylbut-3-yn-2-ol **7** (300 mg, 1.0 mmol) and KOH (300 mg, 5.3 mmol) were heated either under reflux for 1 hour or under microwave irradiation for 8 minutes. The mixture was filtered, and then purified by column chromatography using as a solvent hexane to yield 180 mg (75%) by the conventional heating method or 236 mg (98%) by the microwave assisted method of a pale yellow solid. m.p. 117.3-118.3 ^{o}C. ^{1}H NMR (500 MHz, $CDCl_3$) δ 8.03 (d, *J*=8.21Hz, 1H, Ph-H), 7.86 (d, *J*=8.21Hz, 1H, Ph-H), 7.51 (d, *J*=3.94 Hz, 1H, Thy-H), 7.48 (m, 1H, Ph-H), 7.39 (m, 1H, Ph-H), 7.28 (d, *J*=3.94 Hz, 1H, Thy-H), 3.50 (s, 1H, C≡C-H). ^{13}C NMR (125 MHz, $CDCl_3$) δ ı60.2, 153.6, 138.5, 134.8, 133.9, 133.7, 127.8, 126.5, 125.4, 123.2, 121.6, 84.0, 76.5. Anal. Calcd for $C_{13}H_7NS_2$: C, 64.70; H, 2.92; N, 5.80. Found: C, 64.64; H, 2.91; N, 5.75.

Synthesis of 2,2'-(5,5'-(9,9-didecyl-9H-fluorene-2,7-diyl)bis(ethyne-2,1-diyl)bis(thiophene-5,2-diyl))dibenzothiazole (IV): 2,7-dibromo-9,9-didecyl-9H-fluorene **6** (300 mg, 0.50 mmol), 2-(5-ethynylthiophen-2-yl)benzothiazole **8** (263 mg, 1.09 mmol), $Pd(PPh_3)_2Cl_2$ (30 mg, 0.04 mmol) and CuI (8 mg, 0.04 mmol), were dissolved in a 1:4 mixture of Et_3N:toluene (5 mL). The mixture was heated under reflux for 12 hour or in the microwave for 1h. The mixture was filtered through a celite plug, and purified by column chromatography using as a solvent a mixture of hexane:ethyl acetate (10:1) to yield 252 mg (55%) of a yellow solid by conventional heating and 298 mg (65%) when microwave irradiation was used. m.p. 74.0-75.5

^{o}C. ^{1}H NMR (500 MHz, $CDCl_3$) δ 8.04 (dd, *J*=8.09 Hz, *J*=0.54 Hz, 2H, Ph-H), 7.87 (dd, *J*=8.04 Hz, *J*=0.53 Hz, 2H, Ph-H), 7.70 (d, *J*=7.83 Hz,2H, Ph-H), 7.57 (d, *J*=3.89 Hz, 1H, Thy-H), 7.55 (m, 2H, Ph-H), 7.53 (m, 2H, Ph-H), 7.49 (m, 2H, Ph-H), 7.39 (m, 2H, Ph-H), 7.31 (d, *J*=3.89 Hz, 1H, Thy-H), 2.00 (m, 4H, CH_2), 1.15 (m, 28H, CH_2), 0.84 (t, *J*=6.96 Hz, 6H, CH_3), 0.61 (m, 4H, CH_2). ^{13}C NMR (125 MHz, $CDCl_3$) δ 160.5, 153.7, 151.3, 141.1, 138.0, 134.7, 132.6, 130.8, 128.4, 127.1, 126.6, 125.9, 125.5, 123.1, 121.5, 121.3, 120.2, 97.0, 82.8, 55.4, 40.3, 31.9, 30.0, 29.6, 29.5, 29.3, 29.3, 23.8, 22.7, 14.1. Anal. Calcd for $C_{59}H_{60}N_2S_4$: C, 76.58; H, 6.54; N, 3.03. Found: C, 76.79; H, 6.75; N, 2.79.

2.4.3 Measurements

Absorption spectra were recorded with an Agilent 8453 UV–visible spectrophotometer. Steady-state fluorescence spectra were measured with a PTI Quantamaster spectrofluorimeter in the photon counting regime of the PMT using an L-format configuration. The fluorescence spectra were corrected for the spectral dependence of the PMT. All measurements were performed in hexane at room temperature in 1 cm quartz cuvettes, with dye concentrations in the order of 10^{-6} M. Fluorescence quantum yields were determined relative to 9, 10-diphenylanthracene in cyclohexane as a standard.

Two-photon absorption spectra of **IV** were measured at 700, 750 and 800 nm in spectroscopic grade nonpolar cyclohexane, polar DMSO and aqueous mixtures by a typical two-photon fluorescence 2PF method relative to Rhodamine B in methanol as a standard.[*53*] The setup comprised a PTI QuantaMaster spectrofluorimeter coupled to a femtosecond Clark-MXR CPA-2010 laser that pumped optical parametric generator/amplifiers (TOPAS) with tuning range 600-950 nm, pulse duration ≈ 140 fs (FWHM), 1 kHz repetition rate and pulse energies up to ~

0.15 μJ. Two-photon fluorescence measurements were performed in 10 mm quartz cuvettes with dye concentrations ~ 10^{-5} M. The values of 2PA cross section, δ_{2PA}, were determined by the equation (ii):

$$\delta_{2PA}^{S} = \delta_{2PA}^{R} \cdot \frac{\langle F(t)\rangle_S \cdot C_R \cdot \Phi_R \cdot \varphi_R \cdot \langle P(t)\rangle_R^2}{\langle F(t)\rangle_R \cdot C_S \cdot \Phi_S \cdot \varphi_S \cdot \langle P(t)\rangle_S^2} \qquad \text{(ii)}$$

where *<F(t)>, <P(t)>, C* and *φ*, are the averaged fluorescence intensity, excitation power, molecular concentration and geometric factor, respectively. Subscripts *S* and *R* refer to the sample and reference compound. [*54*] The quadratic dependence of 2PF intensity on the excitation power was checked for every excitation wavelength, λ_{ex}, and special attention was paid to verify the independence of the fluorescence quantum yield from λ_{ex}.

2.4.4 Cell culture and incubation

HCT 116 cell were cultured in DMEM, supplemented with 10% FBS, and 1% penicillin, 1% streptomycin, at 37 °C, under 5% CO_2 environment. N° 1 round 12mm coverslips were treated with poly-D-lysine, to improve cell adhesion, and washed (3x) with PBS buffer solution. The treated cover slips were placed in 24-well plates and 80,000 cells/well were seeded and incubated at the same conditions as indicated above until 75%-85% confluency was reached on the coverslips. From a 3.03 x 10^{-4} M stock solution of Pluronic® F-127 encapsulated dye **IV** a series of 0.1, 1, 10, 25, and 50 μM solutions in culture media were made all of them also containing 75 nM of Lysotracker Red (Invitrogen). These solutions were used to incubate the cells for 3h. The dye solutions were extracted and the coverslipped cells were washed abundantly with PBS (4x).

Cell fixing and mounting: Cells were fixed with 3.7% solution of paraformaldehyde in pH=7.4 PBS buffer for 10 min. The fixing agent was extracted and washed (2x) with PBS. To reduce autofluorescence, a fresh solution of $NaBH_4$ (1 mg/mL) in pH=8 PBS buffer was used to treat the fixed cells (2x). The coverslipped cells were then washed with buffer PBS (2x) and mounted on microscope slides using Prolong Gold (Invitrogen) as a mounting media.

2.4.5 Cell viability

Cell viability was assessed with CellTiter® 96 AQ (Promega). COS-7 and HCT 116 cells were seeded ($5x10^3$ cells/well) in a 96 well plate and incubated for 24 h in 90 μL of DMEM (Invitrogen) without phenol red, supplemented with 10% FBS (Atlanta Biologicals), and 1% penicillin-streptomycin. The cell was incubated for an additional 24 h with 60, 50, 25, 10 and 1 μM solutions of Pluronic® F-127-encapsulated dye **IV** in FBS complemented (10%) culture media. Then 20 μM of the CellTiter® 96 AQ reagent was added into each well and subsequently incubated for another 4 h, 37 ^oC after which the respective absorbance values were read on a SpectraMax M5 plate reader (Molecular Devices) at 490 nm to determine the relative amount of formazan produced. Cell viability % was calculated by the following expression (iii):

$$Cell \quad viability(\%) = \frac{Abs^{S}_{490nm} - Abs^{B}_{490nm}}{Abs^{C}_{490nm} - Abs^{B2}_{490nm}} x100\% \qquad \text{(iii)}$$

where Abs^{S}_{490nm} is the absorbance of the cells at the different concentrations of micelle encapsulated dye **IV**, Abs^{B}_{490nm} is the absorbance of a cell-free well containing only encapsulated dye **IV** in at the concentrations that were studied, Abs^{C}_{490nm} is the absorbance of cells incubated in media without any other component, and Abs^{B2}_{490nm} is the absorbance of a cell-free well.

2.4.6 Confocal one-photon fluorescence imaging

One-photon fluorescence microscopy images were recorded on an Olympus IX-81confocal microscope equipped with a Hamamatsu EM-CCD C9100 digital camera. One-photon confocal fluorescence images of the fixed cells were taken using a custom made filter cube (Ex:377/50; DM: 409; Em:525/40) and a Texas Red filter cube (Ex:562/40; DM: 593; Em:624/40) for dye **IV** and Lysotracker Red, respectively.

2.4.7 Two-photon upconverted fluorescence imaging

Two-photon fluorescence imaging was performed on a modified Olympus Fluoview FV300 laser scanning confocal microscopy system equipped with a broadband, tunable Coherent Mira Ti:sapphire laser (115 fs pulse width, 76 MHz repetition rate), pumped by a 10 W Coherent Verdi frequency doubled Nd:YAG laser. The laser was tuned and modelocked to 700 nm and used as the two-photon excitation source. The two-photon induced fluorescence was collected by a 60x microscope objective (UPLANSAPO 60x, N.A.=1.35 Olympus). A high transmittance (>95%) short-pass filter (cutoff 685 nm, Semrock) was placed in front of the PMT detector within the FV300 scanhead in order to filter off background radiation from the laser source (700 nm).

2.5 Conclusions

Encapsulation of hydrophobic 2PA probe **IV** in Pluronic® F-127 is a viable method for delivering the fluorescent probes into the the lysosomes of HCT 116 cells. After photophysical characerization, the fluorene-based fluorescent probe **IV** proved to have high 2PA cross sections in polar solvents, and good fluorescence quantum yields. The yields and reaction times of this probe were significantly improved by the use of microwave-assisted

synthetic procedures. 2PFM imaging revealed remarkable contrast when compared to the one-photon fluorescence, suggesting the potential that this probe-micelle formulation has in bioimaging. Cell viability assays, carried out for HCT 116 and COS-7 cells, indicate that the probe concentrations used for imaging purposes are virtually harmless to HCT 116 and COS-7 cells.

CHAPTER 3. NEW TWO-PHOTON ABSORBING PROBE WITH EFFICIENT SUPERFLUORESCENT PROPERTIES

Reproduced with permission from: Kevin D. Belfield, Carolina D. Andrade, Ciceron O. Yanez, Mykhailo V. Bondar, Florencio E. Hernandez, Olga V. Przhonska, *Journal of Physical Chemistry B*, **2010**, *114*, 14087-14095.

3.1 Abstract

The synthesis, linear photophysical and photochemical parameters, two-photon absorption (2PA), and superfluorescence properties of 2,2'-(5,5'-(9,9-didecyl-9*H*-fluorene-2,7-diyl)bis(ethyne-2,1-diyl)bis(thiophene-5,2-diyl))dibenzo[*d*]thiazole (**IV**) were investigated, suggesting its potential as an efficient fluorescent probe for bioimaging applications. The steady-state absorption, fluorescence, and excitation anisotropy spectra of **IV** were measured in several organic solvents and aqueous media. Probe **IV** exhibited high fluorescence quantum yield (~ 0.7-0.8) and photochemical stability (photobleaching quantum yield ~ $(3 - 7)\cdot 10^{-6}$). The 2PA spectra were determined over a broad spectral range (640-920 nm) using a standard two-photon induced fluorescence method under femtosecond excitation. A well-defined two-photon allowed absorption band at 680-720 nm with corresponding 2PA cross sections δ_{2PA} ≈ 800-900 GM was observed. The use of probe **IV** in bioimaging was shown via one- and two-photon fluorescence imaging of HCT-116 cells. An amplification of the stimulated emission of **IV** was demonstrated in organic solvents and thin polystyrene films, which potentially can be used for the development of new fluorescent labels with increased spectral brightness.

3.2 Introduction

The development of new highly fluorescent organic compounds with efficient two-photon absorption (2PA) properties is a subject of broad scientific and technological interest for a number of multidisciplinary applications,[*1, 33, 55-59*] including 3D biological imaging by two-photon fluorescence microscopy (2PFM) methods.[*1, 58, 59*] Directional synthesis of new fluorescent labels and comprehensive investigations of their linear photophysical, nonlinear-optical and photochemical properties can appreciably extend the abilities of bioimaging applications. High fluorescence quantum yield, Φ, large values of 2PA cross sections, δ_{2PA}, as well as their product, $\Phi \cdot \delta_{2PA} = \delta_{2PA}^{act}$ (so-called two-photon action cross section[*60*]), and photochemical stability under high intensity laser irradiation are the primary properties required for 2PFM-based applications of organic chromophores.[*54, 61, 62*] A number of potential fluorescence labels with suitable 2PA properties have been synthesized for two-photon bioimaging use (see, e.g., nonlinear optical properties of water soluble [2.2]paracyclophane-based fluorophores with high values of δ_{2PA}^{act},[*60*] 2,6-bis(*p*-dialkylaminostyryl)anthracene derivatives,[*63*] and dipyrrylmetheneboron difluoride compounds[*64*]). Among these, high two-photon absorbing fluorene-based derivatives are promising fluorescent labels for 2PFM bioimaging applications.[*8, 34, 65*] In addition to strong 2PA transitions, fluorene derivatives exhibit efficient stimulated emission depletion[*66*] and lasing properties,[*15*] which can dramatically improve the quality and scope of microscopic images and techniques.

In this paper, we report a new fluorene-based probe, 2,2'-(5,5'-(9,9-didecyl-9*H*-fluorene-2,7-diyl)bis(ethyne-2,1-diyl)bis(thiophene-5,2-diyl))dibenzo[*d*]thiazole (**IV**), [*52*] and comprehensive characterization of its linear photophysical, 2PA, superfluorescence, and lasing

properties in isotropic solutions. The rationale for the molecular design of this compound was previously described. [*52*] Linear photophysical investigations include a detailed analysis of the nature of absorption bands by excitation anisotropy, [*67*] along with fluorescence lifetime and quantum yield measurements, in various organic solvents and aqueous media. 2PA spectra of probe **IV** were obtained over a broad spectral range by a two-photon induced fluorescence (2PF) method.[*54*] Probe **IV** was encapsulated in Pluronic® F127 and used as a fluorescent probe to image endosomes and lysosomes via one- and two-photon fluorescence microscopy in HCT-116 cells. The investigation of the broad range of excited state absorption (ESA) spectra, superfluorescence, and lasing potential of **IV** is just the first step in the development of new types of organic labels with high spectral brightness for fluorescence microscopy applications.

3.3 Results and Discussion

3.3.1 Linear photophysical properties

Probe **IV** was prepared in three steps as shown in Figure 3-1. Each of the three steps was accomplished by either thermal or microwave-facilitated heating. In each case, the microwave-assisted reaction occurred at significantly shorter times. While the conventional (thermal) and microwave-assisted reaction yields were the same for the first step, microwave-facilitated reactions provided high yields of product for the latter two steps.

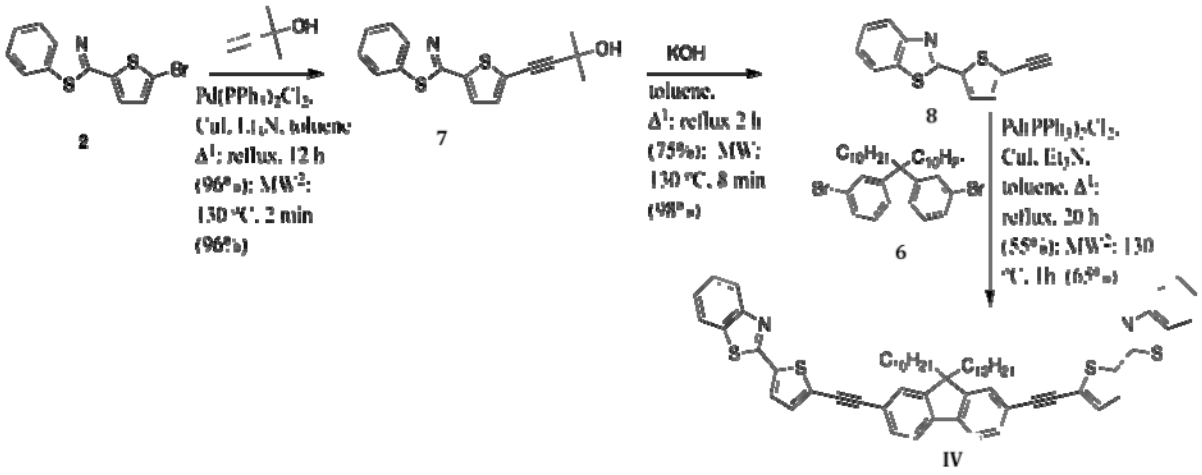

Figure 3-1 Multistep synthesis of probe **IV**.

The main linear photophysical and photochemical parameters of new symmetrical fluorene derivative **IV** with alkynyl triple bonds in the chromophore system, along with the steady-state absorption and fluorescence spectra in various organic solvents are presented in Table 3-1 and Figure 3-2, respectively. The shape of absorption spectra and maximum values of extinction coefficients, ε^{max}, were independent of molecular concentration up to $C \approx 10^{-2}$ M, which is indicative of negligible aggregation effects. As can be seen in Figure 3-2, linear one-photon absorption spectra of **IV** in all of the investigated solvents were nearly independent of solvent polarity, Δf, and exhibited relatively high extinction coefficients $\varepsilon^{max} \sim 10^5$ $M^{-1} \cdot cm^{-1}$ in the long wavelength absorption bands. In contrast, the steady-state fluorescence spectra of **IV** (Figure 3-2, curves 1'-7') exhibited noticeable solvatochromic behavior with relatively strong vibronic structure, even in the polar solvent DMSO. Dramatic changes in the shape of the fluorescence spectra of symmetrical fluorene derivatives with extended π-conjugation are typical for donor-acceptor fluorenes[*66, 68*] and can be explained by symmetry breaking effects

occurring in the first excited state, S_1, after electronic excitation.[*69*] All fluorescence spectra of **IV** were independent of excitation wavelength, λ_{ex}, and exhibited high fluorescence quantum yield ($\Phi \sim 0.7$ - 0.8) in all organic solvents. The fluorescence decay curves corresponded to a single-exponential decay process with $\tau \sim 0.7$ - 0.8 ns (see Table 3-1), indicative of the relatively fast spontaneous relaxation, with velocity $1/\tau_n = \Phi/\tau \sim 10^9$ s^{-1}, where τ_n is the natural lifetime. [*67*]

In aqueous solution probe **IV** exhibited nearly the same steady-state absorption spectrum as in organic media, with an increased Stokes shift, substantial decrease in fluorescence quantum yield, and bi-exponential fluorescence decay (see Table 3-1) with the primary short component ≈ 0.46 ns (~ 95 % amplitude). It should be noted that in an aqueous medium, the shape of fluorescence spectrum of **IV** and the value of its quantum yield, Φ, were also independent of λ_{ex}. The nature of this spectral behavior is not sufficiently clear and will be the subject of further investigation.

Table 3-1 Major linear photophysical parameters of **IV** in different solvents with corresponding polarity Δf and viscosity η: absorption λ_{abs}^{max} and fluorescence λ_{fl}^{max} maxima, Stokes shifts, maximum extinction coefficients ε^{max}, quantum yields Φ, fluorescence lifetimes τ and photobleaching quantum yields, Φ_{Ph}, under one-photon excitation.

N/N	Hexane	Cyclo-hexane	Toluene	THF	DCM	DMSO	ACN	Aqueous mixture*
Δf	$8 \cdot 10^{-5}$	$7 \cdot 10^{-4}$	0.0135	0.209	0.217	0.263	0.305	0.321
η, cP	0.313	0.97	0.59	0.48	0.4	2.0	0.34	0.6
λ_{abs}^{max}, nm	397 ± 1	399 ± 1	402 ± 1	401 ± 1	403 ± 1	404 ± 1	398 ± 1	406 ± 1
λ_{fl}^{max}, nm	433 ± 1	436 ± 1	441 ± 1	441 ± 1	445 ± 1	451 ± 1	441 ± 1	488 ± 1
Stokes shift, nm	36 ± 2	37 ± 2	39 ± 2	40 ± 2	42 ± 2	47 ± 2	43 ± 2	82 ± 2
$\varepsilon^{max} \cdot 10^{-3}$, $M^{-1} \cdot cm^{-1}$	110 ± 7	105 ± 5	104 ± 5	104 ± 5	107 ± 5	90 ± 10	-	63 ± 10
Φ	0.81 ± 0.05	0.80 ± 0.05	0.8 ± 0.05	0.77 ± 0.05	0.78 ± 0.07	0.72 ± 0.05	0.76 ± 0.05	0.14 ± 0.02
τ, ns	0.73 ± 0.04	0.72 ± 0.04	0.70 ± 0.04	0.75 ± 0.04	0.73 ± 0.05	0.80 ± 0.04	0.80 ± 0.04	0.46±0.05 1.7 ± 0.3
$\Phi_{Ph} \cdot 10^{6}$	7.0 ± 1.0	3.1 ± 0.6	3.2 ± 0.6	3.3 ± 0.7	35 ± 6	5.7 ± 0.9	-	45 ± 10

***** Water (95 wt%) and DMSO (5 wt%).

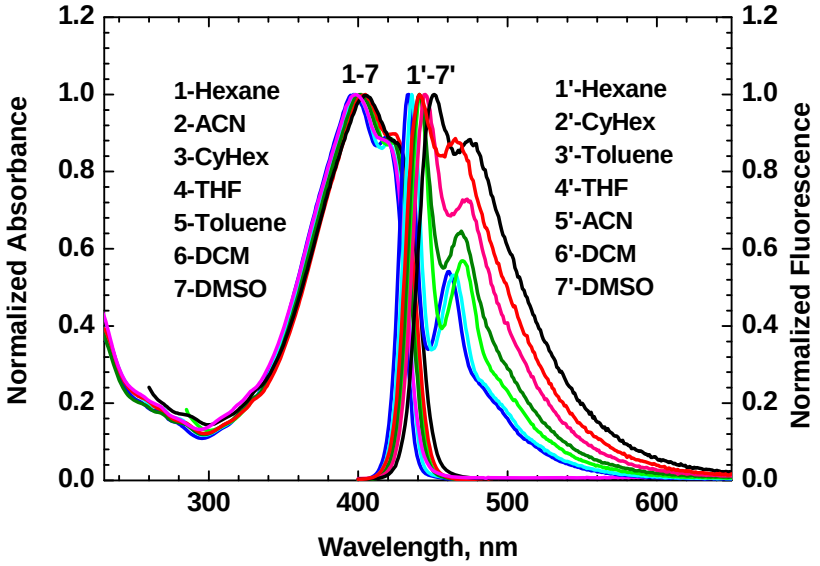

Figure 3-2 Normalized one-photon absorption (1-7) and fluorescence (1'-7') spectra of **IV** in organic solvents. Corresponding solvents are listed in the order of increasing wavelength λ_{abs}^{max} and λ_{fl}^{max}.

The excitation anisotropy spectra of **IV** in organic solvents and in viscous polyTHF (pTHF) are presented in Figure 3-3. In low viscosity solvents (hexane, toluene, ACN, etc.) the anisotropy values, r, decreased due to rotational movement of the molecule in accordance with $r = r_0/(1+\tau/\theta)$, where $r_0 = (3\cos^2\alpha - 1)/5$ is the fundamental anisotropy value (α is the angle between absorption $S_0 \rightarrow S_1$ and emission $S_1 \rightarrow S_0$ transition dipole moments) and θ is the rotational correlation time.[*67*] In viscous pTHF at room temperature the fluorescence lifetime $\tau << \theta$ ($\theta = \eta V/kT >$ 10 ns; V is the volume of the molecule, k and T are the Boltzmann constant and absolute temperature, respectively). Therefore, in pTHF excitation anisotropy reached its maximum value $r \approx r_0 \approx$ 0.38 (Figure 3-3a, curve 1), which is close to theoretical limit 0.4,

reflecting a nearly parallel orientation of the absorption and emission transition dipoles. In this case, it is possible to determine the mutual dipole orientation for the $S_0 \rightarrow S_1$ and higher excited $S_0 \rightarrow Sn$ (n = 2, 3, …) electronic transitions.

Excitation anisotropy spectra provided information regarding the nature of the one-photon absorption bands. From Figure 3-3a, curve 1, the value of anisotropy was not sufficiently constant in the main long wavelength absorption band (see, for comparison, anisotropy spectra of typical fluorene derivatives[*50, 68, 70*]). This suggests that more than one electronic transition with different dipole orientations corresponded to the main absorption band. Following extremes or constant values in the anisotropy spectra in the short wavelength region, the spectral positions of another $S_0 \rightarrow Sn$ absorption band was indicated. Normalization of excitation anisotropy spectra in different organic solvents, $r(\lambda_{ex})$, with respect to the excitation anisotropy spectrum in hexane, $r_{hex}(\lambda_{ex})$, are presented Figure 3-3b and d. Nearly constant values of r / r_{hex} in the spectral range 280 nm $\leq \lambda_{ex} \leq$ 450 nm (Figure 3-3b) reflect similar mutual orientations of the corresponding electronic transitions $S_0 \rightarrow Sn$ (n = 1, 2, 3,…) of **IV** in hexane, cyclohexane, THF, DCM, and ACN. In contrast, mutual orientation of the electronic transitions in toluene, DMSO, and pTHF (see corresponding functions $r / r_{hex} = f(\lambda_{ex})$ in Fig. 3-3d) exhibited different types of solvent influence on the electronic structure of **IV**.

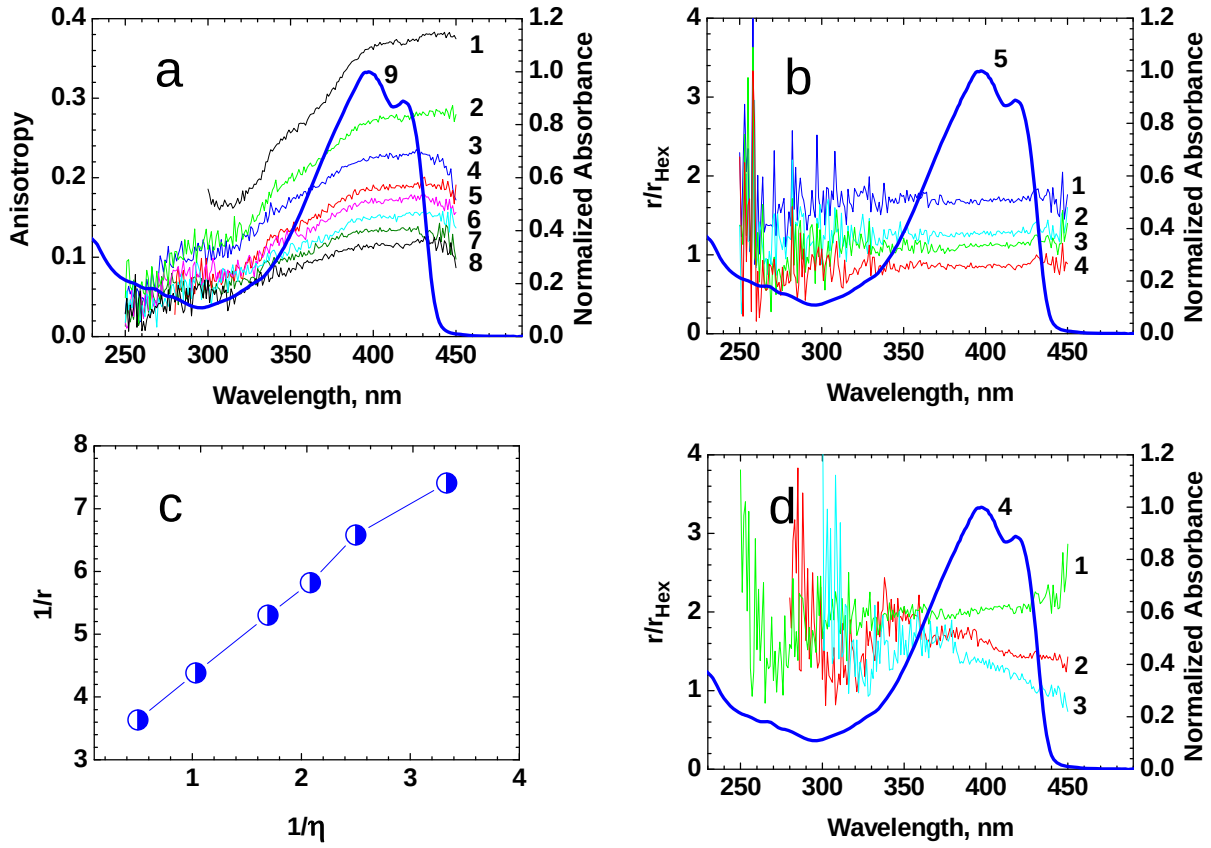

Figure 3-3 (a) Excitation anisotropy spectra of **IV** in pTHF (1), DMSO (2), cyclohexane (3), toluene (4), THF (5), DCM (6), hexane (7), and ACN (8). (b) Dependences $r/r_{hex} = f(\lambda_{ex})$ for IV in cyclohexane (1), THF (2), DCM (3), and ACN (4). (c) Dependence $1/r(\lambda_{abs}^{max}) = f(1/\eta)$ for **IV** in organic media. (d) Dependences $r/r_{hex} = f(\lambda_{ex})$ for **IV** in DMSO (1), toluene (2), and pTHF (3). Normalized one-photon absorption spectrum of **IV** in hexane: (a) curve 9; (b) 5, and (d) 4.

The analysis of the experimental dependence $1/r(\lambda_{abs}^{max}) = f(1/\eta)$ (Figure 3-3c) revealed good agreement with a theoretical linear function:[*67*]

$$\frac{1}{r} = \frac{1}{r_0} + \left(\frac{\tau \cdot kT}{r_0 \cdot V}\right) \cdot \frac{1}{\eta} \quad , \qquad \text{(iv)}$$

which is indicative of the weak dependence of the fundamental anisotropy r_0 on the solvent properties and nearly constant effective rotational molecular volume V in all of the investigated organic solvents. This means that the effective size of the solvate cages in different solvents are sufficiently close and correspond to $V \approx 5000$ Å^3.

The photochemical stability of probe **IV** was investigated by an absorption method[*71*] in the investigated organic solvents and aqueous media, except for ACN, in which a relatively low solubility of **IV** was observed. Corresponding values of the photobleaching quantum yields, Φ_{Ph} are presented in Table 3-1. A high level of photostability ($\Phi_{Ph} \sim (3 - 7)\cdot 10^{-6}$) was observed for **IV** in all investigated solvents except for electron-accepting DCM and aqueous media. Polar DCM exhibits specific photochemical interaction with fluorene derivatives,[*72, 73*] resulting in a dramatic decrease in their photostability (by ca. one order of magnitude) and efficient formation of nonfluorescent photoproducts in the visible region. The estimations of the photochemical stability of **IV** were performed under one-photon excitation conditions, since reactions from the first exited state are nearly independent of the type of excitation (one- or two-photon) for typical fluorene derivatives in organic solvents.[*71-73*] It should be mentioned that the observed level of photostability of probe **IV** is one of the highest among known fluorescent probes used in bioimaging applications.

3.3.2 2PA properties of IV and bioimaging

The efficiency of two-photon processes of **IV** was investigated in cyclohexane, DMSO, and aqueous solution by a relative 2PF method,[*54*] with the corresponding broad range 2PA spectra presented in Figure 3-4. The symmetrical probe **IV** exhibited one well defined 2PA band

at λ_{ex} ≈ 680-720 nm with maxima cross sections δ_{2PA} ~ 800-900 GM and weak dependence on solvent polarity. The spectral position of this band corresponded to the shoulder at λ_{ex} ≈ 340-360 nm in the excitation anisotropy spectrum of **IV** (Figure 3-3a, curve 1) and could not be extracted from the linear absorption spectrum (curve 9). Dramatic decrease in the 2PA efficiency in the main one-photon allowed absorption band is typical, consistent with the relatively symmetrical structure of **IV**. Regardless of the decrease in 2PA efficiency, the values of δ_{2PA} and δ_{2PA}^{act} remain sufficiently high (~ 50-500 GM) in the main tuning range of Ti:sapphire laser, which is the most convenient excitation source for bioimaging applications. In aqueous solution (95 wt% water and 5 wt% DMSO) probe **IV** exhibited decreased 2PA efficiency in the main two-photon allowed absorption band relative to pure DMSO, and nearly the same values of δ_{2PA} in the spectral range λ_{ex} ≥ 750 nm.

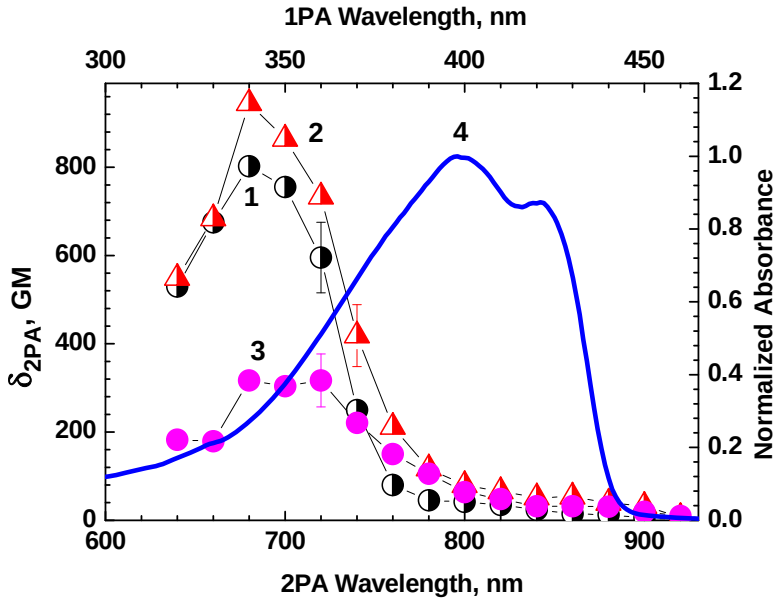

Figure 3-4 2PA spectra of **IV** in cyclohexane (1), DMSO (2), and aqueous solution (95 wt% water and 5 wt% DMSO) (3). Normalized one-photon absorption spectrum of IV in cyclohexane (4).

The hydrophobic character of probe **IV** made it challenging to attempt delivering the dye directly in a solution that was compatible to the solubility of the cell media. This made it an ideal candidate for encapsulating this dye in a poloxomer micelle. The poloxomer of choice was Pluronic® F-127, an FDA approved triblock copolymer that consists of a propylene oxide portion flanked by two ethylene oxide chains. Pluronic® F-127 has been used in drug delivery applications to enhance the solubility of hydrophobic substances such as anticancer drugs.[*45, 46*] Pluronic micelles are known to be uptaken by MDCK cells by means of clathrin-mediated endocytosis when present above critical micelle concentration (CMC).[*47*] Probe **IV** was encapsulated in Pluronic® F-127, with the purpose of it being endocytosed, and subsequently tracked through the vesicle maturation process.

HCT 116 cells were incubated for 3 h in Pluronic® F-127 encapsulated probe **IV**. A series of 0.1, 1, 10, 25, and 50 μM solutions of the micelle-encapsulated probe in culture media was prepared. These samples were coincubated with 75 nM of Lysotracker™ Red (Invitrogen) for colocalization studies to determine whether the micelle-encapsulated probe reached the lysosomes. After fixation, the one-photon fluorescence images exhibited good agreement between the Lysotracker™ Red (Figure 3-5b) and the Pluronic® F-127 encapsulated 2PA probe **IV** (Figure 3-5c), as shown by the overlay of micrographs of these two channels (Figure 3-5d). The excellent colocalization agreement was further confirmed by determining the colocalization coefficient (≅ 0.91).[*51*]

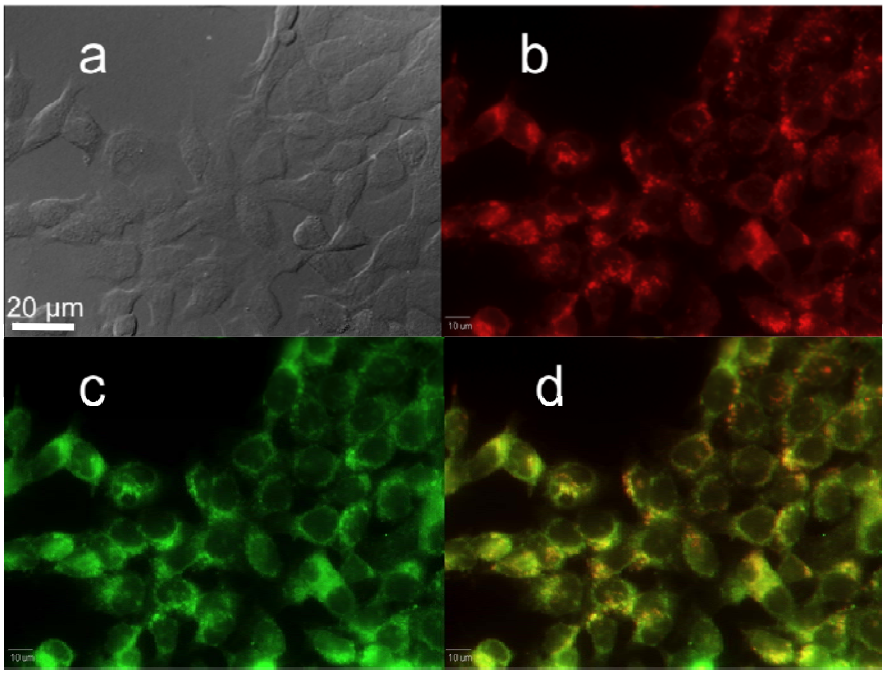

Figure 3-5 Confocal fluorescence images of HCT 116 cells incubated with probe **IV** encapsulated in Pluronic® F-127 (25 µM, 3 h) and Lysotracker™ Red (100 nM, 3 h). (a) differential interference contrast (DIC) image; (b) one-photon fluorescence image showing Lysotracker™ Red; (c) probe **IV** encapsulated in Pluronic® F-127 micelles, and (d) colocalization (overlay of b and c).

Two-photon fluorescence microscopy (2PFM) images of fixed HCT 116 cells incubated with probe **IV** encapsulated in Pluronic® F-127(50 µM, 3 h) were collected on a modified Olympus Fluoview FV300 microscope system coupled to a tunable Coherent Mira 900F Ti:sapphire, 76 MHz, modelocked, 200 fs laser tuned to 700 nm (Figure 3-6c). The 2PFM image, Figure 3-6c, revealed remarkable contrast when compared to one-photon fluorescence image (Figure 3-6b), and revealing the potential that this probe-micelle formulation has for following the endocytotic process by 2PFM.

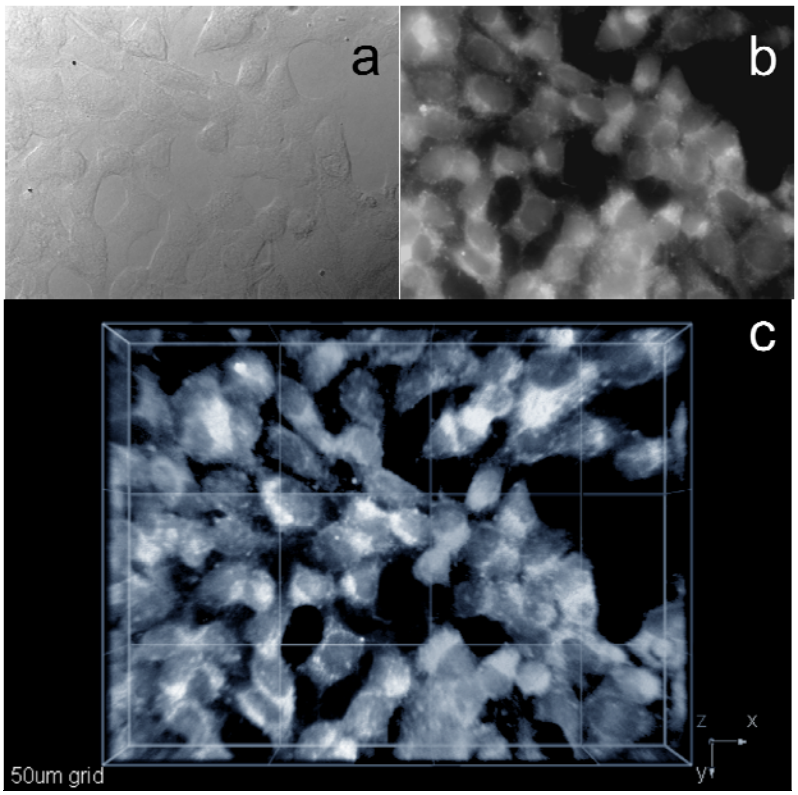

Figure 3-6 One-and two-photon fluorescence micrographs of HCT 116 cells incubated with probe **IV** encapsulated in Pluronic® F-127 (50 μM, 3 h). (a) DIC image; (b) one-photon fluorescence and (c) 3D reconstruction from overlaid 2PFM images, 76 MHz, 200 fs laser, 700 nm, 60x objective (NA= 1.35, Olympus).

3.3.3 ESA superfluorescence and lasing properties

The ESA spectra of **IV** (Figure 3-7) were obtained in the region of its fluorescence (420-700 nm) in order to estimate potential superfluorescence and lasing abilities of this new probe in organic media with different polarity and in aqueous solution. Deduced from the data in Figure 3-7, potential amplification (i.e. negative values of ESA) was obtained only in nonpolar media (hexane, cyclohexane) in the fluorescence region of **IV**. In the aqueous mixture, the ESA spectrum was completely positive (Figure 3-7d) and the existence of small negative regions in

ESA spectrum of **IV** in DMSO (Figure 3-7c) was not sufficient to reach real amplification. Therefore, superfluorescence and lasing properties of **IV** were investigated in nonpolar media, such as hexane, cyclohexane, and polystyrene films.

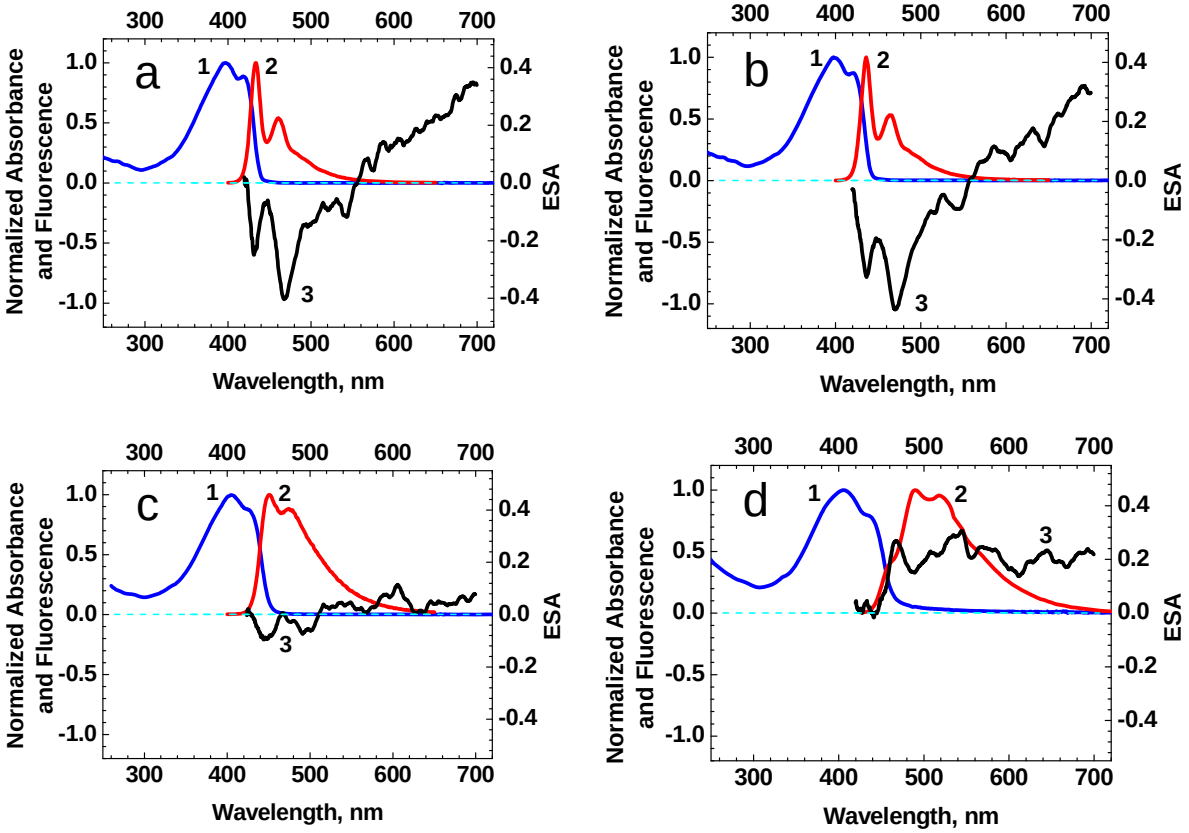

Figure 3-7 Normalized absorption (1), fluorescence (2), and ESA (3) spectra of **IV** in hexane (a), cyclohexane (b), DMSO (c), and aqueous solution (95 wt% water and 5 wt% DMSO) (d).

Efficient superfluorescence and lasing effects under longitudinal pumping at 355 nm were observed for **IV** in hexane and cyclohexane solutions placed in 10 mm regular spectrofluorometric cuvettes. The corresponding fluorescence and amplified stimulated emission

spectra are presented in Figure 3-8. The lasing spectra of **IV** (curves 1) are characterized by spectral width ~ 8-10 nm (FWHM), which are typical for organic dyes in a nondispersive resonator (consisting of the exit uncoated surfaces of the cuvette).[*74*] Under the experimental conditions, a low resonator quality facilitated simultaneous observation of superfluorescence phenomenon in the pumping direction, which was not completely suppressed by resonator's oscillation.

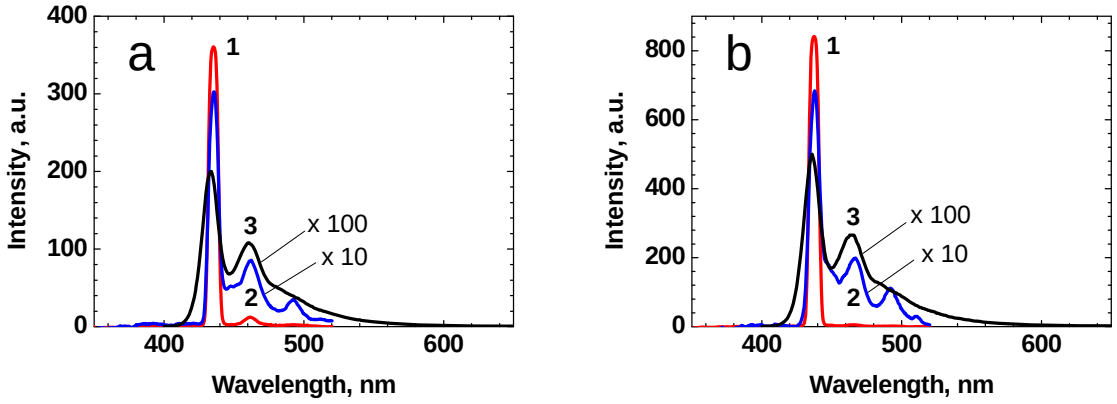

Figure 3-8 Lasing (1), superfluorescence (2), and fluorescence (3) spectra of **IV** in hexane (a) and cyclohexane (b) under 355 nm longitudinal pumping in 10 mm quartz cuvettes.

Polystyrene samples with small thickness (< 100 μm) were used in order to check superfluorescence potential of **IV** in the case of small length amplification, which may have application in bioimaging if the probe were contained within a hydrophobic medium (such as the micelles above). The superfluorescence spectra of **IV** in the polystyrene films with different thicknesses are presented in Figure 3-9. According to these spectra, even for a 5 μm polymeric layer, some degree of amplification was observed for **IV**. This suggests that sufficiently high amplification per unit length in nonpolar medium can be utilized for increasing of the spectral

brightness of fluorescence labels. These amplification conditions potentially can be realized inside specially constructed micelles with high concentrated solution of **IV** and high reflective envelope. The development of such fluorescent labels for bioimaging with increased spectral brightness is currently ongoing in our lab.

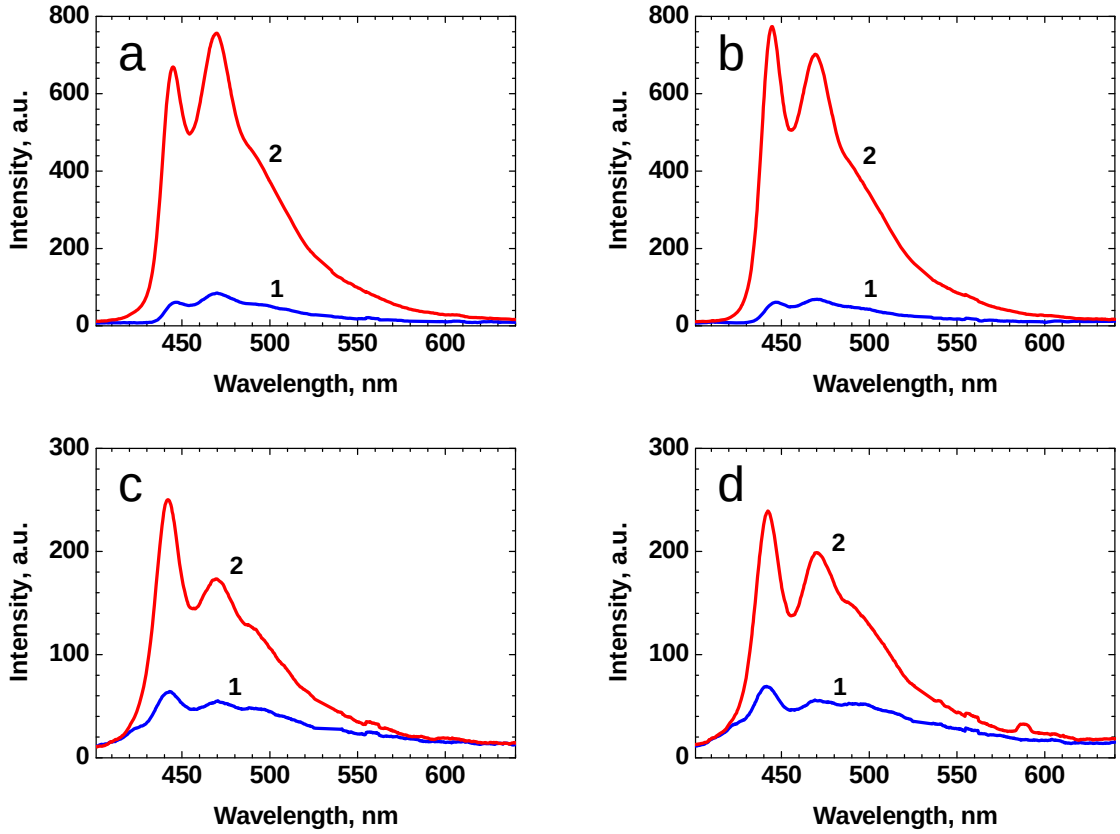

Figure 3-9 Fluorescence (1) and superfluorescence (2) spectra of **IV** in polystyrene films with thicknesses: 85 μm (a), 50 μm (b), 15 μm (c), and 5 μm (d) under 355 nm longitudinal pumping.

3.4 Experimental Section

*3.4.1 Synthesis of probe **IV***

2-(5-Bromothiophen-2-yl)benzothiazole **1** and 2,7-dibromo-9,9-didecyl-9H-fluorene **6** were prepared as described in the literature.[*27, 28*] Microwave-facilitated reactions were carried out under N_2 in a CEM Discover microwave reactor in 10 mL closed vessels, programmed at a maximum temperature of 130 °C, maximum pressure of 100 psi, and maximum power of 100 Watts. All reagents and solvents were used as received from commercial suppliers unless otherwise noted. ^{1}H and ^{13}C NMR spectra were recorded in $CDCl_3$ on a Varian NMR spectrometer at 500 and 125 MHz, respectively. Elemental analyses were performed by Atlantic Microlab, Inc.

Synthesis of 4-(5-(benzothiazol-2-yl)thiophen-2-yl)-2-methylbut-3-yn-2-ol (7): 2-(5-Bromothiophen-2-yl)benzothiazole **2** (200 mg, 0.67 mmol), 2-methyl-3-butyn-2-ol (170 mg, 2.02 mmol), $Pd(PPh_3)_2Cl_2$ (19 mg, 0.027 mmol) and CuI (5 mg, 0.027 mmol) were dissolved in a 1:4 mixture of Et_3N:toluene (5 mL). The mixture was either heated under reflux for 12 h or irradiated by microwave for 2 min, at which time it was determined by TLC that the reaction was completed. The mixture was filtered through a celite plug, and purified by column chromatography using hexanes:EtOAc (1:1) to yield 192 mg (96%) of pale yellow solid by either method; m.p. 164-165 °C. ^{1}H NMR (500 MHz, $CDCl_3$) δ8.02 (d, *J*=8.04Hz, 1H, Ph-H), 7.85 (d, *J*=7.87Hz, 1H, Ph-H), 7.50 (d, *J*=3.95 Hz, 1H, Thy-H), 7.47 (m, 1H, Ph-H), 7.38 (m, 1H, Ph-H), 7.18 (d, *J*=3.95 Hz, 1H, Thy-H), 2.11 (s, 1H, -OH), 1.64 (s, 6H, CH_3). ^{13}C NMR (125 MHz, $CDCl_3$) δ 160.4, 153.6, 137.9, 134.7, 132.9, 128.3, 126.4, 125.4, 123.1, 121.5, 121.4, 100.2, 75.2,

65.8, 31.3.Anal. Calcd for $C_{16}H_{13}NOS_2$: C, 64.18; H, 4.38; N, 4.68. Found: C, 64.10; H, 4.33; N, 4.64.

Synthesis of 2-(5-ethynylthiophen-2-yl)benzothiazole (8): 4-(5-(Benzothiazol-2-yl)thiophen-2-yl)-2-methylbut-3-yn-2-ol **7** (300 mg, 1.0 mmol) and KOH (300 mg, 5.3 mmol) were heated either under reflux for 2 h or under microwave irradiation for 8 min. The mixture was filtered, and purified by column chromatography using hexanes to yield 180 mg (75%) by conventional heating or 236 mg (98%) via microwave of pale yellow solid; m.p. 117-118 °C. ^{1}H NMR (500 MHz, $CDCl_3$) δ 8.03 (d, *J*=8.21Hz, 1H, Ph-H), 7.86 (d, *J*=8.21Hz, 1H, Ph-H), 7.51 (d, *J*=3.94 Hz, 1H, Thy-H), 7.48 (m, 1H, Ph-H), 7.39 (m, 1H, Ph-H), 7.28 (d, *J*=3.94 Hz, 1H, Thy-H), 3.50 (s, 1H, C≡C-H). ^{13}C NMR (125 MHz, $CDCl_3$) δı60.2, 153.6, 138.5, 134.8, 133.9, 133.7, 127.8, 126.5, 125.4, 123.2, 121.6, 84.0, 76.5. Anal. Calcd for $C_{13}H_7NS_2$: C, 64.70; H, 2.92; N, 5.80. Found: C, 64.64; H, 2.91; N, 5.75.

Synthesis of 2,2'-(5,5'-(9,9-didecyl-9H-fluorene-2,7-diyl)bis(ethyne-2,1-diyl)bis(thiophene-5,2-diyl))dibenzothiazole (IV):[*52*] 2,7-Bibromo-9,9-didecyl-9H-fluorene **6** (300 mg, 0.50 mmol), 2-(5-ethynylthiophen-2-yl)benzothiazole **8** (263 mg, 1.09 mmol), $Pd(PPh_3)_2Cl_2$ (30 mg, 0.04 mmol), and CuI (8 mg, 0.04 mmol) were dissolved in a 1:4 mixture of Et_3N:toluene (5 mL). The mixture was heated under reflux for 12 h or by microwave for 1 h. The mixture was filtered through a celite plug and purified by column chromatography using hexanes:EtOAc (10:1) to yield 252 mg (55%) of a yellow solid by conventional heating and 298 mg (65%) when microwave irradiation was used; m.p. 74.0-75.5 °C.^{1}H NMR (500 MHz, $CDCl_3$) δ 8.04 (dd, *J*=8.09 Hz, *J*=0.54 Hz, 2H, Ph-H), 7.87 (dd, *J*=8.04 Hz, *J*=0.53 Hz, 2H, Ph-H), 7.70

(d, *J*=7.83 Hz,2H, Ph-H), 7.57 (d, J=3.89 Hz, 1H, Thy-H), 7.55 (m, 2H, Ph-H), 7.53 (m, 2H, Ph-H), 7.49 (m, 2H, Ph-H), 7.39 (m, 2H, Ph-H), 7.31 (d, J=3.89 Hz, 1H, Thy-H), 2.00 (m, 4H, CH_2), 1.15 (m, 28H, CH_2), 0.84 (t, *J*=6.96 Hz, 6H, CH_3), 0.61 (m, 4H, CH_2). ^{13}C NMR (125 MHz, $CDCl_3$) δ 160.5, 153.7, 151.3, 141.1, 138.0, 134.7, 132.6, 130.8, 128.4, 127.1, 126.6, 125.9, 125.5, 123.1, 121.5, 121.3, 120.2, 97.0, 82.9, 55.4, 40.3, 31.9, 30.0, 29.6, 29.5, 29.3, 29.3, 23.8, 22.7, 14.1. Anal. Calcd for $C_{59}H_{60}N_2S_4$: C, 76.58; H, 6.54; N, 3.03. Found: C, 76.79; H, 6.75; N, 2.79.

3.4.2 Linear photophysical characterization and one-photon bioimaging

The steady-state linear spectral data, fluorescence quantum yields, and lifetimes of **1** were measured in hexane, cyclohexane, toluene, tetrahydrofuran (THF), dichloromethane (DCM), dimethylsulfoxide (DMSO), acetonitrile (ACN), and an aqueous mixture (95 wt% water and 5 wt% DMSO) at room temperature. All solvents were of spectroscopic grade, received from commercial sources, and used without further purification. One-photon absorption spectra of **IV** were obtained with an Agilent 8453 UV–visible spectrophotometer using quartz cuvettes with different path lengths (0.01, 0.1, 1.0 and 10 mm) for a broad range of molecular concentrations 10^{-2} M $\leq C \leq 10^{-6}$ M. The steady-state fluorescence and excitation anisotropy spectra were measured with a PTI QuantaMaster spectrofluorimeter, in 10 mm spectrofluorometric quartz cuvettes for low concentration solutions $C \leq 10^{-6}$ M. All experimentally registered fluorescence spectra were corrected for the spectral responsivity of the PTI detection system. The excitation anisotropy spectra of **IV** were obtained in the L-format configuration geometry,[*67*] with extraction of pure solvent emission and scattered light. Fluorescence quantum yields, Φ, of **IV** at low concentration were determined by a standard relative method with 9,10

diphenylanthracene in cyclohexane as a reference compound.[*67*] The values of fluorescence lifetimes of **IV**, τ, were obtained with a time-correlated single photon counting system PicoHarp 300 under linear polarized (oriented by the magic angle) femtosecond excitation, with time resolution ≈ 80 ps. The values of τ were obtained through the best tail fitting.

Epifluorescence one-photon fluorescence images were obtained using inverted microscope (Olympus IX70) equipped with a QImaging cooled CCD (Model Retiga EXi) and excitation mercury lamp 100 W and an Olympus IX81 DSU equipped with a Hammamatsu EM-CCD C9100. In order to improve the fluorescence background-to-image ratios a customized filter cube (Ex 377/50, DM 409, Em 460/50) was used for the one-photon fluorescence images. The specifications of the filter cube were tailored to match the excitation and emission of **IV**.

3.4.3 Cell culture and incubation

HCT 116 cell were cultured in DMEM, supplemented with 10% FBS, and 1% penicillin, 1% streptomycin, at 37 °C, under 5% CO_2 environment. N° 1 round 12 mm coverslips were treated with poly-D-lysine, to improve cell adhesion, and washed (3x) with PBS buffer solution. The treated cover slips were placed in 24-well plates and 80,000 cells/well were seeded and incubated at the same conditions as indicated above until 75-85% confluency was reached on the coverslips. From a 3.03 x 10^{-4} M stock solution of Pluronic 127 encapsulated probe **IV**, a series of 0.1, 1, 10, 25, and 50 μM solutions in culture media were prepared, all containing 75 nM of Lysotracker™ Red (Invitrogen). These solutions were used to incubate the cells for 3 h. The dye solutions were extracted and the coverslipped cells were washed abundantly with PBS (4x).

Cell fixing and mounting: Cells were fixed with 3.7% solution of paraformaldehyde in pH=7.4 PBS buffer for 10 min. The fixing agent was extracted and washed (2x) with PBS. To reduce autofluorescence, a fresh solution of $NaBH_4$ (1 mg/mL) in pH=8 PBS buffer was used to treat the fixed cells (2x). The coverslipped cells were then washed with buffer PBS (2x) and mounted on microscope slides using Prolong Gold (Invitrogen) as mounting media.

3.4.4 Cell viability

Cell viability was assessed with CellTiter® 96 AQ (Promega). HCT 116 cells were seeded ($5x10^3$ cells/well) in a 96 well plate and incubated for 24 h in 90 μL of DMEM (Invitrogen) without phenol red, supplemented with 10% FBS (Atlanta Biologicals), and 1% penicillin-streptomycin. The cells were incubated for an additional 24 h with 60, 50, 25, 10, and 1 μM solutions of Pluronic® K 127-encapsulated probe **IV** in FBS complemented (10%) culture media. Then 20 μM of the CellTiter® 96 AQ reagent was added into each well and subsequently incubated for another 4 h, 37 °C, after which the respective absorbance values were read on a SpectraMax M5 plate reader (Molecular Devices) at 490 nm to determine the relative amount of formazan produced. [*75*] Cell viability % was calculated by the following expression:

$$Cell \quad viability(\%) = \frac{Abs^{S}_{490nm} - Abs^{B}_{490nm}}{Abs^{C}_{490nm} - Abs^{B2}_{490nm}} x100\% \qquad \text{(iii)}$$

where Abs^{s}_{490nm} is the absorbance of the cells at the different concentrations of micelle encapsulated probe **IV**, Abs^{B}_{490nm} is the absorbance of a cell-free well containing only encapsulated probe **IV** at the concentrations that were studied, Abs^{C}_{490nm} is the absorbance of

cells incubated in media without any other component, and Abs^{B2}_{490nm} is the absorbance of a cell-free well.

The photochemical decomposition quantum yields of **IV**, Φ_{Ph}, were determined in organic solvents and aqueous mixture by the absorption method,[*71*] based on precise measurements of kinetic changes in the corresponding absorption spectra during one-photon UV irradiation (405 nm diode laser with CW irradiance ~ 30 mW/cm^2). In this case, the values of Φ_{Ph} can be expressed by the equation:

$$\Phi_{Ph} = \frac{[D(\lambda,0) - D(\lambda,t_{ir})] \cdot N_A}{10^3 \cdot \varepsilon(\lambda) \cdot I(\lambda) \cdot \int_0^{t_{ir}} [1 - 10^{-D(\lambda,t)}] dt} \quad , \qquad \text{(v)}$$

where $D(\lambda,t)$, N_A, $\varepsilon(\lambda)$, $I(\lambda)$ and t_{ir} are the optical density, Avogadro's number, extinction coefficient, laser irradiance, and total irradiation time, respectively. A comprehensive description of this methodology was described previously.[*71*]

3.4.5 Two-photon spectral and bioimaging measurements

2PA spectra of probe **IV** were measured over a broad spectral region in spectroscopic grade cyclohexane, DMSO, and aqueous media using a typical 2PF method relative to Rhodamine B in methanol as a standard.[*53*] The 2PF technique employed a PTI QuantaMaster spectrofluorimeter coupled with a femtosecond Clark-MXR CPA-2010 laser that pumped an optical parametric generator/amplifiers (TOPAS) with a 600-950 nm tuning range, pulse duration ≈ 140 fs (FWHM), 1 kHz repetition rate, and pulse energies up to ~ 0.15 μJ. Two-photon fluorescence measurements were performed in 10 mm fluorometric quartz cuvettes with dye

concentrations ~ 10^{-5} M. The values of 2PA cross section, δ_{2PA}, were determined by the equation:[*54*]

$$\delta_{2PA}^{S} = \delta_{2PA}^{R} \cdot \frac{\langle F(t)\rangle_S \cdot C_R \cdot \Phi_R \cdot \varphi_R \cdot \langle P(t)\rangle_R^2}{\langle F(t)\rangle_R \cdot C_S \cdot \Phi_S \cdot \varphi_S \cdot \langle P(t)\rangle_S^2}\ , \qquad \text{(ii)}$$

where $\langle F(t)\rangle$, $\langle P(t)\rangle$, C, and φ are the averaged fluorescence intensity, excitation power, molecular concentration, and geometric factor, respectively. Subscripts S and R refer to the sample and reference compound. The quadratic dependence of 2PF intensity on the excitation power was determined for each excitation wavelength, λ_{ex}, while special attention was paid to verify the independence of the fluorescence quantum yield on λ_{ex}.

Two-photon fluorescence imaging was performed on a modified Olympus Fluoview FV300 laser scanning confocal microscopy system equipped with a broadband, tunable Coherent Mira Ti:sapphire laser (200 fs pulse width, 76 MHz repetition rate), pumped by a 10 W Coherent Verdi frequency doubled Nd:YAG laser. The laser was tuned and modelocked to 700 nm and used as the two-photon excitation source. The two-photon induced fluorescence was collected by a 60x microscope objective (UPLANSAPO 60x, N.A.=1.35 Olympus). A high transmittance (>95%) short-pass filter (cutoff 685 nm, Semrock) was placed in front of the PMT detector within the FV300 scanhead in order to filter off background radiation from the laser source (700 nm).

3.4.6 ESA superfluorescence and lasing measurements

The ESA spectra of **IV** were obtained in hexane, cyclohexane, toluene, DMSO, ACN, and aqueous mixtures using a pump-probe technique with a picosecond Nd:YAG laser (PL 2143 B Ekspla). The experimental setup is illustrated in Figure 3-10. A strong pump beam at λ_{ex} = 355 nm, with pulse duration, $\tau_P \approx 35$ ps, (FWHM), pulse energy, $E_P \leq 20$ μJ, and repetition rate 10 Hz, was focused into a 1 mm cuvette with dye concentration $C \sim 5 \cdot 10^{-5}$ M, to a waist radius ≈ 1.5 mm.

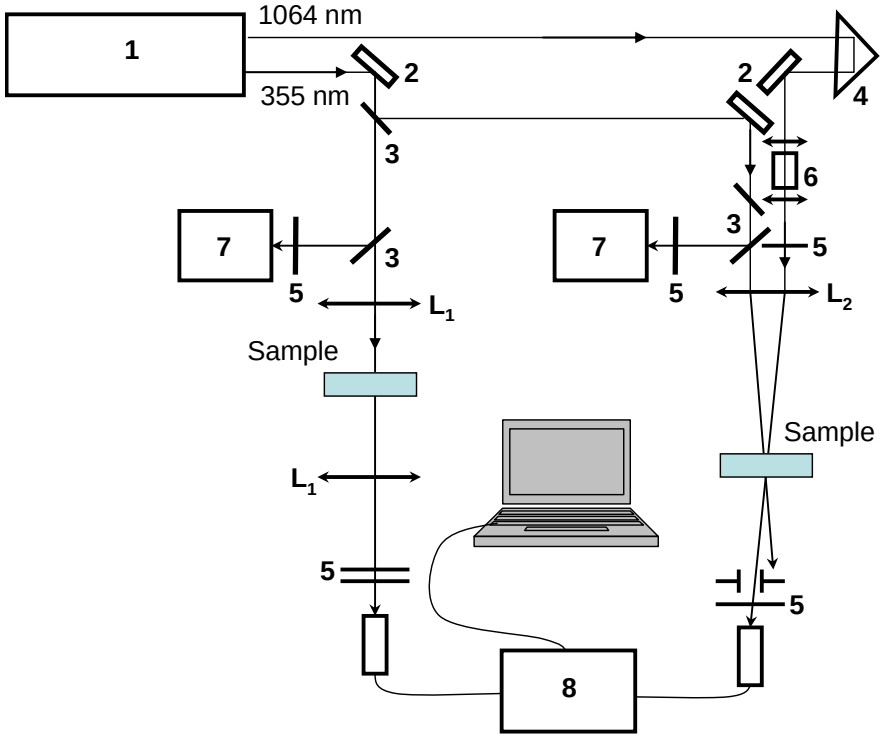

Figure 3-10 Experimental setups for ESA, superfluorescence and lasing measurements: picosecond laser (1); 100% reflection mirrors (2); beam splitters (3); delay line (4); focusing lens (L_1 - 15 cm; L_2 - 25 cm); neutral density and color filters (5); water cell (6); silicon detectors (7); spectrometer (8).

A weak pulse of white light continuum (WLC), generated by the main laser output (1064 nm) in a 10 cm path length quartz cuvette with de-ionized water,[*76*] served as the probe beam. The probe and pump beams were linearly polarized in the vertical direction and spatially overlapped inside the sample. A small delay, ~ 80 ps, was introduced between pump and probe pulses to avoid undesirable interaction. ESA spectra were determined with a Ocean Optics USB-2000 spectrometer. The suprefluorescence and lasing spectra of **IV** were measured in hexane, cyclohexane, and polystyrene matrices with dye concentration $C \sim 5 \cdot 10^{-3}$ - $5 \cdot 10^{-5}$ M, under longitudinal pumping at 355 nm (see Fig. 3-10, left channel) with pulse energy $E_P \leq 20$ μJ. Liquid solutions of **IV** were placed in 0.1, 1.0, and 10 mm quartz cells. Dye-doped polymeric samples were prepared by dissolving polystyrene in a cyclohexane solution containing **IV**, followed by solvent evaporating over 24 h. The resulting polymer films (thickness < 100 μm) were placed between high optical quality quartz plates. The position of the samples inside the focusing caustic (15 cm lens (Figure 3-10, L_1)) was chosen to reach the highest efficiency of the investigated effects. Measurements were performed with the same USB-2000 spectrometer. It should be mentioned, that laser oscillation was observed in the direction perpendicular to the exit surfaces of the quartz cells and served as a resonator, while superfluorescence emission occurred in the direction of the pumping beam. This allowed us to separate the observed superfluorescence and lasing phenomena.

3.5 Conclusions

The synthesis, linear photophysical, and nonlinear optical properties of a new fluorene-based probe **IV** with alkynyl bonds in the chromophore system were investigated in organic

solvents and aqueous solution as a potential fluorescent label for two-photon bioimaging applications. The shape and maximum extinction coefficients of the absorption spectra of **IV** were independent of solvent polarity and no molecular aggregation effects were observed in the range of concentrations up to 10^{-2} M. The fluorescence spectra of relatively symmetrical probe **IV** were independent of λ_{ex} and exhibited noticeable solvatochromic behavior with substantial changes in their shape. The values of the fluorescence quantum yields were sufficiently high in organic media ($\Phi \approx 0.7\text{-}0.8$) and independent of solvent polarity, while single-exponential fluorescence decays were observed. In contrast, an aqueous solution of **IV** exhibited a dramatic decrease in quantum yield accompanied by a bi-exponential decay in fluorescence emission.

The excitation anisotropy spectra revealed a complicated nature of the main long wavelength absorption band of **IV**, consisting of more than one electronic transition. A weak dependence of the fundamental anisotropy r_0 on the solvent properties and nearly constant effective rotational molecular volume V in all investigated organic solvents were shown. Importantly, a high level of photostability ($\Phi_{Ph} \sim (3 - 7)\cdot 10^{-6}$) was observed for probe **IV** under one-photon excitation conditions in several of the investigated solvents.

The 2PA spectra of **IV** were obtained under femtosecond excitation over a broad spectral range (~ 640-920 nm) by a 2PF method. 2PA efficiency was characterized by the one well defined two-photon allowed absorption band at 680-720 nm with corresponding maxima cross sections $\delta_{2PA} \approx$ 800-900 GM.

The potential that probe **IV** has for 2PFM is based on its promising linear and nonlinear photophysical properties, on the excellent contrast obtained with it both in one- and two-photon fluorescence micrographs, and its selectivity to cell lysosomes of HCT 116 cells when encapsulated in Pluronic® F-127. The simplicity of micelle encapsulation and straightforward synthesis make it a probe that can be promptly prepared by the methods described. Furthermore, 2PFM facilitated the observation of cell features that were not entirely resolved in the epifluorescence counterpart. This probe is certainly amenable to other applications in selective imaging of tissue, where further functionalization of the Pluronic® 127 (with a peptide or an antibody for example) could be employed for *in vitro* or *in vivo* tissue 2PFM imaging.

The ESA spectra revealed the possibility of potential light amplification in nonpolar solutions of **IV**. Efficient lasing and superfluorescence effects were shown in hexane, cyclohexane, and polystyrene films under the longitudinal pumping at 355 nm. A possibility for amplification was shown for **IV** in thin polymer films up to 5 μm thickness, which can be used for the development of new fluorescent labels with increased spectral brightness. Based on these results, the new probe **IV**, with its high fluorescence quantum yield, 2PA cross section, photochemical stability, and efficient superfluorescence properties is a promising fluorescent label for two-photon bioimaging applications.

CHAPTER 4. SYNTHESIS AND BIOIMAGING OF NEW FLUORESCENT TWO-PHOTON ABSORBING BIOCONJUGATES SELECTIVE TOWARDS VASCULAR ENDOTHELIAL GROWTH FACTOR RECEPTOR 2

4.1 Abstract

We report the synthesis and characterization of two amine reactive fluorescent dyes with good two-photon absorption (2PA) properties. Bioconjugation of these dyes with a specific antibody and bioimaging of these new materials demonstrated their selectivity towards the vascular endothelial growth factor receptor 2 (VEGFR-2) in cells expressing this receptor and in tissue. In addition, the concentration of dye required for incubation of these bioconjugates is in the picomolar domain, and the fluorescence response obtained from one and 2PA imaging demonstrated high quality and contrast at these low concentrations. We also describe how these new systems offer several advantages compared to previously reported systems.

4.2 Introduction

The development of methodologies and materials to image cancer tumors is an area of increasing interest in the chemical and biomedical communities. The conjugation of fluorescent dyes with antibodies and peptides, used as targeting vectors, is a common strategy to image tumors. In the interest of following tumor growth and drug efficacy, researchers have targeted vasculature instead of the tumor itself to determine tumor size, morphology, and characteristics by different technologies (immunohistochemistry, fluorescence microscopy, photoacoustic microscopy, etc).[*77-81*]

Angiogenesis is the process of forming new blood vessels to support tissue growth. This fundamental physiological process promotes embryonic development, tissue repair, and fertility, although it also promotes chronic inflammation, tumor growth, and tumor metastasis.[*82*] Tumors in particular rely on angiogenesis for their continued growth. It has been demonstrated that solid tumors will not grow larger than 2–3 mm in diameter in the absence of new blood vessels and require angiogenesis to form metastases.[*83*]

Vascular endothelial growth factor (VEGF) is a protein that stimulates vascular endothelial cell growth, survival, and proliferation. Thus, VEGF facilitates survival of existing vessels, contributes to vascular abnormalities that may impede effective delivery of antitumor compounds, and stimulates new vessel growth.[*84-86*]

The VEGF family consists of five members (VEGF-A, VEGF-B, VEGF-C, VEGF-D, and placental growth factor), which show different affinities for one of the three VEGF tyrosine kinase receptors (VEGFR-1, VEGFR-2 and VEGFR-3). VEGFR-1 and VEGFR-2 are expressed in vascular endothelial cells. Moreover, there is evidence that VEGFR-2 is the major mediator of VEGF-driven responses in endothelial cells and it has been considered to be crucial in angiogenic processes.[*86*]

In 2005, Backer and coworkers reported the use of a boronated polyamidoamine dendrimer able to target selectively vasculature by means of a VEGF containing bioconjugate that directed the dendrimer to a specific receptor (VEGFR). The incorporation of a near infrared (NIR) Cy5 dye was employed to track the bioconjugate. The targeting of tumor vasculature endothelial cells, rather than the tumor itself, was achieved since endothelial cells in tumor

neurovasculature express a significantly greater number of VEGFR-2 when compared to quiescent endothelial cells.[*87*] More recent work has demonstrated the use of VEGF bioconjugates containing NIR fluorescent dyes to study the possible expression of VEGFRs in bladder inflammation.[*88*]

The use of 2PA absorbing fluorophores offers several advantages over their one-photon NIR counterparts. In the nonlinear absorption process the fluorescence emission is proportional to the square of the intensity of the incident light providing the system with numerous intrinsic advantages for instance deeper penetration, more confined excitation areas, less scattering and minimal photodamage outside of the focal point.[*31*]

The scientific community has access to a wealth of efficient 1PA fluorescent dyes with emissions that range from the UV to the IR and that are commercially available. However, there is a need to develop new dyes with high fluorescence quantum yields and 2PA cross sections that meet the high photostability demands that two-photon fluorescence microscopy (2PFM) imposes. We have previously described a strategy to create 2PA amine reactive probes that can be conjugated to proteins or antibodies.[*8, 34*] In this work, we introduce the synthesis and characterization of two new fluorescent amine reactive dyes based on a fluorenyl core. With these probes, VEGFR-2 antibody bioconjugates (anti-VEGFR-2) were prepared to selectively bind the VEGFR-2 in cells that overexpress this specific receptor. In this approach, the integration of an antibody to the VEGFR-2, instead of the VEGF itself, as a targeting strategy was achieved. Further studies including the incorporation of VEGF with a similar fluorophores will be done in the future and compared with the current results.

The fluorophore design was based on a small series of efficient 2PA dyes that were recently reported.[*52*] The architecture of the fluorophores involved a fluorenyl core flanked by a triple bond- thiophene bridge (π) that led to an electron withdrawing group on one side (A). On the other, the fluorenyl core was tethered to the anti-VEGFR-2 that served as a donor (D). This resulted in systems that have a D-π-A dipolar structure.

4.3 Results and Discussion

4.3.1 Synthesis of new fluorescent probes and preparation of bioconjugates

The synthesis of the 2PA amine reactive probes **16** and **20** was achieved in short reaction times and high yields by using microwave-assisted synthesis, as illustrated in Scheme 4-1 and Scheme 4-2, respectively. Briefly, fluorene derivative **13** was coupled to previously reported intermediates **2** and **8** either by Stille or Sonogashira coupling to yield nitro derivatives **14** and 1**8**. These nitro derivatives were reduced to the respective amine intermediates **15** and **19**.[*19*] Transformation of these amines into the corresponding isothiocyanates **16** and **20** was performed by a method reported previously by our group. [*8, 34, 35*]

Scheme 4-1

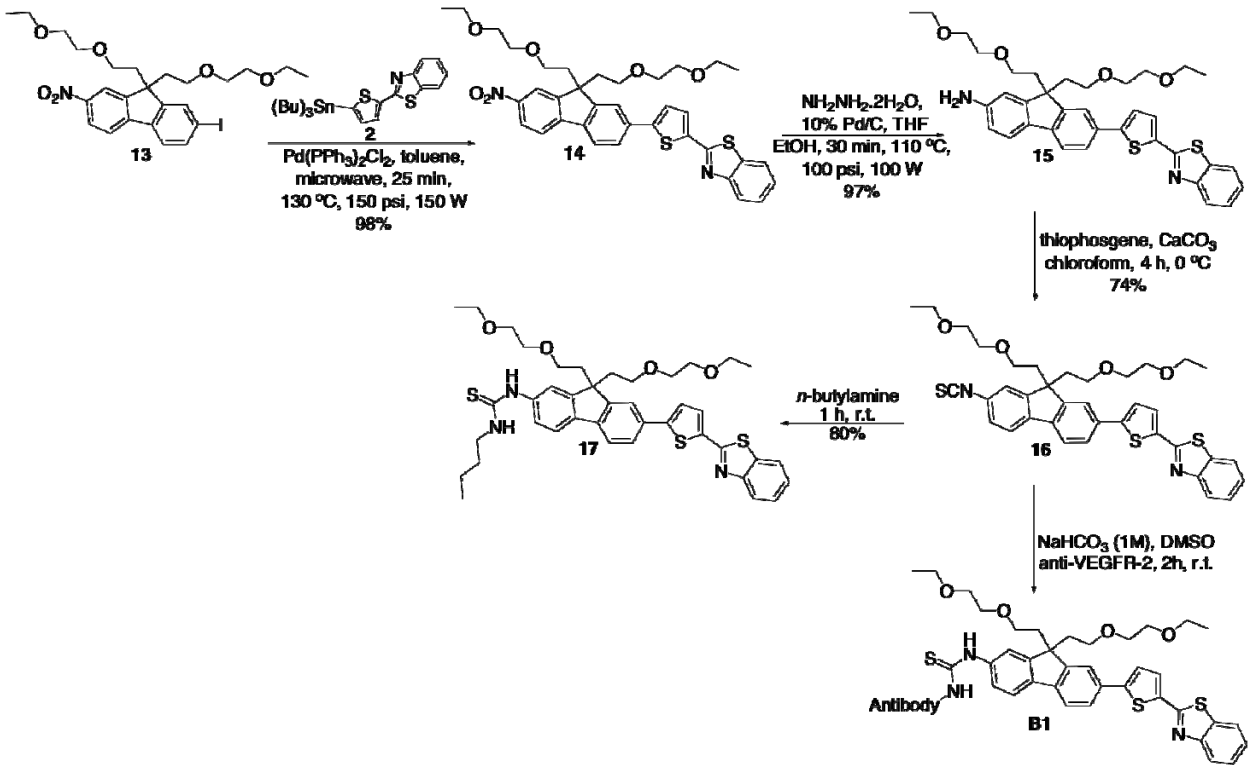

Scheme 4-2

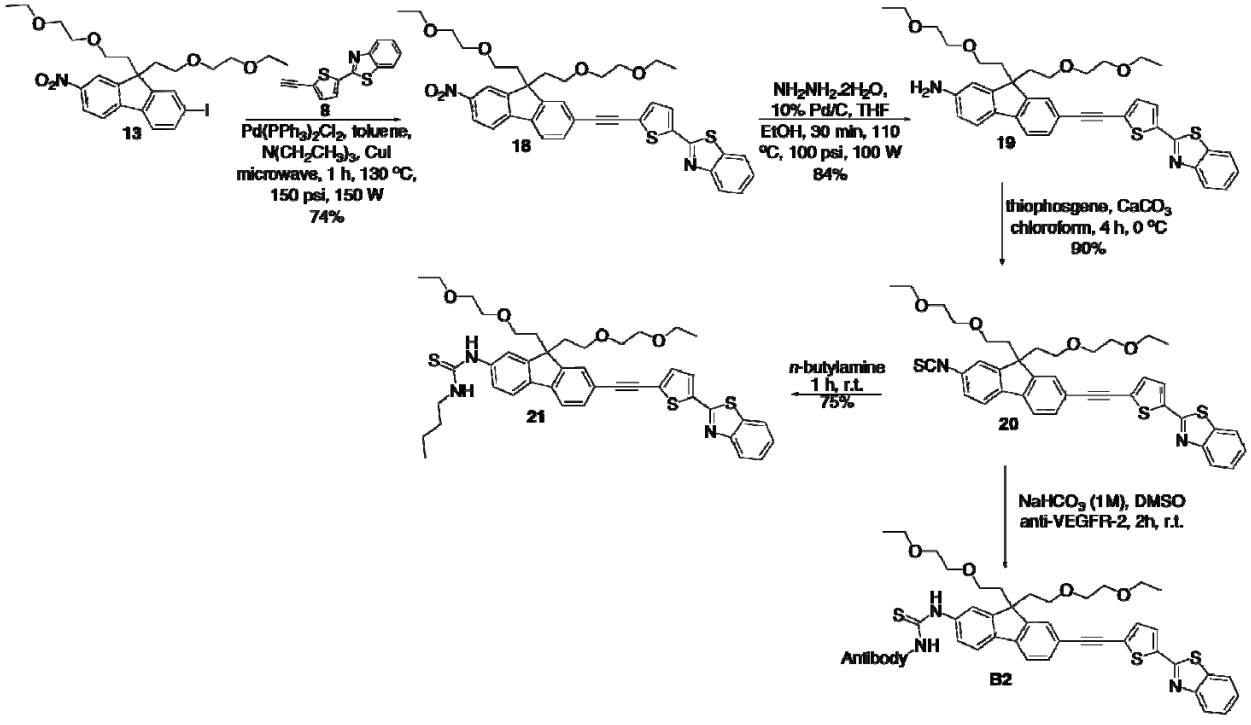

In order to better understand the scope and properties of these probes, conjugation with *n*-butylamine was performed to generate model compounds **17** and **21** that would closely resemble the optical properties of the bioconjugates. Once obtained, amine reactive probes and models were chemically and photophysically characterized.

2PA isothiocyanates **16** and **20** were conjugated to anti-VEGFR-2 for 2 hours at room temperature in a molar proportion 10:1 dye: protein. Purification was achieved by using a commercially available, Sephadex packed, GPC column.

4.3.1 Photophysical properties

Photophysical characterization was performed for amine reactive probes **16** and **20** and model compounds **17** and **21**. Absorption and emission spectra of these compounds were collected at room temperature using DMSO solutions of the compounds at concentrations of approximately 10^{-6} M and are shown in Figure 4-1.

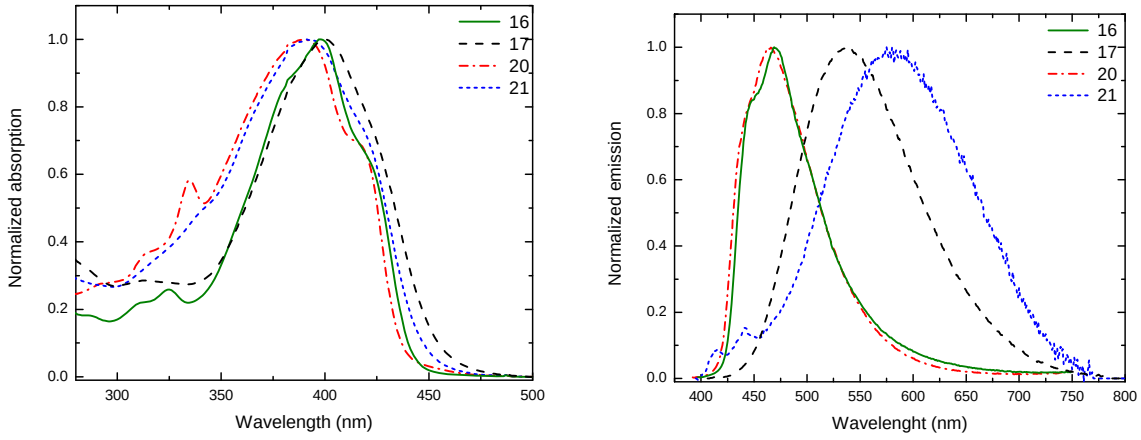

Figure 4-1 Normalized absorption (left) and fluorescence (right) spectra of compounds **16**, **17**, **20** and **21** in DMSO. Absorption and emission spectra were collected at room temperature using DMSO solutions with optical density of ~0.1 (approximately 10^{-6} M) without degassing the solutions. Emission was collected by exciting samples at their λ^{abs}_{max} value.

Table 4-1 reveals that there are intense absorption maxima for amine reactive probes and model compounds located between 390-400 nm, whereas there was a red shift in the emission maxima when the dyes were conjugated to *n*-butylamine. In addition, a larger Stokes shift was observed for the more conjugated model compound **21**.

Table 4-1 Photophysical characterization of compounds 16, 17, 20 and 21 in DMSO.

Compound	λ^{abs}_{max}, nm	λ^{em}_{max}, nm	Φ^{1}	$\varepsilon^{max}\,10^{-3}$, $M^{-1}.cm^{-1}$	τ, ns
16	397±1	469±1	0.80±0.05	61	0.95
17	400±1	583±1	1.00±0.05	53	2.00
20	391±1	466±1	0.70±0.05	60	0.85
21	391±1	580±1	0.20±0.05	54	0.79

[1]Fluorescence quantum yield measured relative to 9,10-diphenylanthracene in cyclohexane.

In our previous studies, we observed that the presence of isothiocyanate groups in the fluorene system plays an important role by quenching the fluorescence of the dye, possibly by inducing intersystem crossing and allowing the molecule to relax by other pathways rather than by fluorescence, but the fluorescence seems to be restored (switch on) upon conjugation.[*8, 34*] Interestingly, in the case of these new dyes, this effect was not observed. Although there was not fluorescence quenching because of the presence of the SCN group, for the first dye **16**, the quantum yield increased upon conjugation, as expected. However, for the more conjugated dye **20**, there was a significant decrease in the fluorescence quantum yield after conjugation with *n*-butylamine. (Table 4-1). This important result suggests that luminescent properties cannot be predicted based only on similarities between structures.

Lifetimes for these series of compounds were also measured in DMSO at concentrations of approximately 10^{-6} M, as shown in Table 4-1. A difference of 1.2 ns was found between the fluorescence lifetime of models **17** and **21**. Even though they have similar fluorescence maxima, with this difference in lifetime it should be possible to distinguish between bioconjugates containing these dyes and different antibodies or vectors by fluorescence lifetime imaging microscopy (FLIM).

Anisotropy of samples were measured under one-photon excitation in poly-THF at concentrations of approximately 10^{-6} M; and two-photon absorption (2PA) cross section of model compounds were determined by the fluorescence method using DMSO solutions in concentrations of ca. 10^{-5} M. Rhodamine B in methanol was employed as a standard.[*53*] (Figure 4-2) Given that the selection rules are not the same for one or two photon excitation, it is not expected that the one-photon and two-photon absorption spectra look the same. Both compounds have a significant 2PA cross section value within the measured range (700-940 nm). Anisotropy spectra exhibited a constant value at wavelengths where the maxima of linear absorption were located, corresponding to the first electronic transition $S_0 \rightarrow S_1$ (one-photon allowed, two-photon forbidden transition); in this region, there is a decrease in the two-photon cross section value. Anisotropy begins to decrease below 350 nm, reaching a minimum at around 325 nm leading to a second "plateau"; this corresponds to the second electronic transition $S_0 \rightarrow S_n$, which is two-photon allowed according the symmetry selection rules, thus, a high value of cross section is obtained at this excitation wavelength.

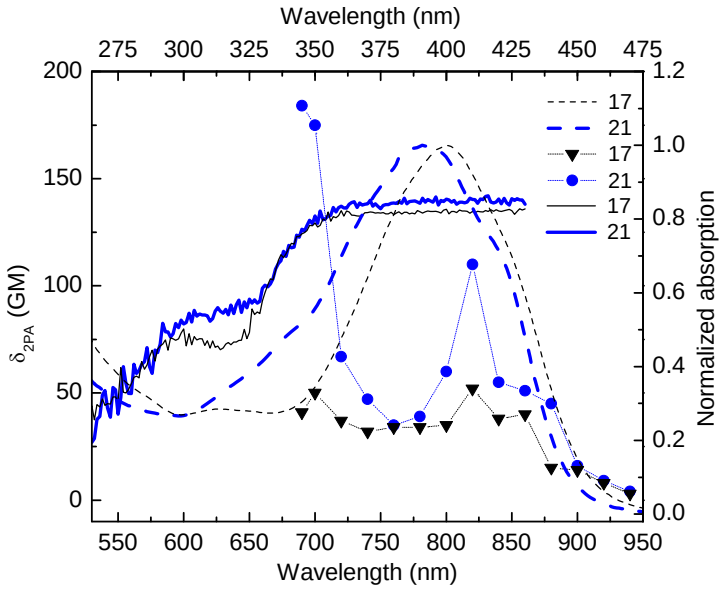

Figure 4-2 Normalized absorption (dash lines), two-photon cross section (symbols and lines) and anisotropy (solid lines) of model compounds **17** (black) and **21** (blue).

Another maximum in the 2PA spectra was observed at around 820 nm for both model compounds. This transition correlated nicely to that responsible for the shoulder located at around 410 nm in the linear absorption spectrum. These dyes can be excited by 2PA at wavelengths as long as 850-900 nm and the fluorescence emission peaks at 580 nm extends ± 190 nm; these dyes have great versatility because they can be efficiently excited by a wide range of wavelengths and their emission is in the far red to NIR range.

After bioconjugation of isothiocyanates with the selected antibody and purification by gel permeation chromatography, fractions containing the bioconjugates were analyzed by UV-vis spectrometry. Figure 4-3 shows the absorption spectrum of isothiocyanate **20** (red) and biconjugate **B2** (green). The concentration of the protein in the bioconjugate was determined to be around 50 μM and the degree of labeling (DOL) was found to be 2. The concentration of the

dye in the purified solution was estimated to be around 0.4 μM by using the extinction coefficient of model compounds. Preparation of bioconjugates following this method was performed more than once to evaluate the reproducibility of the method; repeated preparation of **B1** and **B2** generated these same results consistently.

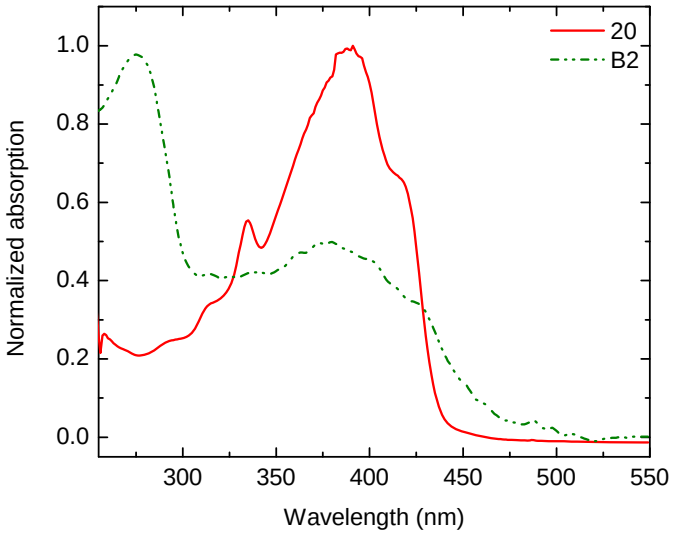

Figure 4-3 Normalized absorption of isothiocyanate **20** (red, solid line) and bioconjugate **B2** (green, dash-dot-dot line).

4.3.2 Cell imaging

To study the scope of the new bioconjugates, probes **B1** and **B2** were incubated with porcine aortic endothelial (PAE-KDR) cells that express VEGFR-2, as it is known that this receptor is found in higher concentrations when angiogenesis is occurring. Preliminary studies demonstrated that fluorescence images obtained with **B2** were superior to those obtained with **B1**; although the latter has a higher quantum yield, but its lower cross section at 700 nm, where the imaging was performed, resulted in lower contrast images (not shown). Thus, due to the

excellent preliminary results obtained with **B2**, this bioconjugate was used for the subsequent experiments. PAE-KDR cells were incubated with a commercially available fluorescent bioconjugate containing fluorescein isothiocyanate and a monoclonal VEGFR-2 antibody, as a positive control, and our bioconjugate **B2**. After 2 h of incubation, epifluorescence micrographs of the incubated cells revealed a high degree of colocalization between the two probes (Figure 4-4).

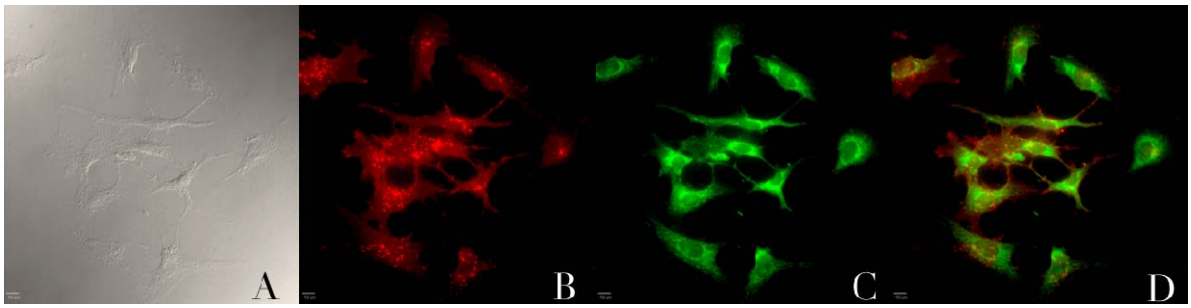

Figure 4-4 Epifluorescence Micrographs PAE-KDR: A) DIC 60x; B) monoclonal VEGR-2 antibody FITC; C) polyclonal VEGR-2 antibody Fluor B2; D) Overlay of B and C.

To examine the selectivity of bioconjugate **B2** towards the VEGFR-2, porcine aortic endothelial (PAE) cells that do not overexpress the receptor were used as a negative control. In this way, **B2** was incubated with porcine aortic endothelial (PAE) cells (control) and porcine aortic endothelial cells that express VEGFR-2 (PAE-KDR). Efficient epifluorescence and 2PA micrographs of PAE-KDR cells were obtained even at the very low concentrations that were employed (0.4 μM) (Figure 4-5).

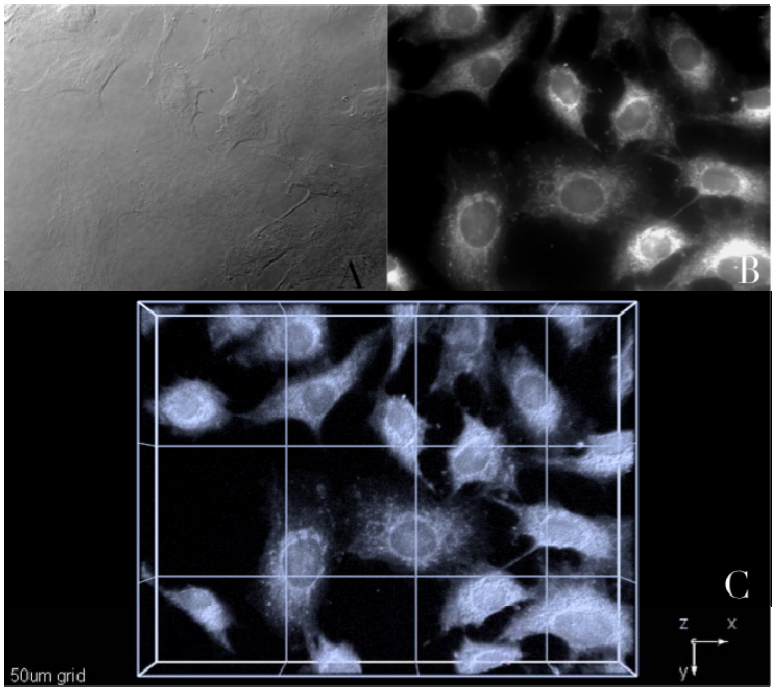

Figure 4-5 One- and two-photon fluorescence micrographs of PAE-KDR (porcine aortic endothelial cells expressing VEGFR-2) incubated with bioconjugate **B2** (≈0.4 μM, 2 h). A) DIC, B) One-photon fluorescence, C) 3D reconstruction from overlaid 2PFM images, 76 MHz, femtosecond laser 700 nm, 60x objective (NA= 1.35, Olympus). Scale: 50 μm grid.

Porcine aortic endothelial (PAE) cells that do not express the receptor incubated under similar conditions (same concentration of **B2**, same incubation time, temperature, etc) demonstrated drastically different results; very little, nonspecific fluorescence was observed in the respective micrographs (Figure 4-6). Fluorescence observed only in those cells that express the receptor suggests that the antibody provides the desired selectivity to the probe. Moreover, the higher resolution resulting from the nonlinearity of the two-photon absorption process is evidenced in Figure 4-5 when images obtained by one photon excitation (B) are compared to images obtained by two-photon excitation (C).

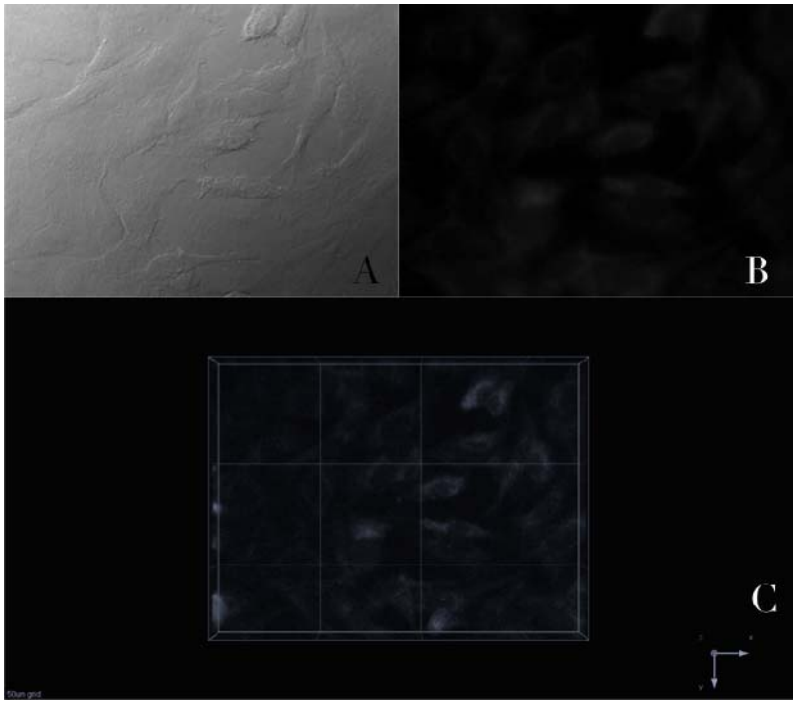

Figure 4-6 One- and two-photon fluorescence micrographs of PAE (porcine aortic endothelial cells) incubated with bioconjugate **B2** (≈0.4 μM, 2 h). A) DIC, B) One-photon fluorescence, C) 3D reconstruction from overlaid 2PFM images, 76 MHz, femtosecond laser 700 nm, 60x objective (NA= 1.35, Olympus). Scale: 50 μm grid.

4.3.3 Tissue imaging

Preliminary tissue staining with bioconjugate **B2** was performed on mouse embryonic tissue sections. Mouse embryo (2 days) tissue sections (200 μm) were incubated with bioconjugate **B2** and epifluorescence micrographs revealed vasculature specificity within the tissue (Figure 4-7 D). Negative control of a neighboring tissue section only showed what appeared to be autofluorescence of white blood cells (as proven by H&E staining), but no vessels were seen (Figure 4-7 B).

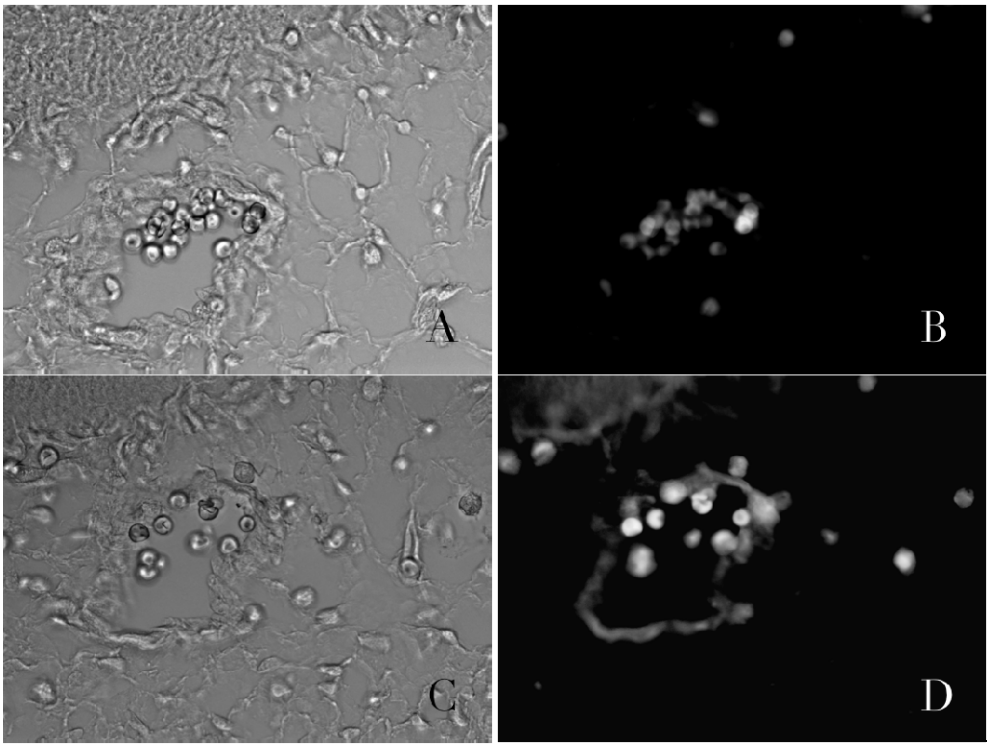

Figure 4-7 Brightfield of mouse embryo negative control (A) and polyclonal VEGR-2 antibody fluorene bioconjugate **B2** (C). Epifluorescence of negative control (B) and polyclonal VEGR-2 antibody fluorene bioconjugate **B2** (D).

Furthermore, 2PFM of this same tissue section (Figure 4-8) indicate that this system is truly promising for imaging nascent micro vessels in tissue by this nonlinear technique. The penetration and reduced scattering that is characteristic of 2PFM will more than likely be successful in intratumor 2PFM of vasculature in live mice models. Work is currently underway in our lab for introducing this dye in Lewis Lung Carcinoma explants in mice and measuring microvessel density in these tumors *ex vivo* and through a dorsal skinfold chamber (*in vivo*).[*78, 89*]

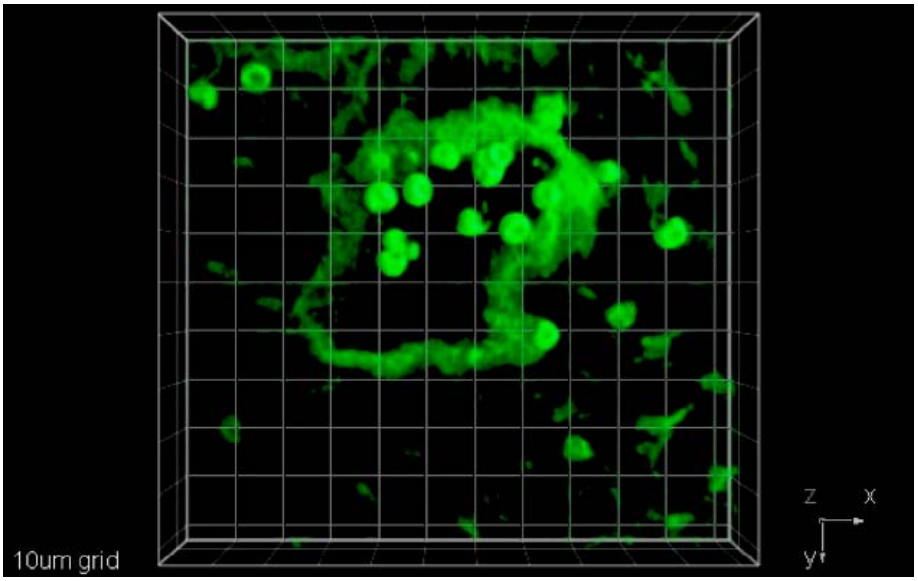

Figure 4-8 Two-photon upconverted fluorescence polyclonal VEGR-2 antibody fluorene bioconjugate **B2.** Excitation 700 nm (20 mW).

4.4 Experimental Section

4.4.1 Materials and methods

Key intermediates **13**, **2** and **8** were prepared as described in the literature.[*34, 52*] All the reactions were carried out under N_2. Microwave assisted procedures were carried out in a CEM Discover unit microwave in 10 mL closed vessels, temperature, pressure and power were programmed at a maximum value, depending on the reaction. All other reagents and solvents were used as received from commercial suppliers. ^{1}H and ^{13}C NMR spectra were recorded in $CDCl_3$ on a Varian NMR spectrometer at 500 and 125 MHz, respectively. Mass analyses (APCI, atmospheric pressure chemical ionization) were performed at University of Florida. The analyses were carried out on a Finnigan LCQ - Quadrupole Ion Trap (Thermo Finnigan, San Jose, CA).

4.4.2 Synthetic procedures and characterization

Synthesis of 2-(5-(9,9-bis(2-(2-ethoxyethoxy)ethyl)-7-nitro-9H-fluoren-2-yl)thiophen-2-yl)benzothiazole (14): In a 10 mL vessel, under nitrogen, 9,9-bis(2-(2-ethoxyethoxy)ethyl)-2-iodo-7-nitro-9H-fluorene **13** (200 mg, 0.335 mmol), 2-(5-(tributylstannyl)thiophen-2-yl)benzothiazole **2** (207 mg, 0.408 mmol) and $Pd(PPh_3)_2Cl_2$ (6 mg, 0.008 mmol) were dissolved in toluene (2 mL). The mixture was heated in the microwave for 25 min, at 130 ^oC, 150 psi and 150W, filtered through a celite plug, and purified by column chromatography using as a solvent a mixture of hexane:ethyl acetate (2:1) to yield 216 mg (98%) of a light orange solid. m.p. 75.7-76.5 ^oC. ^1H NMR (500 MHz, $CDCl_3$) δ 8.26-8.34 (m, 2H, Ph-H), 8.06 (d, *J*=8.06 Hz, 1H, Ph-H), 7.89 (d, *J*=8.06 Hz, 1H, Ph-H), 7.73-7.84 (m, 4H, Ph-H), 7.69 (d, *J*=3.93Hz, 1H, Thy-H), 7.49-7.52 (m, 1H, Ph-H), 7.48 (d, *J*=3.93Hz, 1H, Thy-H), 7.38-7.42 (m, 1H, Ph-H), 3.34-3.40 (m, 4H, CH_2), 3.27-3.31 (m, 4H, CH_2), 3.15-3.22 (m, 4H, CH_2), 2.79-2.93 (m, 4H, CH_2), 2.45-2.56 (m, 4H, CH_2), 1.10 (t, *J*=6.98 Hz, 6H, CH_3). ^{13}C NMR (125 MHz, $CDCl_3$) δ 161.1, 153.9, 152.1, 151.2, 147.7, 147.5, 146.3, 138.6, 137.0, 135.0, 134.8, 129.7, 126.8, 126.0, 125.6, 124.8, 123.9, 123.2, 122.2, 121.7, 121.0, 120.2, 119.3, 70.4, 69.8, 67.1, 66.8, 52.5, 39.6, 15.2. MS (APCI) *m/z* calcd $[M+H]^+$ 659.2244, found 659.2256.

Synthesis of 7-(5-(benzothiazol-2-yl)thiophen-2-yl)-9,9-bis(2-(2-ethoxyethoxy)ethyl)-9*H*-fluoren-2-amine (15): In a 10 mL vessel, under nitrogen, 2-(5-(9,9-bis(2-(2-ethoxyethoxy)ethyl)-7-nitro-9H-fluoren-2-yl)thiophen-2-yl)benzothiazole **14** (300 mg, 0.45 mmol) and 10% Pd/C (30 mg) were dissolved in a 1:1 mixture of THF:EtOH (4 mL). $NH_2NH_2.2H_2O$ (300 mg, 6.0 mmol) was added to the mixture dropwise at room temperature, and then heated in the microwave to 110 ^oC, 100 W and 100 psi for 30 min. The mixture was filtered

though a silica plug with ethyl acetate, and after removing the solvent under reduced pressure, the material was purified by column chromatography using as a solvent ethyl acetate to yield 280 mg (97%) of a dark yellow solid. m.p. 120.8-121.4 ^{o}C. ^{1}H NMR (500 MHz, $CDCl_3$) δ 8.04 (d, *J*=7.88 Hz, 1H, Ph-H), 7.86 (d, *J*=7.88 Hz, 1H, Ph-H), 7.59-7.67 (m, 3H, Ph-H Thy-H), 7.55 (d, *J*=7.69 Hz, 1H, Ph-H), 7.45-7.50 (m, 2H, Ph-H), 7.34-7.40 (m, 2H, Ph-H, Thy-H), 6.75 (d, *J*=7.99Hz, 1H, Ph-H), 6.68 (dd, *J*=7.99Hz, *J*=1.92Hz, 1H, Ph-H), 3.38-3.44 (m, 4H, CH_2), 3.33-3.37 (m, 4H, CH_2), 3.21-3.26 (m, 4H, CH_2), 2.77-2.86 (m, 4H, CH_2), 2.31-2.46 (m, 4H, CH_2), 1.13 (t, *J*=7.05 Hz, 6H, CH_3). ^{13}C NMR (125 MHz, $CDCl_3$) δ 161.3, 153.8, 151.1, 149.0, 148.8, 146.7, 141.6, 135.3, 134.6, 130.8, 130.7, 129.6, 129.6, 125.4, 125.1, 123.3, 122.8, 121.46, 121.1, 120.1, 119.0, 114.5, 109.8, 70.1, 69.7, 67.0, 66.6, 50.9, 39.9, 15.1. MS (APCI) *m/z* calcd $[M+H]^+$ 629.2502, found 629.2508.

Synthesis of 2-(5-(9,9-bis(2-(2-ethoxyethoxy)ethyl)-7-isothiocyanato-9*H*-fluoren-2-yl)thiophen-2-yl)benzothiazole (16): In a two neck round bottom flask and under nitrogen, a solution of 7-(5-(benzothiazol-2-yl)thiophen-2-yl)-9,9-bis(2-(2-ethoxyethoxy)ethyl)-9*H*-fluoren-2-amine **15** (250 mg, 0.398 mmol) in chloroform (2 mL) was combined with an aqueous solution of $CaCO_3$ (103 mg, 1.03 mmol) in an ice bath. Thiophosgene (0.042 mL, 0.44 mmol) was added to the vial dropwise while stirring the mixture and the reaction proceeded for 4 hours. After completion, a 10% HCl solution was added until the gas formation ceased. The mixture was poured into water, extracted with methylene chloride, dried over magnesium sulfate and purified by column chromatography using as a solvent a mixture of hexane:ethyl acetate (2:1) to yield 200 mg (74%) of a light orange solid. m.p. 103.2-104.0 ^{o}C. ^{1}H NMR (500 MHz, $CDCl_3$) δ 8.04 (d, *J*=8.10 Hz, 1H, Ph-H), 7.86 (d, *J*=8.10 Hz, 1H, Ph-H), 7.70-7.73 (m, 1H, Ph-H), 7.61-7.68

(m, 4H, Ph-H, Thy-H), 7.46-7.50 (m, 1H, Ph-H), 7.41 (d, 1H, *J*=4.10 Hz, Thy-H), 7.34-7.39 (m, 1H, Ph-H), 7.32 (d, *J*=1.68 Hz, 1H, Ph-H), 7.21 (dd, *J*=7.97 Hz, *J*=1.68 Hz, 1H, Ph-H), 3.36-3.42 (m, 4H, CH_2), 3.30-3.35 (m, 4H, CH_2), 3.18-3.23 (m, 4H, CH_2), 2.78-2.91 (m, 4H, CH_2), 2.38-2.47 (m, 4H, CH_2), 1.12 (t, *J*=7.11 Hz, 6H, CH_3). ^{13}C NMR (125 MHz, $CDCl_3$) δ 161.0 153.7 151.1 150.3 148.0 139.6 139.0 136.2 135.4 134.7 133.1 130.2 129.6 129.5 124.2 122.9 121.5 121.4 121.1 120.92 120.85 120.7 120.6 120.4 70.1 69.6 66.9 66.6 51.8 39.6 15.1. MS (APCI) *m/z* calcd $[M+H]^+$ 671.2066, found 671.2068. UV-vis (DMSO) λ_{max} 397 nm.

Synthesis of 1-(7-(5-(benzothiazol-2-yl)thiophen-2-yl)-9,9-bis(2-(2-ethoxyethoxy)ethyl)-9*H*-fluoren-2-yl)-3-butylthiourea (17): In a small vial under nitrogen, a mixture of 2-(5-(9,9-bis(2-(2-ethoxyethoxy)ethyl)-7-isothiocyanato-9*H*-fluoren-2-yl)thiophen-2-yl)benzothiazole **16** (56 mg, 0.083 mmol), and *n*-butylamine (0.074 mL, 1.0 mmol) at room temperature was stirred for 1 hour. The remaining amine was removed under vacuum and the residue was purified by column chromatography with hexane:ethyl acetate (1:1) to yield 50 mg (80%) of a bright yellow solid. m.p. 67.0-68.0 ^{o}C. ^{1}H NMR (500 MHz, $CDCl_3$) δ 8.04 (d, *J*=8.13 Hz, 1H, Ph-H), 7.84-7.94 (m, 2H, Ph-H, N-H), 7.67-7.73 (m, 4H, Ph-H), 7.66 (d, *J*=4.01, 1H, Thy-H), 7.47-7.52 (m, 1H, Ph-H), 7.42 (d, 1H, *J*=4.01 Hz, Thy-H), 7.35-7.40 (m, 1H, Ph-H), 7.32 (d, *J*=1.46 Hz, 1H, Ph-H), 7.21 (d, *J*=7.74 Hz, 1H, Ph-H), 6.34-6.39 (m, 1H, N-H), 3.62-3.69 (m, 2H, CH_2), 3.32-3.41 (m, 4H, CH_2), 3.24-3.30 (m, 4H, CH_2), 3.12-3.21 (m, 4H, CH_2), 2.78-2.98 (m, 4H, CH_2), 2.36-2.44 (m, 4H, CH_2), 1.57-1.65 (m, 2H, CH_2), 1.35-1.43 (m, 2H, CH_2), 1.10 (t, *J*=6.96 Hz, 6H, CH_3), 0.95 (t, *J*=7.55 Hz, 3H, CH_3). ^{13}C NMR (125 MHz, $CDCl_3$) δ 180.6 161.1 153.72 173.71 150.1 148.1 140.1 138.3 136.1 134.68 134.67 132.8 129.5 123.8 122.9 121.5 121.4 120.63 120.61 120.60 120.48 120.47 120.0 70.0 69.6 67.1 66.5 51.9 39.6 31.0

20.2, 15.1, 15.0, 13.9 MS (APCI) *m/z* calcd $[M+H]^+$ 744.2958, found 744.2952. UV-vis (DMSO) λ_{max} 400 nm.

Preparation of bioconjugate B1: A mixture containing 100 µL of antibody (1 mg/mL) and 100 µL of $NaHCO_3$ (1 M) was combined with a fresh solution of isothiocyanate **16** in DMSO in a proportion 1:10 molar protein:dye and incubated for 2 hours in the dark at room temperature. The biconjugate was purified by using disposable PD-10 desalting columns from GE equilibrated and eluted with PBS buffer 7.0 (Invitrogen). Fractions containing the bioconjugate were identified using a spectrophotometer by monitoring bands at 280 nm and 400 nm. The degree of labeling was determined to be 1.8.

Synthesis of 2-(5-((9,9-bis(2-(2-ethoxyethoxy)ethyl)-7-nitro-9H-fluoren-2-yl)ethynyl)thiophen-2-yl)benzothiazole (18): In a 10 mL vessel, under nitrogen, 9,9-bis(2-(2-ethoxyethoxy)ethyl)-2-iodo-7-nitro-9H-fluorene **13** (413 mg, 0.725 mmol), 2-(5-ethynylthiophen-2-yl)benzothiazole **8** (175 mg, 0.725 mmol), $Pd(PPh_3)_2Cl_2$ (21 mg, 0.03 mmol), CuI (5.7 mg, 0.03 mmol), were dissolved in a 1:4 mixture of Et_3N:toluene (3 mL). The mixture was heated in the microwave for 1h, at 130 ^oC, 150 psi and 150W, filtered through a celite plug, and purified by column chromatography using as a solvent a mixture of hexane:ethyl acetate (2:1) to yield 505 mg (74%) of a light orange solid. m.p. 105.0-106.5 ^oC. ^1H NMR (500 MHz, $CDCl_3$) δ 8.33 (d, *J*=2.00 Hz, 1H, Ph-H), 8.26 (dd, *J*=8.36 Hz, *J*=2.00 Hz, 1H, Ph-H), 8.02 (d, *J*=7.95 Hz, 1H, Ph-H), 7.85 (d, *J*=7.95 Hz, 1H, Ph-H), 7.73-7.79 (m, 2H, Ph-H, Thy-H), 7.66-7.68 (m, 1H, Ph-H), 7.54-7.60 (m, 2H, Ph-H, Thy-H), 7.46-7.50 (m, 1H, Ph-H), 7.36-7.40 (m, 1H, Ph-H), 7.31 (d, *J*=3.92 Hz, 1H, Thy-H), 3.35-7.42 (m, 4H, CH_2), 3.27-3.31 (m, 4H, CH_2),

3.15-3.21 (m, 4H, CH_2), 2.80-2.93 (m, 4H, CH_2), 2.43-2.54 (m, 4H, CH_2), 1.12 (t, *J*=6.85 Hz, 6H, CH_3). ^{13}C NMR (125 MHz, $CDCl_3$) δ 160.5, 153.8, 151.1, 147.5, 146.0, 138.8, 138.6, 134.9, 133.3, 133.1, 128.6, 128.5, 126.9, 126.7, 126.6, 123.4, 123.3, 121.7, 121.4, 119.2, 119.1, 96.0, 84.2, 70.3, 69.7, 66.9, 66.7, 52.3, 39.4, 15.2. MS (APCI) *m/z* calcd $[M+H]^+$ 683.2244, found 683.2231.

Synthesis of 7-((5-(benzothiazol-2-yl)thiophen-2-yl)ethynyl)-9,9-bis(2-(2-ethoxyethoxy)ethyl)-9H-fluoren-2-amine (19): In a 10 mL vessel, under nitrogen, 2-(5-((9,9-bis(2-(2-ethoxyethoxy)ethyl)-7-nitro-9H-fluoren-2-yl)ethynyl)thiophen-2-yl)benzothiazole **18** (250 mg, 0.366 mmol) and 10% Pd/C (25 mg) were dissolved in a 1:1 mixture of THF:EtOH (4 mL). $NH_2NH_2.2H_2O$ (220 mg, 4.4 mmol) was added to the mixture dropwise at room temperature, and then heated in the microwave to 110 ^oC, 100 W and 100 psi for 30 min. The mixture was filtered though a silica plug with ethyl acetate, and after removing the solvent under reduced pressure, the material was purified by column chromatography using as a solvent a mixture of hexane:ethyl acetate (1:3) to yield 200 mg (84%) of a light orange solid. m.p. 110-111 ^oC. ^1H NMR (500 MHz, $CDCl_3$) δ 8.03 (d, *J*=8.09 Hz, 1H, Ph-H), 7.84 (d, *J*=8.09 Hz, 1H, Ph-H), 7.52-7.57 (m, 2H, Ph-H, Thy-H), 7.43-7.52 (m, 4H, Ph-H), 7.35-7.39 (m, 1H, Ph-H), 7.28 (d, *J*=4.09 Hz, 1H, Thy-H), 6.71-6.74 (m, 1H, Ph-H), 6.64-6.68 (m, 1H, Ph-H), 3.79 (s, 2H, NH_2), 3.39-3.46 (m, 4H, CH_2), 3.32-3.39 (m, 4H, CH_2), 3.20-3.26 (m, 4H, CH_2), 2.74-2.85 (m, 4H, CH_2), 2.29-2.44 (m, 4H, CH_2), 1.15 (t, *J*=7.02 Hz, 6H, CH_3). ^{13}C NMR (125 MHz, $CDCl_3$) δ 160.6, 153.7, 151.3, 148.1, 147.1, 142.0, 137.7, 134.7, 133.0, 131.8, 130.6, 128.1, 127.4, 125.6, 125.5, 122.9, 121.7, 120.8, 118.9, 118.0, 115.1, 113.9, 110.2, 97.2, 82.2, 70.1, 69.7, 67.0, 66.7, 50.9, 39.9, 15.4 MS (APCI) *m/z* calcd $[M+H]^+$ 653.2502, found 653.2510.

Synthesis of 2-(5-((9,9-bis(2-(2-ethoxyethoxy)ethyl)-7-isothiocyanato-9H-fluoren-2-yl)ethynyl)thiophen-2-yl)benzothiazole (20): In a two neck round bottom flask and under nitrogen, a solution of 7-((5-(benzothiazol-2-yl)thiophen-2-yl)ethynyl)-9,9-bis(2-(2-ethoxyethoxy)ethyl)-9H-fluoren-2-amine **19** (178 mg, 0.273 mmol) in chloroform (2 mL) was combined with an aqueous solution of $CaCO_3$ (80 mg, 0.80 mmol) in an ice bath. Thiophosgene (0.026 mL, 0.34 mmol) was added to the vial dropwise while stirring the mixture and the reaction proceeded for 4 hours. After completion, a 10% HCl solution was added until the gas formation ceased. The mixture was poured into water, extracted with methylene chloride, dried over magnesium sulfate and purified by column chromatography using as a solvent a mixture of hexane:ethyl acetate (2:1) to yield 170 mg (90%) of a bright yellow solid. m.p. 86-88 ^{o}C. ^{1}H NMR (500 MHz, $CDCl_3$) δ 8.05 (d, *J*=7.97 Hz, 1H, Ph-H), 7.87 (d, *J*=7.97 Hz, 1H, Ph-H), 7.63-7.67 (m, 2H, Ph-H), 7.53-7.61 (m, 3H, Ph-H Thy-H), 7.47-7.52 (m, 1H, Ph-H), 7.37-7.42 (m, 1H, Ph-H), 7.30-7.33 (m, 2H, Ph-H), 7.21-7.24 (m, 1H, Ph-H), 3.39-3.45 (m, 4H, CH_2), 3.30-3.35 (m, 4H, CH_2), 3.18-3.23 (m, 4H, CH_2), 2.75-2.85 (m, 4H, CH_2), 2.34-2.45 (m, 4H, CH_2), 1.15 (t, *J*=7.01 Hz, 6H, CH_3). ^{13}C NMR (125 MHz, $CDCl_3$) δ 160.4, 153.7, 151.2, 149.4, 139.8, 138.8, 138.1, 135.5, 134.7, 132.3, 130.5, 126.8, 126.5, 126.2, 124.9, 123.1, 123.0, 121.60, 121.58, 121.4, 121.2, 120.9, 120.6, 120.0, 96.4, 83.3, 70.1, 69.6, 67.3, 66.6, 51.7, 39.5, 15.1. MS (APCI) *m/z* calcd $[M+H]^+$ 695.2067, found 695.2076. UV-vis (DMSO) λ_{max} 391 nm.

Synthesis of 1-(7-((5-(benzothiazol-2-yl)thiophen-2-yl)ethynyl)-9,9-bis(2-(2-ethoxyethoxy)ethyl)-9H-fluoren-2-yl)-3-butylthiourea (21): In a small vial under nitrogen, a mixture of 2-(5-((9,9-bis(2-(2-ethoxyethoxy)ethyl)-7-isothiocyanato-9H-fluoren-2-yl)ethynyl)thiophen-2-yl)benzothiazole **20** (58 mg, 0.083 mmol), and *n*-butylamine (0.074 mL,

1.0 mmol) at room temperature was stirred for 1 hour. The remaining amine was removed under vacuum and the residue was recrystallized from hexane:ethyl acetate (9:1) to yield 48 mg (75%) of a light yellow solid. m.p. 118.5-119.5 ^{o}C. ^{1}H NMR (500 MHz, $CDCl_3$) δ 8.05 (d, *J*=8.07 Hz, 1H, Ph-H), 7.88 (d, *J*=8.07 Hz, 1H, Ph-H), 7.78 (s, 1H, N-H), 7.66-7.73 (m, 2H, Ph-H), 7.54-7.62 (m, 3H, Ph-H Thy-H), 7.48-7.53 (m, 1H, Ph-H), 7.37-7.43 (m, 1H, Ph-H), 7.29-7.33 (m, 2H, Ph-H, Thy-H), 7.15-7.22 (m, 1H, Ph-H), 6.36 (s,1H, N-H), 3.62-3.71 (m, 2H, CH_2), 3.34-3.43 (m, 4H, CH_2), 3.22-3.32 (m, 4H, CH_2), 3.10-3.22 (m, 4H, CH_2), 2.74-2.97 (m, 4H, CH_2), 2.34-2.45 (m, 4H, CH_2), 1.61 (quintuplet, *J*=7.05 Hz, 2H, CH_2), 1.40 (sextuplet, *J*=7.05 Hz, 2H, CH_2), 1.13 (t, *J*=7.05 Hz, 6H, CH_3), 0.96 (t, *J*=7.83 Hz, 6H, CH_3). ^{13}C NMR (125 MHz, $CDCl_3$) δ 180.6, 168.1, 160.4, 153.7, 149.2, 140.4, 138.2, 138.1, 134.7, 132.9, 132.7, 128.5, 128.4, 126.9, 126.5, 126.5, 126.3, 123.1, 121.54, 121.5, 121.4, 121.3, 120.2, 120.1, 96.4, 83.1, 70.0, 69.6, 67.1, 66.5, 51.9, 45.5, 39.6, 30.9, 20.2, 15.1, 13.8. MS (APCI) *m/z* calcd $[M+H]^+$ 768.2958, found 768.3010. UV-vis (DMSO) λ_{max} 391 nm.

Preparation of bioconjugate B2: A mixture containing 100 μL of antibody (1 mg/mL) and 100 μL of $NaHCO_3$ (1 M) was combined with a fresh solution of isothiocyanate **20** in DMSO in a proportion 1:10 molar protein:dye and incubated for 2 hours in the dark at room temperature. The bioconjugate was purified by using disposable PD-10 desalting columns from GE equilibrated and eluted with PBS buffer 7.0 (Invitrogen). Fractions containing the bioconjugate were identified using a spectrophotometer by monitoring bands at 280 nm and 391 nm. The degree of labeling was determined to be 2.

4.4.3 Measurements

Spectra of amine reactive probes and model compounds were collected from DMSO solutions with concentrations in the order of 10^{-6} M at room temperature using 1 cm quartz cuvettes. Absorption spectra were recorded with an Agilent 8453 UV–visible spectrophotometer. Steady-state fluorescence spectra were measured with a PTI Quantamaster spectrofluorimeter in the photon counting regime of the PMT using an L-format configuration. The fluorescence spectra were corrected for the spectral dependence of the PMT. Fluorescence quantum yields were determined relative to 9, 10-diphenylanthracene in cyclohexane. Absorption spectra of bioconjugates **B1** and **B2** were measured in PBS buffer using 1 mm quartz cuvettes.

Two-photon absorption spectra were measured by the two-photon fluorescence 2PF method relative to Rhodamine B in methanol [*53*] using solutions with concentrations of approximately 10^{-4} M in spectroscopic grade DMSO following the methodology previously reported [*52*]

4.4.4 Cell culture and incubation

PAE (Porcine aortic endothelial) and PAE/KDR (commercially available Porcine aortic endothelial expressing $2x10^5$ VEGFR-2 per cell), were cultured in F-12 Nutrient mixture (Ham's medium, Invitrogen) containing 10% fetal bovine serum (FBS) (Atlanta Biologicals) and 1% penicillin/ streptomycin, at 37 °C, under 5% CO_2 environment. Monoclonal anti-human VEGFR-2/KDR-Fluorescein isothiocyanate bioconjugate was obtained from R&D Systems and was used as a positive control without further treatment.

N° 1 round 12 mm coverslips were treated with poly-D-lysine, and washed (3x) with PBS buffer solution. The treated cover slips were placed in 24-well plates and 60,000 cells/well were seeded and incubated at the same conditions as indicated above until 75%-85% confluency was reached on the coverslips.

For the positive control, PAE-KDR cells were incubated for 2 hours in a solution containing 0.4 μM solution of bioconjugate **B2** and the monoclonal antibody bioconjugate (25 μg/mL) in culture media. PAE (negative control) and PAE-KDR cells were incubated for 2 hours in a 0.4 μM solution of bioconjugate **B2** in culture media. The dye solutions were extracted and the coverslipped cells were washed abundantly with PBS (4x).

Cell fixing and mounting: Cells were fixed with 3.7% solution of paraformaldehyde in pH=7.4 PBS buffer for 10 min. The fixing agent was extracted and washed (2x) with PBS. To reduce autofluorescence, a fresh solution of $NaBH_4$ (1 mg/mL) in pH=8 PBS buffer was used to treat the fixed cells (2x). The coverslipped cells were then washed with buffer PBS (2x) and mounted on microscope slides using Prolong Gold (Invitrogen) as a mounting media.

4.4.5 Tissue Immunoflurescence staining

2-day old mouse embryo sections were deparaffinized (60 °C for 5 min; then, xylene for 5 min) and rehydrated (EtOH 100%, 95% and 80% twice for 1 min each). Antigen retrieval was performed in sodium citrate buffer solution (6 mM, in conventional microwave 95-100 °C, 10 min) and the tissue sections were allowed to cool for 20 min. Subsequently, tissue sections were permeabilized with Triton X (0.1%, 10 m) and were incubated with bioconjugate **B2** (0.4 μM, for 1.5 h). No dye was added to negative control.

4.4.6 One-photon epifluorescence imaging

One-photon (conventional) fluorescence microscopy images were recorded on an Olympus IX-81 microscope equipped with a Hamamatsu EM-CCD C9100 digital camera. One-photon fluorescence images of the fixed cells were taken using a custom made filter cube (Ex:377/50; DM: 409; Em:525/40) and a FITC filter cube (Ex:477/50; DM: 507; Em:536/40) for bioconjugate **B2** and FITC anti-VEGFR-2, respectively.

4.4.7 Two-photon upconverted fluorescence imaging

Two-photon fluorescence microscopy (2PFM) imaging was performed on a modified Olympus Fluoview FV300 laser scanning microscopy system equipped with a broadband, tunable Coherent Mira Ti:sapphire laser (200 fs pulse width, 76 MHz repetition rate), pumped by a 10 W Coherent Verdi frequency doubled Nd:YAG laser. The Ti:sapphire laser, tuned 700 nm and modelocked, was used as the two-photon excitation source. Two-photon induced fluorescence was collected by a 60x microscope objective (UPLANSAPO 60x, N.A.=1.35 Olympus). A high transmittance (>95%) short-pass filter (cutoff 685 nm, Semrock) was placed in front of the PMT detector within the FV300 scanhead in order to filter off background radiation from the laser source (700 nm).

4.5 Conclusions

We developed and synthesized new two-photon absorbing fluorescent amine reactive probes and bioconjugates. Photophysical characterization was performed for amine reactive probes, model compounds, and bioconjugates. The new probes demonstrated better characteristics and optical properties than those observed for commercially available bioconjugates. Successful imaging by one and two-photon excitation with the bioconjugate **B2** in

cells and tissue was performed, demonstrating that the new bioconjugates selectively bind VEGFR-2 in cell culture and tissue sections.

CHAPTER 5. FUTURE WORK

The development and use of 2PA fluorescent dyes that incorporate a polyclonal antibody to specifically target the vascular endothelial growth factor receptor 2 (VEGFR-2) has been successfully achieved in cells and mouse embryo tissue, as demonstrated in Chapter 4. Although the obtained results proved that the system works satisfactorily, further efforts can be done in order refine the method, improve even more the results, and ultimately, to take maximum advantage of this technology. In this chapter we discuss how this system can be improved. In addition, we comment on the areas where we envision that this system can be useful, as well as further projects that can be completed using this kind of bioconjugates.

5.1 Additional Improvements to the System

The incorporation of a monoclonal antibody (mAb) rather than a polyclonal antibody as the vector that will direct the fluorescent dye towards the desired receptor is a subject that must be studied. Recent reports have demonstrated that in some cases, although more expensive, the use of a monoclonal antibody rather than a polyclonal antibody, will result in a higher specificity of the bioconjugate towards the receptor. For example, Bodor *et al.* developed a series of monoclonal antibodies to study myocardial infarction or heart attack. In their work they compare their results with previous similar studies that used a polyclonal antibody, demonstrating that in this case monoclonal antibodies give the desired response faster and more selectively.[*90*]. On the other hand, studies have demonstrated that the use of monoclonal antibodies instead of polyclonal antibodies not necessarily result in higher specificity; in fact, the use of antibodies microarrays has been suggested and used as a technique to analyze antibody

specificity, since the interactions between the protein and the antibodies cannot be deduced easily.[*91*]

In our future studies, comparison between images obtained with the mAb with those obtained using the polyclonal antibody will reveal if the nature of the antibody is a factor that could derive in a better target resolution or more specific images in this particular case. To perform these series of studies, a mAb selective to the VEGFR-2 must be conjugated with the 2PA fluorescent dye. Specifically, the commercially available monoclonal antibody DC-101 can be used to conjugate the dye following the procedure described in Chapter 4. Monoclonal antibodies DC-101 and IMC-1C11, are currently used in cancer treatment since it is know that they block VEGFR interactions in mice and humans, respectively, thus, inhibiting tumor growth. [*92-94*] Upon completion of these studies, the reproducibility of the method must be proved by repetition of the experiments. The use of monoclonal antibodies may lead not only to imaging of tumors but to therapy, thus, in the future, procedures where VEGFR are blocked with specific antibodies could be used for both imaging and treatment as it has been demonstrated that they result in delayed growth of tumors.[*92, 93*] This is the most important and urgent modification that must be implemented to the system in order to continue with further studies.

Another possible adaptation that the system could undergo would be based on the systematic study of the variation of the degree of labeling (DOL) of the bioconjugate. In the presented work, a DOL of 2 resulted in satisfactory images, but in further studies the quality of the results could be correlated to the variation of the DOL. A low DOL could result in poor fluorescence, while too high DOL could yield poor selectivity because of loss of functionality of the antibody and decrease in the fluorescence due to self-quenching. [*95-97*]

Finally, despite the fact that the dye used to conjugate to the antibody demonstrated to have good optical properties, a new design of the dye based on the structure of compound **III** (Chapter 1) that incorporates the antibody on the 9 position of a fluorene rather than on the conjugated system, could result in a bioconjugate with even better properties than those observed in our model conjugates (Chapter 4).

5.2 Potential Future Projects

Based on the studies performed, the next expected step that involves the use of these bioconjugates is clear: *in vivo* imaging of vasculature in mice. To perform these studies, the bioconjugate will be injected into the vein tail of mice following reported and accepted protocols. Briefly, Lewis Lung Carcinoma will be implanted in the dorsum of 6 week old BALB/c mice. Bioconjugate will be injected in the tail vein several days after tumor implantation. Animals will be sacrificed and sections of tumors removed, treated as necessary and studied with the equipment for one and two-photon fluorescence microscopy described in previous chapters. The same protocol can be used to perform *in vivo* imaging of live small animals. In this case, animals will be anesthetized before imaging.[*87*] The deeper penetration that can be achieved by 2PA excitation will be essential in these series of experiments.

Angiogenesis is an essential factor associated with microvascular density measurements. 3D imaging of blood microvessels results fundamental in areas such as cancer research or heart disease research since the microvessel density (MVD) has been correlated with VEGF; therefore, MVD quantification has been used as a method to evaluate angiogenesis.[*77, 80, 81, 98*] Nonetheless, high resolution imaging of MVD still remains a challenge. In 2000, Callagy and co-workers examined the relationship between VEGF, MVD and tumor stage in breast cancer. One

of the conclusions of this work is that the measurement of MVD seems to be not very reliable with current technologies available, indicating that accurate and reproducible methods for evaluating angiogenesis through MVD measurements are required.[*77*]

Quantification of MVD results very important in heart disease research since an increase in this density means an improvement in the condition of the patient after stroke. Microvascular density might be studied also to not only allow visualization of all vessels, but also distinguish those that are actually perfused.[*98*] Additionally, efficacy of antibody-based oncotherapy can be followed with this methodology.[*77*] Moreover, microvascular density has been associated with measurements of type and degree of tumors, and the prognosis of patients with these tumors through immunohistopathology.[*99*]

Although immunohistochemistry, magnetic resonance imaging (MRI) combined with laser scanning confocal microscopy, and photoacustic microscopy techniques have evolved to be used to image subcutaneous MVD as well as to correlate vessel size with blood volume, the proposed nonlinear fluorescent method (2FPM) provides high contrast, good penetration, and good resolution, which are fundamental to obtain reliable qualitative and quantitative data of the morphology and size of these microvessels in fixed tissue and ultimately *in vivo*. [*77, 80, 81, 98, 100*]

APENDIX A: ^{1}H AND ^{13}C NMR SPECTRA OF NEW MOLECULES IN CHAPTER 1

^{1}H NMR for **2**

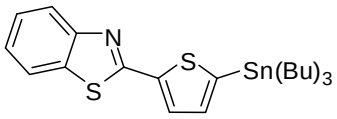
N
S
S
Sn(Bu)3

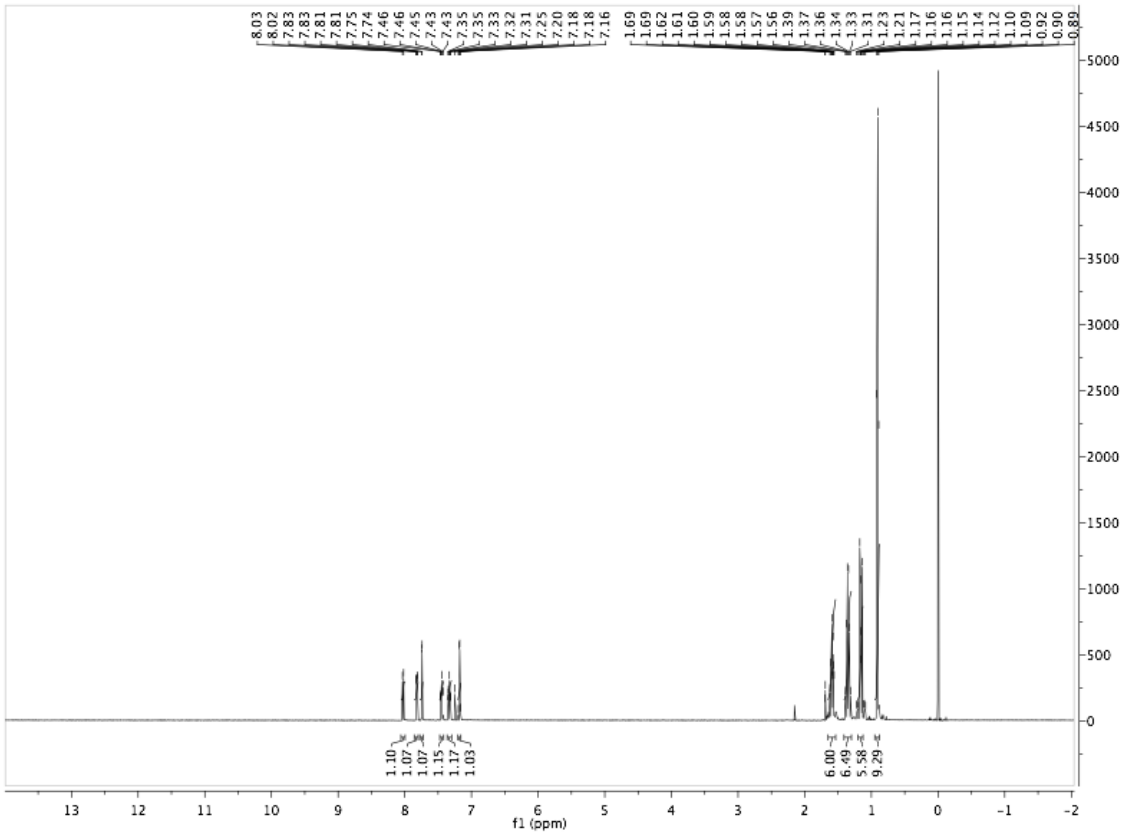
8.03
8.02
7.83
7.83
7.81
7.81
7.75
7.74
7.46
7.46
7.45
7.43
7.43
7.35
7.35
7.33
7.32
7.31
7.25
7.20
7.18
7.18
7.16
1.69
1.69
1.62
1.61
1.60
1.59
1.58
1.58
1.57
1.56
1.39
1.37
1.36
1.34
1.33
1.31
1.23
1.21
1.17
1.16
1.16
1.15
1.14
1.12
1.10
1.09
0.92
0.90
0.89
1.10
1.07
1.07
1.15
1.17
1.03
6.00
6.49
5.58
9.29
f1 (ppm)

^{13}C NMR for **2**

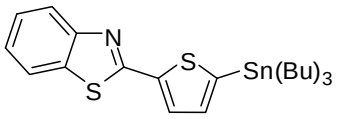
N
S
S
Sn(Bu)3

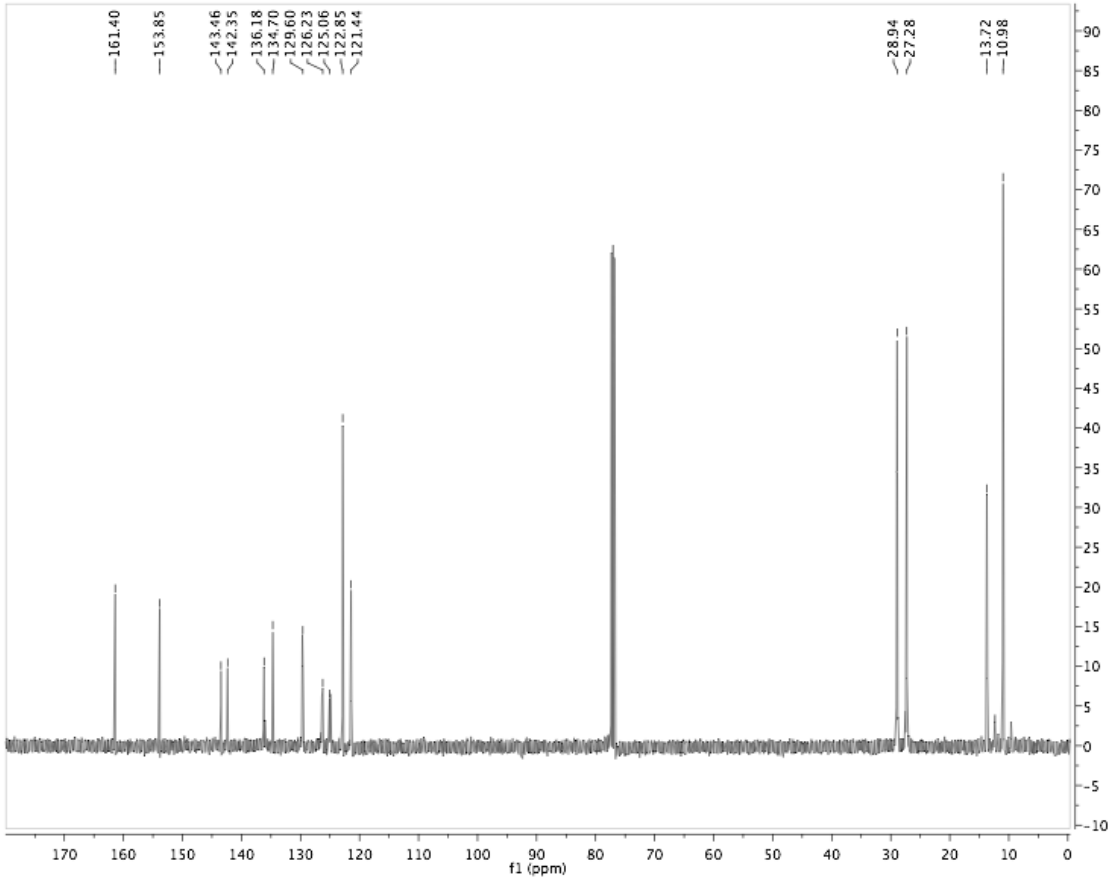
161.40
153.85
143.46
142.35
136.18
134.70
129.60
126.23
125.06
122.85
121.44
28.94
27.28
13.72
10.98
f1 (ppm)

^{1}H NMR for **4**

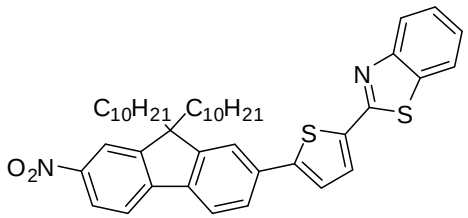
$C_{10}H_{21}$
$C_{10}H_{21}$
O_2N
S
N
S

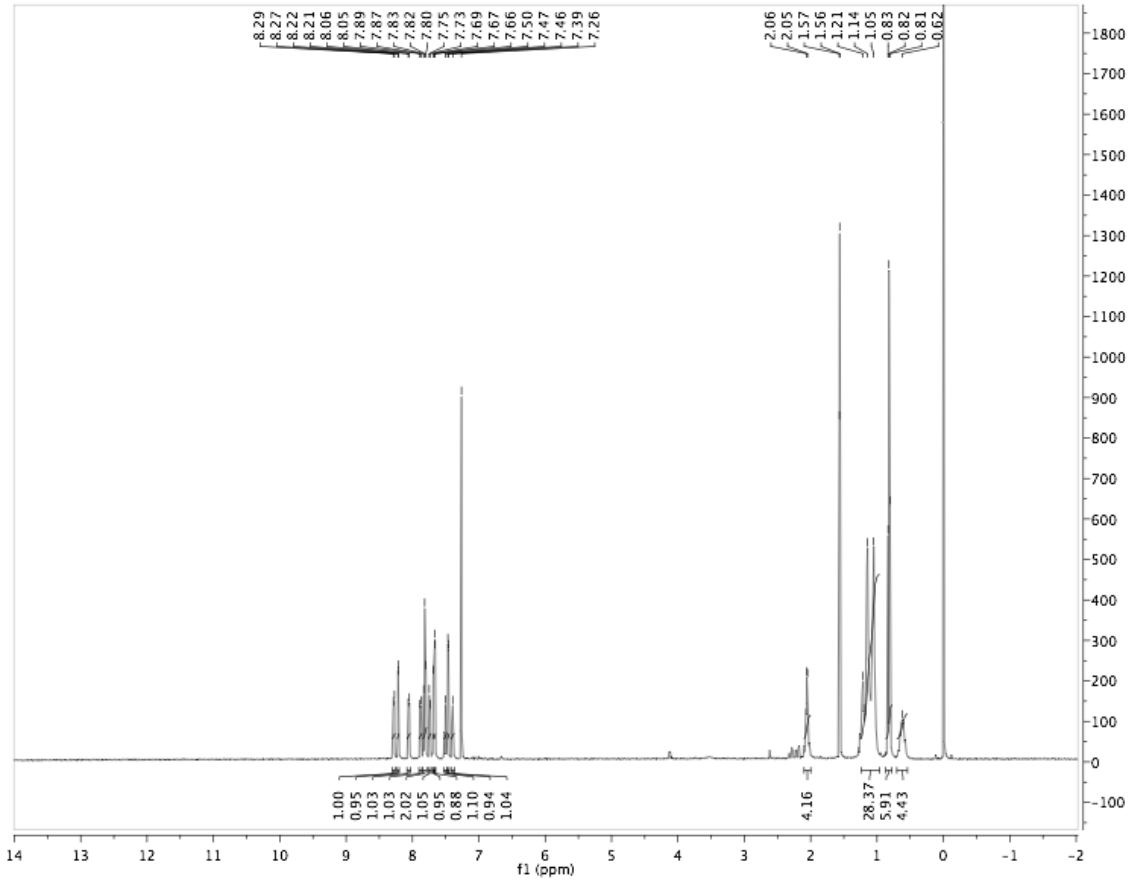
8.29
8.27
8.22
8.21
8.06
8.05
7.89
7.87
7.83
7.82
7.80
7.75
7.73
7.69
7.67
7.66
7.50
7.47
7.46
7.39
7.26
2.06
2.05
1.57
1.56
1.21
1.14
1.05
0.83
0.82
0.81
0.62
1.00
0.95
1.03
1.03
2.02
1.05
0.95
0.88
1.10
0.94
1.04
4.16
28.37
5.91
4.43
f1 (ppm)

^{13}C NMR for **4**

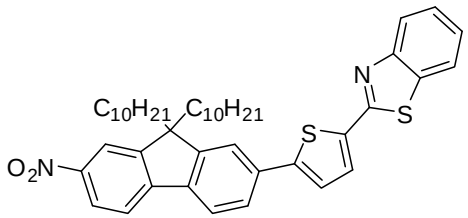
C10H21
C10H21
O2N
S
N
S

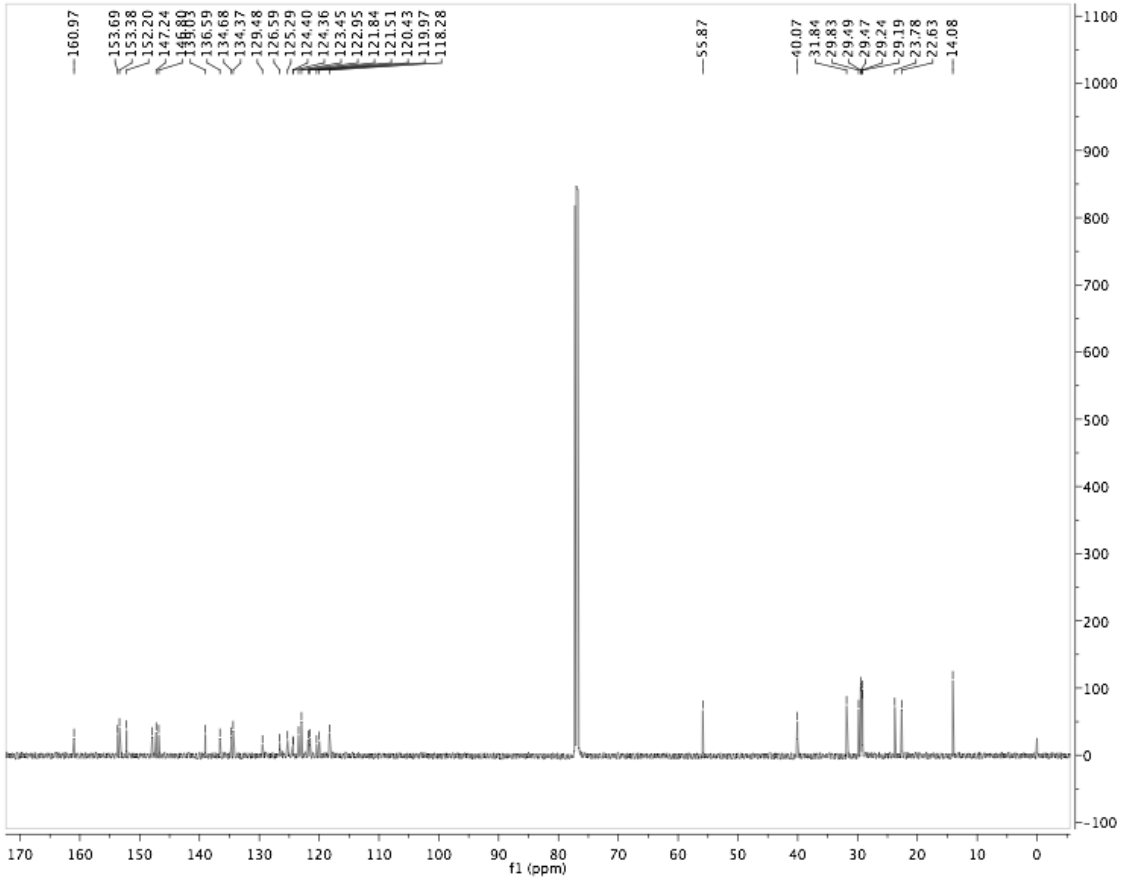
160.97
153.69
153.38
152.20
147.24
136.59
134.68
134.37
129.48
126.59
125.29
124.40
124.36
123.45
122.95
121.84
121.51
120.43
119.97
118.28
55.87
40.07
31.84
29.83
29.49
29.47
29.24
29.19
23.78
22.63
14.08
f1 (ppm)

^{1}H NMR for **5**

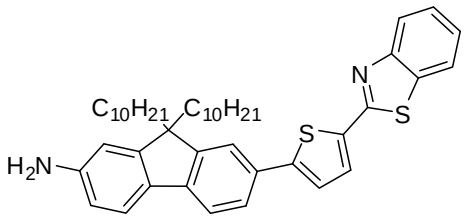
N
S
S
$C_{10}H_{21}$
$C_{10}H_{21}$
H_2N

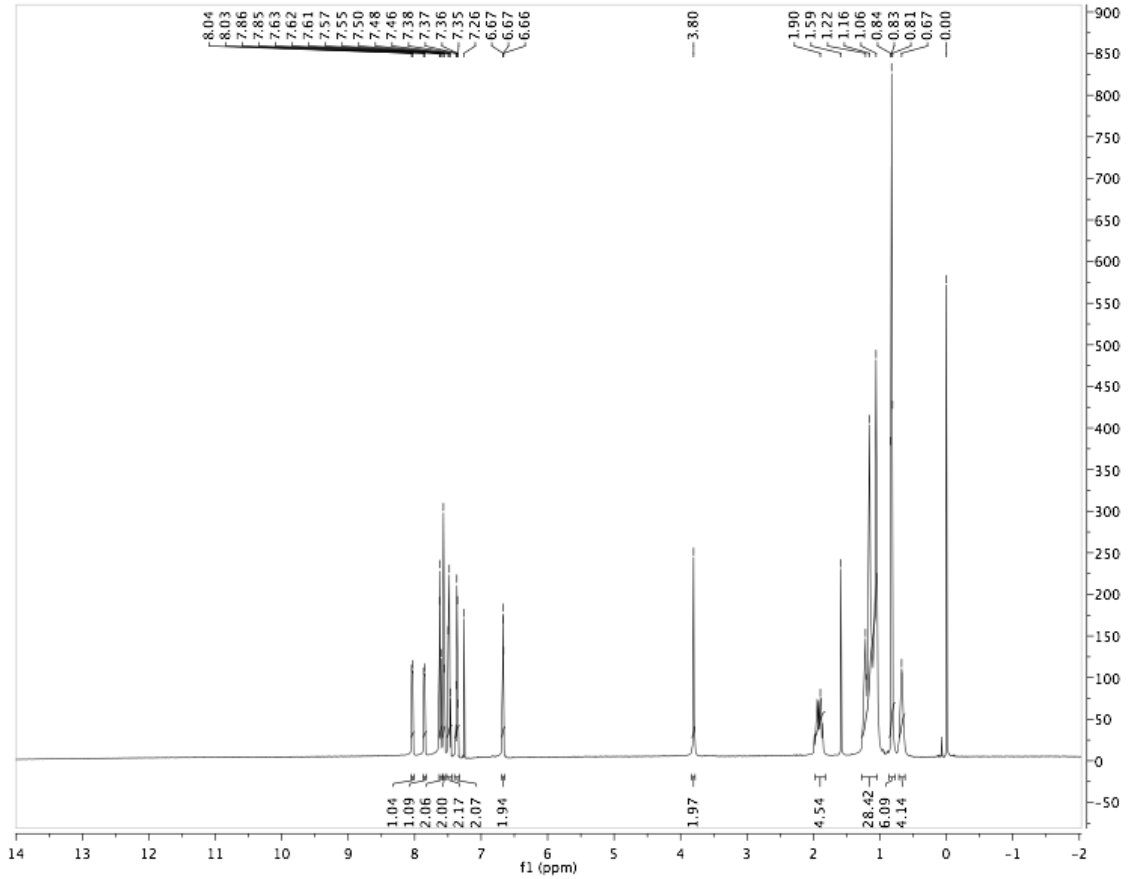
8.04
8.03
7.86
7.85
7.63
7.62
7.61
7.57
7.55
7.50
7.48
7.46
7.38
7.37
7.36
7.35
7.26
6.67
6.67
6.66
3.80
1.90
1.59
1.22
1.16
1.06
0.84
0.83
0.81
0.67
0.00
1.04
1.09
2.06
2.00
2.17
2.07
1.94
1.97
4.54
28.42
6.09
4.14
f1 (ppm)

^{13}C NMR for **5**

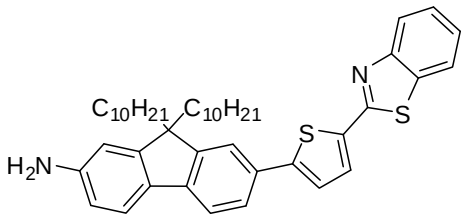
N
S
S
$C_{10}H_{21}$
$C_{10}H_{21}$
H_2N

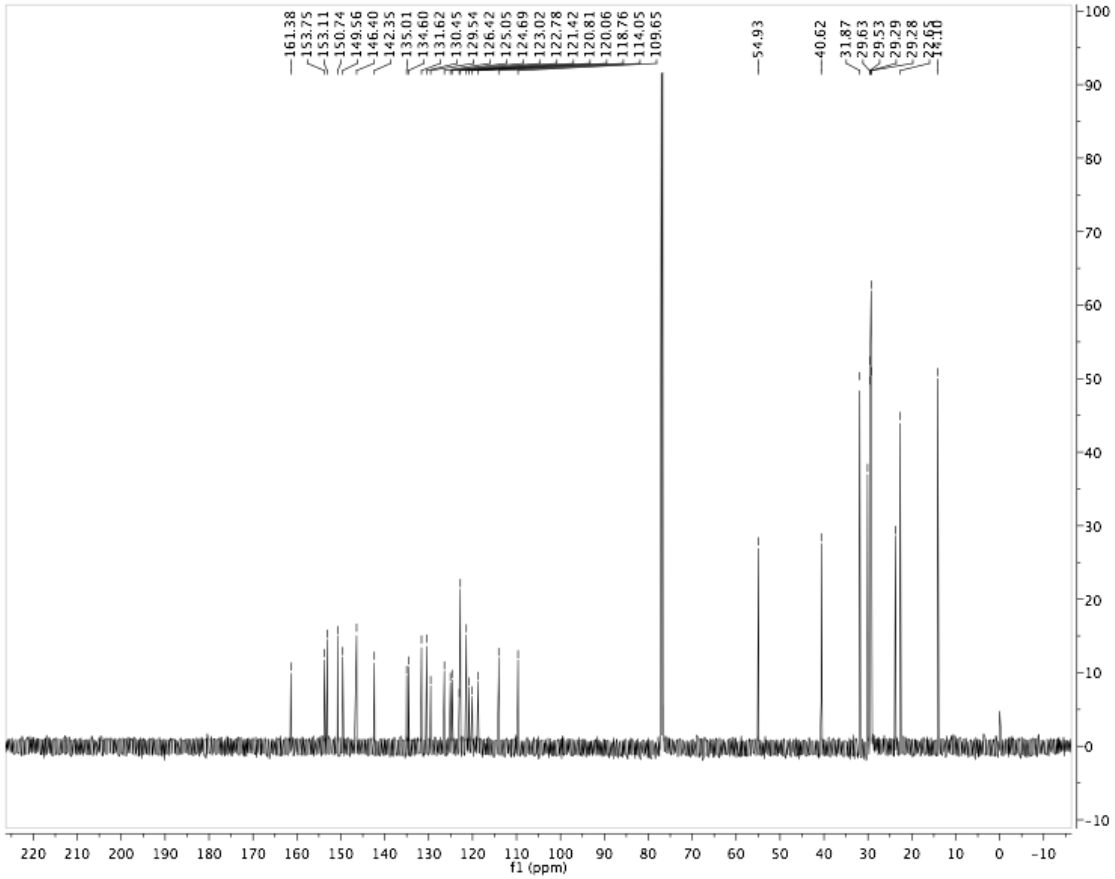
161.38
153.75
153.11
150.74
149.56
146.40
142.35
135.01
134.60
131.62
130.45
129.54
126.42
125.05
124.69
123.02
122.78
121.42
120.81
120.06
118.76
114.05
109.65
54.93
40.62
31.87
29.63
29.53
29.29
29.28
f1 (ppm)

^{1}H NMR for **I**

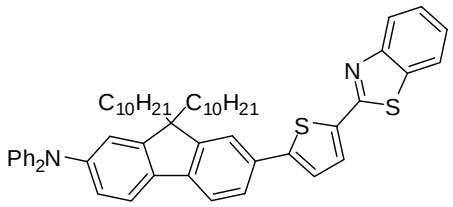
N
S
S
$C_{10}H_{21}$
$C_{10}H_{21}$
Ph_2N

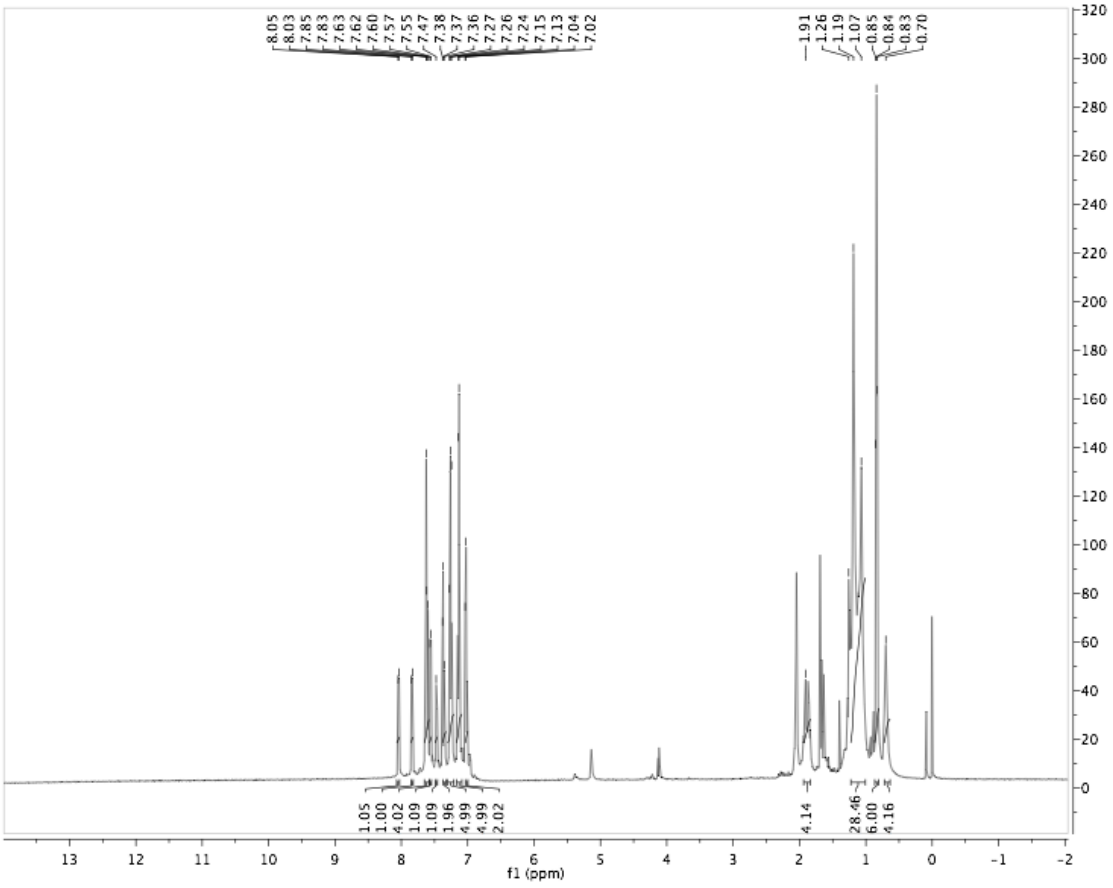
8.05
8.03
7.85
7.83
7.63
7.62
7.60
7.57
7.55
7.47
7.38
7.37
7.36
7.27
7.26
7.24
7.15
7.13
7.04
7.02
1.91
1.26
1.19
1.07
0.85
0.84
0.83
0.70
1.05
1.00
4.02
1.09
1.09
1.96
4.99
4.99
2.02
4.14
28.46
6.00
4.16
f1 (ppm)

^{13}C NMR for **I**

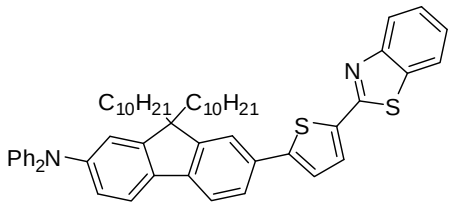
N
S
$C_{10}H_{21}$ $C_{10}H_{21}$
S
Ph_2N

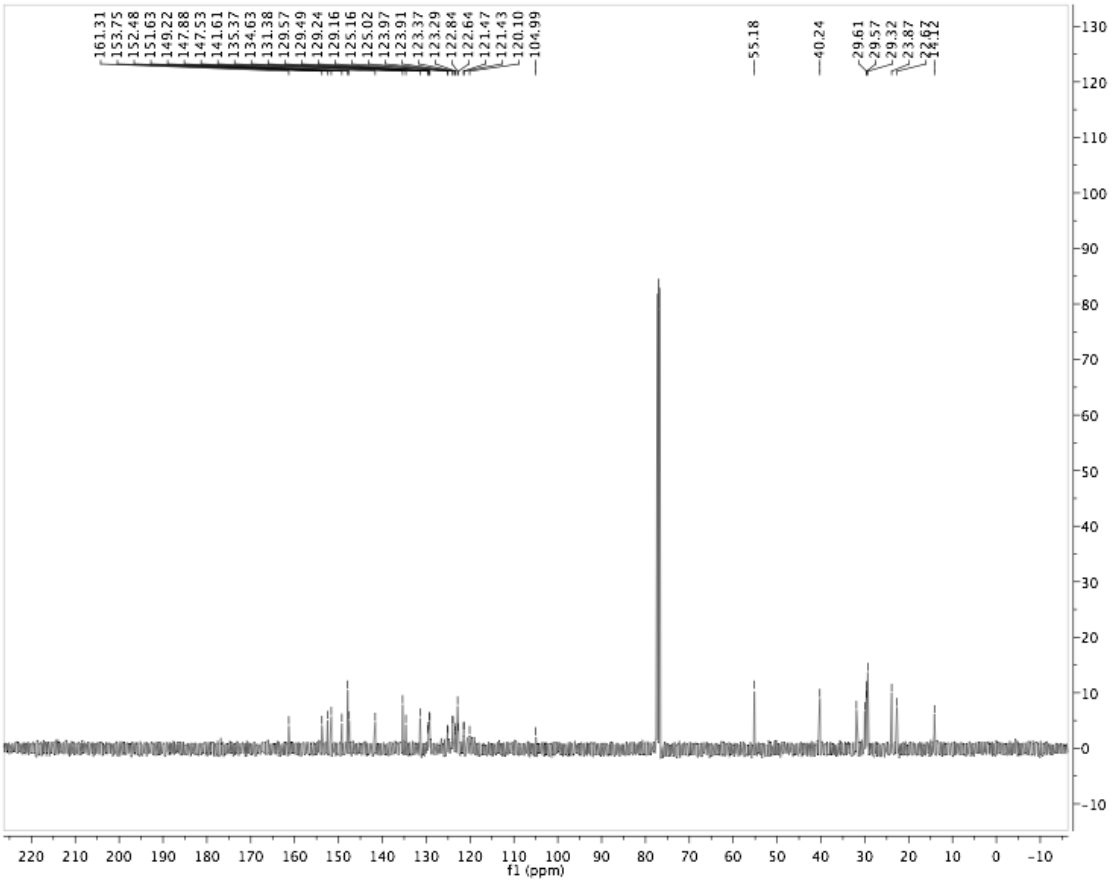
161.31
153.75
152.48
151.63
149.22
147.88
147.53
141.61
135.37
134.63
131.38
129.57
129.49
129.24
128.16
125.16
125.02
123.97
123.91
123.37
123.29
122.84
122.64
121.47
121.43
120.10
104.99
55.18
40.24
29.61
29.57
29.32
23.87
14.12
f1 (ppm)

^{1}H NMR for **II**

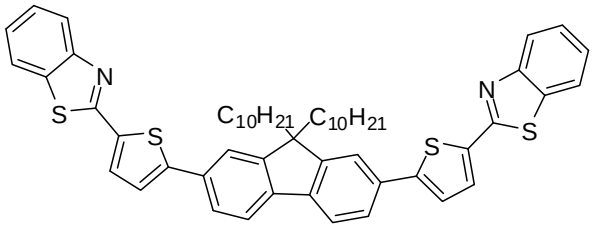
N
S
S
$C_{10}H_{21}$
$C_{10}H_{21}$
S
N
S

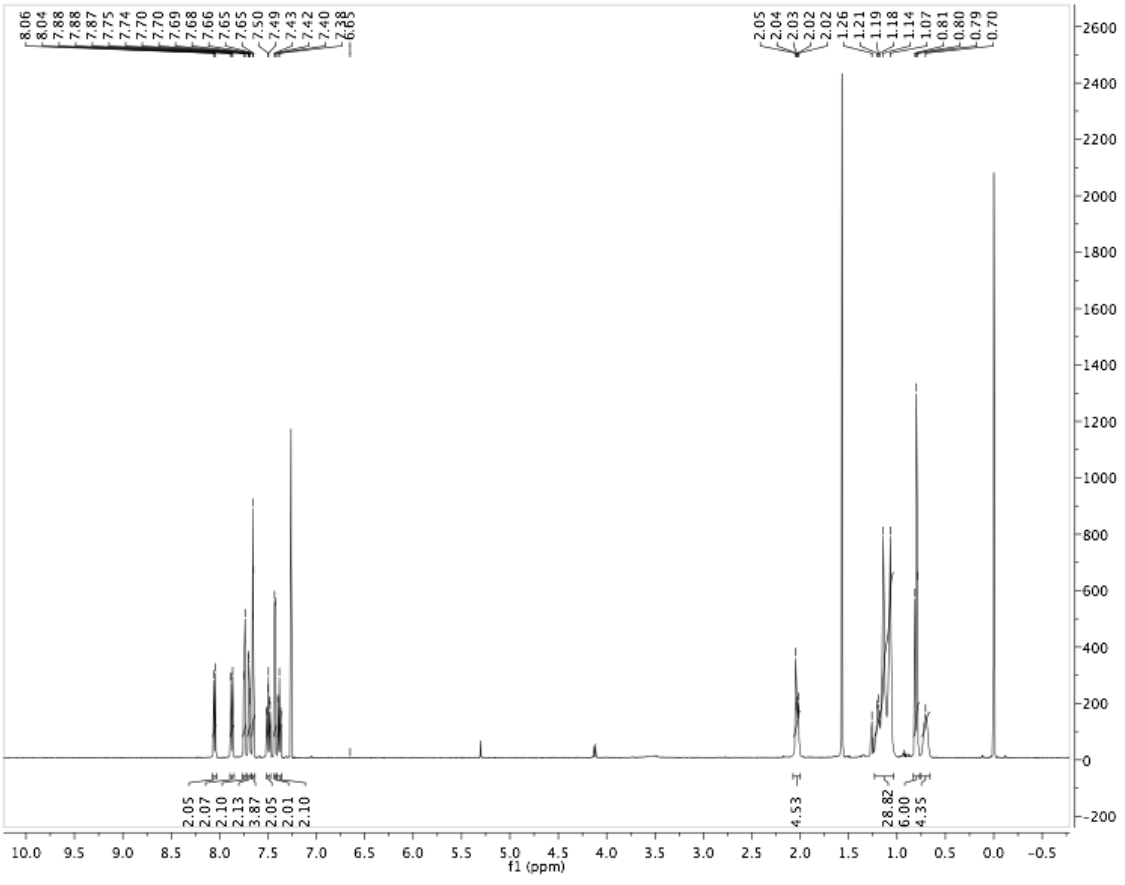
8.06
8.04
7.88
7.87
7.75
7.74
7.70
7.70
7.69
7.68
7.66
7.65
7.65
7.50
7.49
7.43
7.42
7.40
2.05
2.04
2.03
2.02
2.02
1.26
1.21
1.19
1.18
1.14
1.07
0.81
0.80
0.79
0.70
2.05
2.07
2.10
2.13
3.87
2.05
2.01
2.10
4.53
28.82
6.00
4.35
f1 (ppm)

^{13}C NMR for **II**

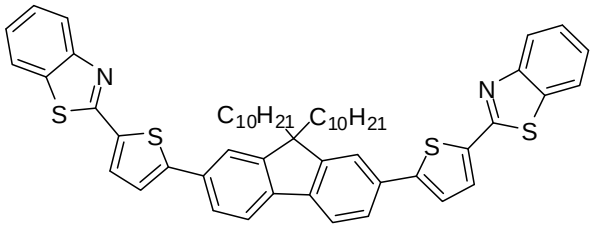

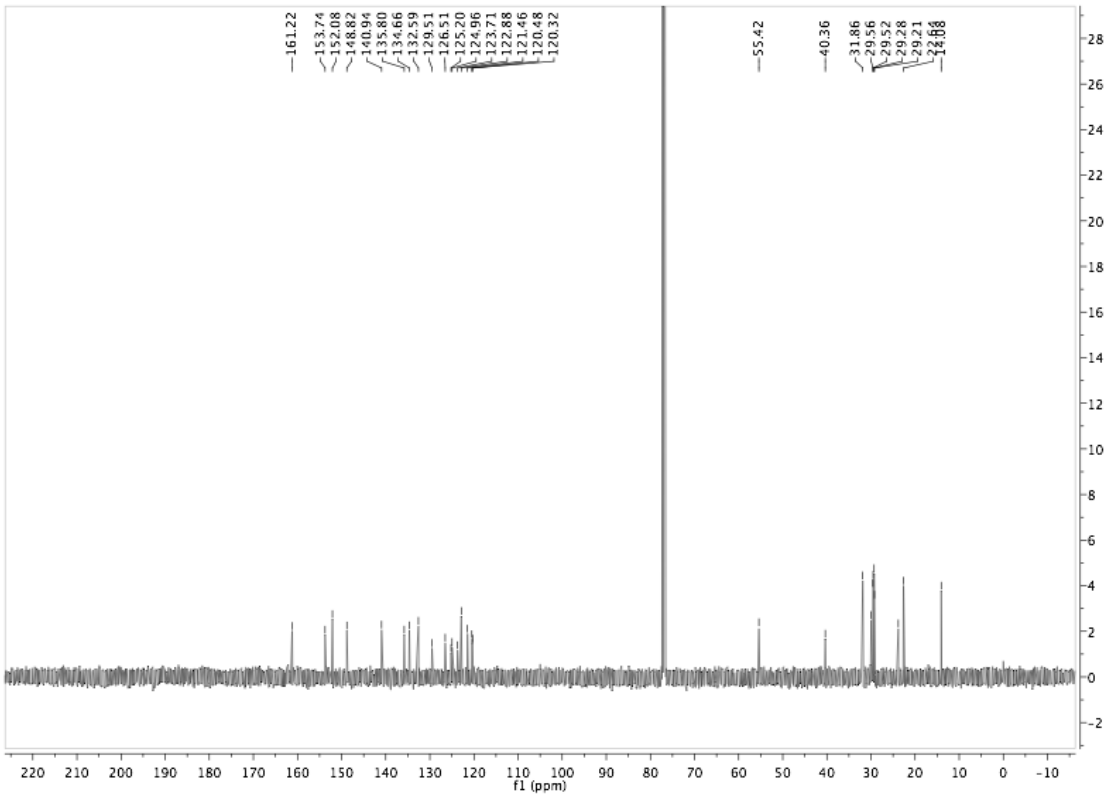

^{1}H NMR for **7**

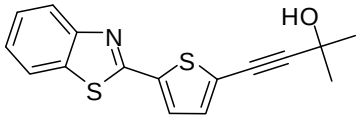
HO
N
S
S

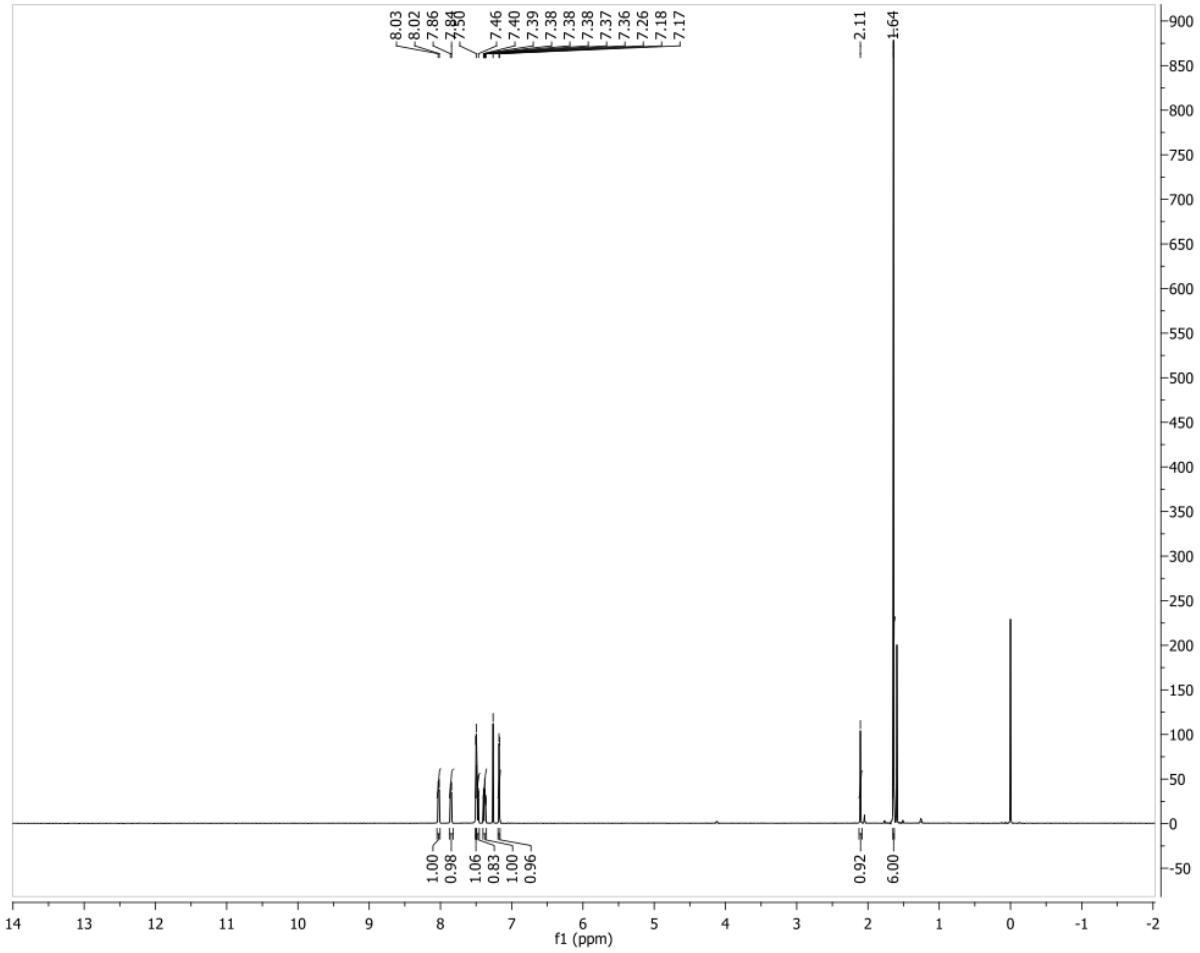
8.03
8.02
7.86
7.84
7.50
7.46
7.40
7.39
7.38
7.38
7.38
7.37
7.36
7.26
7.18
7.17
2.11
1.64
1.00
0.98
1.06
0.83
1.00
0.96
0.92
6.00
f1 (ppm)

^{13}C NMR for **7**

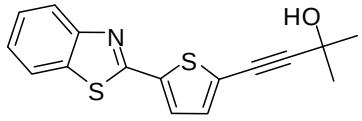
HO
N
S
S

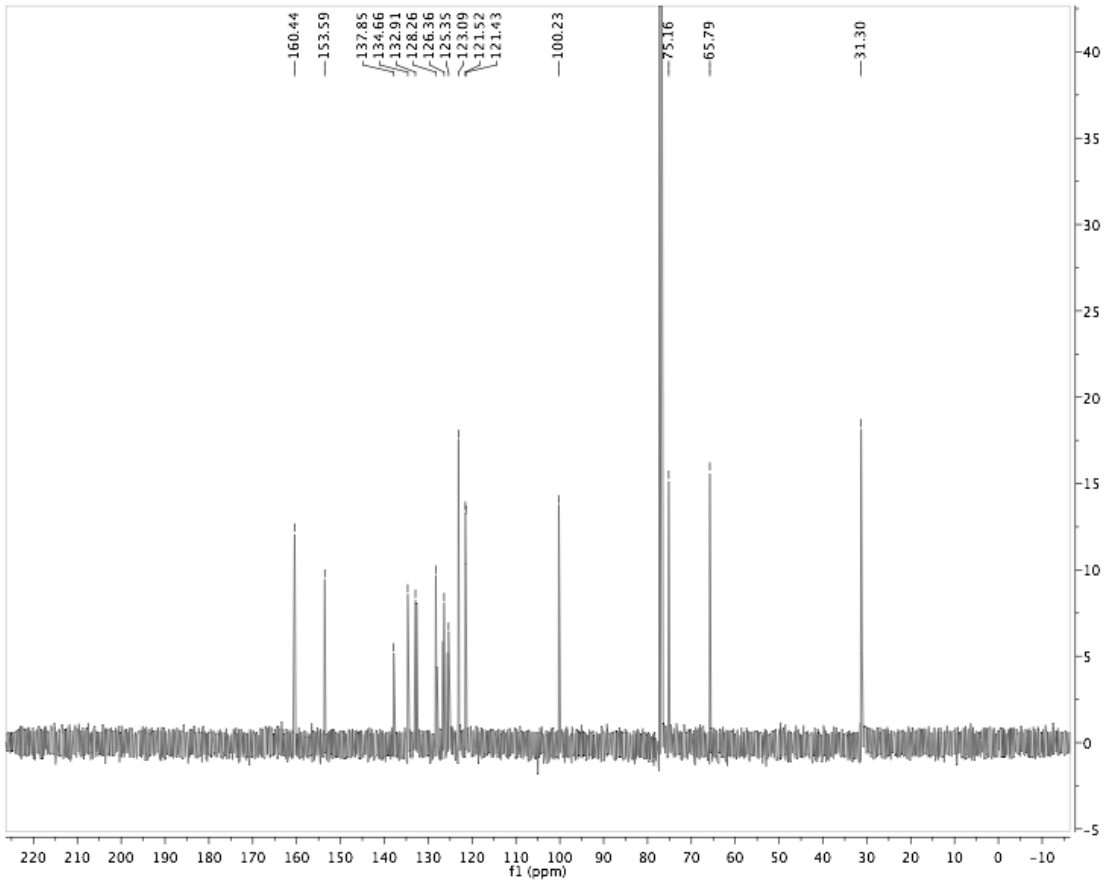
160.44
153.59
137.85
134.66
132.91
128.26
126.36
125.35
123.09
121.52
121.43
100.23
75.16
65.79
31.30
f1 (ppm)

^{1}H NMR for **8**

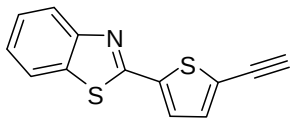
N
S
S

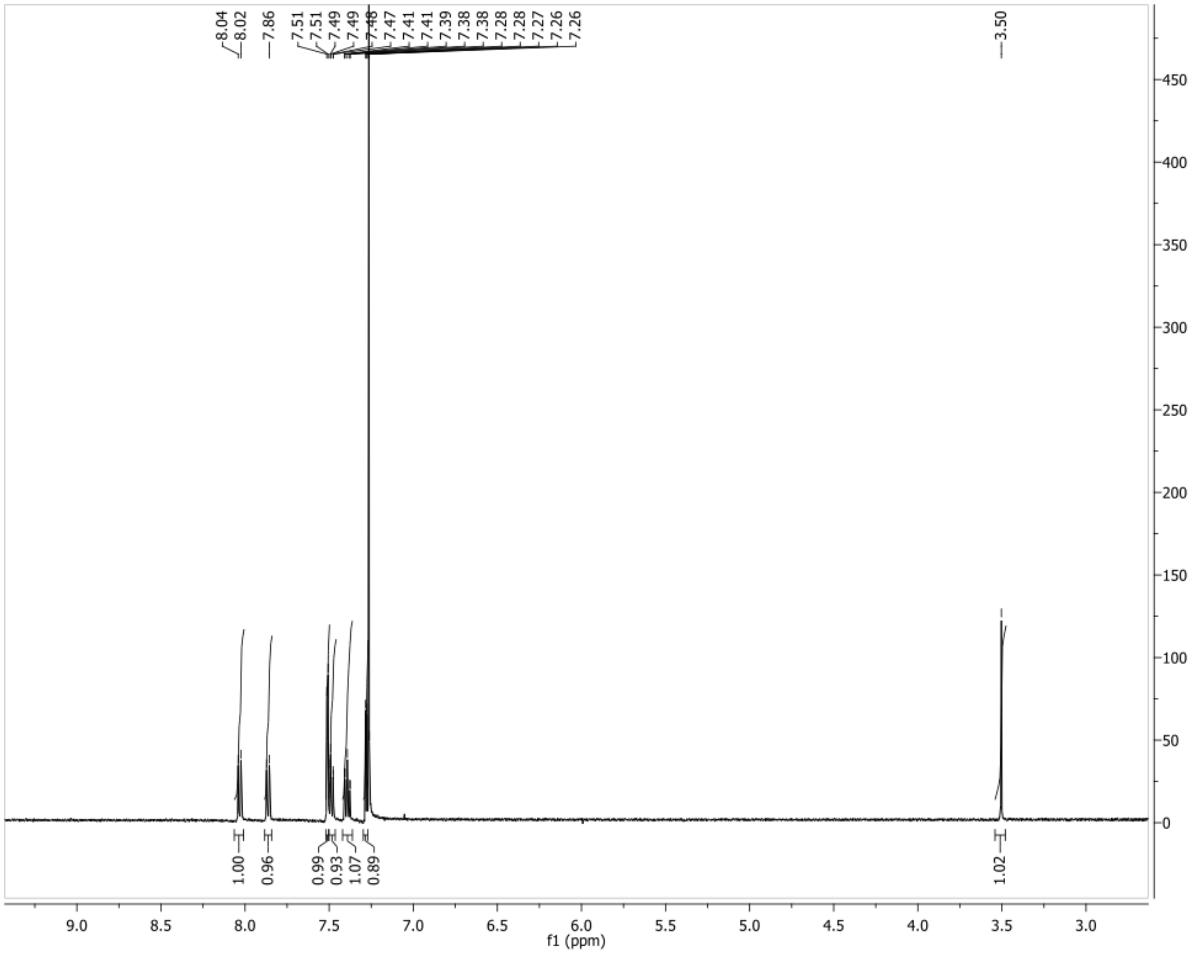
8.04
8.02
7.86
7.51
7.51
7.49
7.49
7.48
7.47
7.41
7.41
7.39
7.38
7.38
7.28
7.28
7.27
7.26
7.26
3.50
1.00
0.96
0.99
0.93
1.07
0.89
1.02
f1 (ppm)

^{13}C NMR for **8**

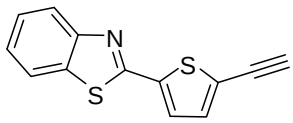
N
S
S

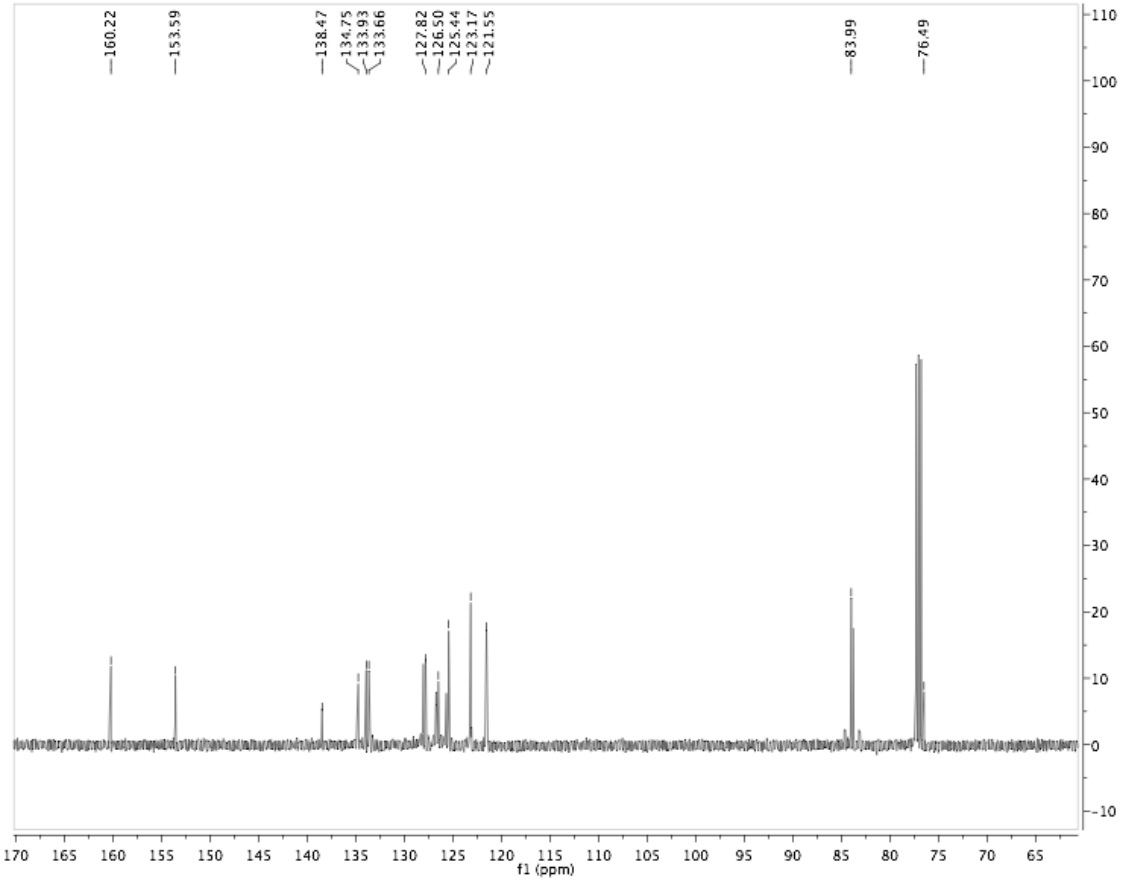
160.22
153.59
138.47
134.75
133.93
133.66
127.82
126.50
125.44
123.17
121.55
83.99
76.49
f1 (ppm)

^{1}H NMR for **9**

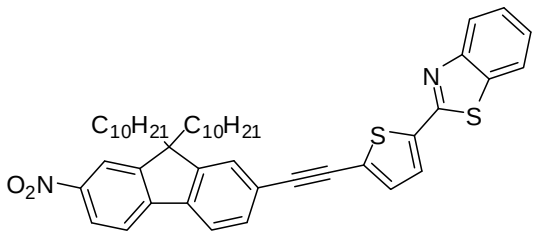
N
S
S
$C_{10}H_{21}$
$C_{10}H_{21}$
O_2N

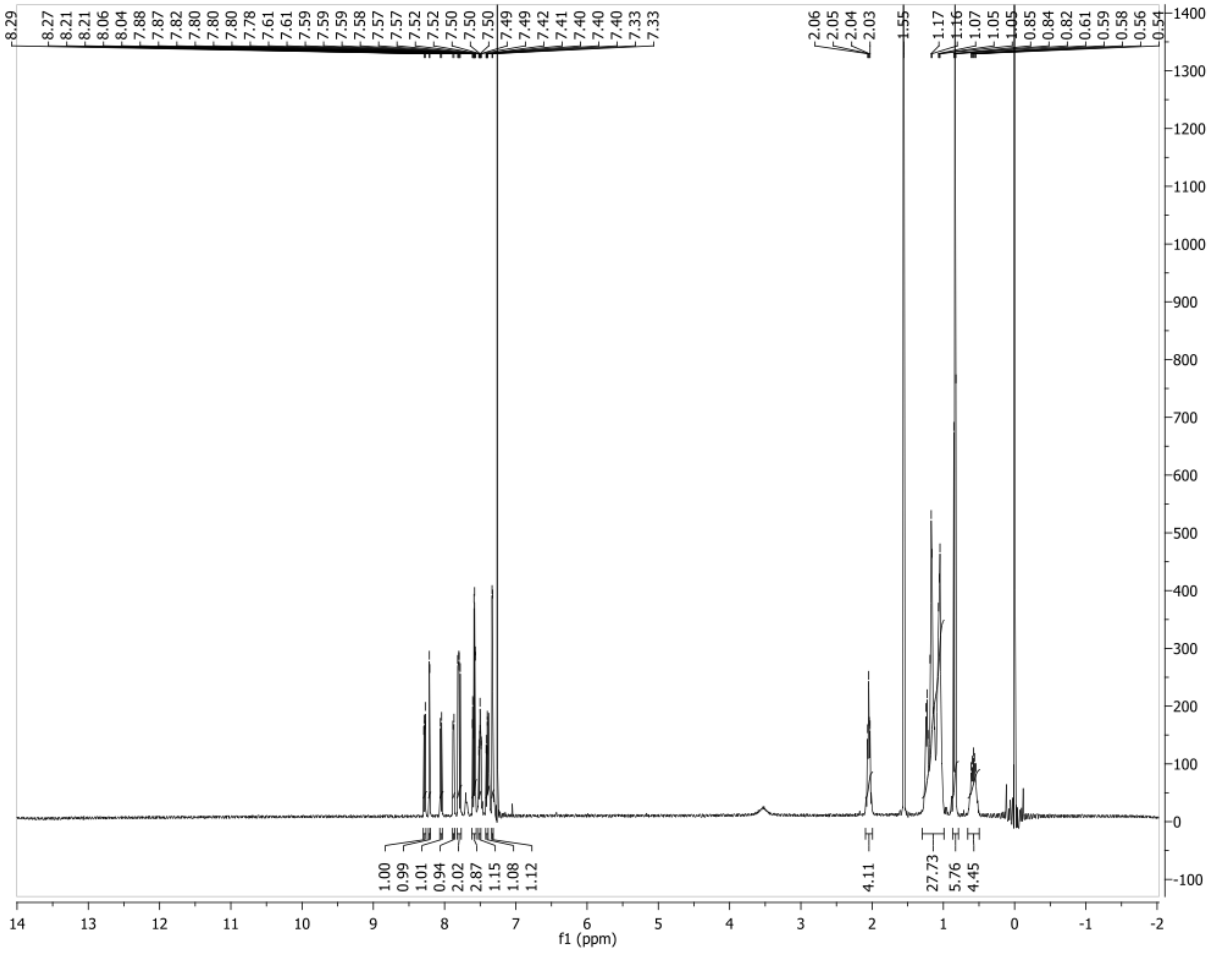
8.29
8.27
8.21
8.21
8.06
8.04
7.88
7.87
7.82
7.80
7.80
7.80
7.78
7.61
7.61
7.59
7.59
7.59
7.58
7.57
7.57
7.52
7.52
7.50
7.50
7.50
7.49
7.49
7.42
7.41
7.40
7.40
7.40
7.33
7.33
2.06
2.05
2.04
2.03
1.55
1.17
1.16
1.07
1.05
1.05
0.85
0.84
0.82
0.61
0.59
0.58
0.56
0.54
1.00
0.99
1.01
0.94
2.02
2.87
1.15
1.08
1.12
4.11
27.73
5.76
4.45
f1 (ppm)

^{13}C NMR for **9**

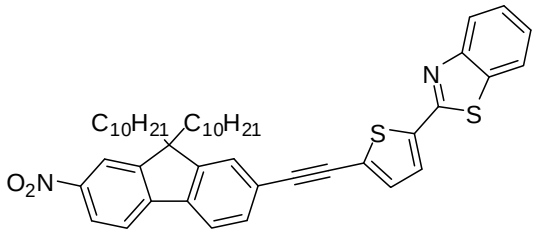
N
S
S
$C_{10}H_{21}$
$C_{10}H_{21}$
O_2N

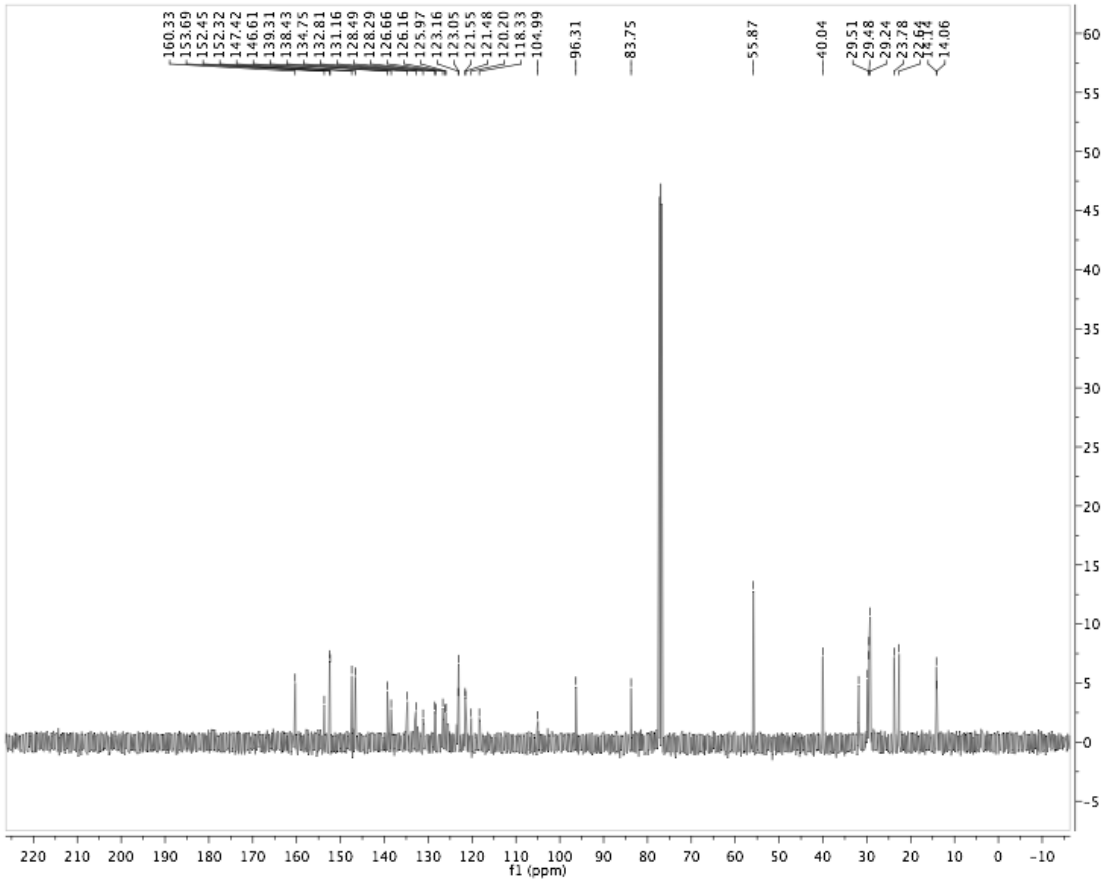
160.33
153.69
152.45
152.32
147.42
146.61
139.31
138.43
134.75
132.81
131.16
128.49
128.29
126.66
126.16
125.97
123.16
123.05
121.55
121.48
120.20
118.33
104.99
96.31
83.75
55.87
40.04
29.51
29.48
29.24
23.78
22.64
14.14
14.06
f1 (ppm)

^{1}H NMR for **10**

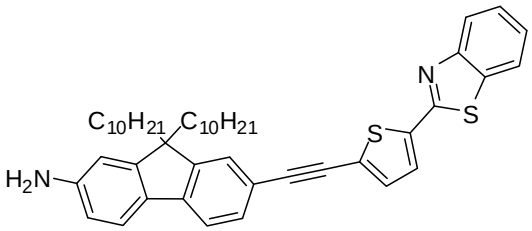
C10H21
C10H21
H2N
S
N
S

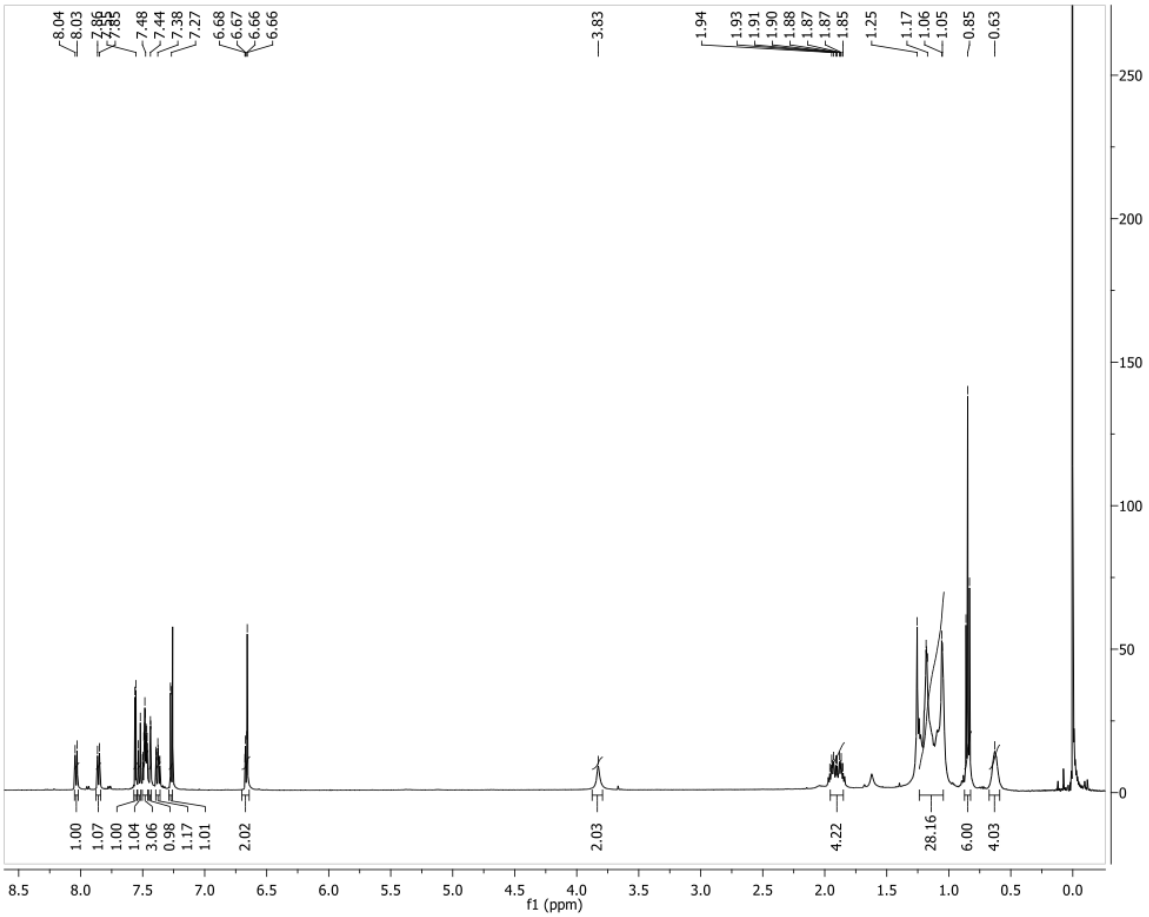
8.04
8.03
7.48
7.44
7.38
7.27
6.68
6.67
6.66
6.66
3.83
1.94
1.93
1.91
1.90
1.88
1.87
1.87
1.85
1.25
1.17
1.06
1.05
0.85
0.63
1.00
1.07
1.00
1.04
3.06
0.98
1.17
1.01
2.02
2.03
4.22
28.16
6.00
4.03
f1 (ppm)

^{13}C NMR for **10**

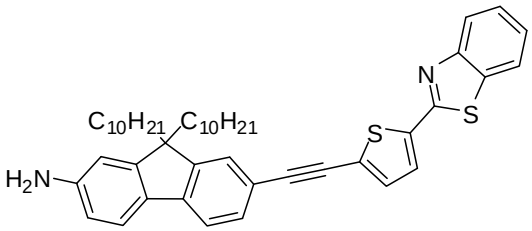

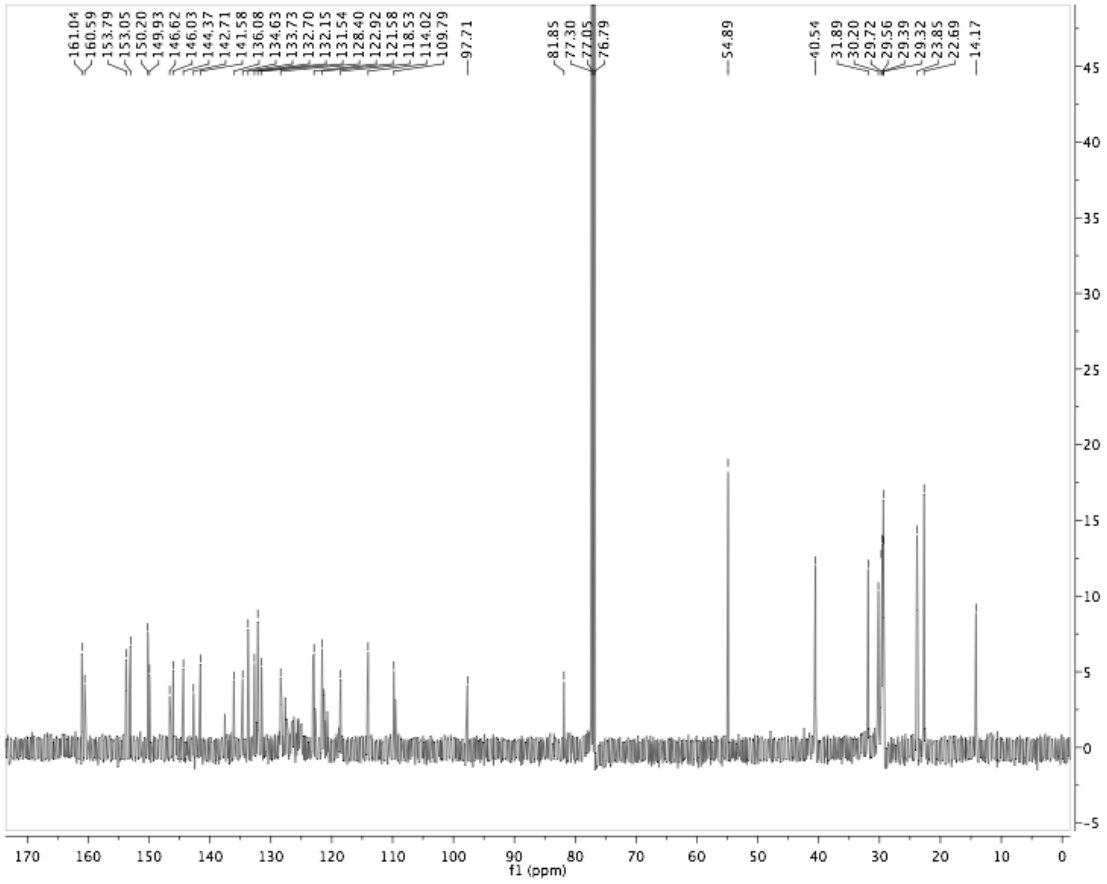

^{1}H NMR for **III**

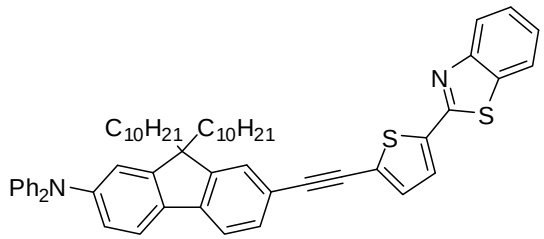

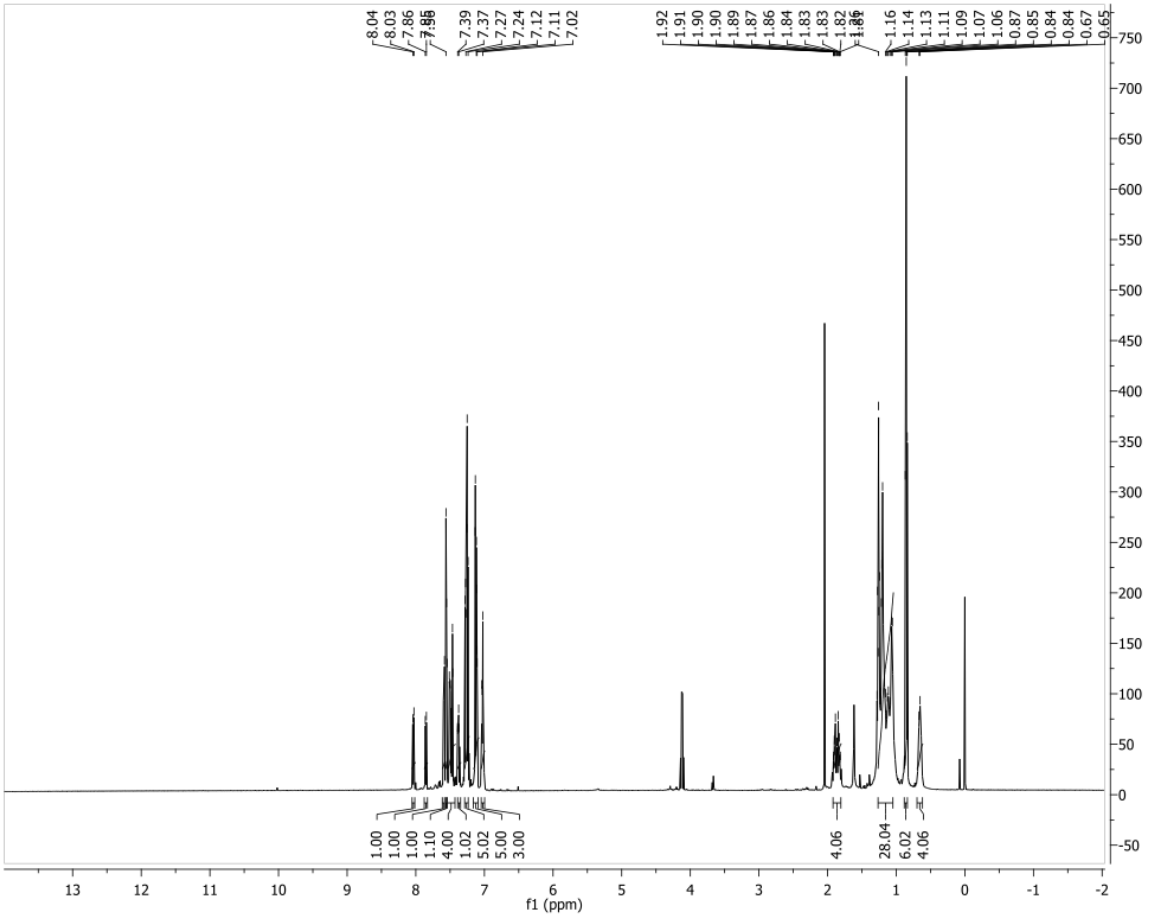

^{13}C NMR for **III**

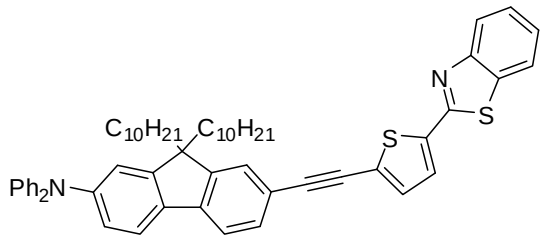

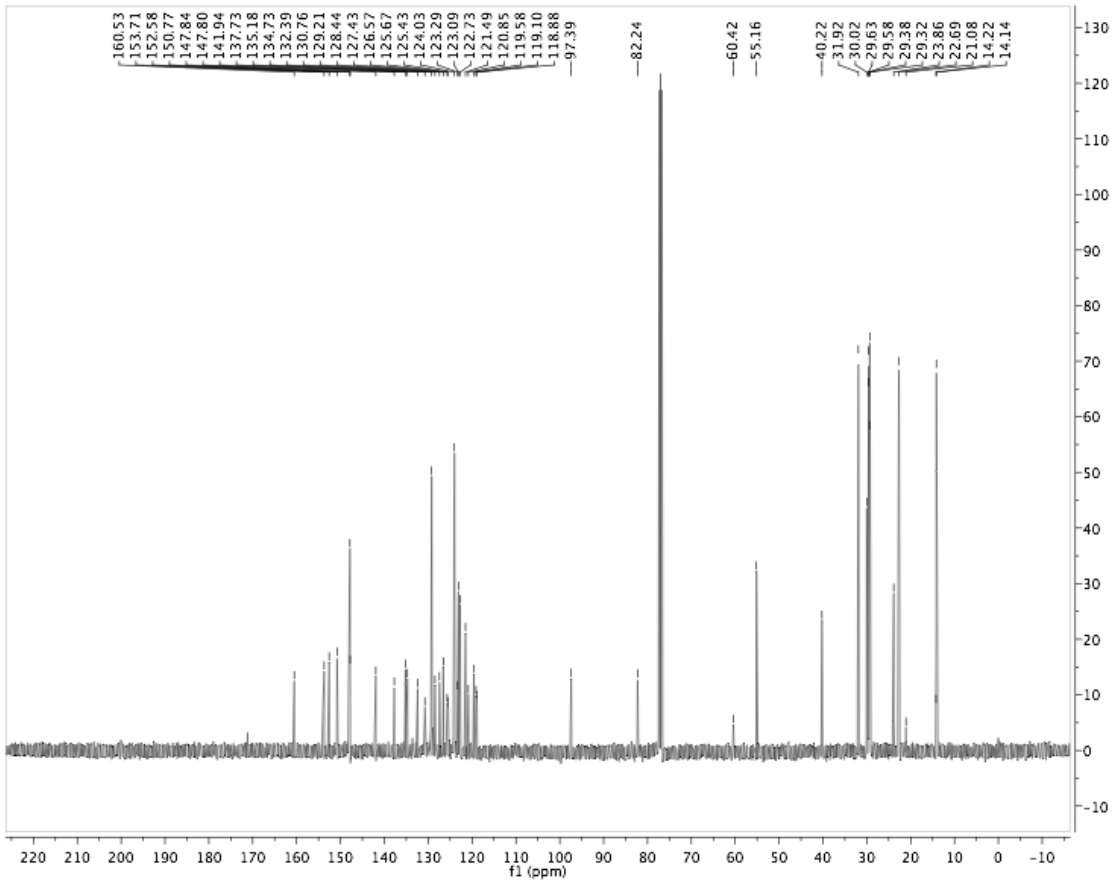

^{1}H NMR for **11**

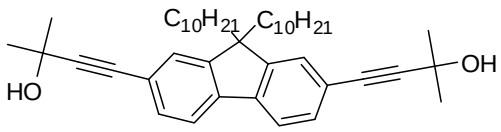
C10H21
C10H21
HO
OH

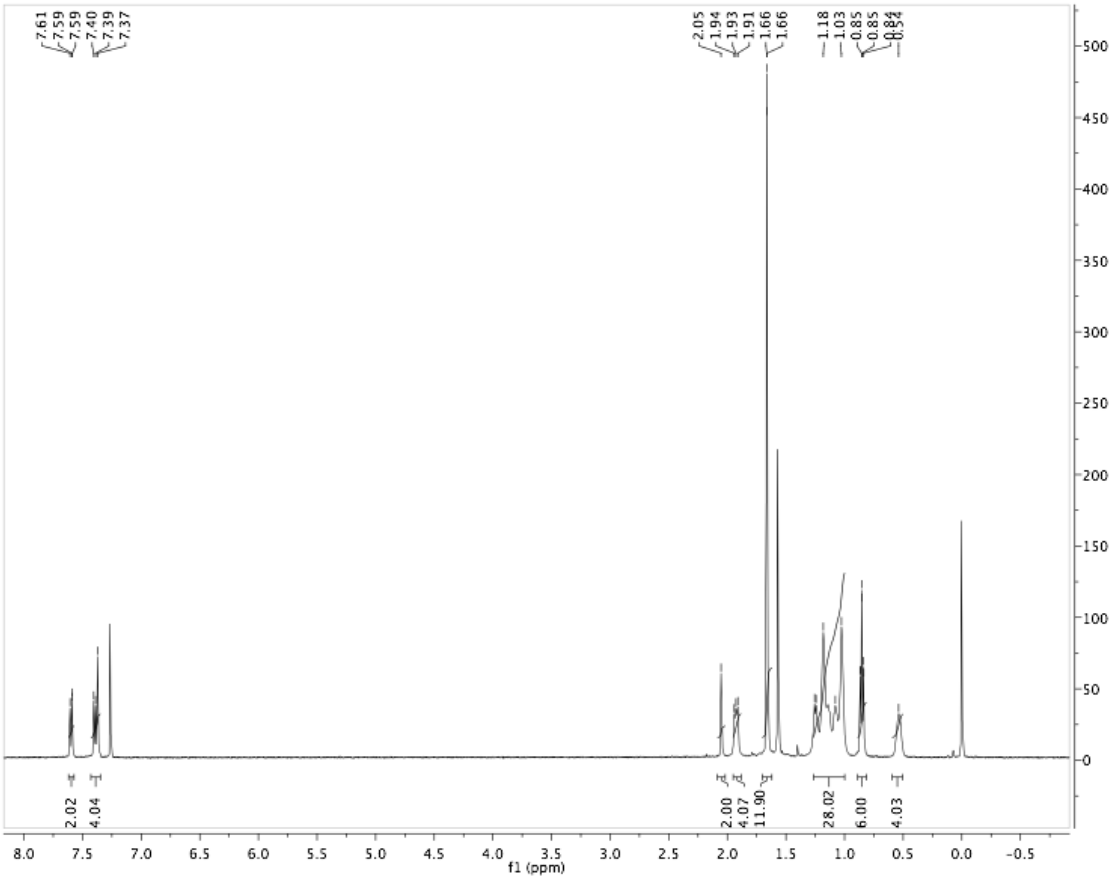
7.61
7.59
7.59
7.40
7.39
7.37
2.05
1.94
1.93
1.91
1.66
1.66
1.18
1.03
0.85
0.85
0.84
0.84
2.02
4.04
2.00
4.07
11.90
28.02
6.00
4.03
f1 (ppm)

^{13}C NMR for **11**

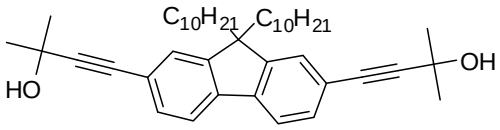

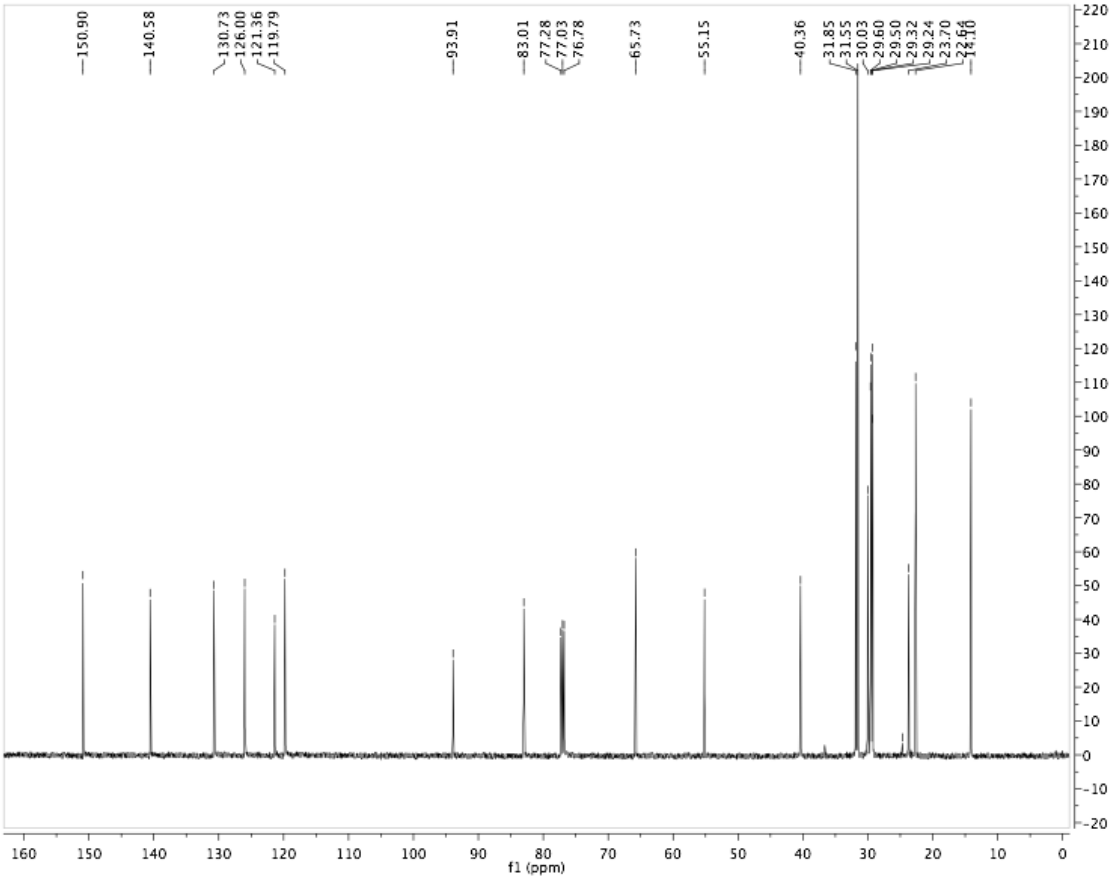

^{1}H NMR for **12**

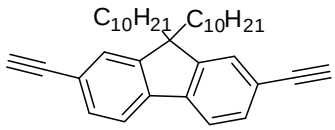
$C_{10}H_{21}$
$C_{10}H_{21}$

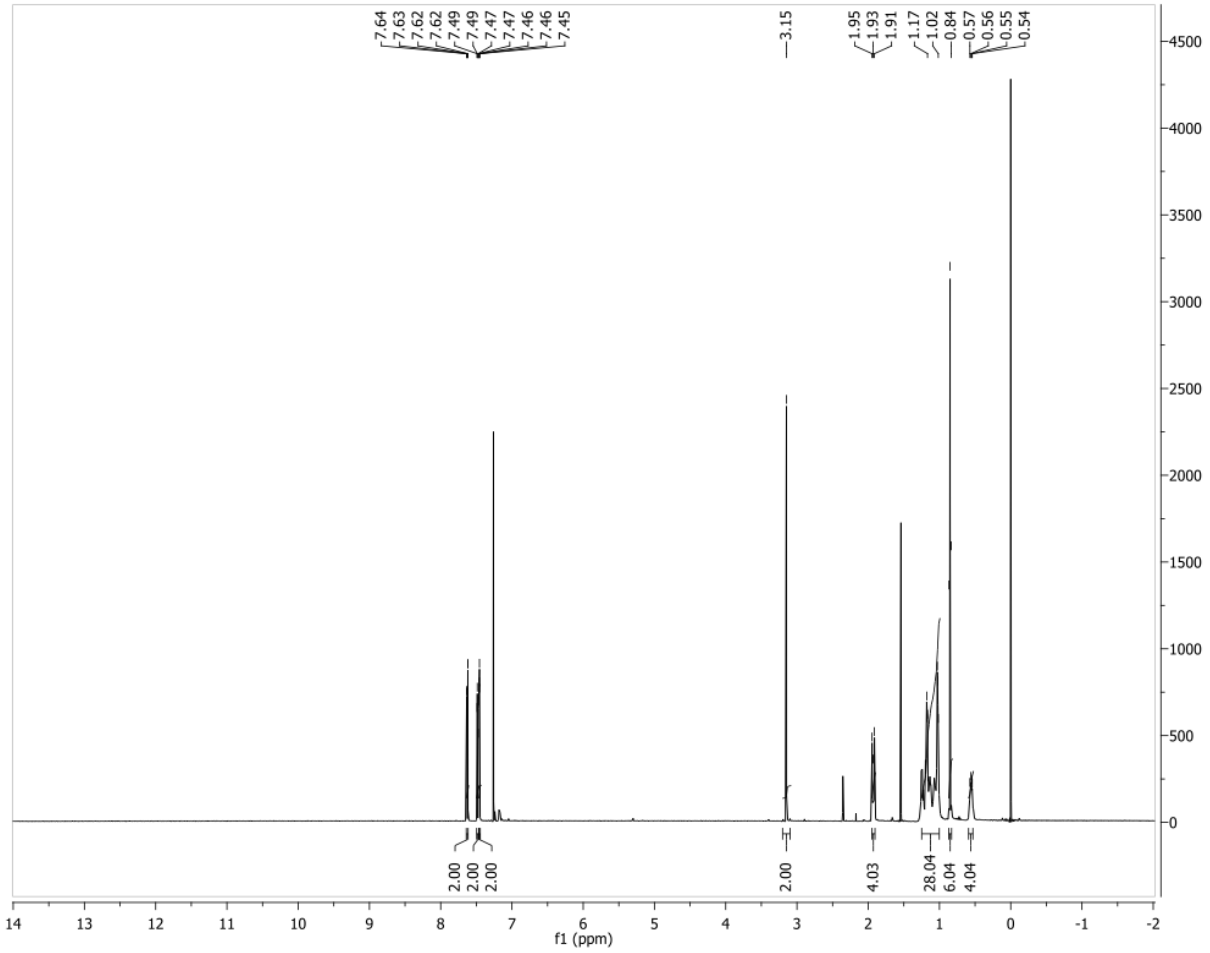
7.64
7.63
7.62
7.62
7.49
7.49
7.47
7.47
7.46
7.46
7.45
3.15
1.95
1.93
1.91
1.17
1.02
0.84
0.57
0.56
0.55
0.54
2.00
2.00
2.00
2.00
4.03
28.04
6.04
4.04
f1 (ppm)

^{13}C NMR for **12**

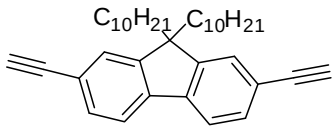

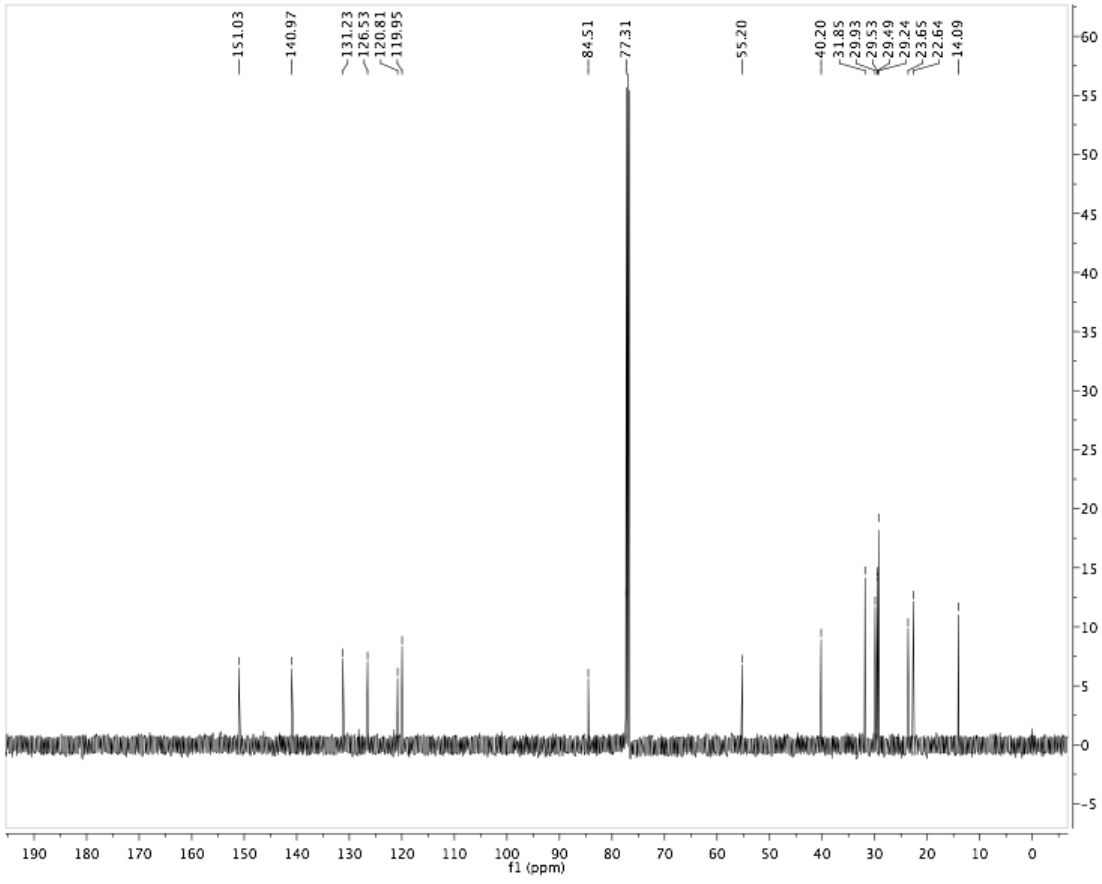

^{1}H NMR for **IV**

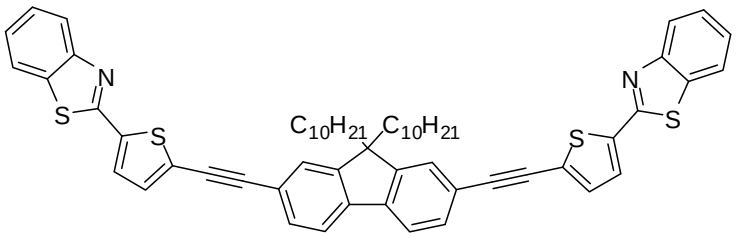
N
S
S
$C_{10}H_{21}$ $C_{10}H_{21}$
S
N
S

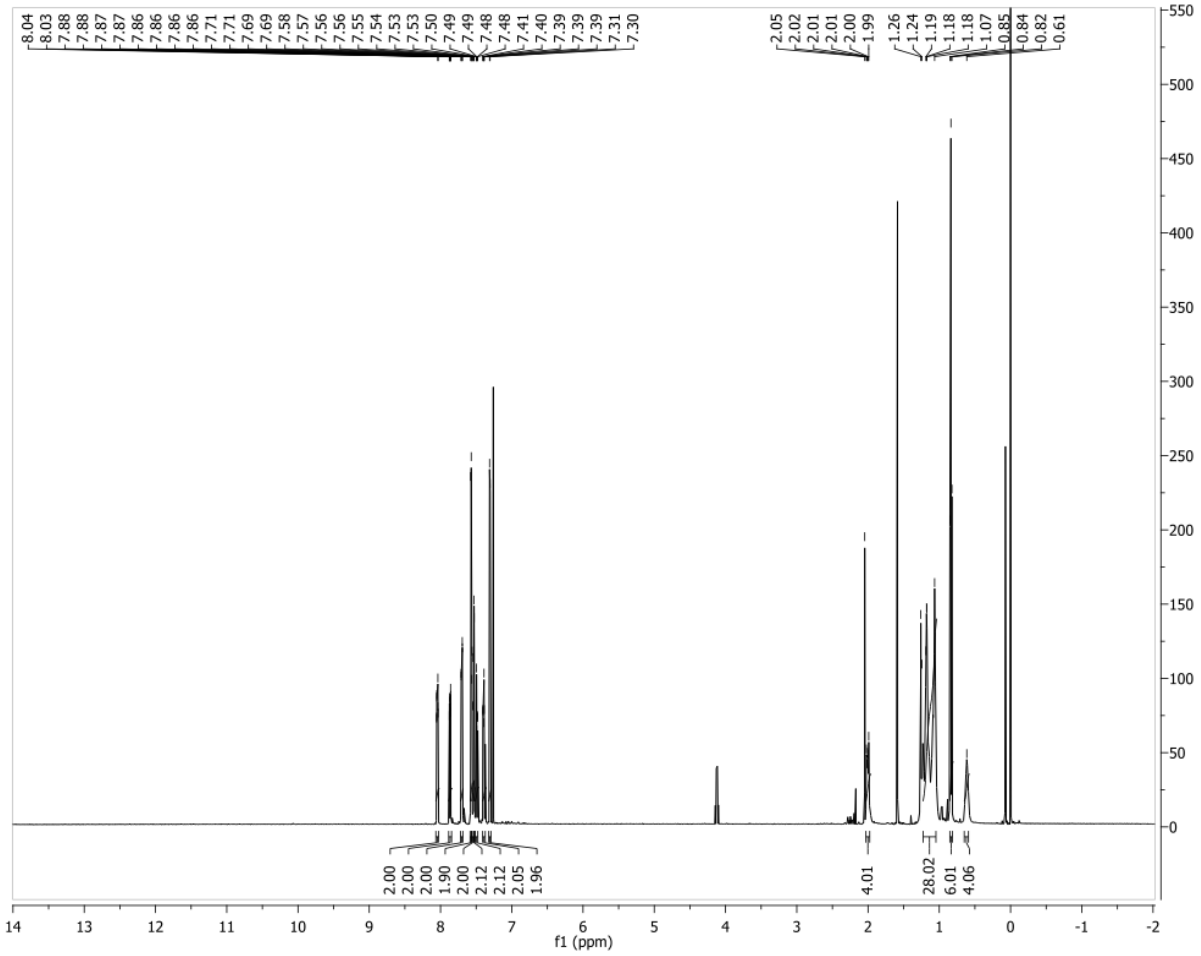
8.04 8.03 7.88 7.88 7.87 7.87 7.86 7.86 7.86 7.86 7.71 7.71 7.69 7.69 7.58 7.57 7.56 7.56 7.55 7.54 7.53 7.53 7.50 7.49 7.49 7.48 7.48 7.41 7.40 7.39 7.39 7.39 7.31 7.30
2.05 2.02 2.01 2.01 2.00 1.99 1.26 1.24 1.19 1.18 1.18 1.07 0.85 0.84 0.82 0.61
2.00 2.00 2.00 1.90 2.00 2.12 2.12 2.05 1.96
4.01 28.02 6.01 4.06
f1 (ppm)

^{13}C NMR for **IV**

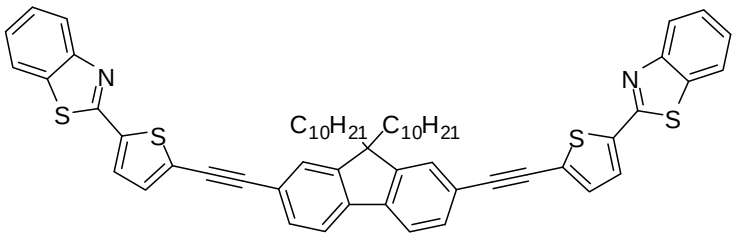

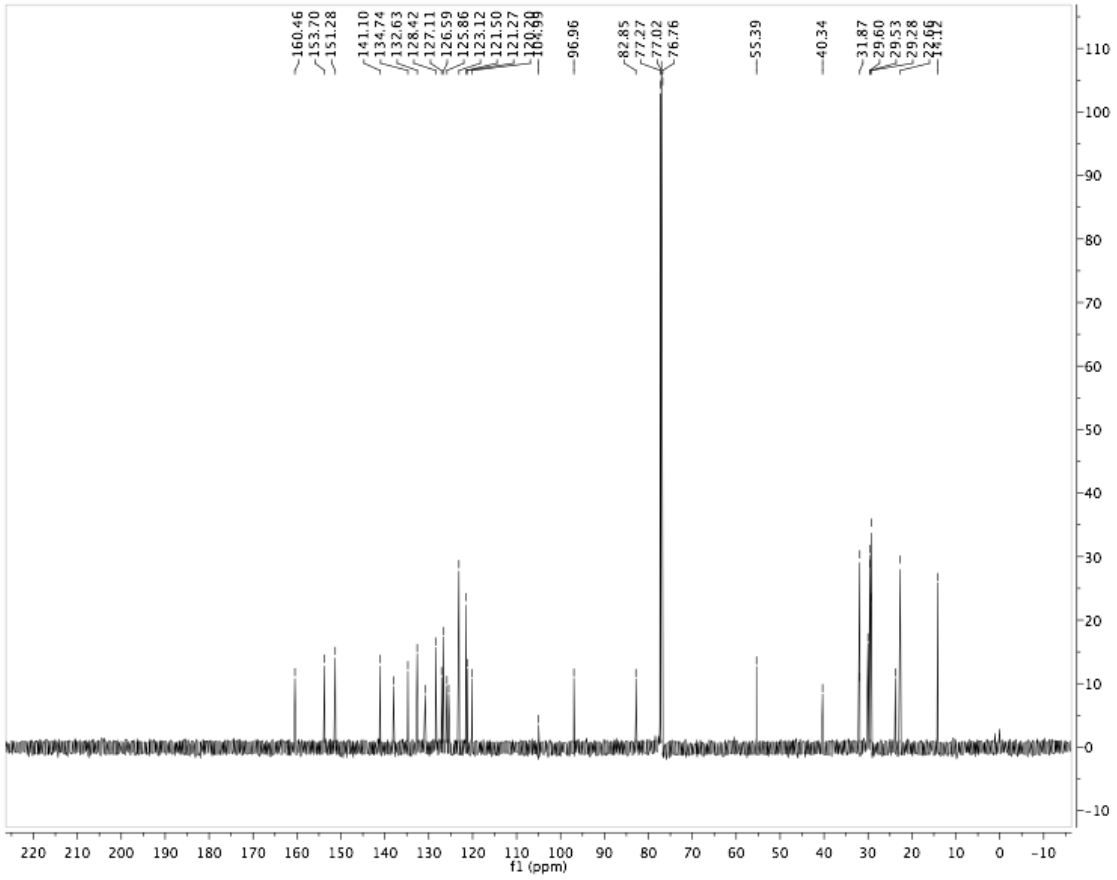

APENDIX B: ^{1}H AND ^{13}C NMR SPECTRA OF NEW MOLECULES IN CHAPTER 4

^{1}H NMR for **14**

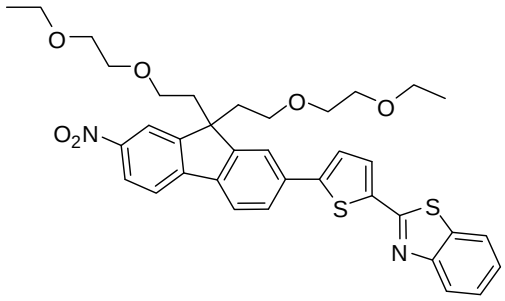
O
O
O
O
O
O_2N
S
S
N

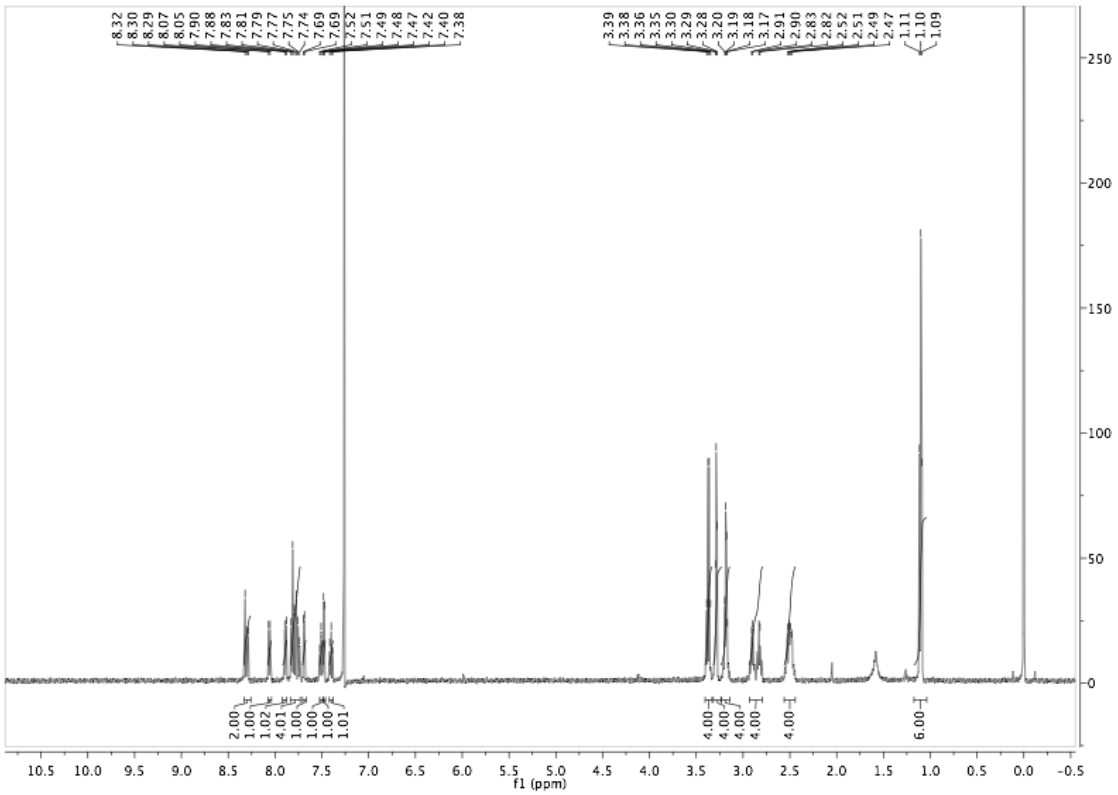
8.32
8.30
8.29
8.07
8.05
7.90
7.88
7.83
7.81
7.79
7.77
7.75
7.74
7.69
7.69
7.52
7.51
7.49
7.48
7.47
7.42
7.40
7.38
3.39
3.38
3.36
3.35
3.30
3.29
3.28
3.20
3.19
3.18
3.17
2.91
2.90
2.83
2.82
2.52
2.51
2.49
2.47
1.11
1.10
1.09
2.00
1.00
1.02
4.01
1.00
1.00
1.00
1.01
4.00
4.00
4.00
4.00
4.00
6.00
f1 (ppm)

^{13}C NMR for **14**

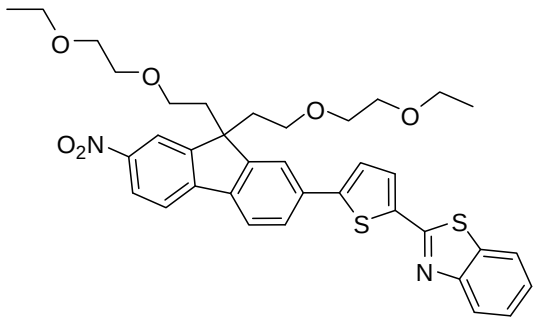

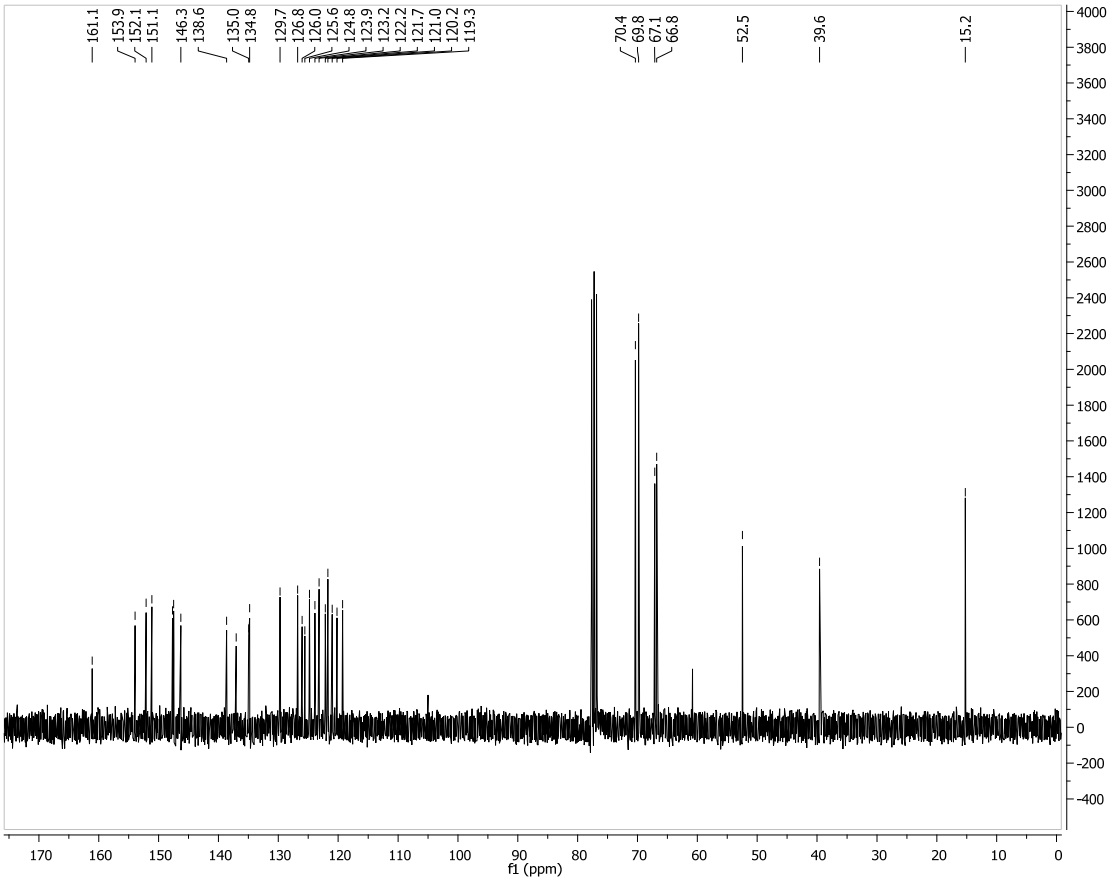

^{1}H NMR for **15**

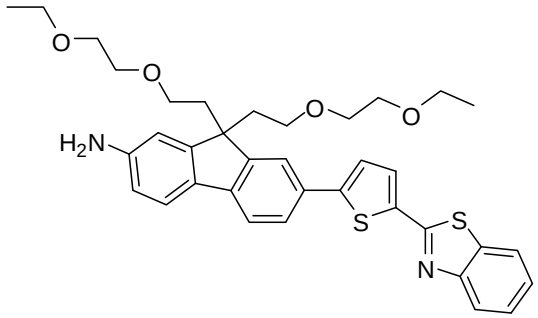
O
O
O
O
O
H2N
S
S
N

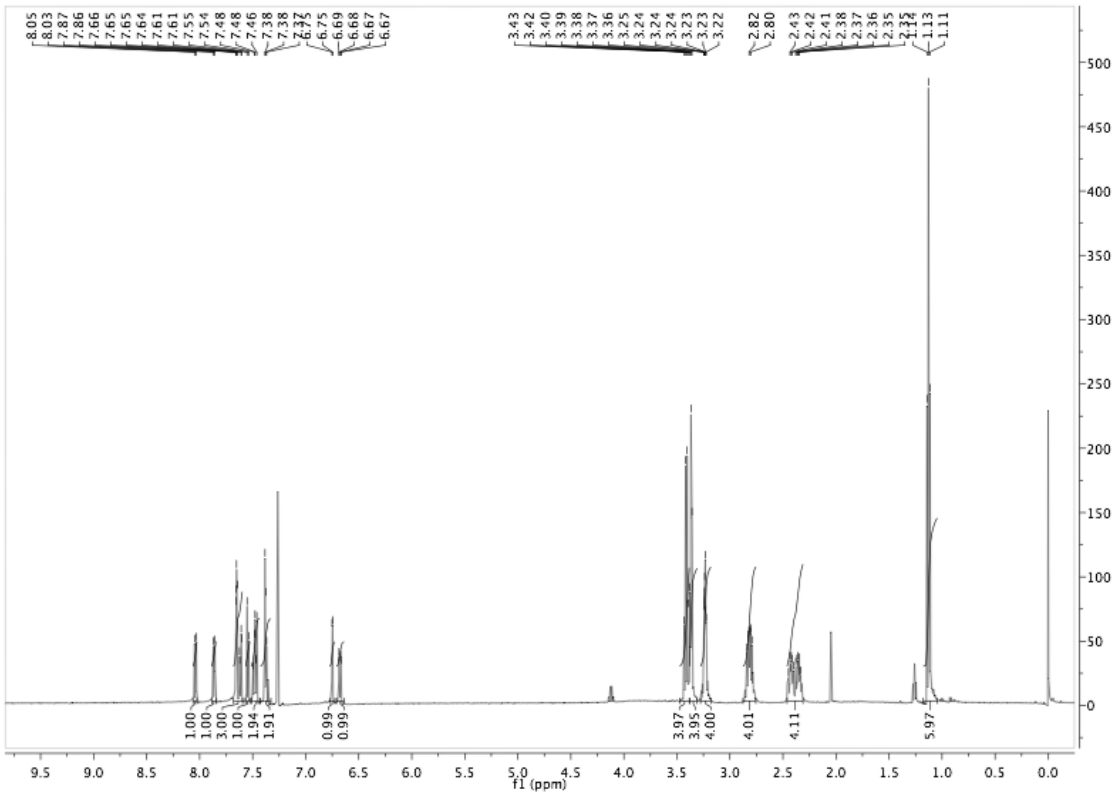
8.05
8.03
7.87
7.86
7.66
7.65
7.65
7.64
7.61
7.61
7.55
7.54
7.48
7.48
7.46
7.38
7.38
7.37
6.75
6.69
6.68
6.67
6.67
3.43
3.42
3.40
3.39
3.38
3.37
3.36
3.25
3.24
3.24
3.24
3.23
3.23
3.22
2.82
2.80
2.43
2.42
2.41
2.38
2.37
2.36
2.35
1.14
1.13
1.11
1.00
1.00
3.00
1.00
1.94
1.91
0.99
0.99
3.97
3.95
4.00
4.01
4.11
5.97
f1 (ppm)

^{13}C NMR for **15**

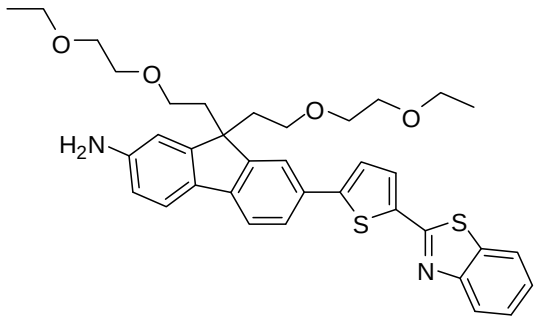

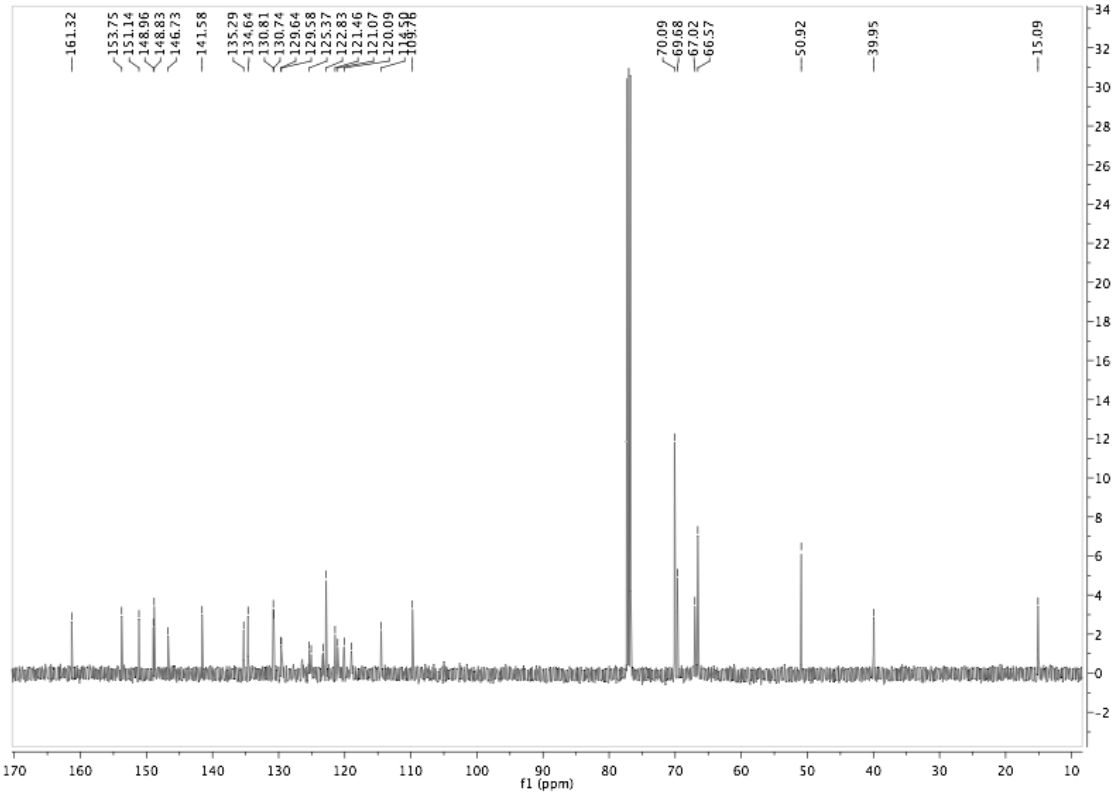

^{1}H NMR for **16**

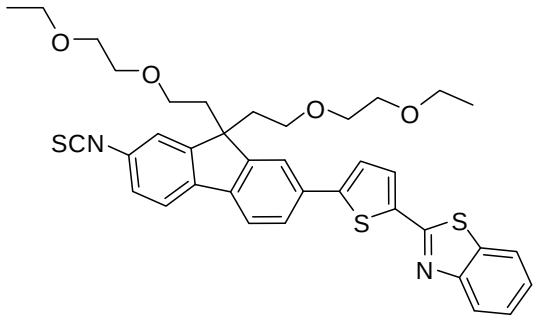
O
O
O
O
O
SCN
S
S
N

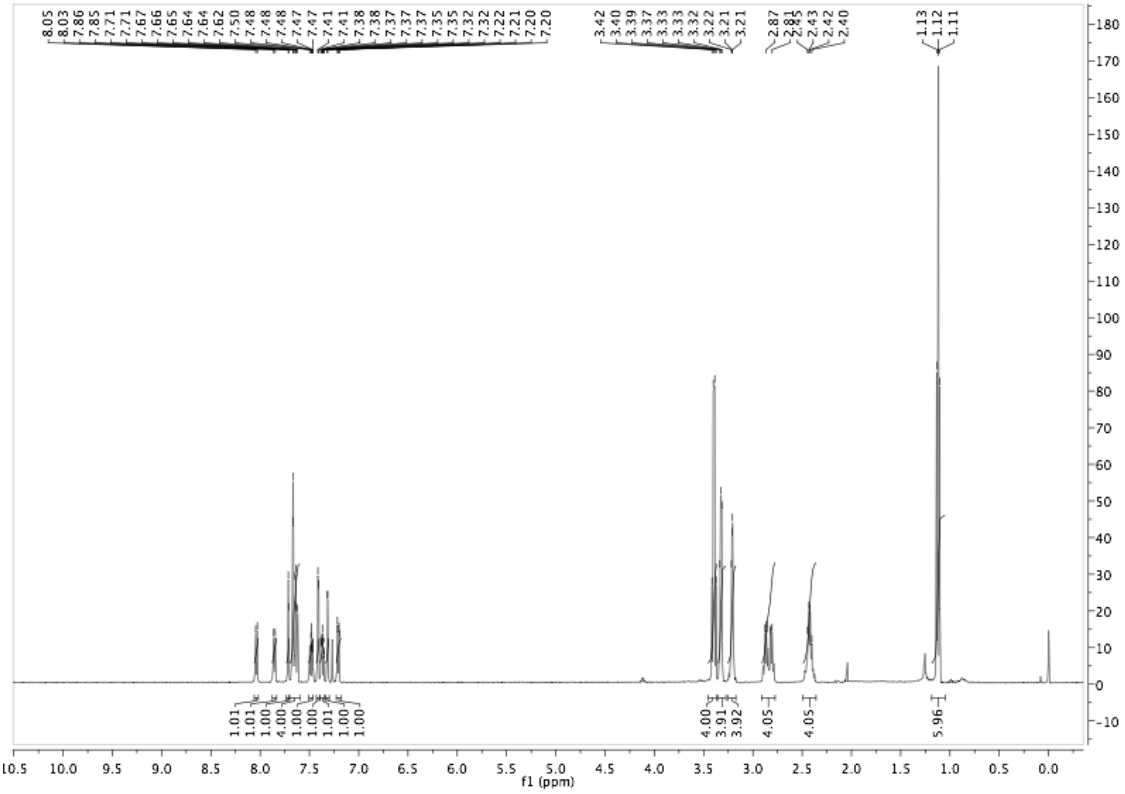
8.05
8.03
7.86
7.85
7.71
7.67
7.66
7.65
7.64
7.62
7.50
7.48
7.48
7.48
7.47
7.47
7.41
7.41
7.38
7.38
7.37
7.37
7.37
7.35
7.35
7.32
7.32
7.22
7.21
7.20
7.20
3.42
3.40
3.39
3.37
3.33
3.33
3.32
3.22
3.21
3.21
2.87
2.81
2.45
2.43
2.42
2.40
1.13
1.12
1.11
1.01
1.01
1.00
4.00
1.00
1.00
1.01
1.00
1.00
4.00
3.91
3.92
4.05
4.05
5.96
f1 (ppm)

^{13}C NMR for **16**

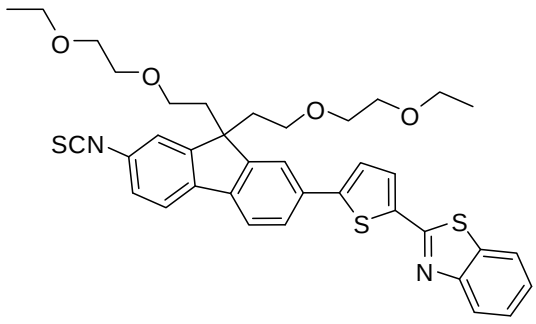

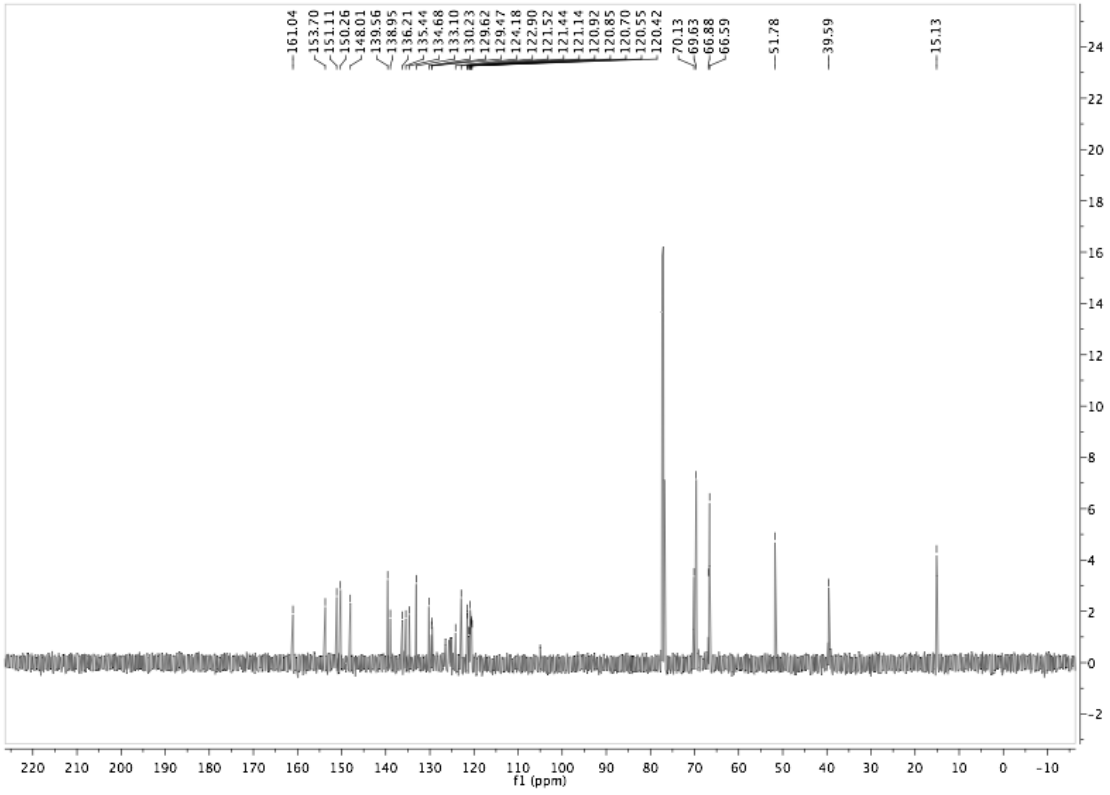

^{1}H NMR for **17**

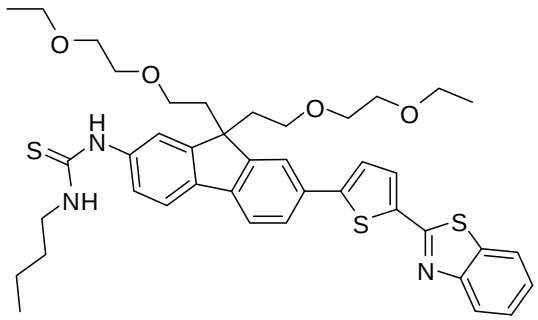

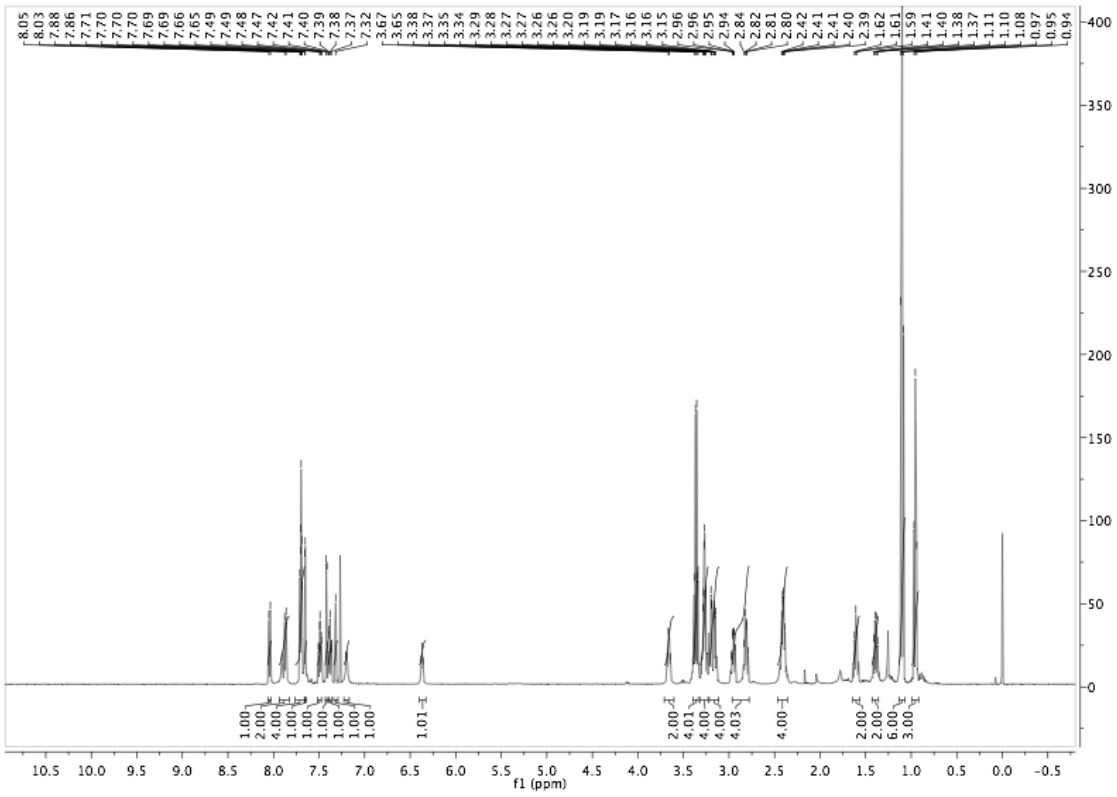

^{13}C NMR for **17**

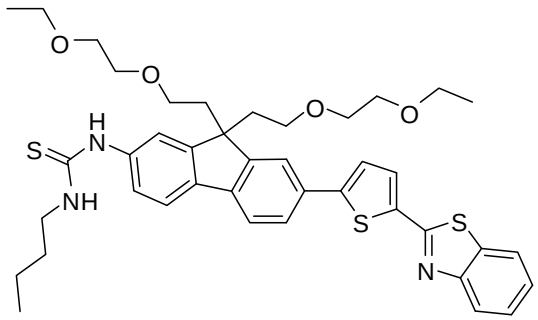

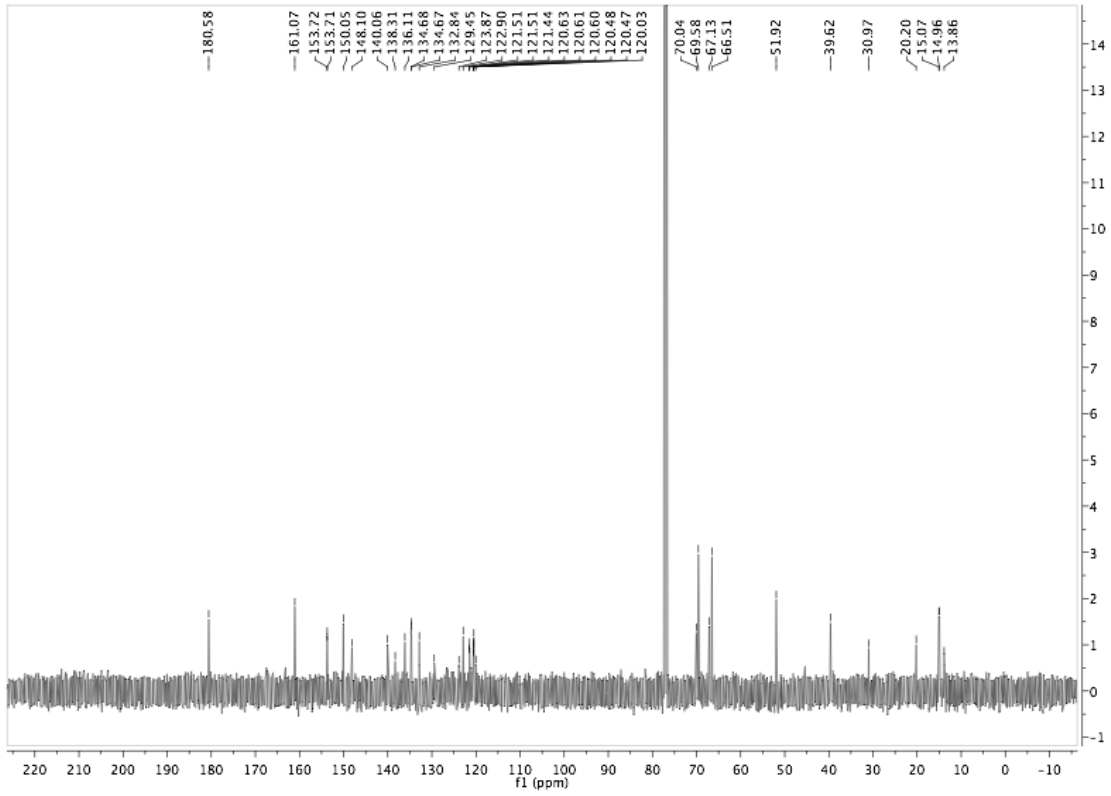

^{1}H NMR for **18**

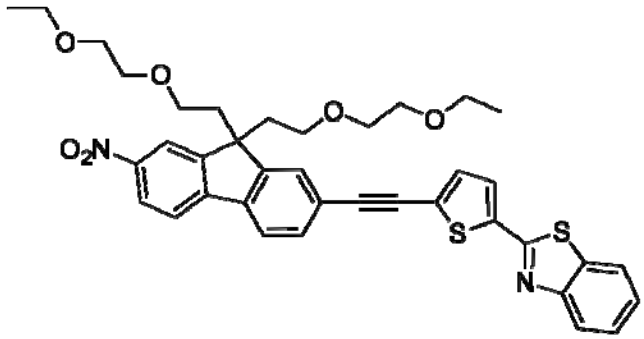

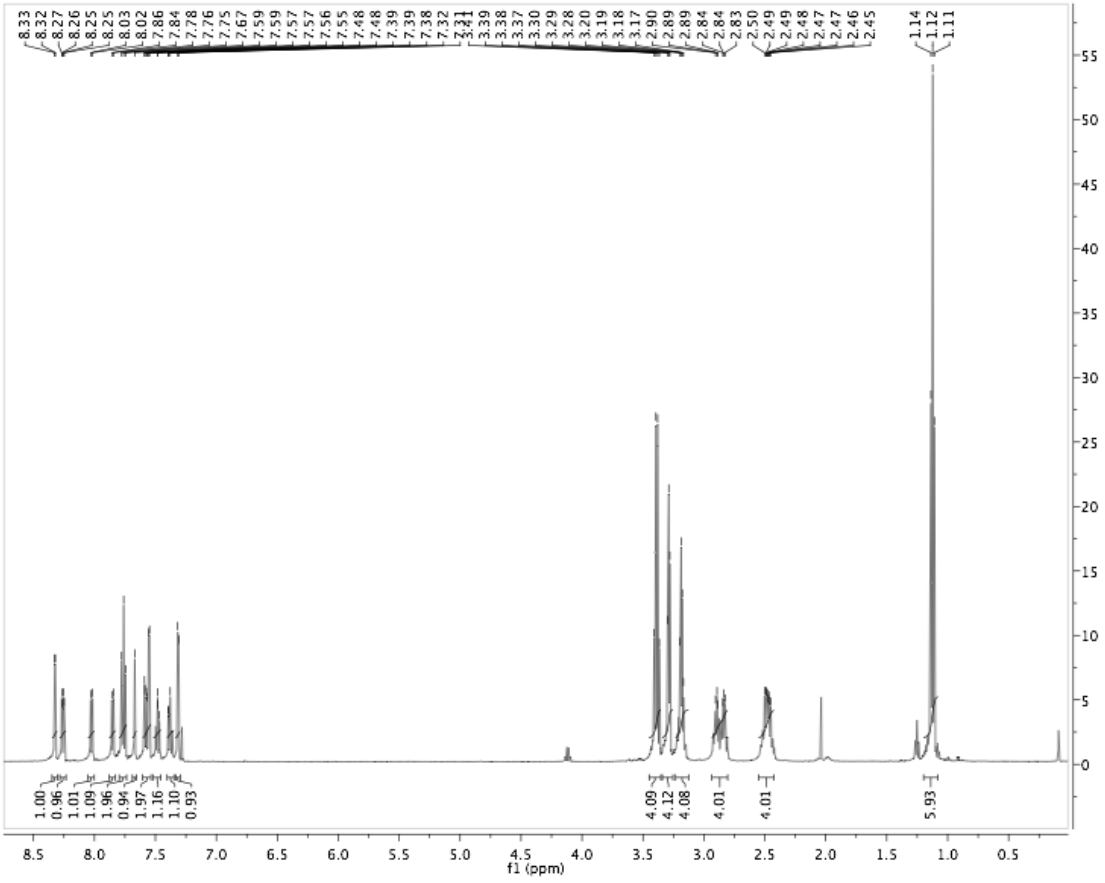

^{13}C NMR for **18**

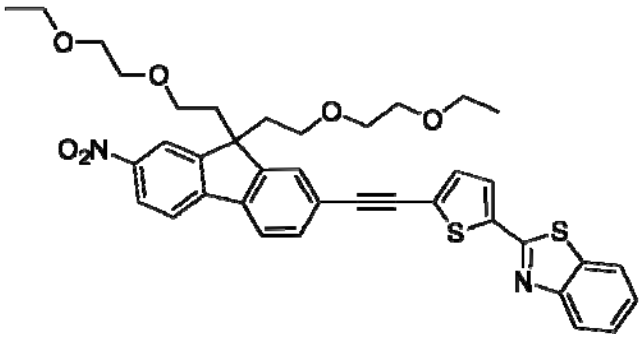

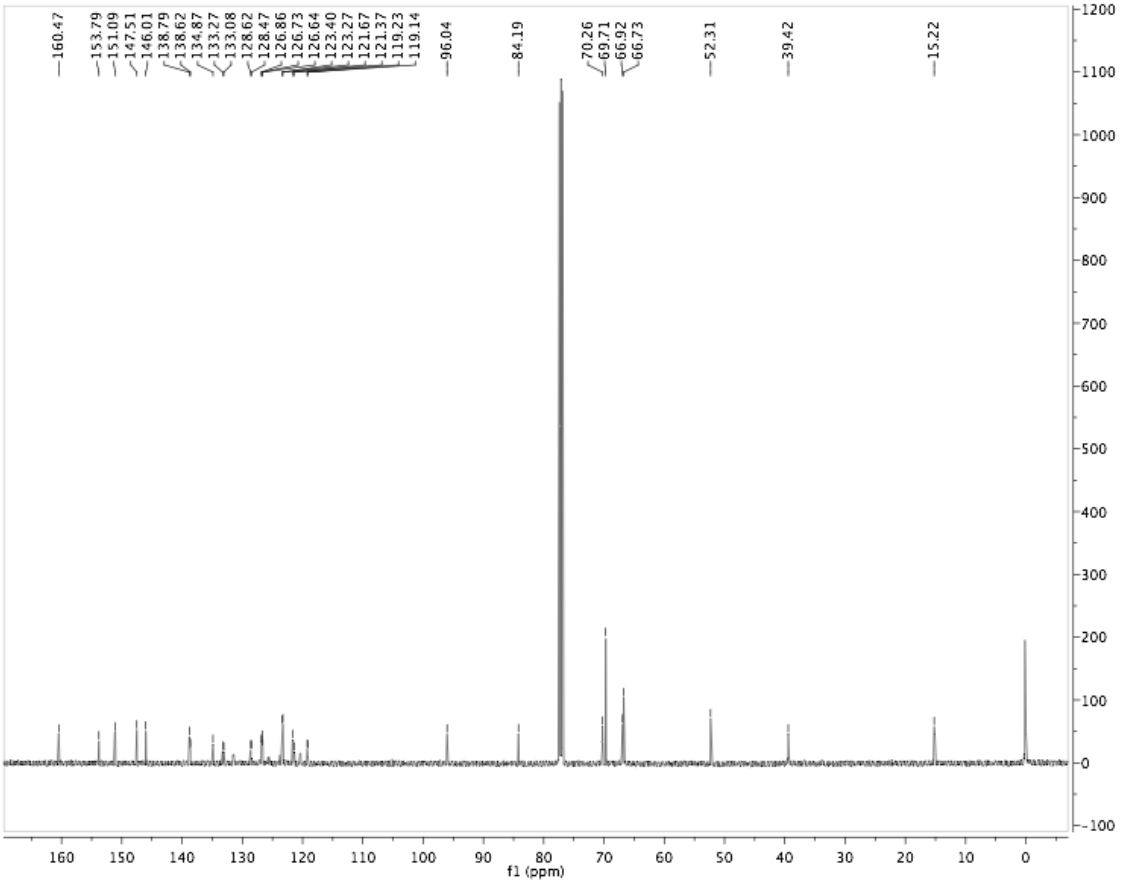

^{1}H NMR for **19**

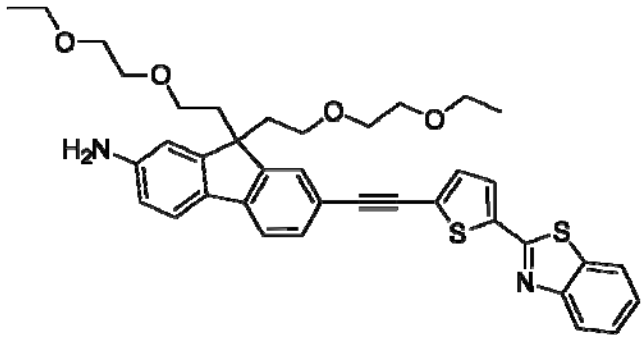
O
O
O
O
H2N
S
S
N

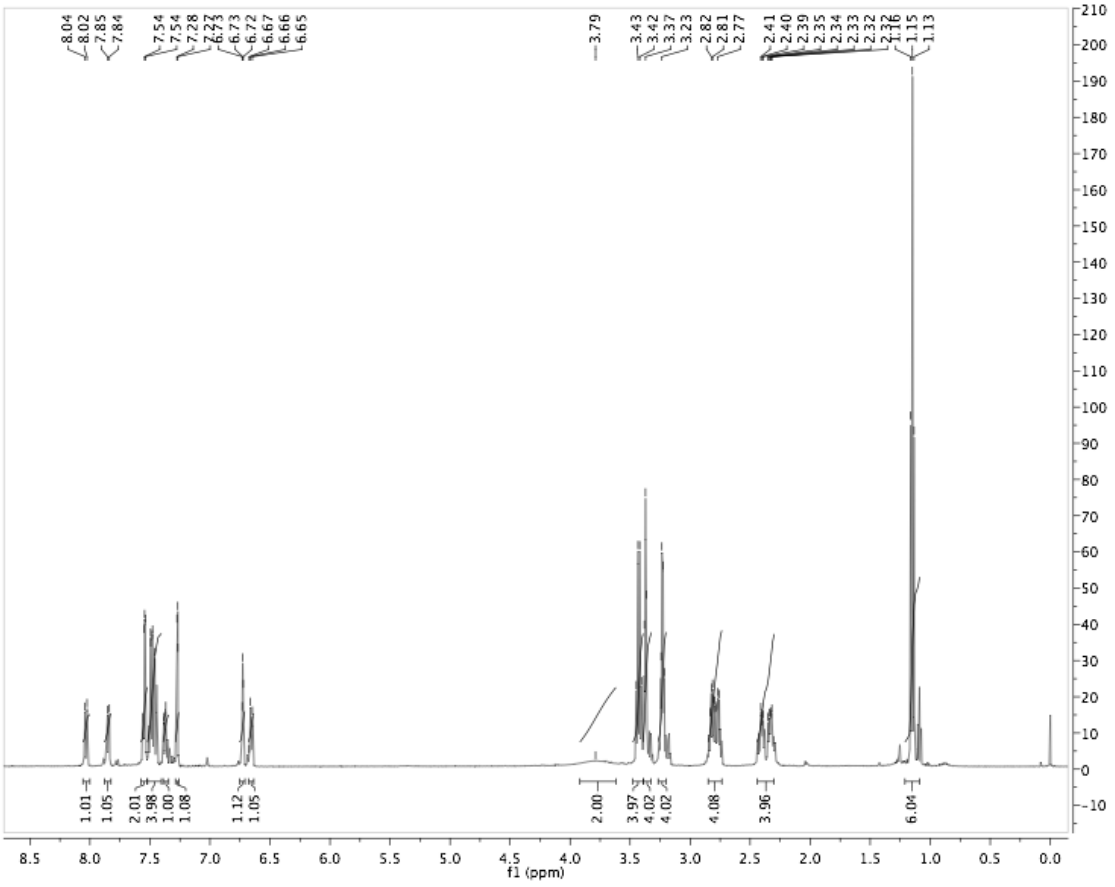
8.04
8.02
7.85
7.84
7.54
7.54
7.28
6.73
6.72
6.67
6.66
6.65
3.79
3.43
3.42
3.37
3.23
2.82
2.81
2.77
2.41
2.40
2.39
2.35
2.34
2.33
2.32
1.16
1.15
1.13
1.01
1.05
2.01
3.98
1.00
1.08
1.12
1.05
2.00
3.97
4.02
4.02
4.08
3.96
6.04
f1 (ppm)

^{13}C NMR for **19**

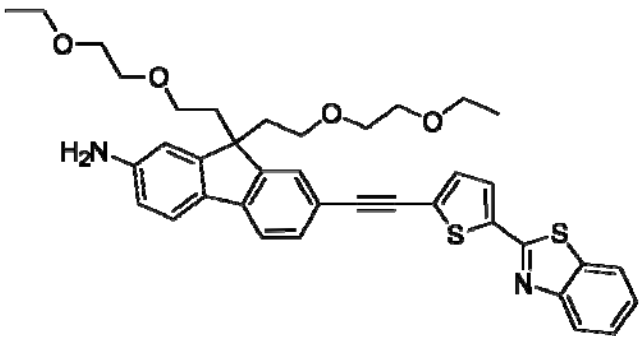

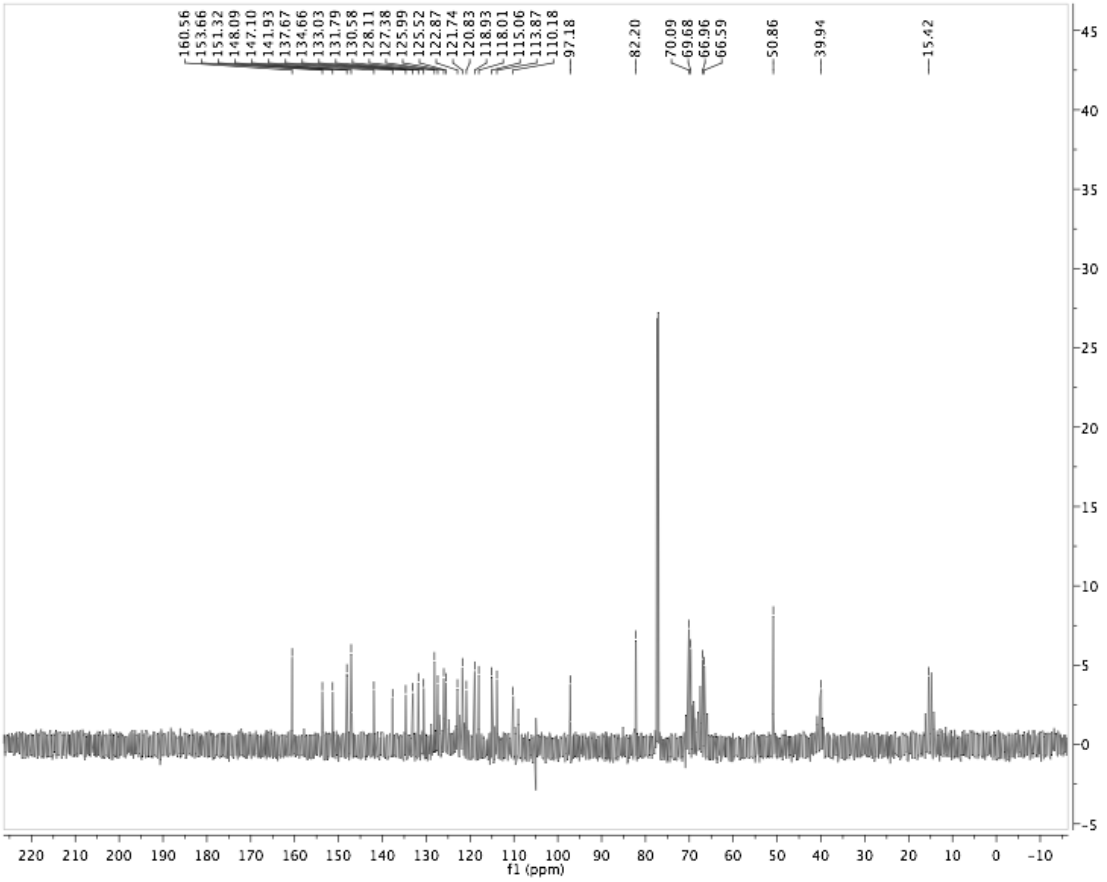

^{1}H NMR for **20**

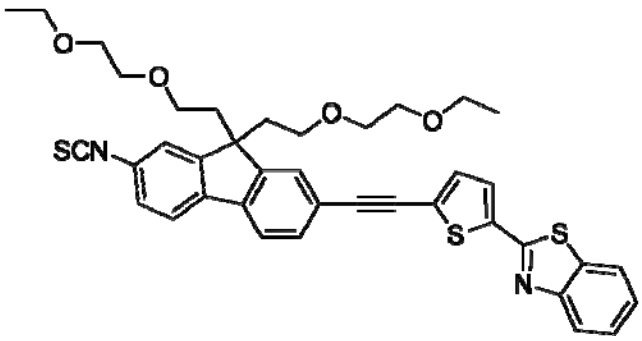

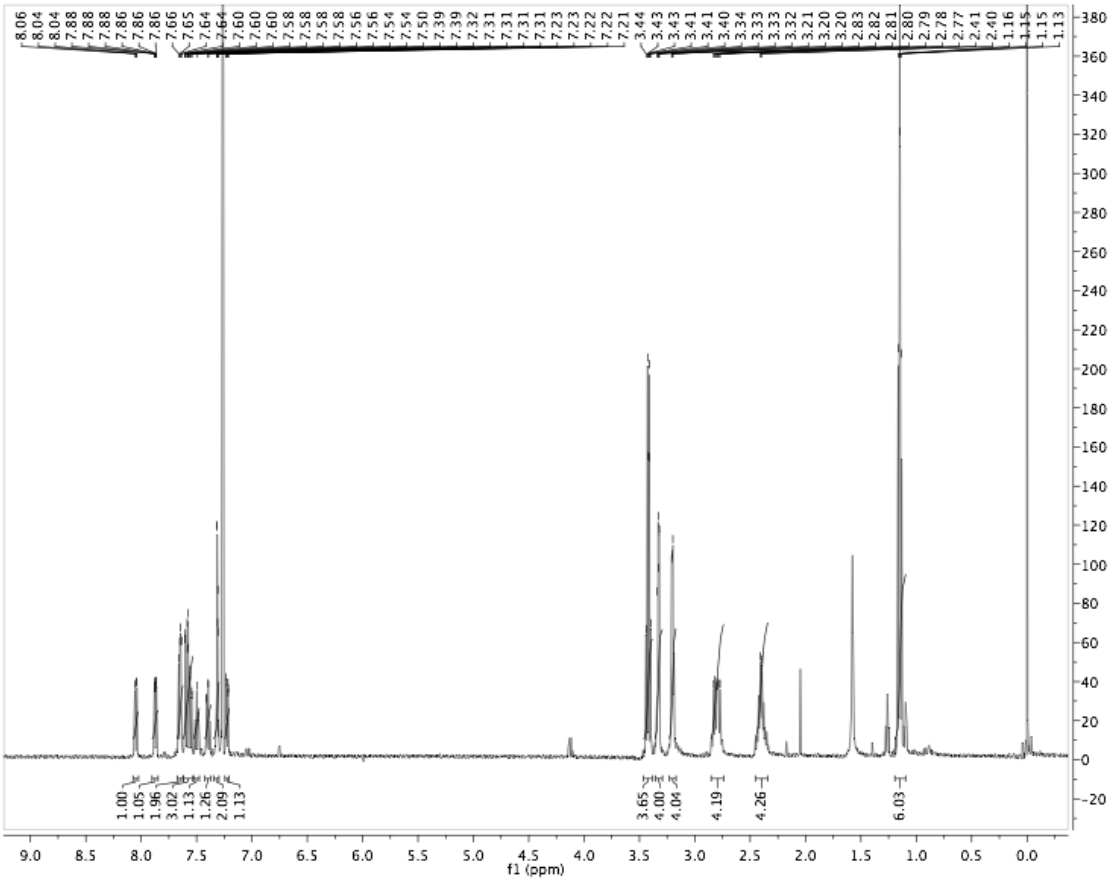

^{13}C NMR for **20**

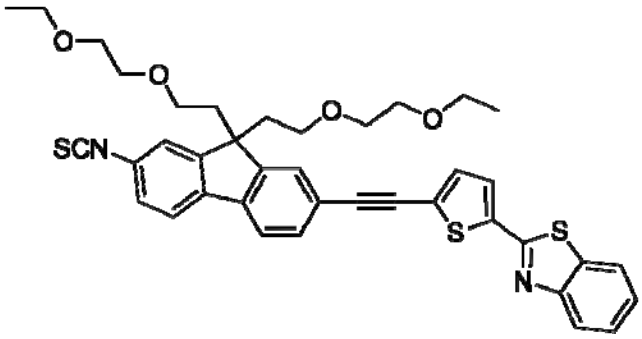

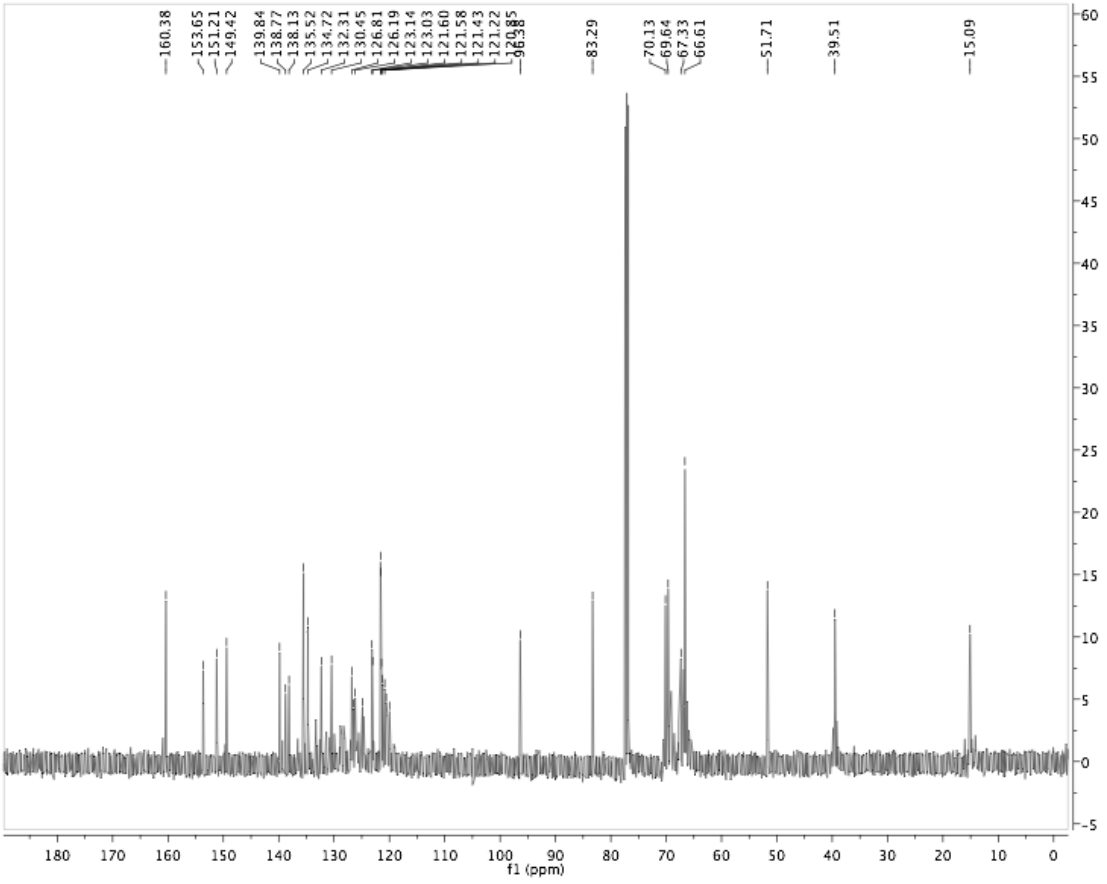

^{1}H NMR for **21**

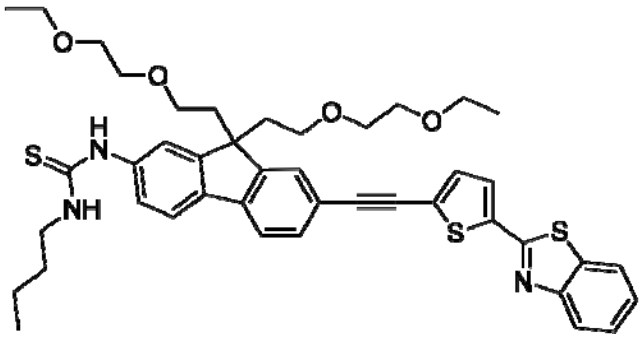

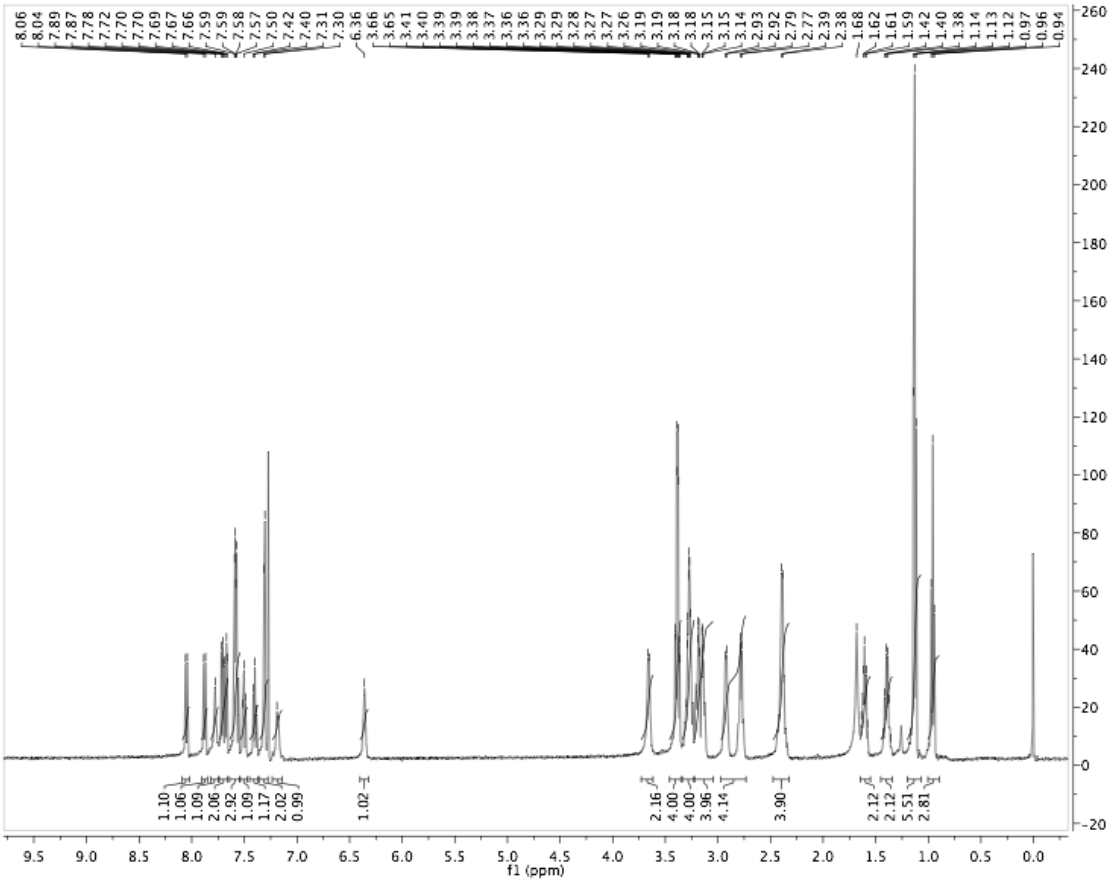
8.06 8.04 7.89 7.87 7.78 7.72 7.70 7.70 7.69 7.67 7.66 7.59 7.59 7.58 7.57 7.50 7.42 7.40 7.31 7.30 6.36 3.66 3.65 3.41 3.40 3.39 3.39 3.38 3.37 3.36 3.36 3.29 3.29 3.28 3.27 3.27 3.26 3.19 3.19 3.18 3.18 3.15 3.15 3.14 2.93 2.92 2.79 2.77 2.39 2.38 1.68 1.62 1.61 1.59 1.42 1.40 1.38 1.14 1.13 1.12 0.97 0.96 0.94
1.10 1.06 1.09 2.06 2.92 1.09 1.17 2.02 0.99
1.02
2.16 4.00 4.00 3.96 4.14
3.90
2.12 2.12 5.51 2.81
f1 (ppm)

^{13}C NMR for **21**

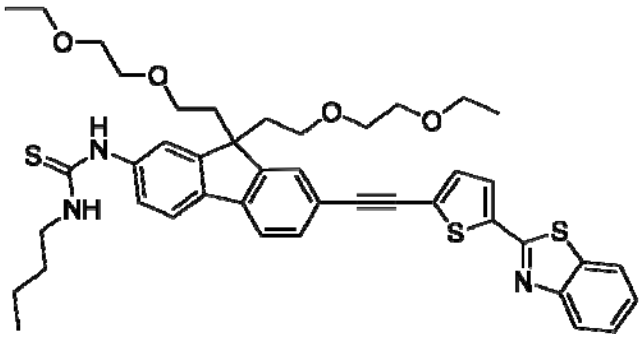

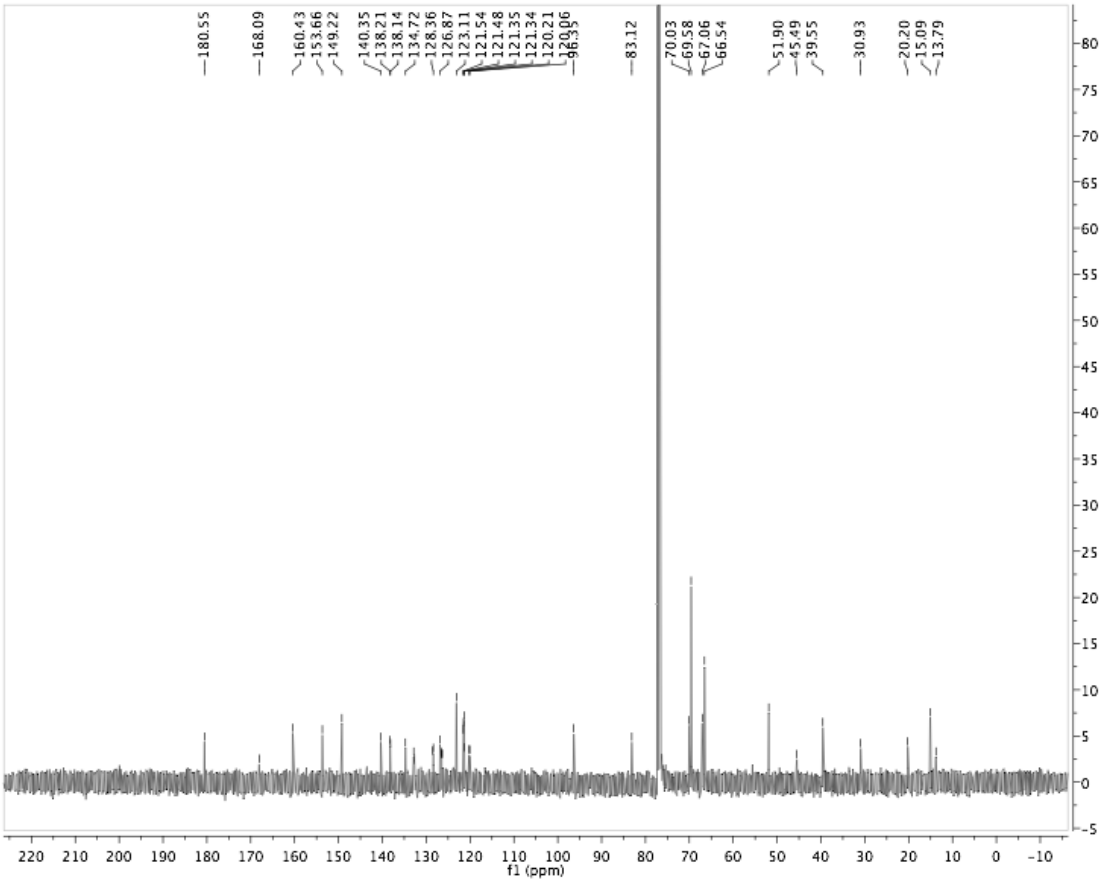

LIST OF REFERENCES

(1) Denk, W., Strickler, J. H., and Webb, W. W. (1990) 2-Photon Laser Scanning Fluorescence Microscopy. *Science 248*, 73-76.

(2) Parthenopoulos, D. A., and Rentzepis, P. M. (1989) 3-Dimensional Optical Storage Memory. *Science 245*, 843-845.

(3) Belfield, K. D., and Schafer, K. J. (2002) A new photosensitive polymeric material for WORM optical data storage using multichannel two-photon fluorescence readout. *Chem Mater 14*, 3656-3662.

(4) Yanez, C. O., Andrade, C. D., Yao, S., Luchita, G., Bondar, M. V., and Belfield, K. D. (2009) Photosensitive Polymeric Materials for Two-Photon 3D WORM Optical Data Storage Systems. *Acs Applied Materials & Interfaces 1*, 2219-2229.

(5) Belfield, K. D., Schafer, K. J., Liu, Y. U., Liu, J., Ren, X. B., and Van Stryland, E. W. (2000) Multiphoton-absorbing organic materials for microfabrication, emerging optical applications and non-destructive three-dimensional imaging. *Journal of Physical Organic Chemistry 13*, 837-849.

(6) Maruo, S., Nakamura, O., and Kawata, S. (1997) Three-dimensional microfabrication with two-photon-absorbed photopolymerization. *Optics Letters 22*, 132-134.

(7) Belfield, K. D., Ren, X. B., Van Stryland, E. W., Hagan, D. J., Dubikovsky, V., and Miesak, E. J. (2000) Near-IR two-photon photoinitiated polymerization using a fluorone/amine initiating system. *Journal of the American Chemical Society 122*, 1217-1218.

(8) Schafer-Hales, K. J., Belfield, K. D., Yao, S., Frederiksen, P. K., Hales, J. M., and Kolattukudy, P. E. (2005) Fluorene-based fluorescent probes with high two-photon action cross-sections for biological multiphoton imaging applications. *Journal of Biomedical Optics 10*, 1-8.

(9) Belfield, K. D., Bondar, M. V., Morales, A. R., Yavuz, O., and Przhonska, O. V. (2003) A new blue light-emitting oligofluorene glass: synthesis, characterization and photophysical properties. *Journal of Physical Organic Chemistry 16*, 194-201.

(10) Belfield, K. D., Morales, A. R., Hales, J. M., Hagan, D. J., Van Stryland, E. W., Chapela, V. M., and Percino, J. (2004) Linear and two-photon photophysical properties of a series of symmetrical diphenylaminofluorenes. *Chemistry of Materials 16*, 2267-2273.

(11) Belfield, K. D., Morales, A. R., Kang, B. S., Hales, J. M., Hagan, D. J., Van Stryland, E. W., Chapela, V. M., and Percino, J. (2004) Synthesis, characterization, and optical properties of new two-photon-absorbing fluorene derivatives. *Chem Mater 16*, 4634-4641.

(12) Yao, S., and Belfield, K. D. (2005) Synthesis of two-photon absorbing unsymmetrical branched chromophores through direct tris(bromomethylation) of fluorene. *J Org Chem 70*, 5126-5132.

(13) Belfield, K. D., Yao, S., and Bondar, M. V. (2008) Two-photon Absorbing Photonic Materials: From Fundamentals to Applications. *Adv Polym Sci 213*, 97-156.

(14) Yanez, C. O., Andrade, C. D., and Belfield, K. D. (2009) Characterization of novel sulfonium photoacid generators and their microwave-assisted synthesis. *Chem Commun*, 827-829.

(15) Belfield, K. D., Bondar, M. V., Yanez, C. O., Hernandez, F. E., and Przhonska, O. V. (2009) Two-photon absorption and lasing properties of new fluorene derivatives. *J Mater Chem 19*, 7498-7502.

(16) Moura, G. L. C., and Simas, A. M. (2010) Two-Photon Absorption by Fluorene Derivatives: Systematic Molecular Design. *J Phys Chem C 114*, 6106-6116.

(17) Reinhardt, B. A., Brott, L. L., Clarson, S. J., Dillard, A. G., Bhatt, J. C., Kannan, R., Yuan, L. X., He, G. S., and Prasad, P. N. (1998) Highly active two-photon dyes: Design, synthesis, and characterization toward application. *Chem Mater 10*, 1863-1874.

(18) Mongin, O., Porres, L., Charlot, M., Katan, C., and Blanchard-Desce, M. (2007) Synthesis, fluorescence, and two-photon absorption of a series of elongated rodlike and banana-shaped quadrupolar fluorophores: A comprehensive study of structure-property relationships. *Chem-Eur J 13*, 1481-1498.

(19) Belfield, K. D., Schafer, K. J., Mourad, W., and Reinhardt, B. A. (2000) Synthesis of new two-photon absorbing fluorene derivatives via Cu-mediated Ullmann condensations. *Journal of Organic Chemistry 65*, 4475-4481.

(20) Kannan, R., He, G. S., Yuan, L. X., Xu, F. M., Prasad, P. N., Dombroskie, A. G., Reinhardt, B. A., Baur, J. W., Vaia, R. A., and Tan, L. S. (2001) Diphenylaminofluorene-based two-photon-absorbing chromophores with various pi-electron acceptors. *Chem Mater 13*, 1896-1904.

(21) Kosugi, M., Koshiba, M., Atoh, A., Sano, H., and Migita, T. (1986) Palladium-Catalyzed Coupling between Organic Halides and Organotin Compounds Involving C-N

Unsaturated Bonds at the Reaction Centers. *Bulletin of the Chemical Society of Japan 59*, 677-679.

(22) Yang, C. P., and Lin, J. H. (1994) Syntheses and Properties of Aromatic Polyamides and Polyimides Based on N-Phenyl-3,3-Bis[4(P-Aminophenoxy)Phenyl]Phthalimidine. *Journal of Polymer Science Part a-Polymer Chemistry 32*, 369-382.

(23) Sonogashira, K., Tohda, Y., and Hagihara, N. (1975) Convenient Synthesis of Acetylenes - Catalytic Substitutions of Acetylenic Hydrogen with Bromoalkenes, Iodoarenes, and Bromopyridines. *Tetrahedron Letters*, 4467-4470.

(24) Umezawa, H., Okada, S., Oikawa, H., Matsuda, H., and Nakanishi, H. (2005) Synthesis and non-linear optical properties of new ionic species: tolan and diphenylbutadiyne with trimethylammonio and dimethylamino groups. *Journal of Physical Organic Chemistry 18*, 468-472.

(25) Mongin, O., Krishna, T. R., Werts, M. H. V., Caminade, A. M., Majoral, J. P., and Blanchard-Desce, M. (2006) A modular approach to two-photon absorbing organic nanodots: brilliant dendrimers as an alternative to semiconductor quantum dots? *Chemical Communications*, 915-917.

(26) Pawlicki, M., Collins, H. A., Denning, R. G., and Anderson, H. L. (2009) Two-Photon Absorption and the Design of Two-Photon Dyes. *Angew Chem Int Edit 48*, 3244-3266.

(27) Zeng, D. X., and Chen, Y. (2007) A selective, fluorescent probe for Hg2+ detection in aqueous solution. *Journal of Photochemistry and Photobiology a-Chemistry 186*, 121-124.

(28) Belfield, K. D., Yao, S., Morales, A. R., Hales, J. M., Hagan, D. J., Van Stryland, E. W., Chapela, V. M., and Percino, J. (2005) Synthesis and characterization absorbing polymers of novel rigid two-photon. *Polym Advan Technol 16*, 150-155.

(29) Belfield, K. D., Bondar, M. V., Przhonska, O. V., and Schafer, K. J. (2002) Steady-state spectroscopic and fluorescence lifetime measurements of new two-photon absorbing fluorene derivatives. *Journal of Fluorescence 12*, 449-454.

(30) Belfield, K. D., Bondar, M. V., Yanez, C. O., Hernandez, F. E., and Przhonska, O. V. (2009) One- and Two-Photon Stimulated Emission Depletion of a Sulfonyl-Containing Fluorene Derivative. *Journal of Physical Chemistry B 113*, 7101-7106.

(31) Göppert-Mayer, M. (1931) Über Elementarakte mit zwei Quantensprüngen. *Annalen der Physik 401*, 273-294.

(32) Corredor, C. C., Huang, Z. L., and Belfield, K. D. (2006) Two-photon 3D optical data storage via fluorescence modulation of an efficient fluorene dye by a photochromic diarylethene. *Adv Mater 18*, 2910-2914.

(33) Corredor, C. C., Huang, Z. L., Belfield, K. D., Morales, A. R., and Bondar, M. V. (2007) Photochromic polymer composites for two-photon 3D optical data storage. *Chemistry of Materials 19*, 5165-5173.

(34) Morales, A. R., Schafer-Hales, K. J., Marcus, A. I., and Belfield, K. D. (2008) Amine-Reactive Fluorene Probes: Synthesis, Optical Characterization, Bioconjugation, and Two-Photon Fluorescence Imaging. *Bioconjugate Chem 19*, 2559-2567.

(35) Morales, A. R., Yanez, C. O., Schafer-Hales, K. J., Marcus, A. I., and Belfield, K. D. (2009) Biomolecule Labeling and Imaging with a New Fluorenyl Two-Photon Fluorescent Probe. *Bioconjugate Chem 20*, 1992-2000.

(36) Levine, B. (2007) Cell biology - Autophagy and cancer. *Nature 446*, 745-747.

(37) Bahr, B. A., and Bendiske, J. (2002) The neuropathogenic contributions of lysosomal dysfunction. *Journal of Neurochemistry 83*, 481-489.

(38) Levine, B., Wei, Y. J., Becker, N., and Anderson, M. (2009) Molecular regulation of the autophagy function of Beclin 1. *Autophagy 5*, 906-906.

(39) Sinha, S., and Levine, B. (2008) The autophagy effector Beclin 1: a novel BH3-only protein. *Oncogene 27*, S137-S148.

(40) Walkley, S. U. (1998) Cellular pathology of lysosomal storage disorders. *Brain Pathology 8*, 175-193.

(41) Donnert, G., Keller, J., Medda, R., Andrei, M. A., Rizzoli, S. O., Lurmann, R., Jahn, R., Eggeling, C., and Hell, S. W. (2006) Macromolecular-scale resolution in biological fluorescence microscopy. *Proceedings of the National Academy of Sciences of the United States of America 103*, 11440-11445.

(42) Hell, S. W., and Wichmann, J. (1994) Breaking the Diffraction Resolution Limit by Stimulated-Emission - Stimulated-Emission-Depletion Fluorescence Microscopy. *Optics Letters 19*, 780-782.

(43) Betzig, E., Patterson, G. H., Sougrat, R., Lindwasser, O. W., Olenych, S., Bonifacino, J. S., Davidson, M. W., Lippincott-Schwartz, J., and Hess, H. F. (2006) Imaging intracellular fluorescent proteins at nanometer resolution. *Science 313*, 1642-1645.

(44) Shtengel, G., Galbraith, J. A., Galbraith, C. G., Lippincott-Schwartz, J., Gillette, J. M., Manley, S., Sougrat, R., Waterman, C. M., Kanchanawong, P., Davidson, M. W., Fetter, R. D., and Hess, H. F. (2009) Interferometric fluorescent super-resolution microscopy resolves 3D cellular ultrastructure. *Proceedings of the National Academy of Sciences of the United States of America 106*, 3125-3130.

(45) Batrakova, E. V., and Kabanov, A. V. (2008) Pluronic block copolymers: Evolution of drug delivery concept from inert nanocarriers to biological response modifiers. *Journal of Controlled Release 130*, 98-106.

(46) Escobar-Chavez, J. J., Lopez-Cervantes, M., Naik, A., Kalia, Y. N., Quintanar-Guerrero, D., and Ganem-Quintanar, A. (2006) Applications of thermoreversible pluronic F-127 gels in pharmaceutical formulations. *Journal of Pharmacy and Pharmaceutical Sciences 9*, 339-358.

(47) Sahay, G., Batrakova, E. V., and Kabanov, A. V. (2008) Different Internalization Pathways of Polymeric Micelles and Unimers and Their Effects on Vesicular Transport. *Bioconjugate Chemistry 19*, 2023-2029.

(48) Kabanov, A. V., Levashov, A. V., and Alakhov, V. Y. (1989) Lipid Modification of Proteins and Their Membrane-Transport. *Protein Eng 3*, 39-42.

(49) Batrakova, E. V., Li, S., Vinogradov, S. V., Alakhov, V. Y., Miller, D. W., and Kabanov, A. V. (2001) Mechanism of pluronic effect on P-glycoprotein efflux system in blood-brain barrier: Contributions of energy depletion and membrane fluidization. *J Pharmacol Exp Ther 299*, 483-493.

(50) Belfield, K. D., Bondar, M. V., Hales, J. M., Morales, A. R., Przhonska, O. V., and Schafer, K. J. (2005) One- and two-photon fluorescence anisotropy of selected fluorene derivatives. *Journal of Fluorescence 15*, 3-11.

(51) Manders, E. M. M., Verbeek, F. J., and Aten, J. A. (1993) Measurement of Colocalization of Objects in Dual-Color Confocal Images. *Journal of Microscopy-Oxford 169*, 375-382.

(52) Andrade, C. D., Yanez, C. O., Rodriguez, L., and Belfield, K. D. (2010) A Series of Fluorene-Based Two-Photon Absorbing Molecules: Synthesis, Linear and Nonlinear Characterization, and Bioimaging. *The Journal of Organic Chemistry 75*, 3975-3982.

(53) Makarov, N. S., Drobizhev, M., and Rebane, A. (2008) Two-photon absorption standards in the 550-1600 nm excitation wavelength range. *Optics Express 16*, 4029-4047.

(54) Albota, M. A., Xu, C., and Webb, W. W. (1998) Two-photon fluorescence excitation cross sections of biomolecular probes from 690 to 960 nm. *Applied Optics 37*, 7352-7356.

(55) He, G. S., Helgeson, R., Lin, T. C., Zheng, Q. D., Wudl, F., and Prasad, P. N. (2003) One-, two-, and three-photon pumped lasing in a novel liquid dye salt system. *Ieee Journal of Quantum Electronics 39*, 1003-1008.

(56) Folling, J., Belov, V., Riedel, D., Schonle, A., Egner, A., Eggeling, C., Bossi, M., and Hell, S. W. (2008) Fluorescence nanoscopy with optical sectioning by two-photon induced molecular switching using continuous-wave lasers. *Chemphyschem 9*, 321-326.

(57) Hagen, S., Leyssner, F., Nandi, D., Wolf, M., and Tegeder, P. (2007) Reversible switching of tetra-tert-butyl-azobenzene on a Au(111) surface induced by light and thermal activation. *Chemical Physics Letters 444*, 85-90.

(58) Konig, K. (2000) Multiphoton microscopy in life sciences. *Journal of Microscopy-Oxford 200*, 83-104.

(59) Zipfel, W. R., Williams, R. M., and Webb, W. W. (2003) Nonlinear magic: multiphoton microscopy in the biosciences. *Nature Biotechnology 21*, 1368-1376.

(60) Woo, H. Y., Korystov, D., Mikhailovsky, A., Nguyen, T. Q., and Bazan, G. C. (2005) Two-photon absorption in aqueous micellar solutions. *Journal of the American Chemical Society 127*, 13794-13795.

(61) Patterson, G. H., and Piston, D. W. (2000) Photobleaching in two-photon excitation microscopy. *Biophysical Journal 78*, 2159-2162.

(62) Ha-Thi, M. H., Penhoat, M., Drouin, D., Blanchard-Desce, M., Michelet, V., and Leray, I. (2008) Synthesis, fluorescence, and two-photon absorption of bidentate phosphane oxide derivatives: Complexation with Pb2+ and Cd2+ cations. *Chemistry-a European Journal 14*, 5941-5950.

(63) Yang, W. J., Seo, M. S., Wang, X. Q., Jeon, S. J., and Cho, B. R. (2008) Two-photon absorption properties of 9,10-disubstituted 2,6-Bis(p-dihexylaminostyryl)Anthracene derivatives. Effect of 9,10-substituents. *Journal of Fluorescence 18*, 403-411.

(64) Meltola, N. J., Wahlroos, R., and Soini, A. E. (2004) Hydrophilic labeling reagents of dipyrrylmethene-BF2 dyes for two-photon excited fluorometry: Syntheses and photophysical characterization. *Journal of Fluorescence 14*, 635-647.

(65) Hernandez, F. E., Belfield, K. D., Cohanoschi, I., Balu, M., and Schafer, K. J. (2004) Three- and four-photon absorption of a multiphoton absorbing fluorescent probe. *Applied Optics 43*, 5394-5398.

(66) Bondar, M. V., Przhonska, O. V., Yanez, C. O., and Belfield, K. D. (2009) New fluorene molecules with efficient two-photon absorption for multidisciplinary nonlinear optical applications. *Ukr. J. Phys. 54*, 14-21.

(67) Lakowicz, J. R. (1999) *Principles of fluorescence spectroscopy*, Kluwer, New York.

(68) Belfield, K. D., Bondar, M. V., Kachkovsky, O. D., Przhonska, O. V., and Yao, S. (2007) Solvent effect on the steady-state fluorescence anisotropy of two-photon absorbing fluorene derivatives. *Journal of Luminescence 126*, 14-20.

(69) Terenziani, F., Painelli, A., Katan, C., Charlot, M., and Blanchard-Desce, M. (2006) Charge instability in quadrupolar chromophores: Symmetry breaking and solvatochromism. *Journal of the American Chemical Society 128*, 15742-15755.

(70) Belfield, K. D., Bondar, M. V., Hernandez, F. E., Przhonska, O. V., and Yao, S. (2007) Two-photon absorption cross section determination for fluorene derivatives: Analysis of the methodology and elucidation of the origin of the absorption processes. *Journal of Physical Chemistry B 111*, 12723-12729.

(71) Corredor, C. C., Belfield, K. D., Bondar, M. V., Przhonska, O. V., and Yao, S. (2006) One- and two-photon photochemical stability of linear and branched fluorene derivatives. *Journal of Photochemistry and Photobiology a-Chemistry 184*, 105-112.

(72) Belfield, K. D., Bondar, M. V., Przhonska, O. V., and Schafer, K. J. (2004) One- and two-photon photostability of 9,9-didecyl-2,7-bis(N,N-diphenylamino)fluorene. *Photochemical & Photobiological Sciences 3*, 138-141.

(73) Belfield, K. D., Bondar, M. V., Przhonska, O. V., and Schafer, K. J. (2004) Photochemical properties of (7-benzothiazol-2-yl-9, 9-didecylfluoren-2-yl)diphenylamine

under one- and two-photon excitation. *Journal of Photochemistry and Photobiology a-Chemistry 162*, 569-574.

(74) Shafer, F. P. (1973) *Dye Lasers*, Springer-Verlag, New York.

(75) Cory, A. H., Owen, T. C., Barltrop, J. A., and Cory, J. G. (1991) Use of an aqueous soluble tetrazolium/formazan assay for cell growth assays in culture. *Cancer Comm. 3*, 207-212.

(76) De Boni, L., Toro, C., and Hernandez, F. E. (2008) Pump polarization-state preservation of picosecond generated white-light supercontinuum. *Optics Express 16*, 957-964.

(77) Callagy, G., Dimitriadis, E., Harmey, J., Bouchier-Hayes, D., Leader, M., and Kay, E. (2000) Immunohistochemical measurement of tumor vascular endothelial growth factor in breast cancer - A more reliable predictor of tumor stage than microvessel density or serum vascular endothelial growth factor. *Applied Immunohistochemistry & Molecular Morphology 8*, 104-109.

(78) Tozer, G. M., Ameer-Beg, S. M., Baker, J., Barber, P. R., Hill, S. A., Hodgkiss, R. J., Locke, R., Prise, V. E., Wilson, I., and Vojnovic, B. (2005) Intravital imaging of tumour vascular networks using multi-photon fluorescence microscopy. *Advanced Drug Delivery Reviews 57*, 135-152.

(79) Gao, J. H., Chen, K., Xie, R. G., Xie, J., Yan, Y. J., Cheng, Z., Peng, X. G., and Chen, X. Y. (2010) In Vivo Tumor-Targeted Fluorescence Imaging Using Near-Infrared Non-Cadmium Quantum Dots. *Bioconjugate Chem 21*, 604-609.

(80) Wang, L. V. (2009) Multiscale photoacoustic microscopy and computed tomography. *Nature Photonics 3*, 503-509.

(81) Zhang, H. F., Maslov, K., Li, M. L., Stoica, G., and Wang, L. H. V. (2006) In vivo volumetric imaging of subcutaneous microvasculature by photoacoustic microscopy. *Optics Express 14*, 9317-9323.

(82) Carmeliet, P. (2005) Angiogenesis in life, disease and medicine. *Nature 438*, 932-936.

(83) Yong, L., and Paul, J. C. (2009) Angiogenesis as a strategic target for prostate cancer therapy. *Medicinal Research Reviews 9999*, n/a.

(84) Ellis, L. M., Curley, S. A., and Grothey, A. (2005) Surgical Resection After Downsizing of Colorectal Liver Metastasis in the Era of Bevacizumab. *J Clin Oncol 23*, 4853-4855.

(85) Ferrara, N., and Kerbel, R. S. (2005) Angiogenesis as a therapeutic target. *Nature 438*, 967-974.

(86) Kowanetz, M., and Ferrara, N. (2006) Vascular Endothelial Growth Factor Signaling Pathways: Therapeutic Perspective. *Clinical Cancer Research 12*, 5018-5022.

(87) Backer, M. V., Gaynutdinov, T. I., Patel, V., Bandyopadhyaya, A. K., Thirumamagal, B. T. S., Tjarks, W., Barth, R. F., Claffey, K., and Backer, J. M. (2005) Vascular endothelial growth factor selectively targets boronated dendrimers to tumor vasculature. *Molecular Cancer Therapeutics 4*, 1423-1429.

(88) Saban, M. R., Backer, J. M., Backer, M. V., Maier, J., Fowler, B., Davis, C. A., Simpson, C., Wu, X.-R., Birder, L., Freeman, M. R., Soker, S., Hurst, R. E., and Saban, R. (2008) VEGF receptors and neuropilins are expressed in the urothelial and neuronal cells in normal mouse urinary bladder and are upregulated in inflammation. *Am J Physiol Renal Physiol 295*, F60-72.

(89) Li, C. Y., Shan, S. Q., Huang, Q., Braun, R. D., Lanzen, J., Hu, K., Lin, P. N., and Dewhirst, M. W. (2000) Initial stages of tumor cell-induced angiogenesis: Evaluation via skin window chambers in rodent models. *Journal of the National Cancer Institute 92*, 143-147.

(90) Bodor, G., Porter, S., Landt, Y., and Ladenson, J. (1992) Development of monoclonal antibodies for an assay of cardiac troponin-I and preliminary results in suspected cases of myocardial infarction. *Clin Chem 38*, 2203-2214.

(91) Michaud, G. A., Salcius, M., Zhou, F., Bangham, R., Bonin, J., Guo, H., Snyder, M., Predki, P. F., and Schweitzer, B. I. (2003) Analyzing antibody specificity with whole proteome microarrays. *Nature Biotechnology 21*, 1509-1512.

(92) Dias, S., Hattori, K., Heissig, B., Zhu, Z. P., Wu, Y., Witte, L., Hicklin, D. J., Tateno, M., Bohlen, P., Moore, M. A. S., and Rafii, S. (2001) Inhibition of both paracrine and autocrine VEGF/VEGFR-2 signaling pathways is essential to induce long-term remission of xenotransplanted human leukemias. *Proceedings of the National Academy of Sciences of the United States of America 98*, 10857-10862.

(93) Posey, J. A., Ng, T. C., Yang, B. L., Khazaeli, M. B., Carpenter, M. D., Fox, F., Needle, M., Waksal, H., and LoBuglio, A. F. (2003) A phase I study of anti-kinase insert domain-containing receptor antibody, IMC-1C11, in patients with liver metastases from colorectal carcinoma. *Clinical Cancer Research 9*, 1323-1332.

(94) Zhu, Z. P., Rockwell, P., Lu, D., Kotanides, H., Pytowski, B., Hicklin, D. J., Bohlen, P., and Witte, L. (1998) Inhibition of vascular endothelial growth factor-induced receptor

activation with anti-kinase insert domain-containing receptor single-chain antibodies from a phage display library. *Cancer Research 58*, 3209-3214.

(95) Berlier, J. E., Rothe, A., Buller, G., Bradford, J., Gray, D. R., Filanoski, B. J., Telford, W. G., Yue, S., Liu, J. X., Cheung, C. Y., Chang, W., Hirsch, J. D., Beechem, J. M., and Haugland, R. P. (2003) Quantitative comparison of long-wavelength Alexa Fluor dyes to Cy dyes: Fluorescence of the dyes and their bioconjugates. *Journal of Histochemistry & Cytochemistry 51*, 1699-1712.

(96) Teske, C. A., Schroeder, M., Simon, R., and Hubbuch, J. (2005) Protein-labeling effects in confocal laser scanning microscopy. *Journal of Physical Chemistry B 109*, 13811-13817.

(97) Vira, S., Mekhedov, E., Humphrey, G., and Blank, P. S. (2010) Fluorescent-labeled antibodies: Balancing functionality and degree of labeling. *Analytical Biochemistry 402*, 146-150.

(98) Bosomtwi, A., Jiang, Q., Ding, G. L., Zhang, L., Zhang, Z. G., Lu, M., Ewing, J. R., and Chopp, M. (2008) Quantitative evaluation of microvascular density after stroke in rats using MRI. *Journal of Cerebral Blood Flow and Metabolism 28*, 1978-1987.

(99) Mertz, K. D., Demichetis, F., Kim, R., Schraml, P., Storz, M., Diener, P. A., Moch, H., and Rubin, M. A. (2007) Automated immunofluorescence analysis defines microvessel area as a prognostic parameter in clear cell renal cell cancer. *Hum Pathol 38*, 1454-1462.

(100) Wu, E. X., Tang, H., and Jensen, J. H. (2004) High-resolution MR imaging of mouse brain microvasculature using the relaxation rate shift index <I>Q</I>. *NMR in Biomedicine 17*, 507-512.